Aus dem Lehrstuhl für Nephrologie

Technische Universität München

Lehrstuhlinhaber: Univ.-Prof. Dr. med. Dr. h.c. Uwe Heemann

Entschlüsselung von erblichen Nierenkrankheiten und monogenen Syndromen mittels Exom-Sequenzierung und Multi-Omics

Zusammenstellung wissenschaftlicher Veröffentlichungen

zur Erlangung der Lehrbefähigung für das Fach Innere Medizin

an der TUM School of Medicine and Health der

Technischen Universität München

vorgelegt von

Dr. med. Korbinian Maria Riedhammer

April 2024

Mit Genehmigung der TUM School of Medicine and Health

der Technischen Universität München

Fachmentorat: Univ.-Prof. Dr. med. Dr. h.c. Uwe Heemann (Vorsitzender)

                       apl. Prof. Dr. med. Julia Höfele

                       Univ.-Prof. Dr. med. Michael Fischereder

Dekanin: Univ.-Prof. Dr. med. Stephanie E. Combs

Tag des Kolloquiums: 08.03.2022

In Gedenken an meinen im November 2023 verstorbenen, geliebten Opa,

Franz Huber.

We wish to suggest a structure for the salt of deoxyribose nucleic acid (D.N.A.).

This structure has novel features which are of considerable biological interest.

Anfang aus Watson JD, Crick FH. Molecular structure of nucleic acids; a structure for deoxyribose nucleic acid. *Nature*. 1953 Apr 25;171(4356):737-8.

Inhaltsverzeichnis

Abkürzungsverzeichnis

Abb.	Abbildung
ADTKD	Autosomal dominant tubulointerstitial kidney disease (autosomal-dominante tubulointerstitielle Nierenkrankheit)
ACMG	American College of Medical Genetics and Genomics
ADAS	Autosomal-dominantes Alport-Syndrom
ARAS	Autosomal-rezessives Alport-Syndrom
AS	Alport-Syndrom
ASD	Atriumseptumdefekt (Vorhofseptumdefekt)
bzw.	beziehungsweise
CAKUT	Congenital anomalies of the kidney and urinary tract (angeborene Nieren- und Harnwegsfehlbildungen)
CKD	Chronic kidney disease (chronische Niereninsuffizienz)
CNS	Central nervous system (Zentralnervensystem)
CNV	Copy number variant (Kopienzahlvariante)
CRISPR	Clustered regularly interspaced short palindromic repeats (gehäufte, kurze palindromische Wiederholungen mit regelmäßigem Abstand)
CVS	Cardiovascular (kardiovaskulär)
d.h.	das heißt
DNA	Deoxyribonucleic acid (Desoxyribonukleinsäure)
ES	Exom-Sequenzierung
ESKD	End-stage kidney disease (dialysepflichtiges Nierenversagen)
FSGS	Fokal segmentale Glomerulosklerose
GFR	Glomeruläre Filtrationsrate
GO	Gene Ontology (Gen-Ontologie)
GS	Genom-Sequenzierung
GWAS	Genomweite Assoziationsstudie
MAF	Minor allele frequency (Frequenz des selteneren Allels)
mRNA	Messenger-RNA (Boten-Ribonukleinsäure)
NGS	Next-Generation-Sequencing
OMIM®	Online Mendelian Inheritance in Man®
PFO	Persistierendes Foramen ovale
qPCR	Real-time quantitative polymerase chain reaction (quantitative Echtzeit-Polymerase-Kettenreaktion)

RAAS	Renin-Angiotensin-Aldosteron-System
RNA	Ribonucleic acid (Ribonukleinsäure)
siRNA	Small interfering RNA (kleine interferierende RNA)
SNP	Single nucleotide polymorphism (Einzelnukleotidpolymorphismus)
SRNS	Steroid-resistentes nephrotisches Syndrom
Tab.	Tabelle
TOF	Tetralogy of Fallot (Fallot'sche Tetralogie)
usw.	und so weiter
v.a.	vor allem
VACTERL	V, vertebrale Anomalien, A, anorektale Fehlbildungen, C, cardiovascular anomalies (kardiovaskuläre Anomalien), T, tracheoösophageale Fisteln; E, esophageal atresia (Ösophagusatresie), R, renale Anomalien, L, limb defects (Extremitätenfehlbildungen)
vs.	versus
VSD	Ventrikelseptumdefekt
VUR	Vesikoureteraler Reflux
XLAS	X-linked Alport Syndrome (X-chromosomales Alport-Syndrom)

Abbildungs- und Tabellenverzeichnis

1. Einleitung

Spätestens mit der von Arthur Cecil Alport 1927 veröffentlichten, bahnbrechenden Arbeit über ein familiär gehäuftes, vor allem Männer betreffendes Syndrom aus Hämaturie, Nierenfunktionsverlust und Taubheit ist die Genetik ein Bestandteil der Nephrologie.[1] Ein weiterer Meilenstein der „Nephrogenetik" sollte bis 1990 dauern, als Forscher um Karl Tryggvason das beim X-chromosomalen Alport-Syndrom betroffene Gen, *COL4A5*, klonieren konnten.[2] Mit der Entschlüsselung der Basenabfolge des menschlichen Erbguts mittels Sanger-Sequenzierung im Rahmen des „Human Genome Projects" zu Beginn des 21. Jahrhunderts wurde die Ära der genomischen Medizin eingeläutet, welche durch die Einführung des Next-Generation-Sequencings (NGS; siehe 1.2) Mitte der 2000er eine unglaubliche Erfolgsgeschichte erfuhr.[3,4] Dadurch hat auch die Nephrogenetik in den letzten zwei Jahrzehnten eine rasante Entwicklung vollzogen, welche im Folgenden beleuchtet werden soll.

1.1 Genetik in der Nephrologie im 21. Jahrhundert - von erblichen zu multifaktoriellen Krankheiten hin zur Präzisionsmedizin

Mittlerweile sind über 600 Gene mit erblichen (= monogenen), nephrologischen Krankheitsentitäten verknüpft worden.[5] Erbliche Nierenkrankheiten betreffen knapp 10% der Erwachsenen mit chronischer Niereninsuffizienz (chronic kidney disease, CKD), bei Beginn der CKD vor einem Alter von 25 Jahren sind es sogar über 70% der Patienten.[6-8]

Daneben konnte u.a. mittels genomweiter Assoziationsstudien (genome-wide association studies, GWAS) gezeigt werden, dass genetische Variation auch bei komplexen Nierenkrankheiten wie der IgA-Nephropathie und renalen Phänotypen wie der Albuminurie eine gewichtige Rolle spielt.[9-11] Weiterhin gibt es Krankheiten wie den systemische Lupus erythematodes, der zu einem kleinen Teil im monogenen Kontext durch seltene Varianten [minor allele frequency (MAF) < 1,0%] erklärt werden kann, bei dem aber auch häufige Varianten (MAF ≥ 1,0%) als Risikoallele die Krankheitsentstehung in einem multifaktoriellen Kontext mitbestimmen.[12] Genannt sei in diesem Zusammenhang zudem der *UMOD*-Locus (16p12.3): Einerseits sind seltene Varianten in *UMOD* mit einer monogenen Krankheit (autosomal dominant tubulointerstitial kidney disease, ADTKD-*UMOD*) verknüpft, daneben ist der *UMOD*-Locus auch von herausragender Bedeutung für das CKD-Risiko in der

Allgemeinbevölkerung.[13] Diese Beispiele zeigen, dass die Grenze zwischen erblichen, durch seltene Varianten mit hoher Effektstärke ausgelöste Krankheiten, und multifaktoriellen, durch häufige Varianten mit geringer Effektstärke beeinflusste Krankheiten, fließend ist (Abbildung 1).[13,14]
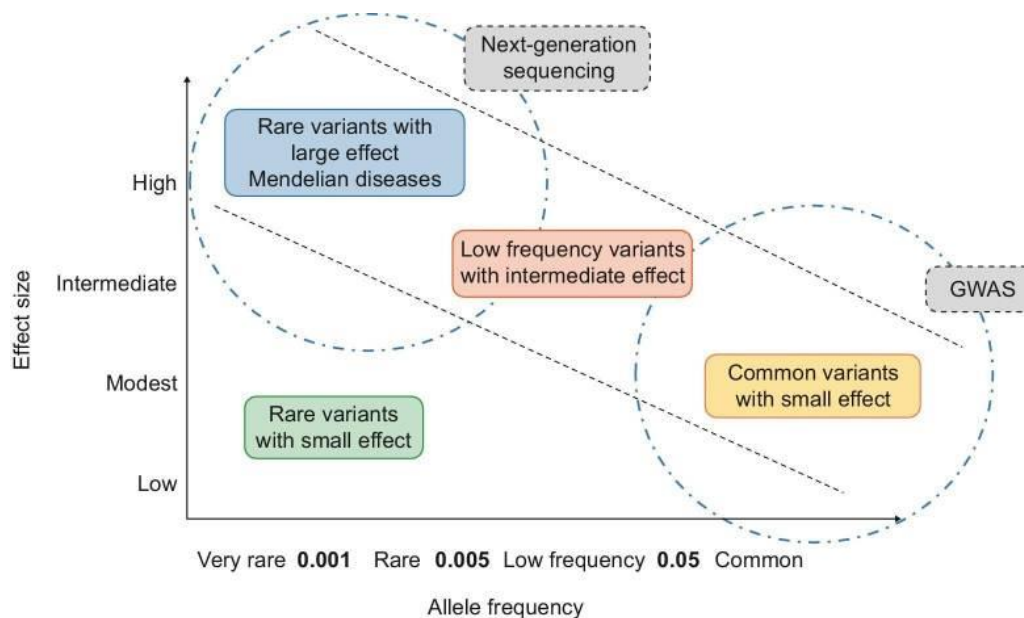
Abbildung 1: Das Kontinuum aus häufiger und seltener genetischer Variation mit variabler Effektstärke und jeweils angewandten molekulargenetischen Techniken (Next-Generation-Sequencing und genomweite Assoziationsstudien, GWAS). Aus [15].

Es ist mittlerweile eindeutig, dass die Kenntnis genetischer Determinanten von Nierenkrankheiten nicht nur zentral in der Diagnostik, sondern auch im therapeutischen Kontext ist.[16] Ein Beispiel hierfür ist die *APOL1*-assoziierte Nephropathie: Patienten mit den gain-of-function-Risikoallelen G1 oder G2 in *APOL1* haben eine erhöhte Aktivität des APOL1-Ionenkanals, was eine Schädigung von Podozyten zufolge hat, was zu einer erhöhten Anfälligkeit für eine proteinurische Nierenkrankheit mit konsekutiver fokal segmentaler Glomerulosklerose (FSGS) führt.[17] In einer kürzlich veröffentlichten Phase-2a-Studie an 16 Individuen mit den Risikoallelen G1 oder G2 in *APOL1* und biopsiegesicherter FSGS mit (sub-)nephrotischer Proteinurie konnte die experimentelle Substanz Inaxaplin, ein Inhibitor der Kanalfunktion von APOL1, die Proteinurie signifikant senken.[18]

Insgesamt lässt sich daher zusammenfassen, dass die Genetik der Schlüssel zur Präzisionsmedizin der Zukunft in der Nephrologie (und der gesamten Medizin) ist.

1.2 Die Entwicklung der Molekulargenetik – eine Erfolgsgeschichte

Neben der Entschlüsselung der Struktur der DNA durch James Watson, Francis Crick, Maurice Wilkins und Rosalind Franklin Anfang der 1950er Jahre kann die 1977 von Frederick Sanger publizierte Kettenabbruchmethode zur DNA-Sequenzierung sicherlich als zentraler Moment der Molekulargenetik gesehen werden.[19,20] Mit der Sanger-Sequenzierung können einzelne DNA-Abschnitte Base für Base sequenziert werden, was auch heute noch für gezielte Untersuchungen, z.B. auf Trägerschaft einer in der Familie bekannten krankheitsverursachenden Variante in einem bestimmten Gen, angewandt wird. Die Effizienz der Methode ist jedoch eingeschränkt: So dauerte die Sanger-Sequenzierung des menschlichen Genoms (ca. drei Milliarden Basenpaare) im Rahmen des „Human Genome Projects" 13 Jahre, von 1990 bis 2003.[21,22] Mit der Etablierung des (short-read-basierten) NGS seit 2005, bei dem nicht eine Base pro Zeiteinheit, sondern Millionen von Basen parallel sequenziert werden können („massively parallel sequencing"), ergab sich ein Quantensprung in der Molekulargenetik.[23] Die Kosten einer Genom-Sequenzierung haben sich damit in den letzten 20 Jahren von knapp drei Milliarden US-Dollar („Human Genome Project") auf unter 1.000 Dollar reduziert (Abbildung 2).[24]
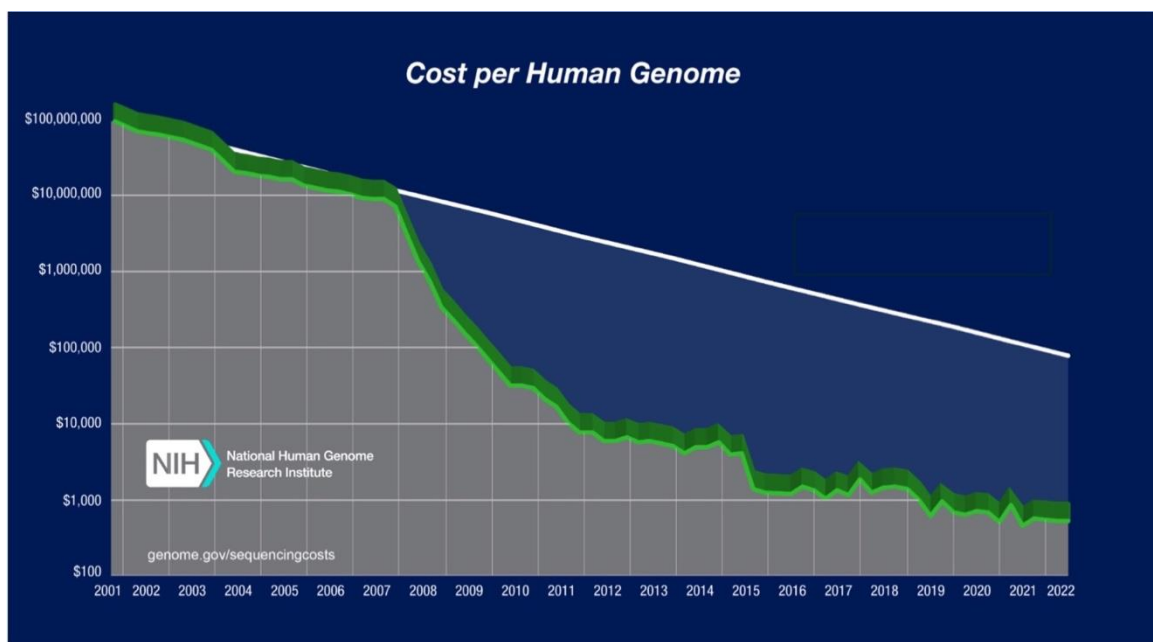
Abbildung 2: Entwicklung der Kosten eines Genoms in US-Dollar zwischen 2001 und 2022 (abgewandelt nach [24]).

Als kostensparende, pragmatische Alternative zur Genom-Sequenzierung (GS) hat sich in den 2010er Jahren die Exom-Sequenzierung (ES) etabliert. Während bei der GS die gesamte Erbanlage sequenziert wird, ist es bei der ES nur der proteinkodierende Bereich, das Exom (ca. 1% des Genoms).[25,26] Gerade in der Erforschung erblicher (monogener) Krankheiten hat die ES zu einem enormen Wissenszuwachs geführt. So wurden in der Enzyklopädie für erbliche Krankheiten, der Mendelian Inheritance in Man, 1998 1.486 monogene Krankheiten und Phänotypen gelistet, 2021 waren es über 25.000 in dessen Online-Version, der Online Mendelian Inheritance in Man® (OMIM®; Abbildung 2).[27,28]
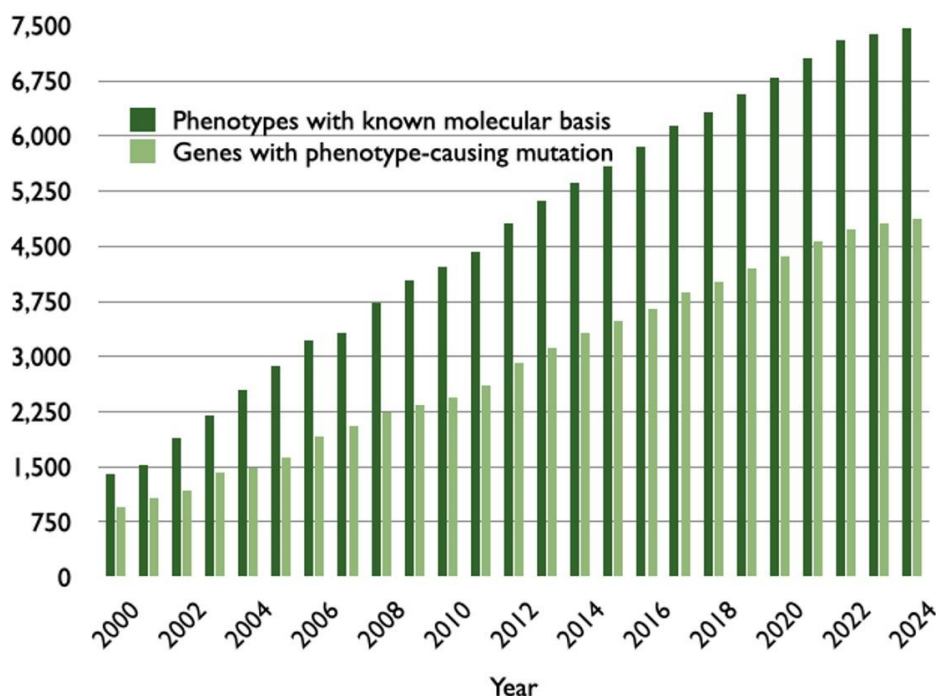
Abbildung 3: Zeitliche Entwicklung der Anzahl der Phänotypen/Krankheiten mit bekannter molekularer Grundlage und der krankheitsassoziierten Gene in der Online Mendelian Inheritance in Man® (OMIM®). Aus [29].

Ein großer methodeninhärenter Nachteil der ES ist die fehlende Analysemöglichkeit nichtkodierender Bereiche. Daher wird, bei weiter fallenden Preisen der GS, die ES sicherlich in den nächsten Jahren einen Bedeutungsverlust erfahren.[26,30] Durch die Integration weiterer „Omics"-Techniken wie Transkriptomik (RNA-Sequenzierung), Proteomik und Epigenomik in Zusammenspiel mit künstlicher Intelligenz wird sich auch die

10

Interpretierbarkeit nichtkodierender Varianten in Zukunft enorm verbessern.[31-34] Außerdem können durch neuere Sequenziermethoden wie dem Long-Read-Sequencing oder dem Optical-Genome-Mapping größere und komplexe strukturelle Varianten (> 10 Kilobasen bzw. > 200 Kilobasen) wie Deletionen, Duplikationen, Inversionen, Insertionen und Translokationen entdeckt werden, was bisher eine Domäne der Zytogenetik ist.[34,35] Zuletzt sei noch erwähnt, dass NGS-Methoden die Erstellung von Gen-Expressions-Atlanten z.B. der Niere auf Einzelzellebene ("Single-Cell-Sequencing") ermöglichen, was enorme Chancen zur Pathway-Analyse und Therapie-Entwicklung bietet.[36]

1.3 Fragestellungen und Ziele der vorliegenden Arbeit

Die folgenden Veröffentlichungen beschäftigen sich mit der Anwendung der Exom-Sequenzierung (ES) bei Individuen mit der klinischen Verdachtsdiagnose einer erblichen Nierenkrankheit. Einerseits werden klinisch-statistische Fragestellungen bearbeitet, die sich aus der umfassenden Diagnostik mittels ES ergeben. So kann die klinische Verdachtsdiagnose einer bestimmten erblichen Nierenkrankheit und die tatsächliche genetische Diagnose in einigen Fällen nicht übereinstimmen ("Phänokopie"), was Konsequenzen in Management und Therapie einer Krankheit haben kann. Weiterhin werden klinische Kohorten mit angeborenen Nieren- und Harnwegsfehlbildungen (congenital anomalies of the kidney and urinary tract, CAKUT) und Typ-IV-Kollagen-assoziierter Nephropathie/Alport-Syndrom beleuchtet, was z.B. zur Hypothese eines dominant-negativen Effekts bei heterozygoten Trägern von krankheitsverursachenden Varianten in *COL4A3*/*COL4A4* (autosomal-dominantes Alport-Syndrom) führt. Anderseits verfolgt die Arbeit auch das Ziel, neue Gene zu charakterisieren, welche zu erblichen Nierenkrankheiten bzw. monogenen Syndromen führen. Hierbei wurde auf eine breite Palette an Methoden zurückgegriffen, welche neben Exom-Sequenzierung auch die RNA-Sequenzierung, Epigenom- und Proteom-Untersuchungen beinhaltet ("Multi-Omics").

2. Identifikation von Phänokopien mittels Exom-Sequenzierung bei Individuen mit klinischer Verdachtsdiagnose einer erblichen Nierenkrankheit

Dieses Kapitel bezieht sich auf die folgende Originalarbeit:

- **Riedhammer KM**, Braunisch MC, Günthner R, Wagner M, Hemmer C, Strom TM, Schmaderer C, Renders L, Tasic V, Gucev Z, Nushi-Stavileci V, Putnik J, Stajić N, Weidenbusch M, Uetz B, Montoya C, Strotmann P, Ponsel S, Lange-Sperandio B, Hoefele J. Exome Sequencing and Identification of Phenocopies in Patients With Clinically Presumed Hereditary Nephropathies. *Am J Kidney Dis*. 2020 Oct;76(4):460-470. doi: 10.1053/j.ajkd.2019.12.008. Epub 2020 Apr 28. PMID: 32359821.

Folgende Beobachtung in der humangenetischen Beratung nephrologischer Patienten führte zur Durchführung dieser Studie: Es kommt immer wieder vor, dass die klinisch gestellte Verdachtsdiagnose [z.B. Alport-Syndrom (AS)] nicht mit der letztlichen genetischen Diagnose einer erblichen Nierenkrankheit übereinstimmt (z.B. eine erbliche Coenzym-Q10-Defizienz).

Diese Situation wird mit dem Begriff „Phänokopie" beschrieben. Der Begriff wurde ursprünglich definiert für einen Phänotyp, der dem einer erblichen Krankheit ähnelt, aber durch einen Umwelteinfluss verursacht ist. Ein vielzitiertes Beispiel ist das Medikament Thalidomid, das, in der Schwangerschaft eingesetzt, zu Fehlbildungen am Ungeborenen führt, welche wiederum dem Phänotyp einer erblichen Krankheit (Holt-Oram-Syndrom, OMIM® #142900) ähneln. Weiterhin wird der Begriff in Linkage-Studien verwendet, wenn ein für einen bestimmten Phänotyp (z.B. Parkinson-Krankheit) etablierter Genotyp (z.B. krankheitsverursachende Variante in *LRRK2)* nicht in allen Betroffenen eines Stammbaums identifiziert werden kann. In der hier besprochenen Publikation wird wiederum die breitere Definition einer Phänokopie benutzt, welche die Ungleichheit aus klinischer Verdachtsdiagnose und genetischer Diagnose ausdrückt.[37]

Phänokopien (klinische Verdachtsdiagnose ≠ genetische Diagnose) wurden in ausgewählten nephrogenetischen Kohorten bereits beschrieben: 10% von 70 Familien mit klinischem Verdacht auf erbliche FSGS hatten krankheitsverursachende Varianten in den mit AS verknüpften Genen *COL4A3* und *COL4A4* und nicht in mit erblicher FSGS/Podozytopathie verknüpften Genen.[38] In einer großen Kohorte mit 300 Familien (335 Individuen) mit der klinischen Verdachtsdiagnose eines steroid-resistenten nephrotischen Syndroms (d.h. einer erblichen Podozytopathie) konnte in 4% der Familien eine Phänokopie entdeckt werden. Neben krankheitsverursachenden Varianten in den AS-Genen *COL4A3* und *COL4A5* wurde auch ein Morbus Fabry (Gen *GLA*) genetisch diagnostiziert, welcher durch Enzymersatztherapie ursächlich behandelt werden kann.[39]

Die nun besprochene Publikation zeigt das genotypische und phänotypische Spektrum von Phänokopien in einer Kohorte aus 174 Index-Individuen mit klinischem Verdacht auf eine erbliche Nierenkrankheit, welche mittels ES molekulargenetisch untersucht wurden.

2.1 Methoden, Studiendesign und -population

Es handelte sich um eine retrospektive Studie an 174 nicht miteinander verwandten Index-Individuen (= Index-Fälle; 53% männlich, 47% weiblich), die zwischen 2015 und 2018 im Rahmen der „NephroGen-Studie" am Institut für Humangenetik des Klinikums rechts der Isar der Technischen Universität München rekrutiert wurden (Arbeitsgruppenleiterin: Prof. Dr. Julia Höfele). Das mediane Alter bei genetischer Testung lag bei 19 Jahren (Interquartilabstand 7,0 – 35,0 Jahre; Tabelle 1). 133/174 (76%) Index-Individuen waren kaukasischer Abstammung („Non-Finnish European descent").

Alle eingeschlossenen Individuen hatten den klinischen Verdacht auf eine spezifische erbliche Nierenkrankheit bzw. -krankheitsentität, gestellt durch den einsendenden Arzt (Kinder-, Erwachsenen-Nephrologe oder externer Humangenetiker) oder hatten den Verdacht auf eine erbliche Nierenkrankheit, weil mindestens eines der folgenden Kriterien zutraf: Beginn der Krankheit im Kindes-/Jugendalter (< 18 Jahre), syndromales Krankheitsbild (weitere Organe neben der Niere betroffen), positive Familienanamnese oder berichtete elterliche Konsanguinität. Der Phänotyp wurde, zusätzlich zu den Arztbriefen, mit einem standardisierten Fragebogen erhoben. Alle Individuen wurden 6 Krankheitsgruppen nach der klinischen Verdachtsdiagnose bzw. Symptomatik zugeordnet (Abbildung 4). Fälle,

die keiner der 6 Krankheitsgruppen zugewiesen werden konnten, wurden in die Gruppe „Andere" („Other") einsortiert (n = 27, 16%).

Alle 174 Index-Individuen wurden mittels ES untersucht (inklusive mitochondriale DNA). Die Variantenbewertung erfolgte nach den Richtlinien des American College of Medical Genetics and Genomics (ACMG).[40] Weiterhin wurde in den Fällen, in denen eine Phänokopie gefunden wurde (n = 10, 6%), untersucht, ob diese Fälle auch durch eine Gen-Panel-Untersuchung eines kommerziellen Anbieters hätten gelöst werden können („enges" Panel mit 6 – 10 Genen bzw. umfassendes Panel mit 272 Genen).
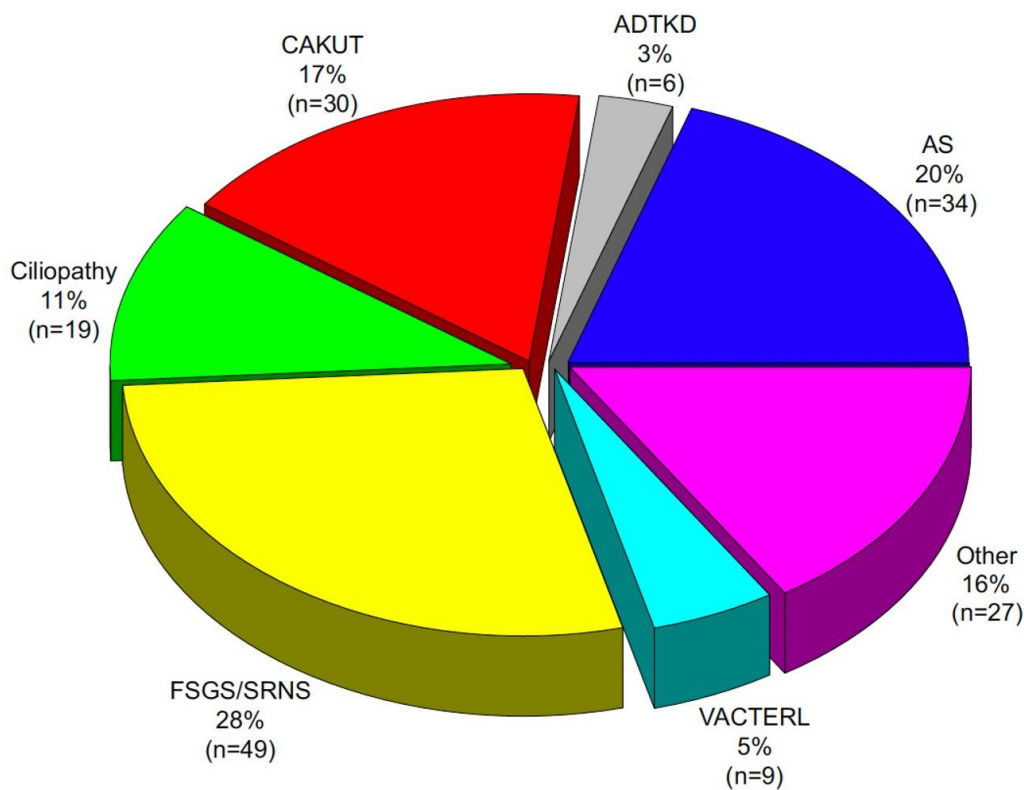
Abbildung 4: Aufteilung der klinischen Krankheitsgruppen (Kohorte mit 174 Index-Individuen mit klinischem Verdacht auf eine erbliche Nierenkrankheit). ADTKD, autosomal dominant tubulointersitial kidney disease (autosomal-dominante tubulointerstitielle Nierenkrankheit); AS, Alport-Syndrom; CAKUT, congenital anomalies of the kidney and urinary tract (angeborene Nieren- und Harnwegsfehlbildungen); FSGS, fokal segmentale Glomerulosklerose; SRNS, steroid-resistentes nephrotisches Syndrom; VACTERL-Assoziation: V, vertebrale Anomalien, A, anorektale Fehlbildungen, C, cardiovascular anomalies (kardiovaskuläre Anomalien), T, tracheoösophageale Fisteln; E, esophageal atresia (Ösophagusatresie), R, renale Anomalien, L, limb defects (Extremitätenfehlbildungen). Aus [41].

2.2 Ergebnisse

2.2.1 Diagnoserate in der Kohorte

Mittels ES konnte bei 52 von 174 Index-Fällen eine genetische Diagnose gestellt werden, was einer Diagnoserate von 30% entspricht. Die Diagnoseraten in den einzelnen Krankheitsgruppen waren sehr unterschiedlich: 3/6 (50%) bei ADTKD, 16/34 bei AS und 9/19 Ziliopathie (je 47%), 8/30 (27%) bei CAKUT und 8/49 (16%) bei FSGS/steroid-resistentes nephrotisches Syndrom (SRNS). In der VACTERL-Gruppe konnte keiner der neun Fälle genetisch gelöst werden [VACTERL: V, vertebrale Anomalien, A, anorektale Fehlbildungen, C, cardiovascular anomalies (kardiovaskuläre Anomalien), T, tracheoösophageale Fisteln; E, esophageal atresia (Ösophagusatresie), R, renale Anomalien, L, limb defects (Extremitätenfehlbildungen)]. In der Gesamtkohorte wurden zehn Phänokopien (10/174, 6%) identifiziert, also in einem von 16 Fällen stimmte die klinische Verdachtsdiagnose nicht mit der genetischen Diagnose überein (Tabelle 1 und Abbildung 5). Wenn man sich nur die genetisch gelösten Fälle ansieht (nur in diesen kann eine Phänokopie aufgedeckt werden), so liegt in ca. jedem fünften Fall (10/52, 19%) eine Phänokopie vor.

	AS	ADTKD	CAKUT	Ciliopathy	FSGS/SRNS	VACTERL	Other	Total
No. of index cases	34/174 (20%)	6/174 (3%)	30/174 (17%)	19/174 (11%)	49/174 (28%)	9/174 (5%)	27/174 (16%)	174
Male sex	20/34 (59%)	3/6 (50%)	19/30 (63%)	7/19 (37%)	25/49 (51%)	5/9 (56%)	14/27 (52%)	93/174 (53%)
Positive family history	18/34 (53%)	5/6 (83%)	9/30 (30%)	8/19 (42%)	19/49 (39%)	0/9 (0%)	10/27 (37%)	69/174 (40%)
Reported consanguinity	0/34 (0%)	0/6 (0%)	2/30 (7%)	2/19 (11%)	5/49 (10%)	0/9 (0%)	1/27 (4%)	10/174 (6%)[a]
Age at genetic testing, y	15 [8.0-26.0]	53 [47.0-65.0]	6 [0.1-25.0]	9 [0.8-19.0]	31 [19.0-42.0]	10 [1.0-12.5]	24 [7.0-37.0]	19 [7.0-35.0]
Diagnostic yield	16/34 (47%)	3/6 (50%)	8/30 (27%)	9/19 (47%)	8/49 (16%)	0/9 (0%)	8/27 (30%)	52/174 (30%)
No. of phenocopies	3/34 (9%)	0/6 (0%)	0/30 (0%)	1/19 (5%)	3/49 (6%)	0/9 (0%)	3/27 (11%)	10/174 (6%)

Tabelle 1: Überblick über die Studienkohorte. Gelöste Fälle sind solche, in denen eine krankheitsverursachende Variante(n) identifiziert wurde und eine genetische Diagnose gestellt werden konnte. Phänokopie (Phenocopy) bedeutet, dass die genetische Diagnose nicht mit der klinischen Verdachtsdiagnose übereinstimmt. Für pränatale Manifestationen/Diagnosen wurde das Alter auf „0 Jahre" festgesetzt. Das „Alter bei genetischer Testung" bezieht sich auf das Alter bei der Exom-Sequenzierung (= „Alter bei genetischer Diagnose" bei gelösten Fällen). Die Werte sind als n/N (Prozent) oder Median [Interquartilabstand] angegeben. ADTKD, autosomal dominant tubulointersitial kidney disease (autosomal-dominante tubulointerstitielle Nierenkrankheit); AS, Alport-Syndrom; CAKUT, congenital anomalies of the kidney and urinary tract (angeborene Nieren- und Harnwegsfehlbildungen); FSGS, fokal segmentale

Glomerulosklerose; SRNS, steroid-resistentes nephrotisches Syndrom; VACTERL-Assoziation: V, vertebrale Anomalien, A, anorektale Fehlbildungen, C, cardiovascular anomalies (kardiovaskuläre Anomalien), T, tracheoösophageale Fisteln; E, esophageal atresia (Ösophagusatresie), R, renale Anomalien, L, limb defects (Extremitätenfehlbildungen). Aus [41].

2.2.2 Identifizierte Phänokopien

Drei Individuen wiesen folgende Phänokopie auf: Genetisch gesicherte erbliche FSGS/SRNS, welche klinisch als AS eingestuft wurde. Bei zwei weiteren Individuen konnte die umgekehrte Situation beobachtet werden, genetisch gesichertes AS bei klinischem Verdacht auf erbliche FSGS/SRNS. Bei einem zusätzlichen Individuum wurde klinisch eine IgA-Nephropathie vermutet (keine Biopsie aufgrund des jungen Alters des Betroffenen), genetisch konnte ein X-chromosomales AS nachgewiesen werden. In einem weiteren Fall deutete das Ergebnis der Nierenbiopsie auf eine Typ-IV-Kollagen-assoziierte Nephropathie hin (elektronenmikroskopisch verschmälerte Basalmembran), genetisch konnte jedoch das Dent-Syndrom diagnostiziert werden (krankheitsverursachende hemizygote Variante in *CLCN5*). Bei einem Individuum wurde klinisch eine autosomal-rezessive polyzystische Nierenkrankheit, eine Ziliopathie, diagnostiziert, bei der molekulargenetischen Untersuchung ergab sich dann aber eine heterozygote 1,2-Megabasen-Deletion in 17q12, welche das CAKUT-Gen *HNF1B* beinhaltet. Die letzten zwei Fälle präsentierten sich klinisch als Tubulopathien, hatten aber einerseits genetisch eine Mitochondriopathie (homoplasmische krankheitsverursachende Variante m.616T>C in *MT-TF*), andererseits einen Prohormon-Prozessierungsdefekt mit compound-heterozygoten krankheitsverursachenden Varianten in *PCSK1*. Genaue genotypische und phänotypische Informationen können in der Originalpublikation nachgelesen werden.
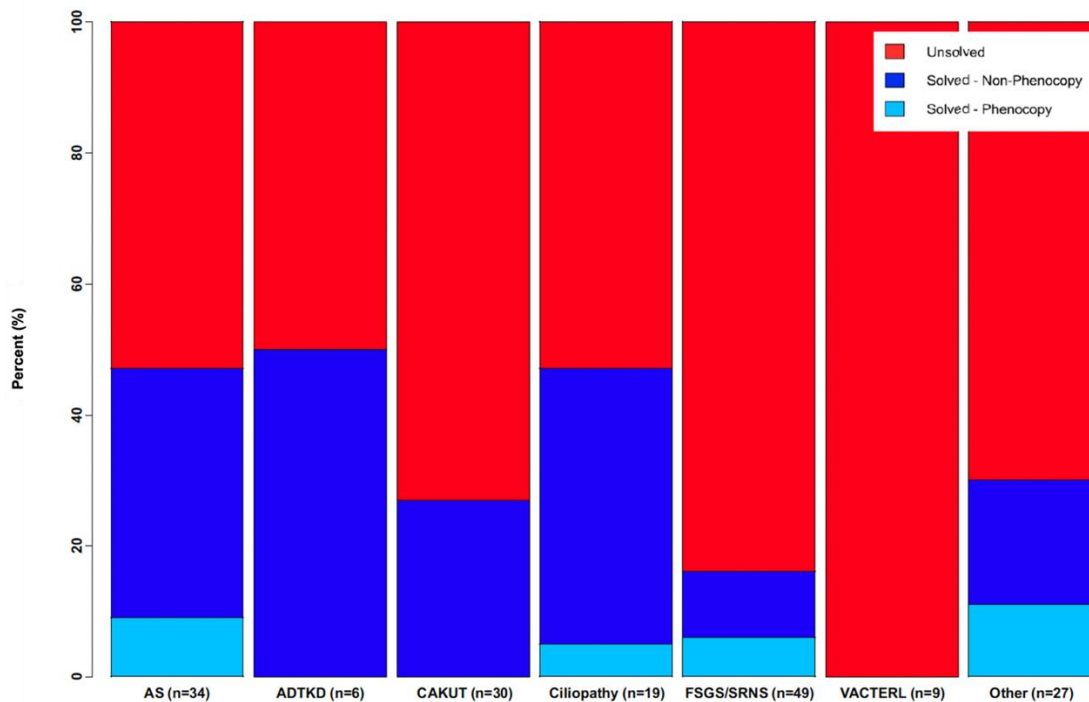
Abbildung 5: Diagnoserate der jeweiligen Krankheitsgruppe. Gelöste Fälle (Solved) sind solche, in denen eine krankheitsverursachende Variante(n) identifiziert wurde und eine genetische Diagnose gestellt werden konnte. Phänokopie (Phenocopy) bedeutet, dass die genetische Diagnose nicht mit der klinischen Verdachtsdiagnose übereinstimmt. Die gelösten Fälle sind in „Gelöst – keine Phänokopie" (dunkelblau) und „Gelöst – Phänokopie" (hellblau) aufgeteilt. Die Diagnoserate der Gesamtkohorte (n = 174 Index-Individuen) liegt bei 30%. ADTKD, autosomal dominant tubulointersitial kidney disease (autosomal-dominante tubulointerstitielle Nierenkrankheit); AS, Alport-Syndrom; CAKUT, congenital anomalies of the kidney and urinary tract (angeborene Nieren- und Harnwegsfehlbildungen); FSGS, fokal segmentale Glomerulosklerose; SRNS, steroid-resistentes nephrotisches Syndrom; VACTERL-Assoziation: V, vertebrale Anomalien, A, anorektale Fehlbildungen, C, cardiovascular anomalies (kardiovaskuläre Anomalien), T, tracheoösophageale Fisteln; E, esophageal atresia (Ösophagusatresie), R, renale Anomalien, L, limb defects (Extremitätenfehlbildungen). Aus [41].

2.2.3 Exom-Sequenzierung vs. Gen-Panel-Untersuchung

„Enge" NGS-Genpanel nach klinischer Verdachtsdiagnose mit < 25 Kilobasen Größe (6-10 Gene; zum Zeitpunkt der Publikation mit den gesetzlichen Krankenkassen abrechenbare Panelgröße) hätten keine der zehn Phänokopien aufdecken können. Ein umfassendes NGS-Genpanel auf erblichen Nierenkrankheiten mit 272 Genen (siehe Tabelle S3 in der Originalpublikation) hätte 8/10 (80%) Phänokopien aufgedeckt. Die beiden Fälle, die klinisch als Tubulopathie imponierten und letztlich genetisch eine Mitochondriopathie und ein Prohormon-Prozessierungsdefekt waren, hätten auch nicht mit einem umfassenden Gen-Panel aufgedeckt werden können.

2.3 Diskussion und Zusammenfassung

Anders als in vorherigen Studien wurde in dieser Publikation das Spektrum an Phänokopien über die gesamte Breite der Nephrogenetik illustriert. Die Rekategorisierung einer Krankheit durch die genetische Diagnose hat mehrere klinische Implikationen: Zum einen kann diese Auswirkungen im therapeutischen Management haben, wie z.B. Hormonersatz bei einem *PCSK1*-assoziierten Prohormon-Prozessierungsdefekt, aber auch die Prognose der Krankheit ändern (autosomal-rezessive polyzystische Nierenkrankheit vs. 17q12-Deletion). Außerdem ändert sich auch die Wiederholungswahrscheinlichkeit bei Nachkommen, je nach Erbgang (z.B. X-chromosomal vs. autosomal-rezessiv), was Konsequenzen für die Reproduktionswünsche von Ratsuchenden haben kann.

Man muss in diesem Zusammenhang natürlich anmerken: Ein klinisch tätiger Arzt muss sich auf Grundlage der Anamnese, Symptome und Befunde zu einem bestimmten Zeitpunkt Differentialdiagnosen überlegen und dann eine Verdachtsdiagnose stellen. Mit dem Verlauf der Krankheit und zunehmenden Diagnosemöglichkeiten können sich Differentialdiagnosen auch ändern bzw. angepasst werden. Jedoch zeigt diese Arbeit, dass aufgrund der genetischen und phänotypischen Heterogenität von erblichen Nierenkrankheiten eine umfassende genomweite Untersuchung wichtig ist, zumindest wenn eine erste umschriebene Gen-Panel-Untersuchung unauffällig war. Es ist auffallend, dass keine einzige der identifizierten Phänokopien durch eine enggefasste Gen-Panel-Untersuchung auf Grundlage der klinischen Verdachtsdiagnose hätte diagnostiziert werden können. Siehe hierzu auch das zugehörige Editorial.[42]

3. Phänotypische, genotypische und funktionelle Charakterisierung des Gens *TASP1* als krankheitsassoziiertes Gen für das Suleiman-El-Hattab-Syndrom

Dieses Kapitel bezieht sich auf folgende Originalarbeit:

- **Riedhammer KM**, Burgemeister AL, Cantagrel V, Amiel J, Siquier-Pernet K, Boddaert N, Hertecant J, Kannouche PL, Pouvelle C, Htun S, Slavotinek AM, Beetz C, Diego-Alvarez D, Kampe K, Fleischer N, Awamleh Z, Weksberg R, Kopajtich R, Meitinger T, Suleiman J, El-Hattab AW. Suleiman-El-Hattab syndrome: a histone modification disorder caused by TASP1 deficiency. *Hum Mol Genet*. 2022 Sep 10;31(18):3083-3094. doi: 10.1093/hmg/ddac098. PMID: 35512351; PMCID: PMC9476618.

Wie in der Einleitung dargelegt, hat die ES zu einem enormen Anstieg des Wissens um krankheitsassoziierte Gene geführt. Die folgende Publikation befasst sich mit der Charakterisierung eines neuen krankheitsassoziierten Gens, *TASP1*. Biallelische loss-of-function-Varianten, die zu TASP1-Defizienz führen, konnten bereits 2019, unter Mitwirkung des Habilitanden, mit einem komplexen Syndrom aus Entwicklungsverzögerung, Verhaltensauffälligkeiten, fazialen Dysmorphien und angeborenen Fehlbildungen verknüpft werden (Suleiman-El-Hattab-Syndrom, OMIM® #618950).[43]

TASP1 kodiert für Taspase 1 (Threonin-Aspartase 1, TASP1), eine heterodimere Endopeptidase, welche u.a. Histonmethyltransferasen der KMT2-Proteinfamilie im Zellkern aktiviert. Damit spielt das Enzym eine Rolle in der Methylierung der DNA (Epigenetik) und beeinflusst mittelbar die Gentranskription.[44] Defekte der „epigenetischen Maschinerie" wie z.B. eine Haploinsuffizienz von *KMT2A* (auch *MLL*; kodiert für eine Histonmethyltransferase, welche durch TASP1 aktiviert wird) sind bereits mit monogenen Syndromen verknüpft worden (Wiedemann-Steiner-Syndrom, OMIM® #605130).[45]

Die obige Publikation beschreibt sechs Individuen (darunter drei aus der Arbeit von 2019 und drei bisher nicht publizierte Individuen) und zeigt, mittels internationaler Kollaboration, die funktionelle Auswirkungen einer TASP1-Defizienz. Hierfür erfolgten u.a. Transkriptom, Proteom, Epigenom und *in-vivo*-Untersuchung an Zebrafischen.

3.1 Methoden

Die sechs Individuen wurden durch Pädiater oder Genetiker rekrutiert. Die internationale Vernetzung bzgl. *TASP1* erfolgte teilweise mittels GeneMatcher.[46] Der Fall aus dem Institut für Humangenetik der Technischen Universität München ist Individuum 5, bei dem mittels ES die homozygote Nonsense-Variante NM_017714.3:c.199C>T, p.(Arg67*) in *TASP1* priorisiert wurde. Um eine reproduzierbare, distinkte faziale Dysmorphie aus den vorhandenen Gesichtsbildern der Betroffenen zu erstellen, wurde der Algorithmus DeepGestalt verwendet (Face2Gene, FDNA Inc., USA).[47]

Western Blotting von TASP1 erfolgte aus primären Fibroblasten von Individuen 5 und 6. Fibroblasten von Individuum 5 wurden auch zur RNA-Sequenzierung und für das Proteom verwendet. Die RNA-Sequenzierung erfolgte mit dem TruSeq Stranded mRNA Sample Prep Guide auf einem NovaSeq 6000 (Illumina, USA). Die Methode OUTRIDER wurde verwendet, um eine differentielle Genexpression im Vergleich zu einer Kontrollkohorte von 269 Proben zu detektieren.[48] Für die Proteomik wurde eine quantitative Tandem-Mass-Tag-Methode angewandt (beschrieben in [49]).

Zur Untersuchung der DNA-Methylierung (Epigenomik) wurde genomische DNA aus Blut mit dem EpiTect PLUS Bisulfite Kit (Qiagen, Deutschland) behandelt und dann mit dem Illumina Infinium Human Methylation EPIC BeadChip hybridisiert (Illumina, USA), um über 850 000 CpG-Stellen zu analysieren. Die *TASP1*-Proben (Individuen 4 und 5) wurden mit alters- und geschlechtsübereinstimmenden gesunden Kontrollen (n = 65) und mit Individuen mit Kabuki-Syndrom-1 (n = 5) mit einer heterozygoten Variante in *KMT2D* (kodiert für eine Histonmethyltransferase) verglichen.

tasp1 wurde mittels CRISPR (clustered regularly interspaced short palindromic repeats) /Cas9 in Zebrafischen ausgeknockt. Homozygote Larven wurden kryosektioniert zur weiteren histologischen Untersuchung.

3.2 Ergebnisse

3.2.1 Phänotypische und genotypische Informationen

Die sechs Individuen stammten aus fünf nicht verwandten Familien und tragen alle bialllelische (angenommene) Loss-of-function-Varianten in *TASP1*. Das Alter lag zwischen 9 Monaten und 10 Jahren. Alle Betroffenen hatten eine Entwicklungsverzögerung mit schwerer Sprachentwicklungsverzögerung (nur wenige Wörter konnten gesprochen werden) und motorischer Entwicklungsverzögerung (das Gehen wurde im Alter zwischen zwei und vier Jahren erlernt), Muskelhypotonie und Mikrozephalie. Auffällig war ein freundliches Auftreten.

Die Betroffenen hatten typische faziale Dysmorphien mit bauschigen und gebogenen Augenbrauen, fülligen Augenlidern, Synophrys, Epikanthus, einem breiten Nasenrücken, einer breiten Mundöffnung mit langem Philtrum, dünner Ober- und dicker Unterlippe, und niedrigsitzenden, dysplastischen Ohren (siehe Abbildung 6A – I, inklusive Stammbäume). Es konnte eine spezifische faziale Gestalt durch den Algorithmus DeepGestalt etabliert werden (Abbildung 6K).

Angeborene Fehlbildungen umfassten Gehirnfehlbildungen (v.a. Malformationen der Fossa posterior), kardiovaskuläre Fehlbildungen [Vorhof- (Atriumseptumdefekt, ASD) und Ventrikelseptumdefekt (VSD), Fallot'sche Tetralogie] und auch eine linksseitige Hydronephrose bei Individuum 4. Die Phänotypen und Genotypen der einzelnen Individuen sind in Tabelle 2 gezeigt, Abbildung 6L zeigt die Verteilung der Varianten im Gen bzw. Protein.

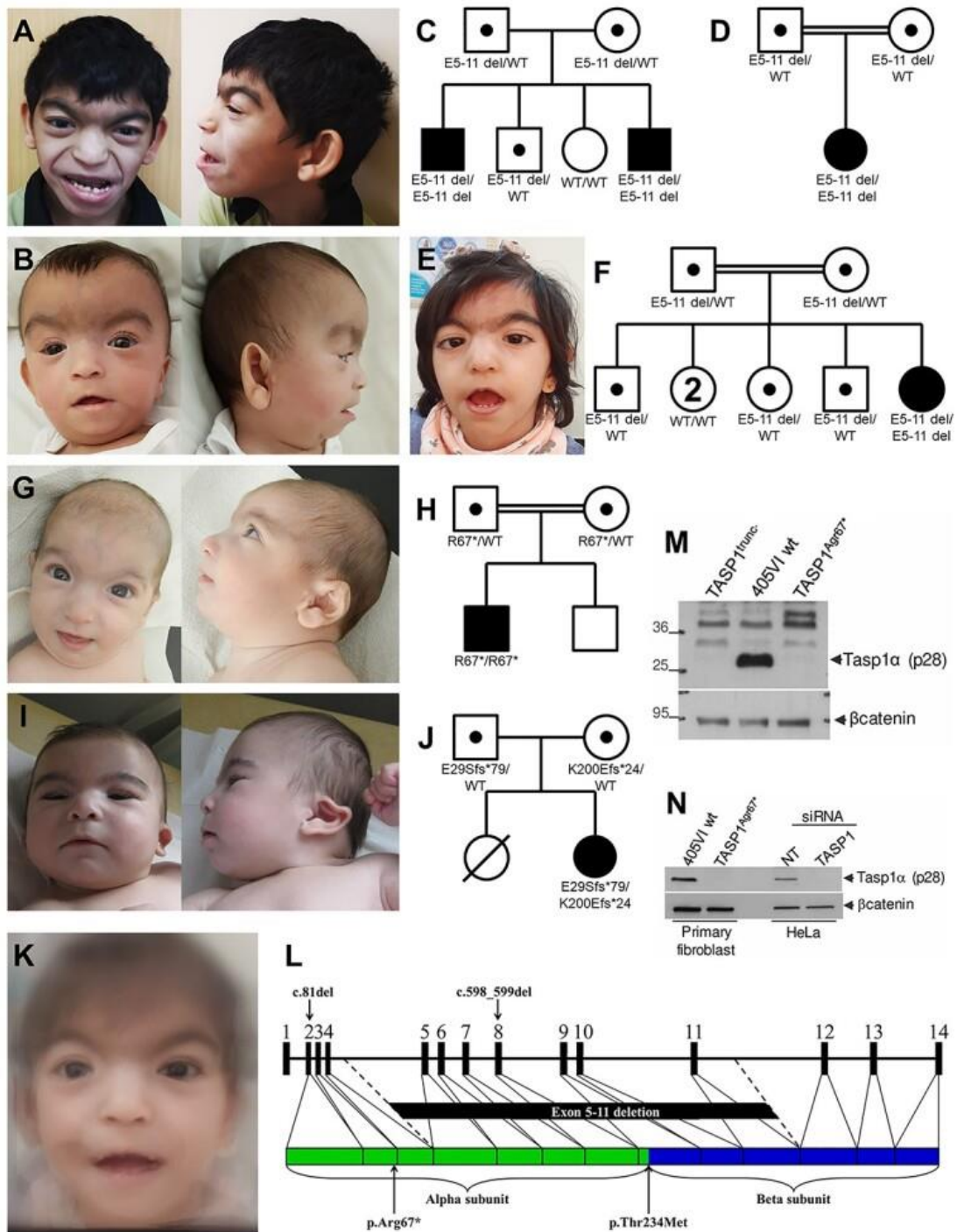**Abbildung 6:** Fotografien der Betroffenen mit Stammbäumen und Genotypen (A – J), durch DeepGestalt[47] zusammengesetztes Gesichtsbild (K), Ergebnisse der Western Blots mit TASP1-Defizienz (Alpha-Untereinheit p28; M und N), schematisches Bild des Gens *TASP1* (NM_017714.3) und des Proteins TASP1 (NP_060184.2) mit identifizierten Varianten (L). WT/wt, Wildtyp. Details siehe Ergebnisse. Aus [50].

Individual	1	2	3	4	5	6	Case 3[a]	
Gender	Male	Male	Female	Female	Male	Female	Male	
Ethnicity	Arabian Peninsula	Arabian Peninsula	Arabian Peninsula	Arabian Peninsula	Turkish	North Africa	Arabian Peninsula	
Age	7 years	9 months	19 months	3 years	6 years	10 years	3 years	
TASP1 allele 1	Exon 5–11 deletion	Exon 5–11 deletion	Exon 5–11 deletion	Exon 5–11 deletion	c.199C > T p.(Arg67*)	c.81del p.(Glu29Serfs*79)	c.701C > T p.(Thr234Met)	
TASP1 allele 2	Exon 5–11 deletion	Exon 5–11 deletion	Exon 5–11 deletion	Exon 5–11 deletion	c.199C > T p.(Arg67*)	c.(598_599del) p.(Lys200Glufs*24)	c.701C > T p.(Thr234Met)	
Neurodevelopment								
Developmental delay	+	+	+	+	+	+	+	7/7
Hypotonia	+	+	+	+	+	−	+	6/7
Microcephaly	+	−	+	+	+	+	+	6/7
Seizures	−	−	−	−	+	−	+	2/7
Posterior fossa malformation	−	+	+	−	+	+	−	4/7
Dilated ventricles	−	+	−	−	+	+	+	4/7
Feeding and growth								
Feeding difficulties	+	+	+	+	+	+	+	7/7
Salivary drooling	+	−	+	+	−	−	+	4/7
Failure to thrive	+	+	+	+	−	−	+	5/7
Happy demeanor	+	NA (too young)	+	+	+	−	+	5/6
CVS malformation	ASD/VSD	TOF	PFO/VSD	PFO/VSD	VSD	VSD	−	6/7
Cryptorchidism	+	−	NA	NA	+	NA	+	3/4
Hirsutism	+	−	+	+	−	+	−	4/7
Recurrent respiratory infections	+	−	+	+	+	−	−	4/7
Preauricular skin tag	−	+	+	+	+	−	−	4/7
Single palmar crease	+	−	−	+	+	−	−	3/7
Facial features								
Prominent glabella	+	+	+	−	+	−	+	4/7
Excess forehead hair	+	−	+	+	+	−	−	4/7
Thick eyebrows	+	+	+	+	+	+	+	7/7
Arched eyebrows	+	+	+	+	+	+	+	7/7
Synophrys	+	+	+	+	+	+	+	7/7
Epicanthus	+	+	+	+	+	+	+	7/7
Hypertelorism	+	+	+	+	+	+	+	7/7
Downslanted eyes	−	−	+	+	−	−	−	2/7
Thick eyelids	+	+	+	+	+	+	+	7/7
Periorbital fullness	+	+	+	+	+	+	+	7/7
Broad nasal bridge	+	+	+	+	+	+	+	7/7
Long smooth philtrum	+	+	+	+	−	+	+	6/7
Wide mouth	+	+	+	+	−	+	+	6/7
Thin upper lip	+	+	+	+	+	+	+	7/7
Thick lower lip	+	+	+	+	+	+	+	7/7
Microretrognathia	−	+	+	−	+	−	−	3/7
High arched palate	−	−	+	−	+	−	−	2/7
Low-set ears	+	+	+	+	+	+	+	7/7
Dysplastic ears	+	+	+	+	+	+	+	7/7
Webbed neck	+	−	+	+	−	−	−	3/7
Ophthalmologic anomalies	−	−	−	Hyperopia	Strabismus, amblyopia, pale optic disc	Hyperopia	−	
Limb deformities	Brachydactyly, clinodactyly	Overlapping toes	−	Polydactyly	−	Short extremities, brachydactyly, broad thumb and first toe	−	
Skeletal deformities	−	−	−	−	−	Scoliosis, genu recurvatum	Short stature	
Skin	−	Lumbar skin dimple	Sacral hair tuft,	Congenital dermal melanocytosis	−	−	−	
Others	Hearing impairment	−	Umbilical hernia	Left hydronephrosis	Inguinal hernia	Choanal stenosis, anteriorly placed anus, spasticity of the lower limbs	−	

Tabelle 2: Phänotypische und genotypische Informationen der beschriebenen Individuen mit Suleiman-El-Hattab-Syndrom. [a], in [43] beschrieben, keine neuen phänotypischen oder funktionellen Daten. In der Tabelle und der Diskussion genannt, um alle publizierten Individuen mit Suleiman-El-Hattab-Syndrom darzustellen. ASD, Atriumseptumdefekt (Vorhofseptumdefekt); CNS, central nervous system (Zentralnervensystem); CVS, cardiovascular (kardiovaskulär); NA, not applicable (nicht zutreffend); PFO, persistierendes Foramen ovale; TOF, tetralogy of Fallot (Fallot'sche Tetralogie); VSD, Ventrikelseptumdefekt. *TASP1*-Transkript NM_017714.3, TASP1-Protein NP_060184.2. Aus [50].

3.2.2 Western Blot, RNA-Sequenzierung, Proteom, Epigenom und Zebrafisch-Knockout

Im Western Blot aus primären Fibroblasten von Individuum 5 und 6 konnte kein TASP1 im Vergleich zur Kontrolle nachgewiesen werden. Es konnte kein Unterschied in der globalen Histonmethylierung (Histon-Merkmal H3K4me3) bei Individuum 5 im Vergleich zur Kontrolle festgestellt werden. Die Spezifität des Antikörpers wurde mittels Herunterregulierung von *TASP1* durch gezielte siRNAs (small interfering RNA) in HeLa-Zellen gezeigt (Abbildung 6M und N).

In der RNA-Sequenzierung aus primären Fibroblasten von Individuum 5 zeigten sich 20 signifikant differentiell exprimierte Gene. Beachtenswert waren *GTF2A1* (adjustiertes $p = 8{,}15 \times 10^{-7}$), welches hochreguliert war (log2fc = 0,55); *HOXA4* (adjustiertes $p = 5.02 \times 10^{-4}$; log2fc = −5,42), *HOXA7* (adjustiertes $p = 7{,}86 \times 10^{-4}$; log2fc = −5,4), *HOXB2* (adjustiertes $p = 9{,}5 \times 10^{-3}$; log2fc = −1,8) und *HOXA1* (adjustiertes $p = 0{,}0312$, log2fc = 5,15), welche alle herunterreguliert waren. TASP1 konnte in der Proteomik nicht detektiert werden, ansonsten ergaben sich 13 signifikant aberrante Proteinlevel, darunter GTF2A2, welches hochreguliert war (adjustiertes $p = 0{,}001770059$; log2fc = 1,74).

Eine spezifische epigenetische Signatur für das Suleiman-El-Hattab-Syndrom konnte mit DNA-Proben von nur zwei Individuen (4 und 5) nicht etabliert werden. Im Vergleich zu Proben von Individuen mit Kabuki-Syndrom-1 zeigte sich ein DNA-Methylierungsprofil, das zwischen demjenigen von Kabuki-Syndrom-1-Fällen und gesunden Kontrollen liegt (Abbildung 7).
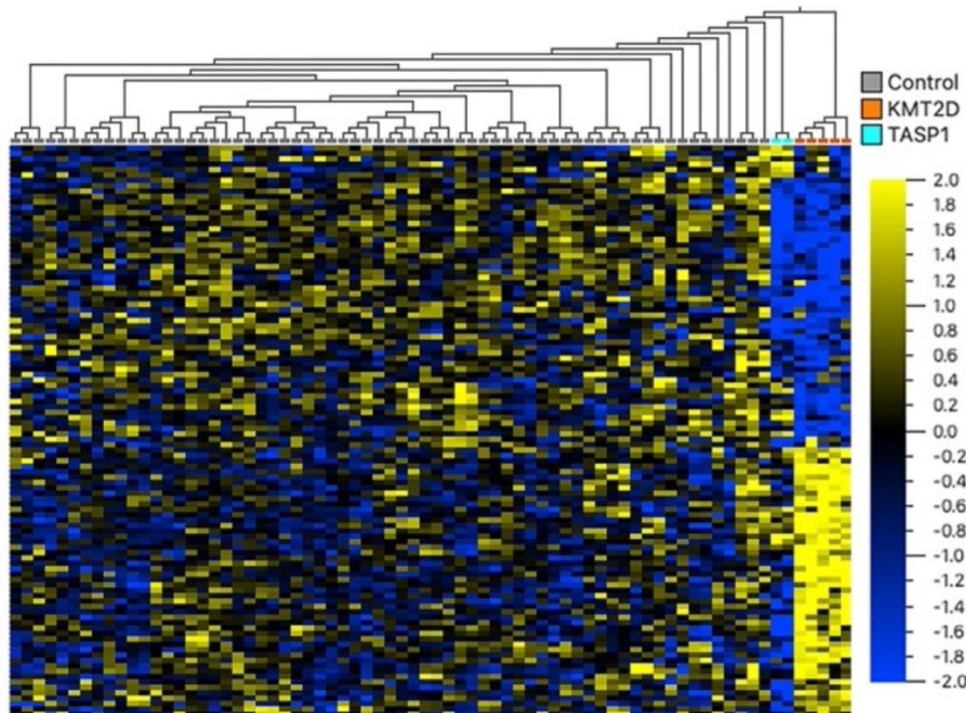
Abbildung 7: Hierarchische Gruppierung der DNA-Methylierungsprofile für gesunde Kontrollen (Control), Individuen mit Kabuki-Syndrom-1 (KMT2D) und Individuen mit Suleiman-El-Hattab-Syndrom (TASP1). Die Farbgraduierung erfolgte nach den normalisierten β-Werten[51] der untersuchten DNA-Methylierungs-Loci [von −2,0 (blau) bis +2.0 (gelb)]. Aus [50].

In den homozygoten Zebrafisch-*tasp1*-Knockouts konnte u.a. eine kleinere Gehirngröße im Vergleich zum Wildtyp (15.596 µm^2 vs. 14.747 µm^2) und auch kraniofaziale Veränderungen festgestellt werden.

3.3 Diskussion und Zusammenfassung

In dieser Arbeit wurde die bisher größte Kohorte von Individuen mit Suleiman-El-Hattab-Syndrom auf phänotypischer, genotypischer und funktioneller Ebene beschrieben. Insgesamt wurden 6 Individuen mit biallelischen Loss-of-function-Varianten eingeschlossen (plus Fall 3 aus [43]. Ohne neue Daten; genannt, um alle publizierten Individuen mit Suleiman-El-Hattab-Syndrom darzustellen). Die Individuen hatten einen überlappenden Phänotyp u.a. mit globaler Entwicklungsverzögerung (7/7), Mikrozephalie (6/7), Hirnfehlbildungen (4/7), muskulärer Hypotonie (6/7) und kardiovaskulären Fehlbildungen wie ASD/VSD (6/7;

Individuum 2 mit Fallot'scher Tetralogie; Tabelle 2). Es zeigte sich auch eine distinkte faziale Gestalt, was durch einen Algorithmus (DeepGestalt) bestätigt wurde (Abbildung 6K).

TASP1 kodiert für die Endopeptidase Taspase 1 (TASP1), ein Proenzym, das autokatalytisch in zwei Untereinheiten (Alpha und Beta, Abbildung 6L) gespalten wird, welche wiederum das aktive Heterodimer bilden. Heterodimerisiertes TASP1 spaltet verschiedene Proteine im Zellkern, darunter Histonmethyltransferasen der KMT2-Proteinfamilie wie z.B. KMT2A und KMT2B, welche dadurch aktiviert werden. Die Spaltung von KMT2A ist u.a. entscheidend für die Expression von *HOX*-Genen, welche für Transkriptionsfaktoren kodieren.[44,52] Passend dazu zeigte sich in der RNA-Sequenzierung von Individuum 5, welches eine homozygote Nonsense-Variante in *TASP1* trägt und daher kein TASP1 exprimiert (siehe Western Blot in Abbildung 6M und N), eine signifikante Herunterregulation der *HOX*-Gene *HOXA4*, *HOXA7*, *HOXA1* and *HOXB2*. Die koordinierte *HOX*-Expression ist zentral für eine normale Körperentwicklung und eine Störung derselbigen könnte die Fehlbildungen bei TASP1-defizienten Individuen erklären.[53]

Ein weiteres Substrat von TASP1 ist der Transkriptionsfaktor TFIIAα−β (*GTF2A1)*, welcher ubiquitär exprimiert wird und ebenfalls aus einer Alpha- und Beta-Untereinheit besteht. TFIIAα−β ist an TFIIAγ (*GTF2A2*) gebunden. Bei Spaltung des Heterotrimers TFIIAα/β/γ (kodiert durch *GTF2A1* und *GTF2A2*, als TFIIA zusammengefasst) durch TASP1, wird dieses Heterotrimer durch das Proteasom abgebaut und dadurch deaktiviert.[44,54] Der regelhafte Umsatz von TFIIA ist wichtig für eine korrekte Embryonalentwicklung.[55] Interessanterweise ist in der RNA-Sequenzierung bei Individuum 5 *GTF2A1* (kodiert für TFIIAα−β) hochreguliert, in der Proteom-Untersuchung ist wiederum *GTF2A2* (kodiert TFIIAγ) herunterreguliert. Also könnte der Phänotyp der Betroffenen auch durch eine TFIIA-Dysregulation erklärt werden.

TASP1 spaltet und aktiviert Histonmethyltransferasen der KMT2-Proteinfamilie. Passenderweise haben Individuen mit Defekten in *KMT2*-Genen mit dem Suleiman-El-Hattab-Syndrom überlappende Phänotypen. Darunter sind z.B. das Wiedemann–Steiner-Syndrom (OMIM® #605130) mit Haploinsuffizienz in *KMT2A* oder das Kabuki-Syndrom-1 (OMIM® #147920) mit Haploinsuffizienz in *KMT2D* zu nennen.[45,56] Aufgrund des damit einhergehenden Einflusses von TASP1 auf die DNA-Methylierung wurde in dieser Arbeit auch untersucht, ob ein spezifisches DNA-Methylierungsmuster, eine sogenannte

26

„epigenetische Signatur", bei Individuen mit TASP1-Defizienz vorliegt.[57] Leider war die Anzahl von nur zwei Proben (Individuum 4 und 5) zu gering, um eine Signatur zu etablieren. Dennoch konnte nachgewiesen werden, dass es eine unterscheidbare Signatur in der Blut-DNA von Individuum 4 und 5 gibt, in der Mitte zwischen Kontrollen und der Signatur des Kabuki-Syndrom-1 (Abbildung 7). Das Suleiman-El-Hattab-Syndrom kann daher in die Gruppe der Krankheiten mit Histonmethylierungsdefekt eingegliedert werden.[58]

Zuletzt konnten *in-vivo*-Studien an Zebrafischen mit *tasp1*-Knockout einen Teil des Phänotyps beim Menschen bestätigen (Mikrozephalie und kraniofaziale Auffälligkeiten).

Zusammenfassend konnte in dieser Arbeit durch Multi-Omics (Transkriptom, Proteom, Epigenom) und *in-vivo*-Untersuchungen umfassend das Gen *TASP1* funktionell charakterisiert werden und der Phänotyp und Genotyp des Suleiman-El-Hattab-Syndroms an der bisher größten Kohorte dargestellt werden.

4. Exom-Sequenzierung bei angeborenen Nieren- und Harnwegsfehlbildungen (CAKUT) – höhere Diagnoserate bei beidseitiger Nierenbeteiligung

Dieses Kapitel bezieht sich auf die folgende Originalarbeit:

- **Riedhammer KM**, Ćomić J, Tasic V, Putnik J, Abazi-Emini N, Paripovic A, Stajic N, Meitinger T, Nushi-Stavileci V, Berutti R, Braunisch MC, Hoefele J. Exome sequencing in individuals with congenital anomalies of the kidney and urinary tract (CAKUT): a single-center experience. *Eur J Hum Genet.* 2023 Jun;31(6):674-680. doi: 10.1038/s41431-023-01331-x. Epub 2023 Mar 16. PMID: 36922632; PMCID: PMC10250376.

Patienten mit angeborenen Nieren- und Harnwegsfehlbildungen (CAKUT) haben ein sehr breites Krankheitsspektrum, welches von „milderen" Verläufen wie vesikoureteralem Reflux bis hin zur Maximalvariante, der beidseitigen Nierenagenesie, reicht. CAKUT kann zudem isoliert, also nur die Nieren und die Harnwege betreffend, oder als Teil eines Syndroms mit einer oder mehreren extrarenalen Manifestationen auftreten. CAKUT ist hauptsächlich ein multifaktorielles Krankheitsbild, das durch genetische, epigenetische und Umwelteinflüsse verursacht werden kann. Es sind jedoch bereits über 50 Gene mit erblichem CAKUT verknüpft worden und Mausmodelle legen eine noch größere Zahl an monogenem CAKUT nahe. Auch Kopienzahlvarianten (copy number variants, CNVs) spielen eine bedeutende Rolle in der Entstehung von CAKUT.[59] Die Diagnoseraten für monogenes CAKUT sind nichtsdestotrotz gering mit ca. 16%, schwankend je nach eingeschlossener Kohorte zwischen 6 und 33%.[60-62]

Die nun besprochene Arbeit hat ihren Ausgangspunkt erneut in der nephrogenetischen Praxis: Trotz der insgesamt geringen Diagnoserate für monogenes CAKUT beobachtete man, dass diese bei „schwereren" Phänotypen wie z.B. beidseitiger

Nierenbeteiligung oder syndromaler Krankheit höher ist. Dies sollte nun systematisch an allen in der „NephroGen-Studie" mit ES untersuchten CAKUT-Index-Fällen überprüft werden.

4.1 Methoden, Studiendesign und -population

In diese retrospektive Studie wurden 86 Index-Individuen, die im Rahmen der „NephroGen-Studie" am Institut für Humangenetik des Klinikums rechts der Isar der Technischen Universität München zwischen Oktober 2015 und Februar 2019 rekrutiert wurden, inkludiert. Alle eingeschlossenen Individuen hatten CAKUT und wurden mit ES molekulargenetisch analysiert. Die priorisierten Varianten wurden mit den Kriterien des ACMG und aktuellen Erweiterungen bewertet.[40,63-65] Der Phänotyp wurde durch die Arztbriefe und einen standardisierten Fragebogen erfasst.

Die Fälle wurden verschiedenen Gruppen nach einem zweistufigen Verfahren zugewiesen. Als erstes erfolgte eine Einstufung nach CAKUT-Phänotyp (nach [59]): Gruppe I: Doppelung von Ureter oder Nierenbecken/Doppelniere. Gruppe II: Ektopie der Niere und/oder Hufeisenniere. Gruppe III: Anderweitige Nierenfehlbildung. Gruppe IV: Obstruktive Uropathie. Gruppe V: Vesikoureteraler Reflux. Gruppe VI: Posteriore Urethralklappen. Gruppe VII: Anderweitige Fehlbildungen der Harnwege.

Als zweites erfolgte eine Einteilung nach einem breiteren phänotypischen Spektrum, welches die Schwere des CAKUT-Phänotyps beleuchtet:
Gruppe I: Beidseitige Nierenbeteiligung (jeder Fall, der eine beidseitige Nierenbeteiligung jedweder Schwere hatte, wurde hier eingruppiert). Gruppe II: Einseitige Nierenbeteiligung (inklusive einseitige Nierenektopie und Hufeisenniere). Gruppe III: Isolierte Harntransportstörung (ohne bekannte parenchymatöse Nierenbeteiligung).

Abbildung 8 zeigt die Aufteilung der Kohorte auf die verschiedenen phänotypischen Gruppen.
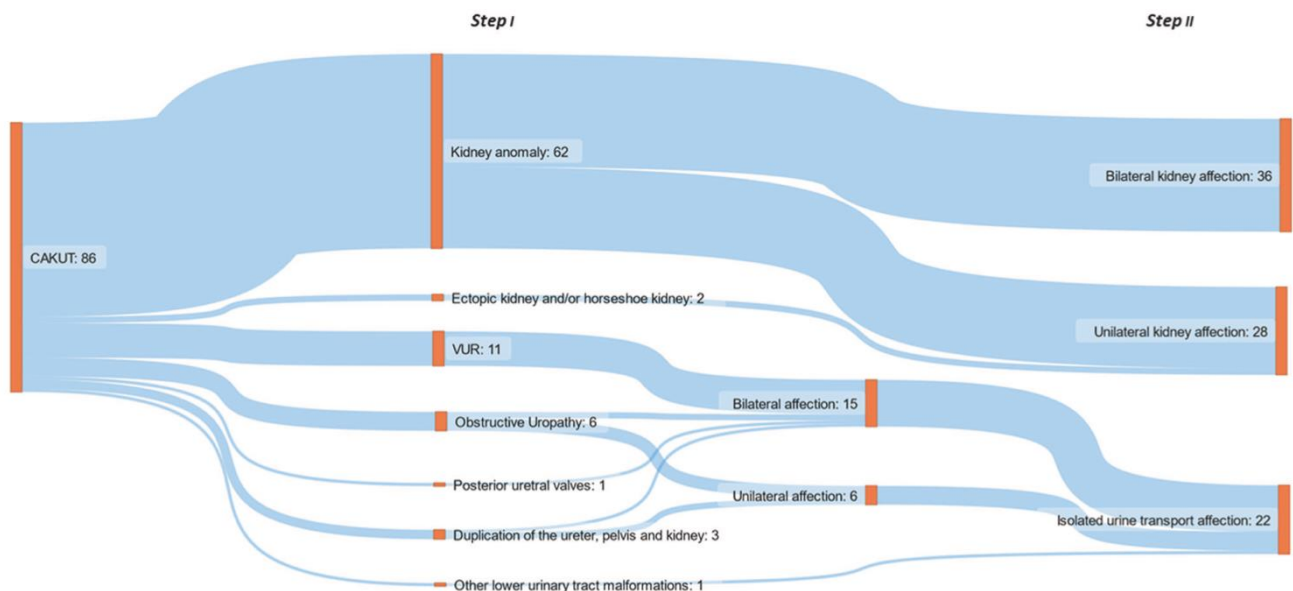
Abbildung 8: Überblick über die Kohorte, eingeteilt nach einem zweistufigen Verfahren (siehe Methoden). CAKUT, congenital anomalies of the kidney and urinary tract (angeborene Nieren- und Harnwegsfehlbildungen); VUR, vesikoureteraler Reflux. Aus [66].

4.2 Ergebnisse

Bzgl. der Schwere des CAKUT-Phänotyps zeigte sich, dass 42% (36/86) der Fälle eine beidseitige Nierenbeteiligung hatten, 32% (28/86) eine einseitige Nierenbeteiligung und 26% (22/86) eine isolierte Harntransportstörung (Abbildung 8). Tabelle 3 fasst die klinischen Parameter zusammen.

Clinical characteristics	Total cohort (n = 86 index cases)
Sex	
Female	29 (34%)
Male	57 (66%)
Non-Finnish European descent	
Yes	74 (86%)
No	12 (14%)
Reported family history regarding CAKUT	Familial CAKUT
Yes	15 (17%)
No	71 (83%)
Reported parental consanguinity	
Yes	7 (8%)
No	79 (92%)
Syndromic CAKUT	
Yes	33 (38%)
No	53 (62%)
Syndromic features	
Skeletal malformations	9 (27%)
Eye anomalies	3 (9%)
Hearing impairment	3 (9%)
Intellectual disability	6 (18%)
Heart defect	6 (18%)
Complex CAKUT	
Yes	24 (30%)
No	62 (72%)
CAKUT phenotype	
Bilateral kidney affection	36 (42%)
Unilateral kidney affection	28 (33%)
Isolated urine transport affection	22 (25%)
Solved cases*	
Yes	8 (9%)
No	78 (91%)

Tabelle 3: Klinische Informationen zu den 86 Index-Fällen der Kohorte. *„Solved cases" (gelöste Fälle) sind solche, bei denen eine genetische Diagnose durch Exom-Sequenzierung gestellt werden konnte. CAKUT, congenital anomalies of the kidney and urinary tract (angeborene Nieren- und Harnwegsfehlbildungen). Aus [66].

Eine genetische Diagnose konnte in 9% (8/86) der Fälle gestellt werden. Alle gelösten Fälle hatten eine bilaterale Nierenbeteiligung (Diagnoserate in dieser Gruppe: 22%, 8/36; Abbildung 9). In den anderen Gruppen nach phänotypischer Schwere („einseitige Nierenbeteiligung" und „isolierte Harntransportstörung") konnte kein einziger Fall molekulargenetisch gelöst werden. 75% (6/8) der gelösten Fälle hatten extrarenale Manifestationen (syndromales CAKUT).
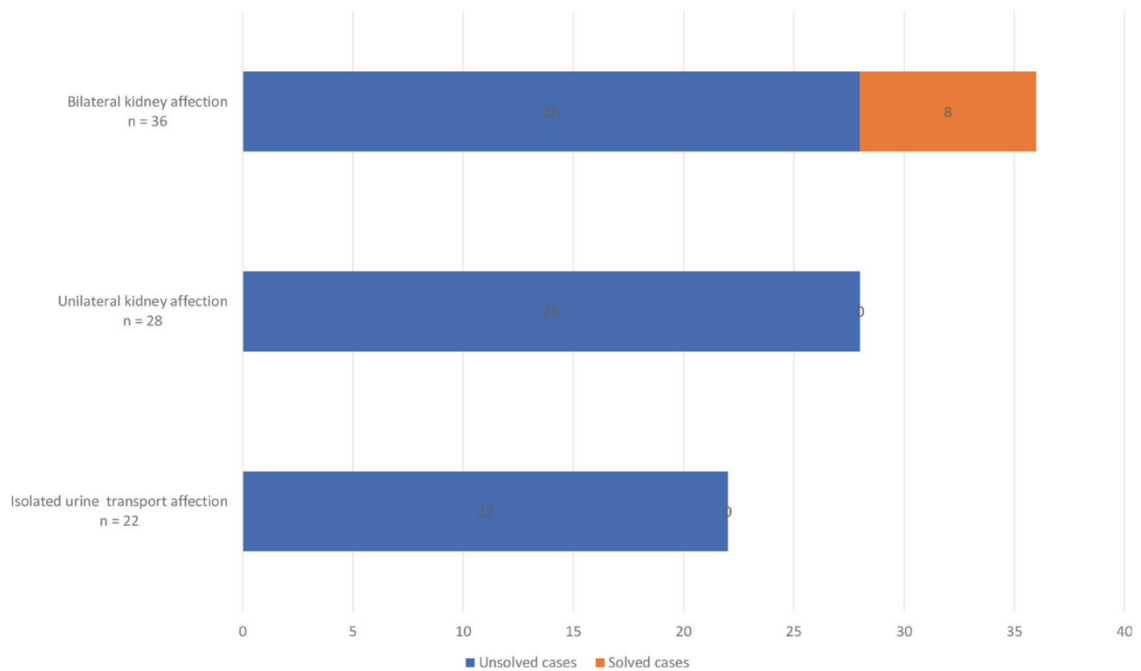
Abbildung 9: Verteilung der ungelösten und gelösten Fälle [„Unsolved cases" (blau) und „Solved cases" (orange)] auf die phänotypischen Kategorien „Bilateral kidney affection" (beidseitige Nierenbeteiligung), „Unilateral kidney affection" (einseitige Nierenbeteiligung) und „Isolated urine transport affection" (isolierte Harntransportstörung). Aus [66].

Von den acht gelösten Fällen waren zwei mit krankheitsverursachenden Varianten in *PBX1* (Krankheit „CAKUTHED", OMIM® #617641), zwei mit Varianten in *SALL1* (Townes-Brocks-Syndrom-1, OMIM® #107480), zwei mit Varianten in *EYA1* (Branchiootorenales Syndrom 1, OMIM® # 113650), einer mit einer Variante in *PAX2* (Papillorenales Syndrom, OMIM® #120330) und einer mit einer 17q12-Deletion (OMIM® #614527), das CAKUT-Gen *HNF1B* inkludierend. 63% (5/8) der Varianten waren noch nicht in der Literatur beschrieben. Genaue genotypische und phänotypische Informationen können in der Originalpublikation nachgelesen werden.

4.3 Diskussion und Zusammenfassung

Die Diagnoserate lag mit 9% im Bereich bekannter Werte für CAKUT-Kohorten.[62] Interessanterweise hatten alle acht gelösten Fälle eine beidseitige Nierenaffektion (Diagnoserate von 22% in dieser Subgruppe). In einer Studie aus 2018 hatten Fälle mit „schwerem CAKUT" (Nierendysplasie oder -agenesie) eine Diagnoserate von 17% im Vergleich zu 13% in der Gesamtkohorte mit 232 Index-Individuen.[67] Die Studie differenzierte jedoch nicht zwischen unilateraler und bilateraler Nierenbeteiligung.

Alle acht gelösten Fälle waren autosomal-dominante Krankheiten des CAKUT-Spektrums. Alle betroffenen Gene/chromosomalen Bereiche (*EYA1*, 17q12-Deletion/*HNF1B*, *PAX2*, *PBX1*, *SALL1*) sind mit syndromalen Krankheitsbildern verknüpft, jedoch zeigten nur 6/8 (75%) der Betroffenen eine extrarenale Manifestation. Auch ein „Reverse Phenotyping" nach genetischer Diagnose konnte in den beiden Fällen mit heterozygoter krankheitsverursachender Deletion in 17q12 (inklusive *HNF1B*) und Variante in *PAX2* keinen syndromalen Phänotyp erkennen lassen. Dabei sind *HNF1B* und *PAX2* die Gene, die am häufigsten mit syndromalem autosomal-dominanten CAKUT verknüpft sind (5 – 15% der Fälle).[68] Es kann aber nicht ausgeschlossen werden, dass subtile extrarenale Manifestationen übersehen wurden, zudem sind manche Manifestationen auch altersabhängig (wie z.B. „Maturity-onset diabetes of the young" und neuropsychiatrische Auffälligkeiten beim 17q12-Deletionssyndrom).[68]

Zusammenfassend zeigte die Studie, dass monogene Formen bei „schweren" CAKUT-Phänotypen wie beidseitiger Nierenbeteiligung und extrarenalen Manifestationen zu beachten sind und eine genetische Testung rechtfertigen. Außerdem können sich eigentlich syndromale monogene CAKUT-Krankheiten aufgrund variabler Expressivität auch ohne klar ersichtliche extrarenale Manifestationen präsentieren. Die beschriebenen Beobachtungen sollten in größeren Studien überprüft werden, um idealerweise einen klinisch erhebbaren Score zu entwickeln, wann eine genetische Testung bei CAKUT sinnvoll ist.

5. *FOXD2* – ein neues krankheitsassoziiertes Gen für syndromale angeborene Nieren- und Harnwegsfehlbildungen (CAKUT)

Dieses Kapitel bezieht sich auf die folgende Originalarbeit:

- **Riedhammer KM**, Nguyen TT, Koşukcu C, Calzada-Wack J, Li Y, Assia Batzir N, Saygılı S, Wimmers V, Kim GJ, Chrysanthou M, Bakey Z, Sofrin-Drucker E, Kraiger M, Sanz-Moreno A, Amarie OV, Rathkolb B, Klein-Rodewald T, Garrett L, Hölter SM, Seisenberger C, Haug S, Schlosser P, Marschall S, Wurst W, Fuchs H, Gailus-Durner V, Wuttke M, Hrabe de Angelis M, Ćomić J, Akgün Doğan Ö, Özlük Y, Taşdemir M, Ağbaş A, Canpolat N, Orenstein N, Çalışkan S, Weber RG, Bergmann C, Jeanpierre C, Saunier S, Lim TY, Hildebrandt F, Alhaddad B, Basel-Salmon L, Borovitz Y, Wu K, Antony D, Matschkal J, Schaaf CW, Renders L, Schmaderer C, Rogg M, Schell C, Meitinger T, Heemann U, Köttgen A, Arnold SJ, Ozaltin F, Schmidts M, Hoefele J. Implication of transcription factor FOXD2 dysfunction in syndromic congenital anomalies of the kidney and urinary tract (CAKUT). Kidney Int. 2024 Apr;105(4):844-864. doi: 10.1016/j.kint.2023.11.032. Epub 2023 Dec 26. PMID: 38154558; PMCID: PMC10957342.

Wie im vorherigen Kapitel besprochen, ist die Diagnoserate bei klinischem Verdacht auf monogenes CAKUT mit ca. 16% gering, aber Knockout-Mausmodelle legen weit mehr monogene Formen nahe.[60,61] Die folgend zusammengefasste Arbeit zeigt die funktionelle Charakterisierung eines neuen krankheitsassoziierten Gens, *FOXD2*, für autosomal-rezessives, syndromales CAKUT. In drei konsanguinen Familien mit Index-Individuen mit syndromalem CAKUT wurden homozygote seltene Varianten in *FOXD2* priorisiert (eine Frameshift-, zwei Missense-Varianten). *FOXD2* (auch *FKHL17*, *FREAC9*, *MF-2*) gehört zur „forkhead box"-Genfamilie (*FOX*) und kodiert für einen Transkriptionsfaktor. Bereits in einer Publikation aus dem Jahr 2000 wurde gezeigt, dass ein Knockout von *Foxd2* in Mäusen zu CAKUT (Nierenhypoplasie, Hydroureter) mit reduzierter Penetranz von ca. 40% führt.[69]

Es erfolgte, im Rahmen einer internationalen Kollaboration, eine funktionelle Charakterisierung des Gens, sowohl *in vitro* mit RNA-Sequenzierung an metanephrischen-Mesenchym-*Foxd2*-Knockout-Zellen und *in vivo* an *Foxd2*-Knockout-Mäusen. Weiterhin legten Daten aus GWAS nahe, dass der *FOXD2*-Locus (1p33) eine Rolle bei der Albuminurie durch Aufrechterhaltung der Podozytenintegrität im Erwachsenenalter spielt, was eine Verknüpfung zwischen monogenen und multifaktoriellen Phänotypen darstellt.

5.1 Methoden

Das Index-Individuum aus Familie 1, eine konsanguinen Familie von der Arabischen Halbinsel, wurde in der Abteilung für Nephrologie am Klinikum rechts der Isar der Technischen Universität München vorgestellt (Leiter: Prof. Dr. Uwe Heemann). Aufgrund des syndromalen CAKUT (beidseitige Nierenhypoplasie, faziale Dysmorphien, Verhaltensauffälligkeiten; siehe Ergebnisse) wurde es in die „NephroGen"-Studie am Institut für Humangenetik des Klinikums rechts der Isar der Technischen Universität München eingeschlossen und mittels ES untersucht. Da keine krankheitsverursachenden Varianten in bekannten krankheitsassoziierten Genen identifiziert werden konnten, erfolgte eine Auswertung auf wissenschaftlicher Basis. Dabei wurde die homozygote Variante NM_004474.4:c.789dup, p.(Gly264Argfs*228), eine Frameshift-Variante, in *FOXD2* priorisiert, da ein *Foxd2*-Knockout in Mäusen bereits mit CAKUT verknüpft worden war.[69] Die Variante ist nicht in der Kontrolldatenbank gnomAD (Genome Aggregation Database, v.2.1.1) gelistet.[70]

Das Index-Individuum aus Familie 2, eine konsanguine Familie aus der Türkei, mit der homozygoten Missense-Variante NM_004474.4:c.628A>G, p.(Met210Val) in *FOXD2*, wurde über GeneMatcher vermittelt.[46] Auch hier wurde die Variante mittels ES priorisiert und ist nicht in gnomAD gelistet. Krankheitsverursachende Varianten in bekannten krankheitsassoziierten Genen konnten ebenfalls nicht nachgewiesen werden.

Das Index-Individuum aus Familie 3, eine konsanguinen Familie aus Israel, trug die homozygote Missense-Variante NM_004474.4:c.629T>G, p.(Met210Arg) in *FOXD2*, welche das gleiche Codon wie in Familie 2 betrifft. Diese Variante wurde ebenfalls

mittels ES priorisiert und ist nicht in gnomAD gelistet. Krankheitsverursachende Varianten in bekannten krankheitsassoziierten Genen konnten auch hier nicht nachgewiesen werden. Die verantwortliche Arbeitsgruppe kontaktierte uns als Reaktion auf den Pre-Print unser Studie an Familie 1 und 2, welcher auf medRxiv hochgeladen worden war.[71]

Die Auswirkungen der beiden Missense-Varianten p.(Met210Val) und p.(Met210Arg) wurde *in silico* modelliert.

Da der bisher beschriebene Phänotyp aus *Foxd2*-Knockout-Mäusen auf die Niere beschränkt war[69], erfolgte mittels CRISPR/Cas9 ein erneuter Knockout von *Foxd2* in Mäusen, und es wurde eine umfassende, systematisierte Phänotypisierung durchgeführt. Diese wurde durch die German Mouse Clinic am Helmholtz Zentrum München in Neuherberg ausgeführt.

Um die Folgen eines *Foxd2*-Knockouts auf Nierenzellebene zu untersuchen, wurden mittels CRISPR/Cas9 murine metanephrische *Foxd2*-Knockout-Mesenchymzellen (mk4-Zellen) erstellt und 3D-Zellkulturen, eine RNA-Sequenzierung und Western Blots angefertigt. Dies erfolgte in den Laboren von Dr. Miriam Schmidts in Nijmegen, Niederlande, und Freiburg im Breisgau.

Da der *FOXD2*-Locus (1p33) in GWAS-Metaanalysen mit Albuminurie verknüpft worden war, erfolgte, in Zusammenarbeit mit der Arbeitsgruppe von Prof. Dr. Anna Köttgen, Freiburg im Breisgau, aus vorhandenen UK-Biobank-Daten (436.392 Individuen) noch ein Locus-Fine-Mapping, um die Varianten (single nucleotide polymorphisms, SNPs) im *FOXD2*-Locus zu identifizieren, die ursächlich für die Albuminurie-Assoziation sind.

5.2 Ergebnisse

5.2.1 Phänotypische Informationen

Das Index-Individuum (VI-3 in Abbildung 10a) aus der konsanguinen Familie 1 (Arabische Halbinsel) hatte faziale Dysmorphien (niedrig-sitzende Ohren, Hypertelorismus, abfallende Lidspalten und eine Retrognathie), eine Entwicklungsverzögerung (besuchte eine Förderschule) und eine angeborene, beidseitige Nierenhypoplasie (Abbildung 10d). Mit sieben Jahren hatte er eine CKD G4A3 mit einer errechneten GFR (glomeruläre Filtrationsrate) von 26 ml/min/1,73 m^2 (modifizierte Schwartz-Formel[72]) und einer Proteinurie von 2,7 g/24 h. Mit elf Jahren wurde er nierentransplantiert. Zwei Cousins und eine Cousine zweiten Grades (V-13, V-14 und V-19 in Abbildung 10a) waren ähnlich betroffen. Die Cousine zweiten Grades (V-19) hatte ebenfalls eine beidseitige Nierenhypoplasie, eine Entwicklungsverzögerung und eine Retrognathie. Im Alter von sieben Jahren hatte sie eine CKD G5A3 mit einer errechneten GFR von 11 ml/min/1,73 m^2 und einer Proteinurie von 5,0 g/24 h, woraufhin sie im gleichen Jahr nierentransplantiert wurde.

Das Index-Individuum (II-1 in Abbildung 10b) aus der konsanguinen Familie 2 (Türkei) erhielt mit sechs Jahren eine präemptive Nierentransplantation (Lebendspende durch den Vater). Sie hatte ebenfalls eine beidseitige kongenitale Nierenhypoplasie mit fazialen Dysmorphien (u.a. Retrognathie, Abbildung 10e und f). Ihre Schwester (II-2) entwickelte im Alter von sieben Jahren eine persistierende Proteinurie bei unauffälliger Nierenfunktion (errechnete GFR 138 ml/min/1,73 m^2). Im Ultraschall zeigte sich eine linksseitige Nierenhypoplasie bei beidseitig erhöhter Echogenität im Nierenparenchym. In der ebenfalls durchgeführten Nierenbiopsie fand sich eine FSGS (Abbildung 10i). Auch sie hatte faziale Dysmorphien, u.a. eine Retrognathie (Abbildung 10g und h). Mit 17 Jahren hatte sie eine CKD G3 mit einer errechneten GFR von 38 ml/min/1,73 m^2.

Beim Index-Individuum (IV-5 in Abbildung 10c) der konsanguinen Familie 3 (Israel) wurden bereits während der Schwangerschaft (35. Schwangerschaftswoche) beidseitige hypoplastische Nieren im Ultraschall diagnostiziert. Das Serumkreatinin war am dritten Lebenstag erhöht bei 1,7 mg/dl. Im Alter von zwei Jahren entwickelte die Betroffene ein nephrotisches Syndrom, welches steroidrefraktär verlief. Mit fünfeinhalb Jahren erhielt sie erstmals Peritonealdialyse, mit sieben Jahren wurde sie

nierentransplantiert. Auch sie war leicht entwicklungsverzögert und hatte faziale Dysmorphien, u.a. eine Retrognathie.

5.2.2 Genotypische Informationen

In allen drei Index-Individuen wurden seltene (nicht in gnomAD gelistete) homozygote Varianten in *FOXD2* priorisiert, nachdem die Routine-Diagnostik auf krankheitsverursachende Varianten in bekannten krankheitsassoziierten Genen unauffällig war.

Individuum VI-3 aus Familie 1 trug die homozygote Frameshift-Variante NM_004474.4:c.789dup, p.(Gly264Argfs*228) in *FOXD2*. Diese Variante führt vorhergesagt zu einem Protein mit ähnlicher Länge wie das Wildtyp-Protein, aber unterschiedlicher Aminosäurezusammensetzung, wobei die DNA-bindende Domäne von FOXD2 erhalten bleibt (NP_004465.3; Abbildung 10j). *FOXD2* ist ein Ein-Exon-Gen (NM_004474.4), und daher kann ein Nonsense-mediated decay nicht angenommen werden. Es finden sich in gnomAD (v.2.1.1) übrigens keinerlei homozygote Loss-of-function-Varianten. Die Variante segregierte in der Familie und konnte auch bei der ähnlich betroffenen Cousine zweiten Grades (V-19) mittels Sanger-Sequenzierung nachgewiesen werden.

Individuum II-1 aus Familie 2 trug die homozygote Missense-Variante NM_004474.4:c.628A>G, p.(Met210Val) in *FOXD2*. Die Variante liegt in der DNA-bindenden Domäne von FOXD2 (Abbildung 10j). Die betroffene Aminosäure Methionin ist evolutionär stark konserviert bis zum Zebrafisch (*Danio rerio*, Abbildung 10k). Die Variante konnte auch in der ähnlich betroffenen Schwester (II-2) nachgewiesen werden.

Individuum IV-5 aus Familie 3 trug die homozygote Missense-Variante NM_004474.4:c.629T>G, p.(Met210Arg). Die Variante führt zu einem Austausch der gleichen hochkonservierten Aminosäure (p.Met210) wie diejenige in Familie 2.

Beide Missense-Varianten sind in *in-silico*-Vorhersageprogrammen als schädlich (deleterious) vorhergesagt (u.a. CADD).[73] Sie haben beide in der Proteinmodellierung eine destabilisierende Wirkung (Abbildung 10l).

a
Family 1
NM_004474.4:c.789dup, p.(Gly264Argfs*228)

b
Family 2
NM_004474.4:c.628A>G, p.(Met210Val)

c
Family 3
NM_004474.4:c.629T>G, p.(Met210Arg)

j

Human FOXD2 (NP_004465.3)

p.(Met210Arg)
p.(Met210Val)
p.(Gly264Argfs*228)

DNA binding (forkhead domain)

k

H.sapiens	GKNYWTLDPESADMDNGSFLRRRKRFK
P.troglodytes	GKNYWTLDPESADMDNGSFLRRRKRFK
M.mulatta	GKNYWTLDPESADMDNGSFLRRRKRFK
C.familiaris	GKNYWTLDPESADMDNGSFLRRRKRFK
M.musculus	GKNYWTLDPESADMDNGSFLRRRKRFK
R.norvegicus	GKNYWTLDPESADMDNGSFLRRRKRFK
X.tropicalis	GKNYWTLDPESADMDNGSFLRRRKRFK
D.rerio	GKNYWTLDPESADMDNGSFLRRRKRFK

l

FOXD2: Met210 (wild type)

FOXD2: c.628A>G, p.(Met210Val)

FOXD2: c.629T>G, p.(Met210Arg)

van der Waals forces | Polar interactions | Hydrophobic interactions | Ionic bonds | Hydrogen bonds

Abbildung 10: Stammbäume der arabischen (a), türkischen (b) und der israelischen Familie (c). (d) Nierenultraschall des Index-Individuums (VI-3) aus der arabischen Familie (rechte Niere). (e – h) Gesichtsbilder der betroffenen Geschwister (II-1 und II-2) der türkischen Familie (i) Lichtmikroskopisches Bild der Nierenbiopsie von Individuum II-2 der türkischen Familie (Hämatoxylin-Eosin-Färbung) mit glomerulärer Hypertrophie, Vermehrung des Mesangiums und segmentaler Sklerose (schwarzer Pfeil). (j) Schematische Darstellung des Proteins FOXD2 mit Lage der priorisierten Varianten. (k) Illustration der evolutionären Konservierung des Methionins (M) an Position 210 in FOXD2 (erstellt mit der Clustal X software[74]). (l) Dreidimensionale Darstellung der veränderten Interaktion mit den umgebenden Aminosäuren aufgrund der jeweiligen Missense-Variante p.(Met210Val) and p.(Met210Arg) in FOXD2. Aus [75].
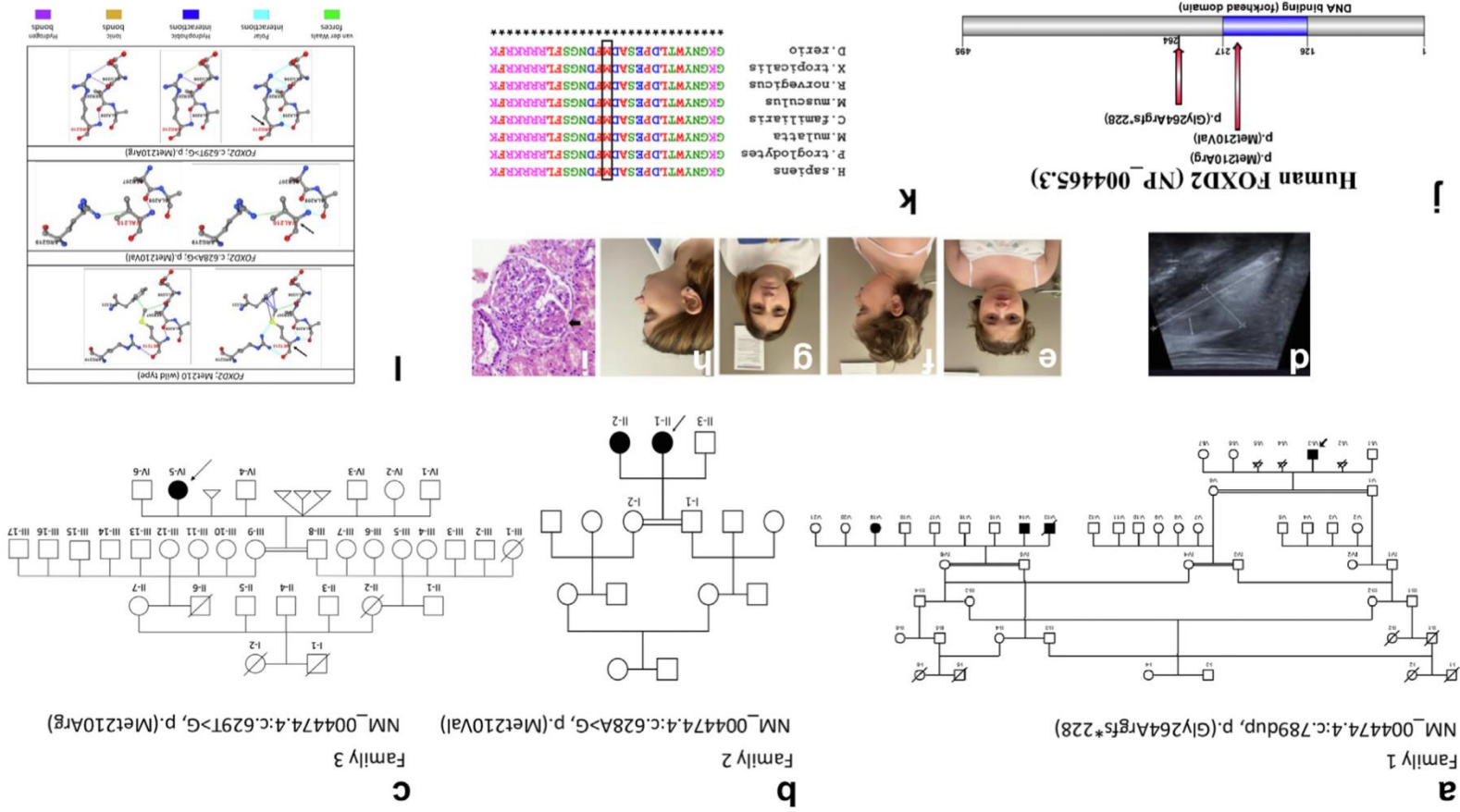
5.2.3 *Foxd2*-Knockout-Mäuse

Die mittels CRISPR/Cas9 erzeugten homozygoten *Foxd2*-Knockout-Mäuse waren überlebensfähig und wurden systematisch phänotypisiert, um neben dem renalen auch den extrarenalen Phänotyp zu untersuchen. Im Alter von 16 Wochen wurde eine Mikro-Computertomographie angefertigt, welche eine veränderte Kiefermorphologie, v.a. einen verkleinerten Unterkiefer (Mandibula), zeigte (Abbildung 11a – d).
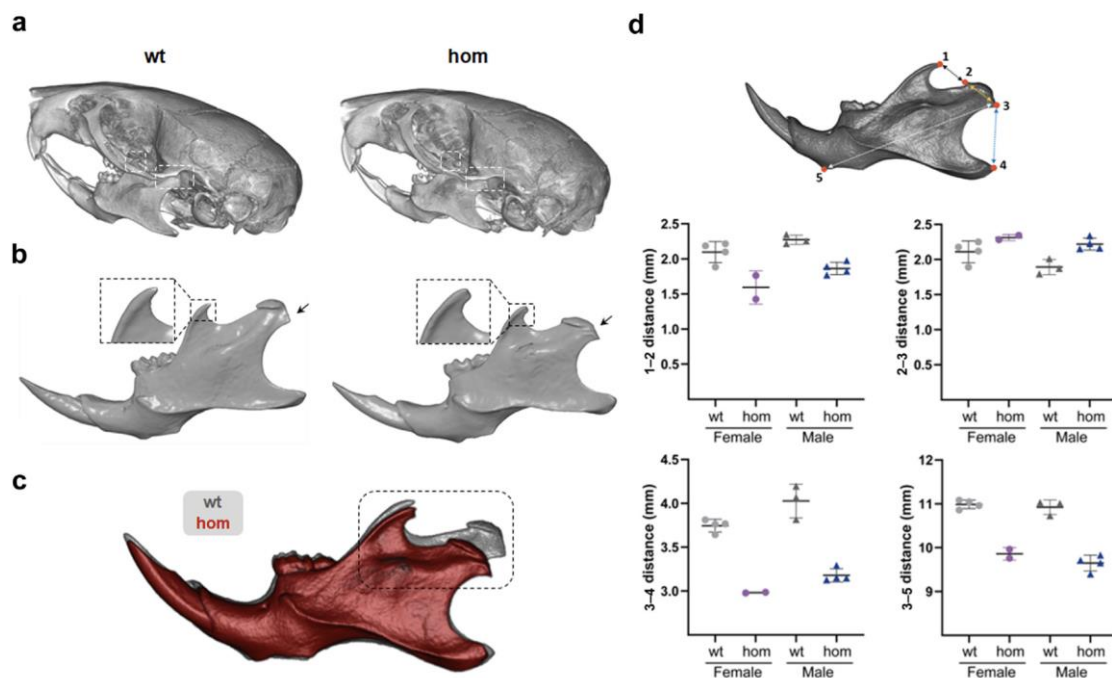

Abbildung 11: Darstellung der mandibulären Veränderungen in der Mikro-Computertomographie bei homozygoten *Foxd2*-Kockout-Mäusen. (a) Schädelknochen, (b) Mandibula von jeweils Wildtyp-Maus (wt) vs. homozygoter Knockout-Maus (hom). (c) Vergleich des Mandibula-Volumens zwischen wt und hom (kleiner). (d) Exakte morphometrische Vermessung der Mandibula anhand anatomischer Landmarken mit Vergleich zwischen wt und hom. Der Processus condylaris ist kürzer (Strecke 1 – 2 und 3 – 4) und weiter (Strecke 2 – 3) in hom vs. wt. n = 4 wt und n = 2 weibliche homozygote Knockout-Mäuse und n = 4 wt und n = 4 männliche homozygote Knockout-Mäuse. In den Graphen in (d) werden Einzelwerte mit Mittelwert ± Standardabweichung gezeigt. Aus [75].

Makroskopisch zeigte sich keine veränderte Nierenmorphologie bei homozygoten Knockouts im Alter von 16 Wochen. Mikroskopisch zeigte sich in der Hämatoxylin-Eosin-Färbung ein erweitertes Nierenbecken mit einer Penetranz von 33% (Abbildung

12a – c). Eine Obstruktion der ableitenden Harnwege als Ursache hierfür konnte ausgeschlossen werden. Als Zeichen verstärkter Nierenfibrose konnte weiterhin eine signifikant erhöhte Cytokeratin-8-Expression im Nierenkortex von Knockout-Mäusen festgestellt werden (Abbildung 13a-h).
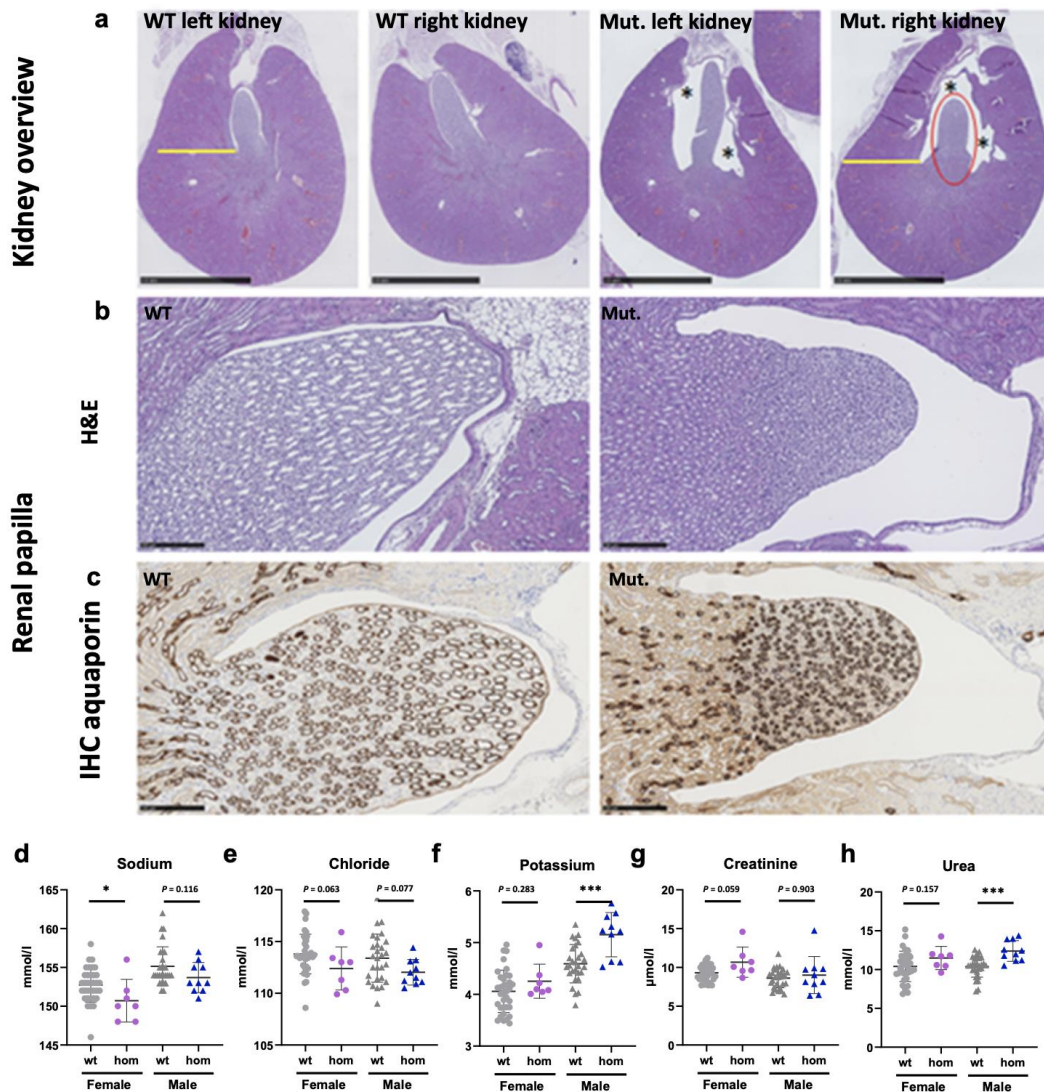

Abbildung 12: Histopathologische Veränderungen in der Niere bei 16 Wochen alten Mäusen. (a) Übersichtsbilder der linken und rechten Niere von Wildtyp- (WT) und homozygoten *Foxd2*-Knockout-Mäusen (Mut.). Es zeigt sich bei Knockout-Mäusen eine leichte beidseitige Nierenbeckenerweiterung (Stern), eine Verkleinerung der Papilla (rot eingekreist) und eine verschmälerte Nierenrinde (gelber Strich) im Vergleich zu WT-Mäusen. (b) Papilla vergrößert dargestellt. (a) und (b), Hämatoxylin-Eosin-Färbung. (c) Immunhistochemische Untersuchung auf Aquaporin 2 als Marker der Sammeltubuli (braun) mit Nachweis einer Verkleinerung des Umfangs der Sammeltubuli bei Knockout-Mäusen im Vergleich zu WT. (d – h) Veränderungen der Elektrolyte Natrium (Sodium), Chlorid (Chloride) und Kalium (Potassium), Veränderungen bei Kreatinin (Creatinine) und Harnstoff (Urea) im Plasma zwischen Wildtyp-Mäusen (wt) und homozygoten *Foxd2*-Knockout-Mäusen (hom). $*p < 0,05$; $***p < 0,001$. Aus [75].

Es zeigte sich auch eine auffällige Plasmachemie: Weibliche Knockout-Mäuse hatten u.a. leicht erniedrigte Plasmanatriumwerte, evtl. aufgrund einer Volumenüberladung bei abfallender Nierenfunktion. Männliche Knockout-Mäuse hatten ein signifikant erhöhtes Plasma-Kalium und -Harnstoff, evtl. auch aufgrund abnehmender Nierenfunktion. Zwei Knockout-Mäuse zeigten zudem stark erhöhte Plasmakreatininwerte (Abbildung 12d – h).
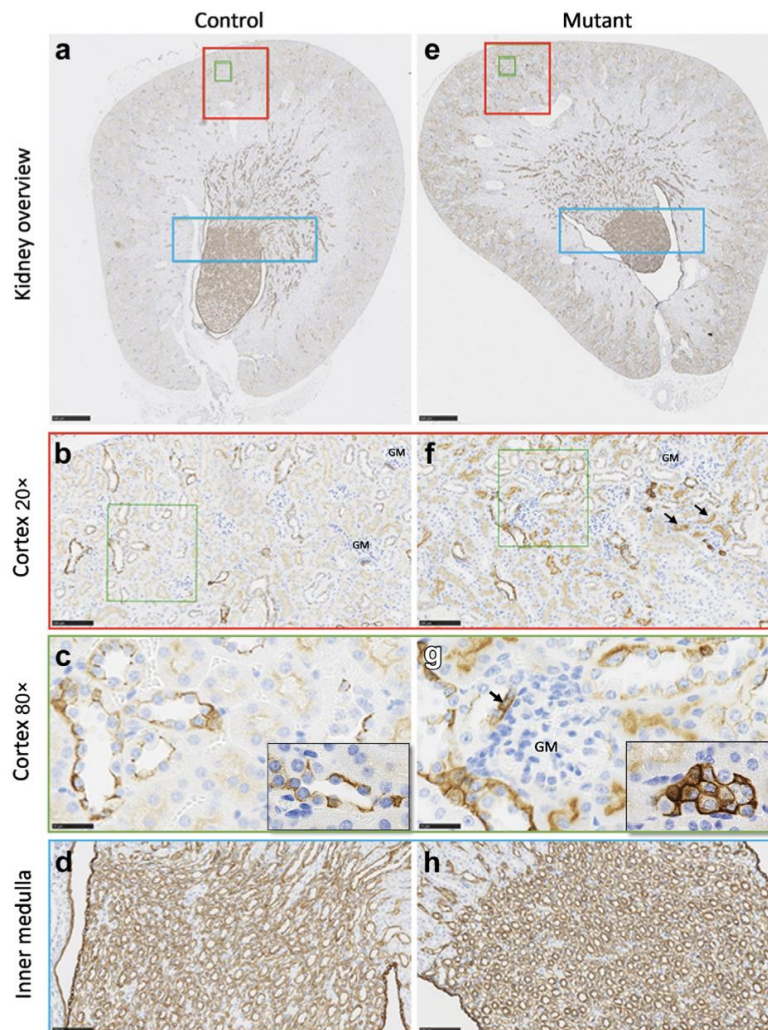

Abbildung 13: Erhöhte Cytokeratin-8-Expression (CK8) in den Nieren homozygoter *Foxd2*-Knockout-Mäuse (Mutant) vs. Wildtyp (Control). Hier dargestellt anhand repräsentativer Nierenbilder [Nierenrinde (Cortex) und inneres Nierenmark (Inner medulla)] unterschiedlicher Vergrößerung mit immunhistochemischer Untersuchung auf CK8 (braun).

GM, Glomerulus. Aus [75].

Schließlich zeigen sich Verhaltensauffälligkeiten bei den homozygoten *Foxd2*-Knockout-Mäusen. Im „Open field test" waren Knockout-Mäuse eindeutig weniger explorativ in einer neuen Umgebung im Vergleich zu Wildtyp-Mäusen.

5.2.4 *Foxd2*-Knockout in murinen metanephrischen Nierenzellen

Foxd2 wurde mittels CRISPR/Cas9 in murinen metanephrischen Nierenzellen (mk4) homozygot ausgeknockt. Daraufhin erfolgte eine RNA-Sequenzierung. Im Vergleich zu Wildtyp-Zellen waren hier v.a. Gene signifikant herunterreguliert, die unter die Gene-Ontology(GO)-Termini „extrazelluläre Matrixorganisation" (GO:0043062, $p = 3{,}46 \times 10^{-8}$) und „renale/urogenitale Entwicklung" fallen, wie z.B. „Entwicklung des Nierensystems" („Renal system development", GO:0072001, $p = 6{,}57 \times 10^{-7}$; Tabelle 4). Die Top-Ergebnisse der differentiell exprimierten Gene wurden mittels qPCR validiert. Wichtige differentiell exprimierte Gene waren u.a. *Pax2* und *Wnt4*, welche herunterreguliert waren (Abbildung 14a). Reduzierte Pax2-Proteinlevel in Knockouts vs. Kontrollen konnten mittels Western Blot bestätigt werden (Abbildung 14b und c).

	P	Adjusted P
Down		
Extracellular matrix organization	3.456442E−8	0.000152
Renal system development	6.571659E−7	0.000655
Urogenital system development	7.447146E−7	0.000655
Positive regulation of the steroid metabolic process	3.479562E−6	0.002186
Inner ear development	3.807702E−6	0.002186
Up		
Cell chemotaxis	6.340431E−11	4.250202E−8
Positive regulation of vasculature development	1.506551E−10	7.765204E−8
Antigen processing and presentation of endogenous antigen	1.544546E−10	7.765204E−8
Regulation of MAP kinase activity	2.957847E−10	1.321828E−7
Regulation of protein serine/threonine kinase activity	1.459391E−9	3.668544E−7

MAP, mitogen-activated protein.

Tabelle 4: Vergleich der differentiell exprimierten Gene zwischen *Foxd2*-Knockout- und Wildtyp-Zellen (mk4-Zellen) nach Gene-Ontology-Termini. Aus [75].
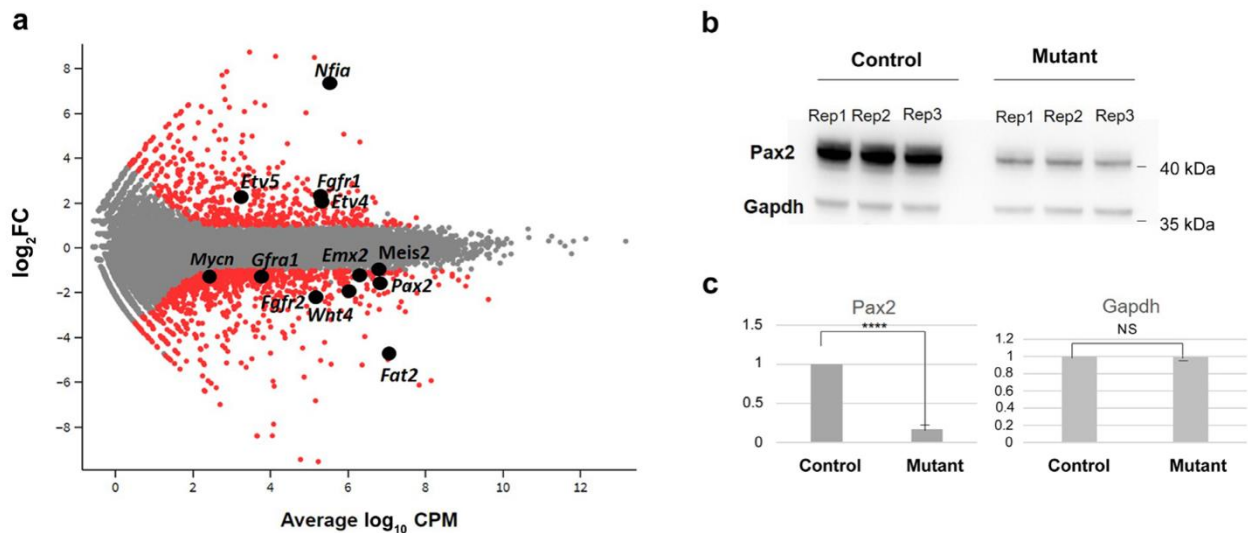
Abbildung 14: (a) Differentielle Genexpression in *Foxd2*-Knockout-Zellen vs. Wildtyp-Zellen (mk4-Zellen) im Glimma-Plot. (b) Western Blot mit Pax2-Reduktion in *Foxd2*-Knockout-Zellen vs. Wildtyp-Zellen. (c) Quantitative Analyse der Pax2-Proteinlevel aus dem Western-Blot-Experiment (3 biologische Replikate). ****p < 0,0001. CPM, counts per million (Zählungen pro Million); FC, fold change (X-fache Veränderung); NS, nicht signifikant; Rep, Replikat. Aus [75].

In der 3D-Zellkultur mit *Foxd2*-Knockouts konnte eine signifikant reduzierte Tubulusformation im Vergleich zu Wildtyp-Zellen nachgewiesen werden.

5.2.5 Fine-Mapping des mit Albuminurie verknüpften *FOXD2*-Locus

Um diejenigen Varianten zu identifizieren, welche am stärksten mit dem Albuminurie-Assoziationssignal am *FOXD2*-Locus aus GWAS-Metaanalysen[9] verknüpft sind, wurde eine sogenanntes Fine-Mapping von Albuminurie-assoziierten Varianten aus Teilnehmern der UK Biobank durchgeführt (Abbildung 15a).[76] Zwei SNPs, rs17453832 und rs1337526, hatten die höchste Wahrscheinlichkeit ursächlich für die Verknüpfung zu sein (Abbildung 15b). Interessanterweise überlappt rs17453832 zugängliche Chromatinbereiche in der Niere nur in Podozyten und hat eine angenommene Verbindung zum *FOXD2*-Promotor (Abbildung 15c und d), was dessen Funktion als regulatorische Variante stützt.[77,78]
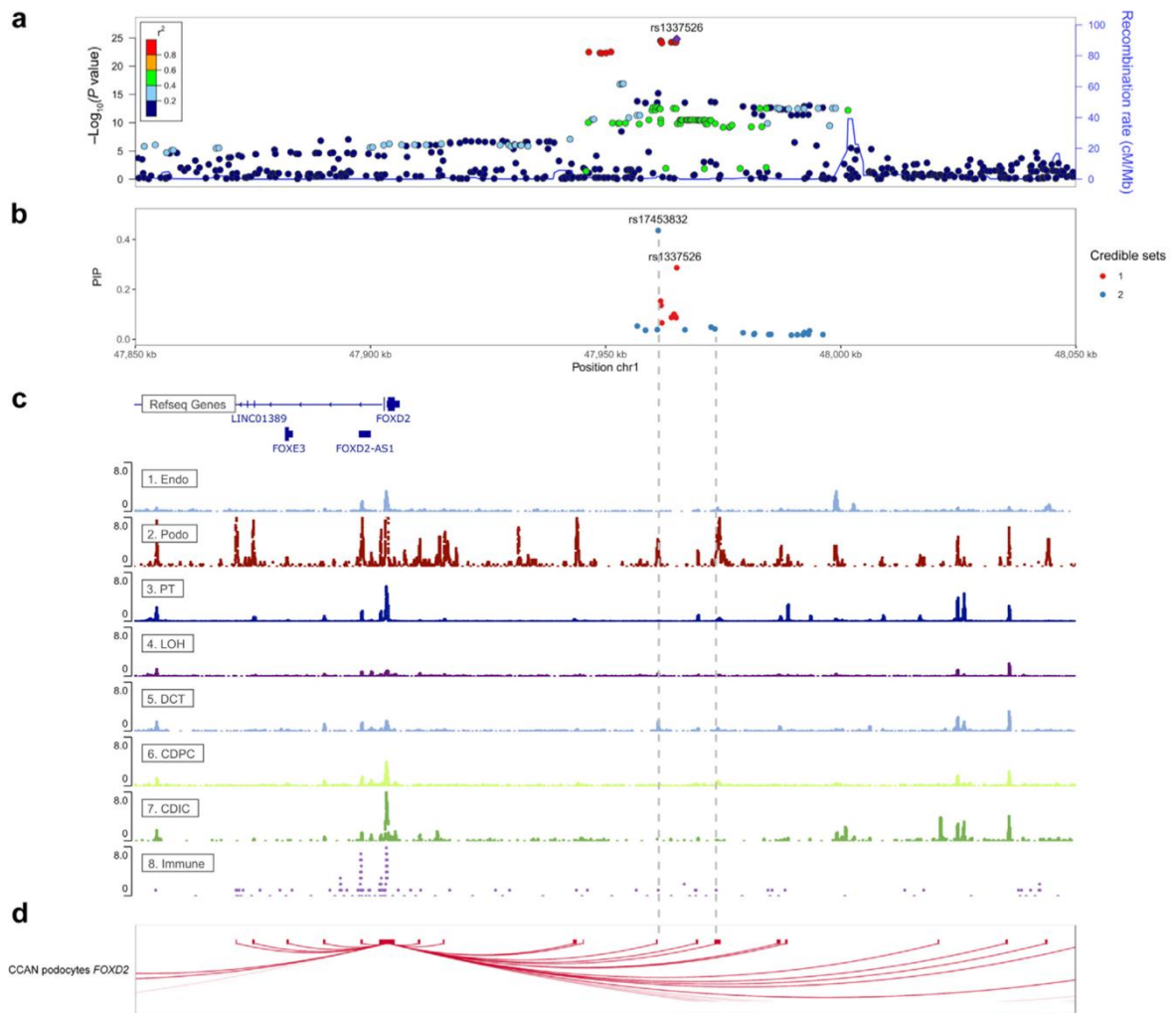
Abbildung 15: (a) Regionaler Assoziationsplot, (b) "Posterior inclusion probability"-Plot ("PIP plot"), (c) Refseq-Gen-Umgebung und acht snATAC-Sequenzierungs-Spuren (aus [79]), (d) „Podocyte cis-coaccessibility network" (CCAN) am *FOXD2*-Locus (1p33). Die Single nucleotide polymorphisms (SNPs) rs17453832 und rs1337526 hatten die höchste Wahrscheinlichkeit ursächlich für die Verknüpfung zwischen Albuminurie und dem *FOXD2*-Locus zu sein (b). Der SNP rs17453832 überlappt zugängliche Chromatinbereiche in der Niere nur in Podozyten und hat eine angenommene Verbindung zum FOXD2-Promotor (c und d).[77,78] CDIC, collecting duct intercalated cell (interkalierende Zelle des Sammeltubulus); CDPC, collecting duct principal cell (Prizipalzelle des Sammeltubulus); chr1, Chromosom 1; DCT, distal convoluted tubule (distales Tubuluskonvolut); Endo, endotheliale Zelle; Immune, Immune cell (Immunzelle); LOH, loop of Henle (Henlesche Schleife); Podo, Podozyt; PT, proximaler Tubulus. Aus [75].

5.3 Diskussion und Zusammenfassung

FOXD2 ist Teil einer evolutionär konservierten Gen-Familie, welche für Transkriptionsfaktoren kodiert. Verschiedene *FOX*-Gene wurden bereits mit monogenen Krankheiten assoziiert. Darunter *FOXC1*, welches mit dem Axenfeld-Rieger-Syndrom Typ 3 verknüpft ist (OMIM® #602482) und zuletzt auch mit einem CAKUT-Phänotyp in Verbindung gebracht wurde.[80]

Ein Vertreter der „D"-Gruppe der *FOX*-Gene wurde jedoch noch nicht mit einer monogenen Krankheit assoziiert. *FOXD2* (*FKHL17*, *FREAC9*, *MF-2*) wird gut in der Nierenrinde exprimiert.[81] *Foxd2*-Knockout-Mäuse haben einen CAKUT-Phänotyp (Nierenhypoplasie, Hydroureter) mit unvollständiger Penetranz von ca. 40%.[69] *Foxd2*-RNA ist außerdem stark in Podozyten angereichert und wurde mit der Aufrechterhaltung der Podozyten-Integrität verknüpft.[82] Weiterhin wurde der *FOXD2*-Locus (1p33) in GWAS-Metaanalysen mit Albuminurie assoziiert.[9] Die Betroffenen in dieser Arbeit haben alle einen CAKUT-Phänotyp und auch eine (nephrotische) Proteinurie bzw. es konnte eine FSGS in einer Nierenbiopsie nachgewiesen werden.

Es sollte daher mit dieser Studie gezeigt werden, ob eine FOXD2-Dysfunktion den Phänotyp der betroffenen Individuen der drei Familien erklären könnte. Die generierten homozygoten *Foxd2*-Knockout-Mäuse zeigen einen (milden) CAKUT-Phänotyp mit reduzierter Penetranz von 33% (Abbildung 12a – c). *Foxd2* hat eine große Sequenzhomologie mit *Foxd1*, und eine (teilweise) Redundanz der beiden kodierten Transkriptionsfaktoren könnte die verminderte Penetranz erklären.[69,83] Auch die fazialen Auffälligkeiten bei den betroffenen Individuen (v.a. Retrognathie; Abbildung 10e – h) konnten in homozygoten *Foxd2*-Knockout-Mäusen mittels Kiefervermessung nachempfunden werden (Abbildung 11a – d). Die Knockout-Mäuse hatten auch Verhaltensauffälligkeiten (Hypoaktivität im „Open field test"), was zu den Entwicklungsauffälligkeiten bei den Betroffenen passen könnte. All dies ist übereinstimmend damit, dass *Foxd2*-mRNA in der Niere, fazialen Regionen (u.a. Kiefer) und Gehirn in Northern-Blot-Experimenten nachgewiesen werden konnte.[83]

Die *in-vitro*-Ergebnisse der RNA-Sequenzierung aus murinen metanephrischen Nierenzellen (mk4) mit homozygoten *Foxd2*-Knockout stützen die *in-vivo*-Ergebnisse. Die Pathway-Analyse zeigte eine Anreicherung von differentiell exprimierten Genen,

die mit der Entwicklung der Nieren und des Urogenitaltrakts verknüpft sind, in Knockout- vs. Wildtyp-Zellen (Tabelle 4).

Berichtenswerterweise war *Pax2* in allen mk4-Klonen signifikant herunterreguliert, wie auch Pax2-Proteinlevel im Western Blot reduziert waren (Abbildung 14a – c). Eine PAX2-Haploinsuffizienz ist mit monogenem CAKUT verknüpft (Papillorenales Syndrom, OMIM® #120330). *Foxd2* ist wie *Pax2* stark im kondensierten Mesenchym in embryonalen Mausnieren exprimiert.[69] Eine regelrechte Pax2-Funktion ist zentral für eine Mesenchymal-Epitheliale-Zelltransition: Bei reduzierten Pax2-Proteinleveln kann im Nierenmesenchym keine epitheliale Zellformation erfolgen.[84] Interessanterweise ist *Pax2* auch wichtig, damit sich in der Embryonalentwicklung der Niere eine Grenze zwischen Nephron und Interstitium bildet. Nephron-Vorläuferzellen ohne Pax2 können sich nicht in Nephrone differenzieren und entwickeln sich stattdessen in interstitielle Zellen.[85] Die *Foxd2*-Knockout-Zellen hatten eine reduzierte *Pax2*-Expression und Pax2-Proteinlevel. Dies könnte darauf hindeuten, dass eine Foxd2-Dysfunktion zu vermehrter Bildung von Stroma-Zellen anstatt Nephronen in der Nierenentwicklung führt. Passend hierzu konnte eine erhöhte Expression des Fibrosemarkers Cytokeratin 8 in Nieren von homozygoten *Foxd2*-Knockout-Mäusen festgestellt werden (Abbildung 13), und in der Nierenbiopsie der Schwester des Index-Individuums aus Familie 2 (II-2) fand sich eine FSGS (Abbildung 10i).

Pax2 aktiviert zudem *Wnt4* im metanephrischen Mesenchym während der Nierenentwicklung.[86] Dies könnte die reduzierte *Wnt4*-Expression in *Foxd2*-Knockout-Zellen erklären (Abbildung 14a). Wnt4 spielt ebenfalls eine Rolle bei der Mesenchymal-Epithelialen-Zelltransition und ist wichtig für eine korrekte Tubulogenese.[87,88] Es konnte in dieser Arbeit anhand 3D-Zellkultur-Experimenten tatsächlich gezeigt werden, dass die Tubuologenese in *Foxd2*-Knockout-Zellen signifikant gestört ist.

Schlussendlich konnte ein Fine-Mapping einen Podozyten-spezifischen regulatorischen SNP (rs17453832) am *FOXD2*-Locus priorisieren, der mit Albuminurie in der Allgemeinbevölkerung verknüpft ist. Dieser Teil der Arbeit zeigt einmal mehr das Kontinuum zwischen seltener und häufiger Variation, zwischen monogenen und multifaktoriellen Phänotypen.

Zusammenfassend konnte mit der Arbeit das Gen *FOXD2* als krankheitsassoziiertes Gen für autosomal-rezessives CAKUT etabliert werden. Eine FOXD2-Dysfunktion

könnte über eine Verschiebung der zellulären Identität von Nephron-Vorläuferzellen hin zu Stromazellen in der Nierenentwicklung zu CAKUT führen. Es ist faszinierend, dass *FOXD2* neben CAKUT im Sinne einer monogenen Krankheit auch mit Albuminurie in einem multifaktoriellen Kontext verknüpft ist. FOXD2 könnte daher eine interessante Zielstruktur sein, um Proteinurie und Nierenfibrose in Zukunft zu behandeln.

6. Gibt es einen dominant-negativen Effekt bei Individuen mit heterozygoten krankheitsverursachenden Varianten in *COL4A3*/*COL4A4*?

Dieses Kapitel bezieht sich auf die folgende Originalarbeit:

- **Riedhammer KM,** Simmendinger H, Tasic V, Putnik J, Abazi-Emini N, Stajic N, Berutti R, Weidenbusch M, Patzer L, Lungu A, Milosevski-Lomic G, Günthner R, Braunisch MC, Ćomić J, Hoefele J. Is there a dominant-negative effect in individuals with heterozygous disease-causing variants in *COL4A3*/*COL4A4*? Clin Genet. 2024 Apr;105(4):406-414. doi: 10.1111/cge.14471. Epub 2024 Jan 12. PMID: 38214412.

Die Typ-IV-Kollagen-assoziierte Nephropathie ist ein Überbergriff für das X-chromosomale (X-linked AS, XLAS), autosomal-rezessive (ARAS) und autosomal-dominante Alport-Syndrom (ADAS). ADAS ist durch heterozygote (= monoallelische) krankheitsverursachende Varianten in den autosomalen AS-Genen *COL4A3* und *COL4A4* verursacht. Früher wurde in diesem Zusammenhang auch der Begriff „Syndrom der dünnen Basalmembran" („thin basement membrane nephropathy") benutzt, welcher mittlerweile als veraltet angesehen wird.[89]

Aber auch der Begriff ADAS für heterozygote Träger von krankheitsverursachenden Varianten in *COL4A3* und *COL4A4* ist umstritten: Furlano *et al.* haben in einer Studie 2021 argumentiert, jegliche heterozygote Variantenträger in *COL4A3*/*COL4A4* als ADAS-Betroffene zu bezeichnen, damit Behandlungsindikationen nicht übersehen werden.[90] Judy Savige hat sich bereits 2018 in einem Editorial skeptischer gezeigt: Der Begriff „Alport-Syndrom" beschreibt eine monogene, hochpenetrante Krankheit, bei dem 90% der am Vollbild Betroffenen mit 40 Jahren einen kompletten Nierenfunktionsverlust erleiden (XLAS und ARAS). Beim ADAS haben zwar alle Betroffenen eine Hämaturie, eine dialysepflichtige Niereninsuffizienz entwickeln aber „nur" ca. ¼ der Betroffenen und das auch im Median erst im Alter von über 50 Jahren.[89,91] Hinzu kommt, dass aus Kontrolldatenbanken bekannt ist, dass ca. 1% (!)

der Bevölkerung heterozygote krankheitsverursachende Varianten in *COL4A3*/*COL4A4* trägt, wobei natürlich nicht jeder und jede davon eine dialysepflichtige Niereninsuffizienz bzw. das Vollbild eines AS entwickelt.[89,92]

Ziel dieser Studie war es nun, gerade in Hinblick auf das geringe Wissen bzgl. Genotyp-Phänotyp-Korrelationen beim ADAS, eine Kohorte mit autosomalem AS bzgl. des Genotyps und Phänotyps zu untersuchen.

6.1 Methoden, Studiendesign und -population

Diese retrospektive Studie umfasste 89 Individuen mit krankheitsverursachenden Varianten in *COL4A3* oder *COL4A4* aus 38 nicht miteinander verwandten Familien. Die Rekrutierung fand zwischen Oktober 2015 und Januar 2021 statt und war Teil der „NephroGen-Studie" am Institut für Humangenetik des Klinikums rechts der Isar der Technischen Universität München. Alle eingeschlossenen Individuen wurden molekulargenetisch getestet, entweder mittels ES (33/89, 37%), NGS-basiertem-Gen-Panel (14/89, 16%) oder Sanger-Sequenzierung (42/89, 47%; hier aber nur 5/38 Index-Fälle, der Rest waren Verwandtentestungen). Der Phänotyp wurde aus Arztbriefen und anhand eines standardisierten Fragebogens erfasst. Zusätzlich wurden die eingeschlossenen Individuen und zuweisenden Ärzte telefonisch kontaktiert, um die phänotypischen Informationen sehr genau zu erheben [wie Alter bei Erstmanifestation (= erstmalige Diagnose) der Mikrohämaturie oder Proteinurie].

Alle 89 Index-Individuen wurden folgenden Krankheitsgruppen nach klinischer (Verdachts-)diagnose zugeordnet: ARAS, ADAS und (erbliche) FSGS. Weiterhin wurden die Fälle nach Genotyp folgenden Gruppen zugewiesen: (I) Monoallelische krankheitsverursachende Variante in *COL4A3* oder *COL4A4*; (II) Biallelische krankheitsverursachende Varianten in *COL4A3* oder *COL4A4*. Innerhalb dieser beiden Gruppen wurden weiter Untergruppen nach Art der Variante gebildet: (A) Individuen mit einer monoallelischen nicht-trunkierenden Variante (Missense-Variante, In-frame-Insertion/-Deletion); (B) Individuen mit einer monoallelischen trunkierenden Variante (Nonsense-, Frameshift-, kanonische Spleiß-Site-Variante und CNV); (C) Individuen mit einer biallelischen nicht-trunkierenden Variante; (D) Individuen mit einer nicht-trunkierenden und einer trunkierenden Variante (compound-heterozygot); (E)
50

Individuen mit einer biallelischen trunkierenden Variante (Abbildung 16). Alle Varianten wurden mit den Kriterien des ACMG und aktuellen Erweiterungen überprüft.[40,63-65]
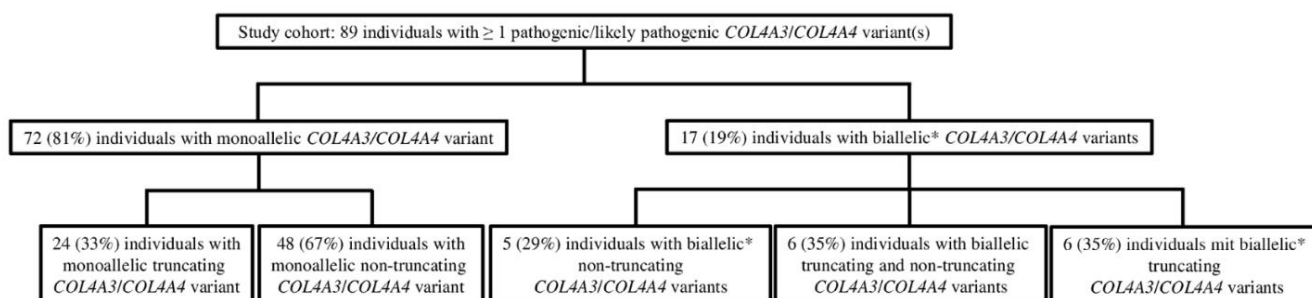

Abbildung 16: Flussdiagramm der Kohorte. *compound-heterozygot oder homozygot. Aus [93].

Das Alter bei Dialysepflichtigkeit wurde als das Alter bei Beginn der Hämodialyse oder Peritonealdialyse oder bei präemptiver Nierentransplantation festgesetzt.

Die statistische Auswertung erfolgte mit SPSS® Statistics 23 (IBM®, Deutschland) und R, Version 4.2.2 (R Foundation for statistical Computing, Österreich).

6.2 Ergebnisse

Die Studienkohorte bestand aus 89 Individuen aus 38 nicht miteinander verwandten Familien. 46/89 (52%) Individuen waren weiblich. 84/89 (94%) waren Kaukasier („Non-Finnish European"). Eine berichtete Konsanguinität der Eltern lag bei 5/89 (6%) Individuen vor. Das mediane Alter bei Datenerhebung war 33 Jahre mit einer Spannbreite von zwei bis 86 Jahren. 60/89 (67%) Individuen waren ≥18 alt. 86/89 (97%) Individuen hatten eine positive Familienanamnese.

Nach klinischer (Verdachts-)diagnose wurden 19 Fälle als ARAS, 56 Fälle als ADAS und 4 Fälle als (erbliche) FSGS eingruppiert. 10/89 (11%) Individuen hatten eine unauffällige Nierenfunktion und wurden nur wegen eines klinisch auffälligen Verwandten rekrutiert.

Tabelle 5 zeigt klinische Informationen und einen Überblick über die Verteilung der krankheitsverursachenden Varianten auf die verschiedenen in den Methoden genannten Gruppen.

Individuals/Variants	Total cohort	*COL4A3*	*COL4A4*
Individuals	89/89	61 (69%)	28 (31%)
Male	43/89	30 (70%)	13 (30%)
Female	46/89	31 (67%)	15 (33%)
Non-Finnish European origin	84/89	57 (68%)	27 (32%)
Consanguinity	5/89	4 (80%)	1 (20%)
Positive family history	86/89	60 (70%)	26 (30%)
Zygosity			
Monoallelic	72/89	47 (65%)	25 (35%)
Biallelic	17/89	14 (82%)	3 (18%)
Compound heterozygous	12/17	11 (92%)	1 (8%)
Homozygous	5/17	3 (60%)	2 (40%)
Variants			
Number of identified variants	106/106	75 (71%)	31 (29%)
Number of different variants	42/42	27 (64%)	15 (36%)
Once in cohort	9/42	6 (67%)	3 (33%)
Multiple times in cohort	33/42	21 (64%)	12 (36%)
Type of variant			
Truncating	42/106	26 (62%)	16 (38%)
Nonsense	19/42	10 (53%)	9 (47%)
Frameshift	7/42	6 (86%)	1 (14%)
Canonical splice site variant	13/42	8 (62%)	5 (38%)
CNV (multi-exon deletion)	1/42	0 (0%)	1 (100%)
Affecting start codon	2/42	2 (100%)	0 (0%)
Non-truncating	64/106	49 (77%)	15 (23%)
Missense	53/64	40 (75%)	13 (25%)
In-frame deletion	4/64	2 (50%)	2 (50%)
In-frame duplication	7/64	7 (100%)	0 (0%)

Tabelle 5: Klinische Informationen und Verteilung der krankheitsverursachenden Varianten in der Kohorte. CNV, copy number variant (Kopienzahlvariante). Aus [93].

Die genaue Aufteilung nach Phänotypen [Mikrohämaturie, Proteinurie, dialysepflichtiges Nierenversagen (end-stage kidney disease, ESKD) und beim AS typische extrarenale Manifestationen (Augenauffälligkeiten, Hörstörungen)] zeigen Tabelle 6 und Abbildung 17.

Abbildung 17: Statistische Auswertung nach Genotyp und Phänotyp [Mikrohämaturie (Microscopic hematuria), Proteinurie (Proteinuria), dialysepflichtiges Nierenversagen (ESKD, end-stage kidney disease) und extrarenale Manifestationen (Extrarenal manifestation; Augenauffälligkeiten, Hörminderung)]. $^{*}p \leq 0,05$. n.t., nicht-trunkierend; t., trunkierend. Aus [93].

Individuen mit monoallelischen nicht-trunkierenden Varianten hatten eine signifikant frühere Diagnose einer Mikrohämaturie als solche mit einer monoallelisch trunkierenden Variante (p = 0,015). Im Alter von 20 Jahren war die Inzidenz der Mikrohämaturie 55% und 25% jeweils in der nicht-trunkierenden und trunkierenden Gruppe. Im Alter von 40 Jahren war sie jeweils 79% und 59% und im Alter von 60 Jahren jeweils 96% und 74% (Abbildung 18A). Ein ähnliches Bild zeigte sich bei der Proteinurie: Individuen mit monoallelischen nicht-trunkierenden Varianten hatten eine signifikant frühere Diagnose einer Proteinurie als solche mit einer monoallelisch trunkierenden Variante (p = 0,046). Im Alter von 20 Jahren war die Inzidenz der Proteinurie 18% und 8% jeweils in der nicht-trunkierenden und trunkierenden Gruppe. Im Alter von 40 Jahren war sie jeweils 37% und 21% (Abbildung 18B).
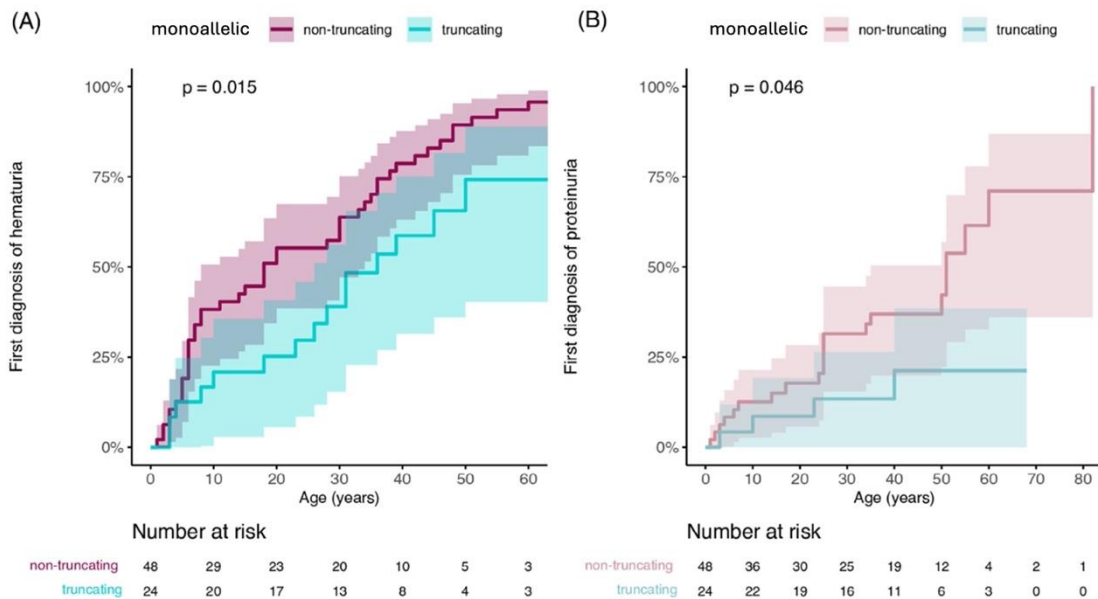
Abbildung 18: Kumulative Inzidenzkurve für Alter bei Erstdiagnose einer (Mikro-)hämaturie (A) oder Proteinurie (B), stratifiziert nach monoallelisch nicht-trunkierender (rot) und trunkierender (blau) krankheitsverursachender Variante. Nach [93].

Für biallelische Variantenträger mit trunkierenden Varianten zeigte sich ein jüngeres Alter bei Erstdiagnose einer Mikrohämaturie und Proteinurie im Vergleich zu Variantenträgern mit nicht-trunkierenden Varianten (drei vs. sechs Jahre für Mikrohämaturie, $p = 0{,}03$; drei vs. neun Jahre für Proteinurie, $p = 0{,}017$; Tabelle 6).

28/89 (31%) Individuen hatten eine berichtete Therapie mit einer RAAS-Blockade (Renin-Angiotensin-Aldosteron-System-Blockade). 13/72 (18%) Individuen mit einer monoallelischen und 15/17 (88%) mit einer biallelischen Variante ($p < 0{,}001$). Individuen mit einer monoallelischen nicht-trunkierenden Variante hatten eine RAAS-Blockade in 12/48 (25%) Fällen, Individuen mit einer monoallelischen trunkierenden Variante in 1/24 (4%) Fällen ($p = 0{,}048$).

6.3 Diskussion und Zusammenfassung

Das Krankheitsspektrum beim AS, welches mit dem Überbegriff Typ-IV-Kollagen-assoziierte Nephropathie zusammengefasst wird, beinhaltet neben dem klassischen, hoch-penetranten AS (ARAS und XLAS) auch „mildere" Formen wie das ADAS mit monoallelischen krankheitsverursachenden Varianten in *COL4A3*/*COL4A4*.[89] Auch in dieser Studie hatten Individuen mit monoallelischen Varianten in *COL4A3*/*COL4A4* (ADAS) im Vergleich zu solchen mit biallelischen Varianten eine signifikant niedrigere Häufigkeit von Proteinurie, ESKD und für das AS typischen extrarenalen Manifestationen (Augenauffälligkeiten, Hörminderung; Abbildung 17). Außerdem entwickelten monoallelische Variantenträger signifikant später im Leben eine Mikrohämaturie oder Proteinurie im Vergleich zu biallelischen Variantenträgern (Tabelle 6). Die Prävalenz der Mikrohämaturie war übrigens nicht signifikant unterschiedlich zwischen monoallelischen und biallelischen Variantenträgern (85% vs. 100%, Tabelle 6). Dies spricht dafür, dass eine Mikrohämaturie das typische Symptom im gesamten Krankheitsspektrum der Typ-IV-Kollagen-assoziierten Nephropathie ist.

Interessanterweise hatten Individuen mit monoallelischen nicht-trunkierenden Varianten signifikant häufiger eine Mikrohämaturie und Proteinurie als solche mit monoallelischen trunkierenden Varianten (Tabelle 6 und Abbildung 17). Außerdem zeigte sich dieser schwerere Phänotyp von monoallelischen nicht-trunkierenden Variantenträgern im Vergleich zu monoallelischen trunkierenden Variantenträgern durch ein signifikant jüngeres Alter bei Erstmanifestation (= Erstdiagnose) einer Mikrohämaturie und Proteinurie (Abbildung 18). Passenderweise hatten monoallelische nicht-trunkierende Variantenträger signifikant häufiger eine RAAS-Blockade im Vergleich zu monoallelischen trunkierenden Variantenträgern.

Diese Beobachtung, dass monoallelische nicht-trunkierende Variantenträger einen schwereren Phänotyp als monoallelische trunkierende Variantenträger haben, ist in der Literatur beim ADAS fast gar nicht beschrieben. Nur die aktuelle Studie von Solanki *et al.* geht darauf in Bezug auf monoallelische *COL4A3*-Variantenträger ein.[94] Furlano *et al.* hatten in ihrer ADAS-Studie mit 252 Individuen keine phänotypischen Unterschiede nach Variantentyp feststellen können.[90] Es ist in diesem Zusammenhang zu erwähnen, dass 28 von 39 (72%) monoallelischen Missense-Varianten in

56

COL4A3/COL4A4 (58% aller nicht-trunkierenden Varianten) die Aminosäure Glycin in der Triple-Helix-Domäne des jeweiligen Gens in stark destabilisierende Aminosäuren tauschen (Arginin, Glutamat, Aspartat, Valin), welche bekannterweise mit einer erhöhten Mikrohämaturie-Rate verknüpft sind.[95,96]

Zusammenfassend deuten unsere Daten, bei insgesamt kleiner Kohortengröße, auf einen schwereren Phänotyp bei monoallelischen nicht-trunkierenden Variantenträgern im Vergleich zu monoallelischen trunkierenden Variantenträgern hin. Dies könnte durch einen dominant-negativen Effekt bedingt sein. Man kennt dieses Phänomen bei anderen autosomal-dominanten Kollagen-assoziierten Krankheiten wie z.B. der Osteogenesis imperfecta (Gene *COL1A1* und *COL1A2*), bei der heterozygote trunkierende Varianten zu einem weniger gravierenden Phänotyp führen als destabilisierende heterozygote nicht-trunkierende Glycin-Varianten in der Triple-Helix-Domäne der Typ-1-Kollagene.[97] Es ist aber anzumerken, dass ein dominant-negativer Effekt noch nicht bei ADAS beschrieben wurde und weitere Studien an größeren Kohorten und Laboruntersuchungen diese Beobachtung bestätigen müssen.

7. Zusammenfassung und Ausblick

Durch die in dieser Arbeit beschriebenen Publikationen konnte die Leistungsfähigkeit der genomweiten Sequenzierung aufgezeigt werden.

Dies ist zum einen in Bezug auf die klinische Praxis der Nephrologie klar ersichtlich: In jedem fünften Fall mit klinischer Verdachtsdiagnose einer erblichen Nierenkrankheit führte eine Exom-Sequenzierung zur Reklassifizierung der Diagnose („Phänokopie").[41] Dies kann erhebliche Auswirkungen auf Management, Prognose und Therapie einer Krankheit haben. So hatten wir, kurz nach der Publikation zu Phänokopien, den Fall eines 38-jährigen Patienten (ATS-F719-II-2), der seit über 30 Jahren die klinische Verdachtsdiagnose eines AS hatte (Hörminderung, beginnend im Alter von drei Jahren, mit 27 Jahren nierentransplantiert) ohne Nachweis einer krankheitsverursachenden Variante in den AS-Genen *COL4A3*, *COL4A4* oder *COL4A5*. Mittels ES konnten wir eine primäre Coenzym-Q10-Defizienz Typ 6 (OMIM® #614650) diagnostizieren, welche inzwischen durch frühzeitige Coenzym-Q10-Supplementation im Verlauf verlangsamt werden kann (Reduktion der Proteinurie).[98] Dies hat zwar keine Auswirkung auf den Verlauf der Nierenkrankheit dieses Patienten mehr (bereits nierentransplantiert), wirft aber ein Schlaglicht darauf, wie wichtig eine – frühzeitige – genetische Diagnose ist.

Außerdem wurde das genetisch komplizierte Feld der angeborenen Nieren- und Harnwegsfehlbildungen (CAKUT) beleuchtet. Wir konnten zeigen, dass gerade bei beidseitiger Nierenbeteiligung und syndromaler Komponente ein vererbbares CAKUT vorliegenden kann. Dies ist eine wichtige Erkenntnis für den Nephrologen, der auf Grundlage des klinischen Bildes entscheiden muss, ob er einen Patienten in die Humangenetik überweist oder nicht, vor allem wenn es sich um ein Krankheitsbild wie CAKUT handelt, das mehrheitlich multifaktoriell bedingt ist.[66] Siehe in diesem Zusammenhang auch das zur beschriebenen Publikation zugehörige Editorial.[99]

Komplex ist auch das genotypische und phänotypische Spektrum beim Alport-Syndrom, zusammengefasst als Typ-IV-Kollagen-assoziierte Nephropathie. Gerade bei heterozygoten (= monoallelischen) Trägern von krankheitsverursachenden Varianten in den autosomalen AS-Genen *COL4A3* und *COL4A4*, welche mit dem immer noch umstrittenen Begriff ADAS (autosomal-dominantes Alport-Syndrom) bezeichnet werden, ist der klinische Verlauf sehr variabel und insgesamt milder als

beim klassischen Alport-Syndrom (ARAS, XLAS). Unsere Daten deuten darauf hin, dass bei monoallelischen Variantenträgern in *COL4A3* und *COL4A4* ein dominant-negativer Effekt vorliegen könnte, der zu einem schwereren Phänotyp bei monoallelischen nicht-trunkierenden Varianten (wie z.B. Glycin-Missense-Varianten in der Triple-Helix-Domäne der jeweiligen Kollagene) im Vergleich zu monoallelischen trunkierenden Varianten führt. Diese Erkenntnis, welche wir als mit die Ersten publiziert haben, ist wichtig in der Beratung und Behandlung von Patienten mit ADAS, z.B. was deren Prognose und Surveillance angeht.[93]

Andererseits zeigte die genomweite Sequenzierung auch Ihren Nutzen in Bezug auf die Entdeckung und Charakterisierung von neuen krankheitsassoziierten Genen.

So konnte an der bisher größten Kohorte mit Suleiman-El-Hattab-Syndrom (OMIM® #618950) das Krankheitsbild phänotypisch und genotypisch aufgearbeitet werden. Diese Arbeit bewies zudem den Nutzen von Multi-Omics, womit das mit dem Suleiman-El-Hattab-Syndrom verknüpfte Gen *TASP1* umfassend funktionell untersucht wurde und als Krankheit mit Histonmethylierungsdefekt kategorisiert werden konnte.[50,58]

Zudem konnte mit *FOXD2* ein neues krankheitsassoziiertes Gen für autosomal-rezessives CAKUT beschrieben und funktionell aufgearbeitet werden. *FOXD2* ist ein in der Nephrologie sehr spannendes Gen/Locus, da es nicht nur im monogenen Kontext mit CAKUT verknüpft ist, sondern auch im multifaktoriellen Kontext mit Albuminurie, was unsere Publikation zeigen konnte. Damit bestätigt sich, dass die Genetik eine Schlüsselposition einnimmt, um molekulare Zielstrukturen für zukünftige Therapien zu identifizieren.[75]

Die chronische Niereninsuffizienz hat eine enorme (und zunehmende) gesundheitspolitische Dimension, mit ca. 850 Millionen betroffenen Menschen weltweit. Durch GWAS, dem Wissen aus monogenen Krankheiten und molekulargenetischen Methoden wie dem Single-Cell-Sequencing kann zunehmend die molekulare Anatomie von Krankheiten und Phänotypen „seziert" werden.[15,36] Damit werden in Zukunft immer präzisere Therapien in der Nephrologie (und natürlich darüber hinaus) möglich, in deren Zentrum die genetische Expertise stehen wird.

Literaturverzeichnis

1.   Alport AC. Hereditary Familial Congenital Haemorrhagic Nephritis. *Br Med J.* 1927;1(3454):504-506.
2.   Barker DF, Hostikka SL, Zhou J, et al. Identification of mutations in the COL4A5 collagen gene in Alport syndrome. *Science.* 1990;248(4960):1224-1227.
3.   Lander ES, Linton LM, Birren B, et al. Initial sequencing and analysis of the human genome. *Nature.* 2001;409(6822):860-921.
4.   Goodwin S, McPherson JD, McCombie WR. Coming of age: ten years of next-generation sequencing technologies. *Nat Rev Genet.* 2016;17(6):333-351.
5.   Participants KC. Genetics in chronic kidney disease: conclusions from a Kidney Disease: Improving Global Outcomes (KDIGO) Controversies Conference. *Kidney Int.* 2022;101(6):1126-1141.
6.   Groopman EE, Marasa M, Cameron-Christie S, et al. Diagnostic Utility of Exome Sequencing for Kidney Disease. *N Engl J Med.* 2019;380(2):142-151.
7.   Devuyst O, Knoers NV, Remuzzi G, et al. Rare inherited kidney diseases: challenges, opportunities, and perspectives. *Lancet.* 2014;383(9931):1844-1859.
8.   Vivante A, Hildebrandt F. Exploring the genetic basis of early-onset chronic kidney disease. *Nat Rev Nephrol.* 2016;12(3):133-146.
9.   Teumer A, Li Y, Ghasemi S, et al. Genome-wide association meta-analyses and fine-mapping elucidate pathways influencing albuminuria. *Nat Commun.* 2019;10(1):4130.
10.   Kiryluk K, Sanchez-Rodriguez E, Zhou XJ, et al. Genome-wide association analyses define pathogenic signaling pathways and prioritize drug targets for IgA nephropathy. *Nat Genet.* 2023;55(7):1091-1105.
11.   Gorski M, Rasheed H, Teumer A, et al. Genetic loci and prioritization of genes for kidney function decline derived from a meta-analysis of 62 longitudinal genome-wide association studies. *Kidney Int.* 2022;102(3):624-639.
12.   Vinuesa CG, Shen N, Ware T. Genetics of SLE: mechanistic insights from monogenic disease and disease-associated variants. *Nat Rev Nephrol.* 2023;19(9):558-572.
13.   Devuyst O, Pattaro C. The UMOD Locus: Insights into the Pathogenesis and Prognosis of Kidney Disease. *J Am Soc Nephrol.* 2018;29(3):713-726.
14.   Katsanis N. The continuum of causality in human genetic disorders. *Genome Biol.* 2016;17(1):233.
15.   Fountoglou A, Deltas C, Siomou E, Dounousi E. Genome-wide association studies reconstructing chronic kidney disease. *Nephrol Dial Transplant.* 2024;39(3):395-402.
16.   Sullivan KM, Susztak K. Unravelling the complex genetics of common kidney diseases: from variants to mechanisms. *Nat Rev Nephrol.* 2020;16(11):628-640.
17.   Giovinazzo JA, Thomson RP, Khalizova N, et al. Apolipoprotein L-1 renal risk variants form active channels at the plasma membrane driving cytotoxicity. *Elife.* 2020;9.
18.   Egbuna O, Zimmerman B, Manos G, et al. Inaxaplin for Proteinuric Kidney Disease in Persons with Two APOL1 Variants. *N Engl J Med.* 2023;388(11):969-979.
19.   Watson JD, Crick FH. Molecular structure of nucleic acids; a structure for deoxyribose nucleic acid. *Nature.* 1953;171(4356):737-738.
20.   Sanger F, Nicklen S, Coulson AR. DNA sequencing with chain-terminating inhibitors. *Proc Natl Acad Sci U S A.* 1977;74(12):5463-5467.
21.   Gibbs RA. The Human Genome Project changed everything. *Nat Rev Genet.* 2020;21(10):575-576.
22.   https://www.genome.gov/about-genomics/educational-resources/fact-sheets/human-genome-project. Abgerufen am 25.03.2024.
23.   Pervez MT, Hasnain MJU, Abbas SH, Moustafa MF, Aslam N, Shah SSM. A Comprehensive Review of Performance of Next-Generation Sequencing Platforms. *Biomed Res Int.* 2022;2022:3457806.
24.   https://www.genome.gov/about-genomics/fact-sheets/Sequencing-Human-Genome-cost. Abgerufen am 25.03.2024.
25.   Majewski J, Schwartzentruber J, Lalonde E, Montpetit A, Jabado N. What can exome sequencing do for you? *J Med Genet.* 2011;48(9):580-589.
26.   Ross JP, Dion PA, Rouleau GA. Exome sequencing in genetic disease: recent advances and considerations. *F1000Res.* 2020;9.

27. Hamosh A, Amberger JS, Bocchini C, Scott AF, Rasmussen SA. Online Mendelian Inheritance in Man (OMIM(R)): Victor McKusick's magnum opus. *Am J Med Genet A.* 2021;185(11):3259-3265.
28. https://www.omim.org. Abgerufen am 25.03.2024.
29. https://www.omim.org/statistics/paceGraph. Abgerufen am 25.03.2024.
30. Nurchis MC, Radio FC, Salmasi L, et al. Cost-Effectiveness of Whole-Genome vs Whole-Exome Sequencing Among Children With Suspected Genetic Disorders. *JAMA Netw Open.* 2024;7(1):e2353514.
31. Yepez VA, Gusic M, Kopajtich R, et al. Clinical implementation of RNA sequencing for Mendelian disease diagnostics. *Genome Med.* 2022;14(1):38.
32. Sadikovic B, Levy MA, Kerkhof J, et al. Clinical epigenomics: genome-wide DNA methylation analysis for the diagnosis of Mendelian disorders. *Genet Med.* 2021;23(6):1065-1074.
33. Colin E, Duffourd Y, Chevarin M, et al. Stepwise use of genomics and transcriptomics technologies increases diagnostic yield in Mendelian disorders. *Front Cell Dev Biol.* 2023;11:1021920.
34. Vilhekar RS, Rawekar A. Artificial Intelligence in Genetics. *Cureus.* 2024;16(1):e52035.
35. Dremsek P, Schwarz T, Weil B, Malashka A, Laccone F, Neesen J. Optical Genome Mapping in Routine Human Genetic Diagnostics-Its Advantages and Limitations. *Genes (Basel).* 2021;12(12).
36. Zhou J, Abedini A, Balzer MS, et al. Unified Mouse and Human Kidney Single-Cell Expression Atlas Reveal Commonalities and Differences in Disease States. *J Am Soc Nephrol.* 2023;34(11):1843-1862.
37. Becherucci F, Landini S, Cirillo L, Mazzinghi B, Romagnani P. Look Alike, Sound Alike: Phenocopies in Steroid-Resistant Nephrotic Syndrome. *Int J Environ Res Public Health.* 2020;17(22).
38. Malone AF, Phelan PJ, Hall G, et al. Rare hereditary COL4A3/COL4A4 variants may be mistaken for familial focal segmental glomerulosclerosis. *Kidney Int.* 2014;86(6):1253-1259.
39. Warejko JK, Tan W, Daga A, et al. Whole Exome Sequencing of Patients with Steroid-Resistant Nephrotic Syndrome. *Clin J Am Soc Nephrol.* 2018;13(1):53-62.
40. Richards S, Aziz N, Bale S, et al. Standards and guidelines for the interpretation of sequence variants: a joint consensus recommendation of the American College of Medical Genetics and Genomics and the Association for Molecular Pathology. *Genet Med.* 2015;17(5):405-424.
41. Riedhammer KM, Braunisch MC, Gunthner R, et al. Exome Sequencing and Identification of Phenocopies in Patients With Clinically Presumed Hereditary Nephropathies. *Am J Kidney Dis.* 2020;76(4):460-470.
42. Ahram DF, Aggarwal VS, Sanna-Cherchi S. Phenocopies, Phenotypic Expansion, and Coincidental Diagnoses: Time to Abandon Targeted Gene Panels? *Am J Kidney Dis.* 2020;76(4):451-453.
43. Suleiman J, Riedhammer KM, Jicinsky T, et al. Homozygous loss-of-function variants of TASP1, a gene encoding an activator of the histone methyltransferases KMT2A and KMT2D, cause a syndrome of developmental delay, happy demeanor, distinctive facial features, and congenital anomalies. *Hum Mutat.* 2019;40(11):1985-1992.
44. Niizuma H, Cheng EH, Hsieh JJ. Taspase 1: A protease with many biological surprises. *Mol Cell Oncol.* 2015;2(4):e999513.
45. Jones WD, Dafou D, McEntagart M, et al. De novo mutations in MLL cause Wiedemann-Steiner syndrome. *Am J Hum Genet.* 2012;91(2):358-364.
46. Sobreira N, Schiettecatte F, Valle D, Hamosh A. GeneMatcher: a matching tool for connecting investigators with an interest in the same gene. *Hum Mutat.* 2015;36(10):928-930.
47. Gurovich Y, Hanani Y, Bar O, et al. Identifying facial phenotypes of genetic disorders using deep learning. *Nat Med.* 2019;25(1):60-64.
48. Brechtmann F, Mertes C, Matuseviciute A, et al. OUTRIDER: A Statistical Method for Detecting Aberrantly Expressed Genes in RNA Sequencing Data. *Am J Hum Genet.* 2018;103(6):907-917.
49. https://www.medrxiv.org/content/10.1101/2021.03.09.21253187v1. Abgerufen am 25.03.2024.
50. Riedhammer KM, Burgemeister AL, Cantagrel V, et al. Suleiman-El-Hattab syndrome: a histone modification disorder caused by TASP1 deficiency. *Hum Mol Genet.* 2022;31(18):3083-3094.
51. Weinhold L, Wahl S, Pechlivanis S, Hoffmann P, Schmid M. A statistical model for the analysis of beta values in DNA methylation studies. *BMC Bioinformatics.* 2016;17(1):480.
52. Hsieh JJ, Cheng EH, Korsmeyer SJ. Taspase1: a threonine aspartase required for cleavage of MLL and proper HOX gene expression. *Cell.* 2003;115(3):293-303.

53. Takeda S, Chen DY, Westergard TD, et al. Proteolysis of MLL family proteins is essential for taspase1-orchestrated cell cycle progression. *Genes Dev.* 2006;20(17):2397-2409.
54. Zhou H, Spicuglia S, Hsieh JJ, et al. Uncleaved TFIIA is a substrate for taspase 1 and active in transcription. *Mol Cell Biol.* 2006;26(7):2728-2735.
55. Takeda S, Sasagawa S, Oyama T, et al. Taspase1-dependent TFIIA cleavage coordinates head morphogenesis by limiting Cdkn2a locus transcription. *J Clin Invest.* 2015;125(3):1203-1214.
56. Ng SB, Bigham AW, Buckingham KJ, et al. Exome sequencing identifies MLL2 mutations as a cause of Kabuki syndrome. *Nat Genet.* 2010;42(9):790-793.
57. Aref-Eshghi E, Kerkhof J, Pedro VP, et al. Evaluation of DNA Methylation Episignatures for Diagnosis and Phenotype Correlations in 42 Mendelian Neurodevelopmental Disorders. *Am J Hum Genet.* 2020;106(3):356-370.
58. Al Ojaimi M, Banimortada BJ, Othman A, Riedhammer KM, Almannai M, El-Hattab AW. Disorders of histone methylation: Molecular basis and clinical syndromes. *Clin Genet.* 2022;102(3):169-181.
59. Verbitsky M, Westland R, Perez A, et al. The copy number variation landscape of congenital anomalies of the kidney and urinary tract. *Nat Genet.* 2019;51(1):117-127.
60. Vivante A, Kohl S, Hwang DY, Dworschak GC, Hildebrandt F. Single-gene causes of congenital anomalies of the kidney and urinary tract (CAKUT) in humans. *Pediatr Nephrol.* 2014;29(4):695-704.
61. Kolvenbach CM, Shril S, Hildebrandt F. The genetics and pathogenesis of CAKUT. *Nat Rev Nephrol.* 2023;19(11):709-720.
62. Kagan M, Pleniceanu O, Vivante A. The genetic basis of congenital anomalies of the kidney and urinary tract. *Pediatr Nephrol.* 2022;37(10):2231-2243.
63. Kearney HM, Thorland EC, Brown KK, Quintero-Rivera F, South ST, Working Group of the American College of Medical Genetics Laboratory Quality Assurance C. American College of Medical Genetics standards and guidelines for interpretation and reporting of postnatal constitutional copy number variants. *Genet Med.* 2011;13(7):680-685.
64. Abou Tayoun AN, Pesaran T, DiStefano MT, et al. Recommendations for interpreting the loss of function PVS1 ACMG/AMP variant criterion. *Hum Mutat.* 2018;39(11):1517-1524.
65. https://www.acgs.uk.com/media/11631/uk-practice-guidelines-for-variant-classification-v4-01-2020.pdf. Abgerufen am 25.03.2024.
66. Riedhammer KM, Comic J, Tasic V, et al. Exome sequencing in individuals with congenital anomalies of the kidney and urinary tract (CAKUT): a single-center experience. *Eur J Hum Genet.* 2023;31(6):674-680.
67. van der Ven AT, Connaughton DM, Ityel H, et al. Whole-Exome Sequencing Identifies Causative Mutations in Families with Congenital Anomalies of the Kidney and Urinary Tract. *J Am Soc Nephrol.* 2018;29(9):2348-2361.
68. Murugapoopathy V, Gupta IR. A Primer on Congenital Anomalies of the Kidneys and Urinary Tracts (CAKUT). *Clin J Am Soc Nephrol.* 2020;15(5):723-731.
69. Kume T, Deng K, Hogan BL. Minimal phenotype of mice homozygous for a null mutation in the forkhead/winged helix gene, Mf2. *Mol Cell Biol.* 2000;20(4):1419-1425.
70. https://gnomad.broadinstitute.org. Abgerufen am 25.03.2024.
71. https://www.medrxiv.org/content/10.1101/2023.03.21.23287206v1. Abgerufen am 25.03.2024.
72. Schwartz GJ, Munoz A, Schneider MF, et al. New equations to estimate GFR in children with CKD. *J Am Soc Nephrol.* 2009;20(3):629-637.
73. https://cadd.gs.washington.edu. Abgerufen am 25.03.2024.
74. http://www.clustal.org/clustal2. Abgerufen am 25.03.2024.
75. Riedhammer KM, Nguyen TT, Kosukcu C, et al. Implication of transcription factor FOXD2 dysfunction in syndromic congenital anomalies of the kidney and urinary tract (CAKUT). *Kidney Int.* 2024;105(4):844-864.
76. https://www.ukbiobank.ac.uk. Abgerufen am 25.03.2024.
77. Sheng X, Guan Y, Ma Z, et al. Mapping the genetic architecture of human traits to cell types in the kidney identifies mechanisms of disease and potential treatments. *Nat Genet.* 2021;53(9):1322-1333.
78. Muto Y, Wilson PC, Ledru N, et al. Single cell transcriptional and chromatin accessibility profiling redefine cellular heterogeneity in the adult human kidney. *Nat Commun.* 2021;12(1):2190.
79. http://www.susztaklab.com/human_kidney/igv/. Abgerufen am 25.03.2024.

80. Wu CW, Mann N, Nakayama M, et al. Phenotype expansion of heterozygous FOXC1 pathogenic variants toward involvement of congenital anomalies of the kidneys and urinary tract (CAKUT). *Genet Med.* 2020;22(10):1673-1681.

81. Ernstsson S, Betz R, Lagercrantz S, et al. Cloning and characterization of freac-9 (FKHL17), a novel kidney-expressed human forkhead gene that maps to chromosome 1p32-p34. *Genomics.* 1997;46(1):78-85.

82. Okabe M, Motojima M, Miyazaki Y, Pastan I, Yokoo T, Matsusaka T. Global polysome analysis of normal and injured podocytes. *Am J Physiol Renal Physiol.* 2019;316(2):F241-F252.

83. Wu SC, Grindley J, Winnier GE, Hargett L, Hogan BL. Mouse Mesenchyme forkhead 2 (Mf2): expression, DNA binding and induction by sonic hedgehog during somitogenesis. *Mech Dev.* 1998;70(1-2):3-13.

84. Rothenpieler UW, Dressler GR. Pax-2 is required for mesenchyme-to-epithelium conversion during kidney development. *Development.* 1993;119(3):711-720.

85. Naiman N, Fujioka K, Fujino M, et al. Repression of Interstitial Identity in Nephron Progenitor Cells by Pax2 Establishes the Nephron-Interstitium Boundary during Kidney Development. *Dev Cell.* 2017;41(4):349-365 e343.

86. Torban E, Dziarmaga A, Iglesias D, et al. PAX2 activates WNT4 expression during mammalian kidney development. *J Biol Chem.* 2006;281(18):12705-12712.

87. Stark K, Vainio S, Vassileva G, McMahon AP. Epithelial transformation of metanephric mesenchyme in the developing kidney regulated by Wnt-4. *Nature.* 1994;372(6507):679-683.

88. Tanigawa S, Wang H, Yang Y, et al. Wnt4 induces nephronic tubules in metanephric mesenchyme by a non-canonical mechanism. *Dev Biol.* 2011;352(1):58-69.

89. Puapatanakul P, Miner JH. Alport syndrome and Alport kidney diseases - elucidating the disease spectrum. *Curr Opin Nephrol Hypertens.* 2024;33(3):283-290.

90. Furlano M, Martinez V, Pybus M, et al. Clinical and Genetic Features of Autosomal Dominant Alport Syndrome: A Cohort Study. *Am J Kidney Dis.* 2021;78(4):560-570 e561.

91. Savige J. Should We Diagnose Autosomal Dominant Alport Syndrome When There Is a Pathogenic Heterozygous COL4A3 or COL4A4 Variant? *Kidney Int Rep.* 2018;3(6):1239-1241.

92. Gibson J, Fieldhouse R, Chan MMY, et al. Prevalence Estimates of Predicted Pathogenic COL4A3-COL4A5 Variants in a Population Sequencing Database and Their Implications for Alport Syndrome. *J Am Soc Nephrol.* 2021;32(9):2273-2290.

93. Riedhammer KM, Simmendinger H, Tasic V, et al. Is there a dominant-negative effect in individuals with heterozygous disease-causing variants in COL4A3/COL4A4? *Clin Genet.* 2024;105(4):406-414.

94. Solanki KV, Hu Y, Moore BS, et al. The Phenotypic Spectrum of COL4A3 Heterozygotes. *medRxiv.* 2023.

95. Gibson JT, Huang M, Shenelli Croos Dabrera M, et al. Genotype-phenotype correlations for COL4A3-COL4A5 variants resulting in Gly substitutions in Alport syndrome. *Sci Rep.* 2022;12(1):2722.

96. Savige J, Huang M, Croos Dabrera MS, Shukla K, Gibson J. Genotype-Phenotype Correlations for Pathogenic COL4A3-COL4A5 Variants in X-Linked, Autosomal Recessive, and Autosomal Dominant Alport Syndrome. *Front Med (Lausanne).* 2022;9:865034.

97. Steiner RD, Basel D. COL1A1/2 Osteogenesis Imperfecta. In: Adam MP, Feldman J, Mirzaa GM, et al., eds. *GeneReviews((R)).* Seattle (WA)2024.

98. Heeringa SF, Chernin G, Chaki M, et al. COQ6 mutations in human patients produce nephrotic syndrome with sensorineural deafness. *J Clin Invest.* 2011;121(5):2013-2024.

99. McNeill A. The complex genomics of single gene disorders. *Eur J Hum Genet.* 2023;31(6):609-610.

Publikationsverzeichnis

Kumulativer Impact-Faktor, Stand 04/2024 (nach Journal Citation Reports 2022, publiziert 06/2023):

336,0.

<u>Originalarbeiten als Erstautor</u>

1. **Riedhammer KM**, Simmendinger H, Tasic V, Putnik J, Abazi-Emini N, Stajic N, Berutti R, Weidenbusch M, Patzer L, Lungu A, Milosevski-Lomic G, Günthner R, Braunisch MC, Ćomić J, Hoefele J. Is there a dominant-negative effect in individuals with heterozygous disease-causing variants in *COL4A3/COL4A4*? *Clin Genet.* 2024 Apr;105(4):406-414. doi: 10.1111/cge.14471. Epub 2024 Jan 12. PMID: 38214412. Impact-Faktor 3,5.

2. **Riedhammer KM***, Nguyen TT, Koşukcu C, Calzada-Wack J, Li Y, Assia Batzir N, Saygılı S, Wimmers V, Kim GJ, Chrysanthou M, Bakey Z, Sofrin-Drucker E, Kraiger M, Sanz-Moreno A, Amarie OV, Rathkolb B, Klein-Rodewald T, Garrett L, Hölter SM, Seisenberger C, Haug S, Schlosser P, Marschall S, Wurst W, Fuchs H, Gailus-Durner V, Wuttke M, Hrabe de Angelis M, Ćomić J, Akgün Doğan Ö, Özlük Y, Taşdemir M, Ağbaş A, Canpolat N, Orenstein N, Çalışkan S, Weber RG, Bergmann C, Jeanpierre C, Saunier S, Lim TY, Hildebrandt F, Alhaddad B, Basel-Salmon L, Borovitz Y, Wu K, Antony D, Matschkal J, Schaaf CW, Renders L, Schmaderer C, Rogg M, Schell C, Meitinger T, Heemann U, Köttgen A, Arnold SJ, Ozaltin F, Schmidts M, Hoefele J. Implication of transcription factor FOXD2 dysfunction in syndromic congenital anomalies of the kidney and urinary tract (CAKUT). *Kidney Int.* 2024 Apr;105(4):844-864. doi: 10.1016/j.kint.2023.11.032. Epub 2023 Dec 26. PMID: 38154558; PMCID: PMC10957342. **geteilte Erstautorenschaft*. Impact-Faktor 19,6.

3. **Riedhammer KM**, Ćomić J, Tasic V, Putnik J, Abazi-Emini N, Paripovic A, Stajic N, Meitinger T, Nushi-Stavileci V, Berutti R, Braunisch MC, Hoefele J. Exome sequencing in individuals with congenital anomalies of the kidney and urinary tract (CAKUT): a single-center experience. *Eur J Hum Genet*. 2023 Jun;31(6):674-680. doi: 10.1038/s41431-023-01331-x. Epub 2023 Mar 16. PMID:36922632; PMCID: PMC10250376. Impact-Faktor 5,2.

4. Najafi M, **Riedhammer KM***, Rad A, Torbati PN, Berutti R, Schüle I, Schroda S, Meitinger T, Ćomić J, Bojd SS, Baranzehi T, Shojaei A, Azarfar A, Khazaei MR, Köttgen A, Backofen R, Karimiani EG, Hoefele J, Schmidts M. High detection rate for disease-causing variants in a cohort of 30 Iranian pediatric steroid resistant nephrotic syndrome cases. *Front Pediatr*. 2022 Sep 22;10:974840. doi: 10.3389/fped.2022.974840. PMID: 36245711; PMCID: PMC9555279. **geteilte Erstautorenschaft*. Impact-Faktor 2,6.

5. **Riedhammer KM**, Burgemeister AL, Cantagrel V, Amiel J, Siquier-Pernet K, Boddaert N, Hertecant J, Kannouche PL, Pouvelle C, Htun S, Slavotinek AM, Beetz C, Diego-Alvarez D, Kampe K, Fleischer N, Awamleh Z, Weksberg R, Kopajtich R, Meitinger T, Suleiman J, El-Hattab AW. Suleiman-El-Hattab syndrome: a histone modification disorder caused by TASP1 deficiency. *Hum Mol Genet*. 2022 Sep 10;31(18):3083-3094. doi: 10.1093/hmg/ddac098. PMID: 35512351; PMCID:PMC9476618. Impact-Faktor 3,5.

6. Stippel M, **Riedhammer KM***, Lange-Sperandio B, Geßner M, Braunisch MC, Günthner R, Bald M, Schmidts M, Strotmann P, Tasic V, Schmaderer C, Renders L, Heemann U, Hoefele J. Renal and Skeletal Anomalies in a Cohort of Individuals With Clinically Presumed Hereditary Nephropathy Analyzed by Molecular Genetic Testing. *Front Genet*. 2021 May 26;12:642849. doi: 10.3389/fgene.2021.642849. PMID: 34122504; PMCID: PMC8188481. **geteilte Erstautorenschaft.* Impact-Faktor 3,7.

7. **Riedhammer KM**, Stockler S, Ploski R, Wenzel M, Adis-Dutschmann B, Ahting U, Alhaddad B, Blaschek A, Haack TB, Kopajtich R, Lee J, Murcia Pienkowski V, Pollak A, Szymanska K, Tarailo-Graovac M, van der Lee R, van Karnebeek CD, Meitinger T, Krägeloh-Mann I, Vill K. *De novo* stop-loss variants in *CLDN11* cause hypomyelinating leukodystrophy. *Brain*. 2021 Mar 3;144(2):411-419. doi: 10.1093/brain/awaa410. Erratum in: *Brain*. 2021 Jun 22;144(5):e48. PMID: 33313762; PMCID: PMC7940174. Impact-Faktor 14,5.

8. **Riedhammer KM**, Braunisch MC, Günthner R, Wagner M, Hemmer C, Strom TM, Schmaderer C, Renders L, Tasic V, Gucev Z, Nushi-Stavileci V, Putnik J, Stajić N, Weidenbusch M, Uetz B, Montoya C, Strotmann P, Ponsel S, Lange-Sperandio B, Hoefele J. Exome Sequencing and Identification of Phenocopies in Patients With Clinically Presumed Hereditary Nephropathies. *Am J Kidney Dis*. 2020 Oct;76(4):460-470. doi: 10.1053/j.ajkd.2019.12.008. Epub 2020 Apr 28. PMID: 32359821. Impact-Faktor 13,2.

9. Suleiman J, **Riedhammer KM***, Jicinsky T, Mundt M, Werner L, Gusic M, Burgemeister AL, Alsaif HS, Abdulrahim M, Moghrabi NN, Nicolas-Jilwan M, AlSayed M, Bi W, Sampath S, Alkuraya FS, El-Hattab AW. Homozygous loss-of-function variants of *TASP1*, a gene encoding an activator of the histone methyltransferases KMT2A and KMT2D, cause a syndrome of developmental delay, happy demeanor, distinctive facial features, and congenital anomalies. *Hum Mutat*. 2019 Nov;40(11):1985-1992. doi: 10.1002/humu.23844. Epub 2019 Jul 22. PMID: 31209944. **geteilte Erstautorenschaft*. Impact-Faktor 3,9.

Originalarbeiten als Ko-Autor

1. Schönauer R, Jin W, Findeisen C, Valenzuela I, Devlin LA, Murrell J, Bedoukian EC, Pöschla L, Hantmann E, **Riedhammer KM**, Hoefele J, Platzer K, Biemann R, Campeau PM, Münch J, Heyne H, Hoffmann A, Ghosh A, Sun W, Dong H, Noé F, Wolfrum C, Woods E, Parker MJ, Neatu R, Le Guyader G, Bruel AL, Perrin L, Spiewak H; Genomics England Research Consortium; Missotte I, Fourgeaud M, Michaud V, Lacombe D, Paolucci SA, Buchan JG, Glissmeyer M, Popp B, Blüher M, Sayer JA, Halbritter J. Monoallelic intragenic *POU3F2* variants lead to neurodevelopmental delay and hyperphagic obesity, confirming the gene's candidacy in 6q16.1 deletions. *Am J Hum Genet.* 2023 Jun 1;110(6):998-1007. doi: 10.1016/j.ajhg.2023.04.010. Epub 2023 May 18. PMID: 37207645; PMCID: PMC10257002. Impact-Faktor 9,8.

2. Patterson V, Ullah F, Bryant L, Griffin JN, Sidhu A, Saliganan S, Blaile M, Saenz MS, Smith R, Ellingwood S, Grange DK, Hu X, Mireguli M, Luo Y, Shen Y, Mulhern M, Zackai E, Ritter A, Izumi K, Hoefele J, Wagner M, **Riedhammer KM**, Seitz B, Robin NH, Goodloe D, Mignot C, Keren B, Cox H, Jarvis J, Hempel M, Gibson CF, Tran Mau-Them F, Vitobello A, Bruel AL, Sorlin A, Mehta S, Raymond FL, Gilmore K, Powell BC, Weck K, Li C, Vulto-van Silfhout AT, Giacomini T, Mancardi MM, Accogli A, Salpietro V, Zara F, Vora NL, Davis EE, Burdine R, Bhoj E. Abrogation of MAP4K4 protein function causes congenital anomalies in humans and zebrafish. *Sci Adv.* 2023 Apr 28;9(17):eade0631. doi: 10.1126/sciadv.ade0631. Epub 2023 Apr 26. Erratum in: *Sci Adv.* 2023 Nov 24;9(47):eadl5515. PMID: 37126546; PMCID: PMC10132768. Impact-Faktor 13,6.

3. Günthner R, Knipping L, Jeruschke S, Satanoskij R, Lorenz-Depiereux B, Hemmer C, Braunisch MC, **Riedhammer KM**, Ćomić J, Tönshoff B, Tasic V, Abazi-Emini N, Nushi-Stavileci V, Buiting K, Gjorgjievski N, Momirovska A, Patzer L, Kirschstein M, Gross O, Lungu A, Weber S, Renders L, Heemann U, Meitinger T, Büscher AK, Hoefele J. Renal X-inactivation in female individuals with X-linked Alport syndrome primarily determined by age. *Front Med* (Lausanne). 2022 Oct 20;9:953643. doi: 10.3389/fmed.2022.953643. PMID: 36341250; PMCID: PMC9630586. Impact-Faktor 3,9.

4. Ćomić J, **Riedhammer KM**, Günthner R, Schaaf CW, Richthammer P, Simmendinger H, Kieffer D, Berutti R, Tasic V, Abazi-Emini N, Nushi-Stavileci V, Putnik J, Stajic N, Lungu A, Gross O, Renders L, Heemann U, Braunisch MC, Meitinger T, Hoefele J. The multifaceted phenotypic and genotypic spectrum of type-IV-collagen- related nephropathy - A human genetics department experience. *Front Med* (Lausanne). 2022 Aug 31;9:957733. doi: 10.3389/fmed.2022.957733. PMID: 36117978; PMCID: PMC9470833. Impact-Faktor 3,9.

5. Drovandi S, Lipska-Ziętkiewicz BS, Ozaltin F, Emma F, Gulhan B, Boyer O, Trautmann A, Xu H, Shen Q, Rao J, **Riedhammer KM**, Heemann U, Hoefele J, Stenton SL, Tsygin AN, Ng KH, Fomina S, Benetti E, Aurelle M, Prikhodina L, Schreuder MF, Tabatabaeifar M, Jankowski M, Baiko S, Mao J, Feng C, Liu C, Sun S, Deng F, Wang X, Clavé S, Stańczyk M, Bałasz-Chmielewska I, Fila M, Durkan AM, Levart TK, Dursun I, Esfandiar N, Haas D, Bjerre A, Anarat A, Benz MR, Talebi S, Hooman N, Ariceta G; PodoNet Consortium; mitoNET Consortium; CCGKDD Consortium; Schaefer F. Oral Coenzyme Q10 supplementation leads to better preservation of kidney function in steroid-resistant nephrotic syndrome due to primary Coenzyme Q10 deficiency. *Kidney Int*. 2022 Sep;102(3):604-612. doi: 10.1016/j.kint.2022.04.029. Epub 2022 May 25. PMID: 35643375. Impact-Faktor 19,6.

6. Drovandi S, Lipska-Ziętkiewicz BS, Ozaltin F, Emma F, Gulhan B, Boyer O, Trautmann A, Ziętkiewicz S, Xu H, Shen Q, Rao J, **Riedhammer KM**, Heemann U, Hoefele J, Stenton SL, Tsygin AN, Ng KH, Fomina S, Benetti E, Aurelle M, Prikhodina L, Schijvens AM, Tabatabaeifar M, Jankowski M, Baiko S, Mao J, Feng C, Deng F, Rousset-Rouviere C, Stańczyk M, Bałasz-Chmielewska I, Fila M, Durkan AM, Levart TK, Dursun I, Esfandiar N, Haas D, Bjerre A, Anarat A, Benz MR, Talebi S, Hooman N, Ariceta G; PodoNet Consortium; mitoNET Consortium; CCGKDD Consortium; Schaefer F. Variation of the clinical spectrum and genotype-phenotype associations in Coenzyme Q10 deficiency associated glomerulopathy. *Kidney Int*. 2022 Sep;102(3):592-603. doi: 10.1016/j.kint.2022.02.040. Epub 2022 Apr 26. PMID: 35483523. Impact-Faktor 19,6.

7. Breuer K, **Riedhammer KM**, Müller N, Schaidinger B, Dombrowsky G, Dittrich S, Zeidler S, Bauer UMM, Westphal DS, Meitinger T, Dakal TC, Hitz MP, Breuer J, Reutter H, Hilger AC, Hoefele J. Exome sequencing in individuals with cardiovascular laterality defects identifies potential candidate genes. *Eur J Hum Genet*. 2022 Aug;30(8):946-954. doi: 10.1038/s41431-022-01100-2. Epub 2022 Apr 26. PMID: 35474353; PMCID: PMC9349204. Impact-Faktor 5,2.

8. Weng R, Nenning KH, Schwarz M, **Riedhammer KM**, Brunet T, Wagner M, Kasprian G, Lehrner J, Zimprich F, Bonelli SB, Krenn M. Connectome Analysis in an Individual with *SETD1B*-Related Neurodevelopmental Disorder and Epilepsy. *J Dev Behav Pediatr*. 2022 Aug 1;43(6):e419-e422. doi: 10.1097/DBP.0000000000001079. Epub 2022 Apr 6. PMID: 35385430. Impact-Faktor 2,4.

9. Boeckhaus J, Hoefele J, **Riedhammer KM**, Nagel M, Beck BB, Choi M, Gollasch M, Bergmann C, Sonntag JE, Troesch V, Stock J, Gross O. Lifelong effect of therapy in young patients with the *COL4A5* Alport missense variant p.(Gly624Asp): a prospective cohort study. *Nephrol Dial Transplant*. 2022 Nov 23;37(12):2496-2504. doi: 10.1093/ndt/gfac006. PMID: 35022790. Impact-Faktor 6,1.

10. Westphal DS, Mastantuono E, Seidel H, **Riedhammer KM**, Hahn A, Vill K, Wagner M. There is more to it than just congenital heart defects - The phenotypic spectrum of *TAB2*-related syndrome. *Gene*. 2022 Mar 10;814:146167. doi: 10.1016/j.gene.2021.146167. Epub 2022 Jan 5. PMID: 34995729. Impact-Faktor 3,5.

11. Dworschak GC, Punetha J, Kalanithy JC, Mingardo E, Erdem HB, Akdemir ZC, Karaca E, Mitani T, Marafi D, Fatih JM, Jhangiani SN, Hunter JV, Dakal TC, Dhabhai B, Dabbagh O, Alsaif HS, Alkuraya FS, Maroofian R, Houlden H, Efthymiou S, Dominik N, Salpietro V, Sultan T, Haider S, Bibi F, Thiele H, Hoefele J, **Riedhammer KM**, Wagner M, Guella I, Demos M, Keren B, Buratti J, Charles P, Nava C, Héron D, Heide S, Valkanas E, Waddell LB, Jones KJ, Oates EC, Cooper ST, MacArthur D, Syrbe S, Ziegler A, Platzer K, Okur V, Chung WK, O'Shea SA, Alcalay R, Fahn S, Mark PR, Guerrini R, Vetro A,

Hudson B, Schnur RE, Hoganson GE, Burton JE, McEntagart M, Lindenberg T, Yilmaz Ö, Odermatt B, Pehlivan D, Posey JE, Lupski JR, Reutter H. Biallelic and monoallelic variants in *PLXNA1* are implicated in a novel neurodevelopmental disorder with variable cerebral and eye anomalies. *Genet Med.* 2021 Sep;23(9):1715-1725. doi: 10.1038/s41436-021-01196-9. Epub 2021 May 30. PMID: 34054129; PMCID: PMC8460429. Impact-Faktor 8,8.

12. Burns W, Bird LM, Heron D, Keren B, Ramachandra D, Thiffault I, Del Viso F, Amudhavalli S, Engleman K, Parenti I, Kaiser FJ, Wierzba J, **Riedhammer KM**, Liptay S, Zadeh N, Porrmann J, Fischer A, Gößwein S, McLaughlin HM, Telegrafi A, Langley KG, Steet R, Louie RJ, Lyons MJ. Syndromic neurodevelopmental disorder associated with *de novo* variants in *DDX23*. *Am J Med Genet A.* 2021 Oct;185(10):2863-2872. doi: 10.1002/ajmg.a.62359. Epub 2021 May 29. PMID: 34050707. Impact-Faktor 2,0.

13. Brunet T, Jech R, Brugger M, Kovacs R, Alhaddad B, Leszinski G, **Riedhammer KM**, Westphal DS, Mahle I, Mayerhanser K, Skorvanek M, Weber S, Graf E, Berutti R, Necpál J, Havránková P, Pavelekova P, Hempel M, Kotzaeridou U, Hoffmann GF, Leiz S, Makowski C, Roser T, Schroeder SA, Steinfeld R, Strobl-Wildemann G, Hoefele J, Borggraefe I, Distelmaier F, Strom TM, Winkelmann J, Meitinger T, Zech M, Wagner M. *De novo* variants in neurodevelopmental disorders-experiences from a tertiary care center. *Clin Genet.* 2021 Jul;100(1):14-28. doi: 10.1111/cge.13946. Epub 2021 Mar 1. PMID: 33619735. Impact-Faktor 3,5.

14. Weng PL, Majmundar AJ, Khan K, Lim TY, Shril S, Jin G, Musgrove J, Wang M, Ahram DF, Aggarwal VS, Bier LE, Heinzen EL, Onuchic-Whitford AC, Mann N, Buerger F, Schneider R, Deutsch K, Kitzler TM, Klämbt V, Kolb A, Mao Y, Moufawad El Achkar C, Mitrotti A, Martino J, Beck BB, Altmüller J, Benz MR, Yano S, Mikati MA, Gunduz T, Cope H, Shashi V; Undiagnosed Diseases Network; Trachtman H, Bodria M, Caridi G, Pisani I, Fiaccadori E, AbuMaziad AS, Martinez-Agosto JA, Yadin O, Zuckerman J, Kim A; UCLA Clinical Genomics Center; John-Kroegel U, Tyndall AV, Parboosingh JS, Innes AM, Bierzynska A, Koziell AB, Muorah M, Saleem MA, Hoefele J, **Riedhammer KM**,

Gharavi AG, Jobanputra V, Pierce-Hoffman E, Seaby EG, O'Donnell-Luria A, Rehm HL, Mane S, D'Agati VD, Pollak MR, Ghiggeri GM, Lifton RP, Goldstein DB, Davis EE, Hildebrandt F, Sanna-Cherchi S. *De novo TRIM8* variants impair its protein localization to nuclear bodies and cause developmental delay, epilepsy, and focal segmental glomerulosclerosis. *Am J Hum Genet.* 2021 Feb 4;108(2):357-367. doi: 10.1016/j.ajhg.2021.01.008. Epub 2021 Jan 27. PMID: 33508234; PMCID: PMC7895901. Impact-Faktor 9,8.

15. Schneider R, Deutsch K, Hoeprich GJ, Marquez J, Hermle T, Braun DA, Seltzsam S, Kitzler TM, Mao Y, Buerger F, Majmundar AJ, Onuchic-Whitford AC, Kolvenbach CM, Schierbaum L, Schneider S, Halawi AA, Nakayama M, Mann N, Connaughton DM, Klämbt V, Wagner M, **Riedhammer KM**, Renders L, Katsura Y, Thumkeo D, Soliman NA, Mane S, Lifton RP, Shril S, Khokha MK, Hoefele J, Goode BL, Hildebrandt F. *DAAM2* Variants Cause Nephrotic Syndrome via Actin Dysregulation. *Am J Hum Genet.* 2020 Dec 3;107(6):1113-1128. doi: 10.1016/j.ajhg.2020.11.008. Epub 2020 Nov 23. PMID: 33232676; PMCID: PMC7820625. Impact-Faktor 9,8.

16. Begemann A, Sticht H, Begtrup A, Vitobello A, Faivre L, Banka S, Alhaddad B, Asadollahi R, Becker J, Bierhals T, Brown KE, Bruel AL, Brunet T, Carneiro M, Cremer K, Day R, Denommé-Pichon AS, Dyment DA, Engels H, Fisher R, Goh ES, Hajianpour MJ, Haertel LRM, Hauer N, Hempel M, Herget T, Johannsen J, Kraus C, Le Guyader G, Lesca G, Mau-Them FT, McDermott JH, McWalter K, Meyer P, Õunap K, Popp B, Reimand T, **Riedhammer KM**, Russo M, Sadleir LG, Saenz M, Schiff M, Schuler E, Syrbe S, Van der Ven AT, Verloes A, Willems M, Zweier C, Steindl K, Zweier M, Rauch A. New insights into the clinical and molecular spectrum of the novel *CYFIP2*-related neurodevelopmental disorder and impairment of the WRC-mediated actin dynamics. *Genet Med.* 2021 Mar;23(3):543-554. doi: 10.1038/s41436-020-01011-x. Epub 2020 Nov 5. PMID: 33149277; PMCID: PMC7935717. Impact-Faktor 8,8.

17. Zech M, Jech R, Boesch S, Škorvánek M, Weber S, Wagner M, Zhao C, Jochim A, Necpál J, Dincer Y, Vill K, Distelmaier F, Stoklosa M, Krenn M, Grunwald S, Bock-Bierbaum T, Fečíková A, Havránková P, Roth J, Příhodová I, Adamovičová M, Ulmanová O, Bechyně K, Danhofer P, Veselý B, Haň V, Pavelekova P, Gdovinová Z, Mantel T, Meindl T, Sitzberger A, Schröder S, Blaschek A, Roser T, Bonfert MV, Haberlandt E, Plecko B, Leineweber B, Berweck S, Herberhold T, Langguth B, Švantnerová J, Minár M, Ramos-Rivera GA, Wojcik MH, Pajusalu S, Õunap K, Schatz UA, Pölsler L, Milenkovic I, Laccone F, Pilshofer V, Colombo R, Patzer S, Iuso A, Vera J, Troncoso M, Fang F, Prokisch H, Wilbert F, Eckenweiler M, Graf E, Westphal DS, **Riedhammer KM**, Brunet T, Alhaddad B, Berutti R, Strom TM, Hecht M, Baumann M, Wolf M, Telegrafi A, Person RE, Zamora FM, Henderson LB, Weise D, Musacchio T, Volkmann J, Szuto A, Becker J, Cremer K, Sycha T, Zimprich F, Kraus V, Makowski C, Gonzalez-Alegre P, Bardakjian TM, Ozelius LJ, Vetro A, Guerrini R, Maier E, Borggraefe I, Kuster A, Wortmann SB, Hackenberg A, Steinfeld R, Assmann B, Staufner C, Opladen T, Růžička E, Cohn RD, Dyment D, Chung WK, Engels H, Ceballos-Baumann A, Ploski R, Daumke O, Haslinger B, Mall V, Oexle K, Winkelmann J. Monogenic variants in dystonia: an exome-wide sequencing study. *Lancet Neurol*. 2020 Nov;19(11):908-918. doi: 10.1016/S1474-4422(20)30312-4. PMID: 33098801; PMCID: PMC8246240. Impact-Faktor 48,0.

18. Boeckhaus J, Hoefele J, **Riedhammer KM**, Tönshoff B, Ehren R, Pape L, Latta K, Fehrenbach H, Lange-Sperandio B, Kettwig M, Hoyer P, Staude H, Konrad M, John U, Gellermann J, Hoppe B, Galiano M, Gessner M, Pohl M, Bergmann C, Friede T, Gross O; GPN Study Group and EARLY PRO-TECT Alport Investigators. Precise variant interpretation, phenotype ascertainment, and genotype-phenotype correlation of children in the EARLY PRO-TECT Alport trial. *Clin Genet*. 2021 Jan;99(1):143-156. doi: 10.1111/cge.13861. Epub 2020 Oct 25. PMID: 33040356. Impact-Faktor 3,5.

19. Braunisch MC, **Riedhammer KM**, Herr PM, Draut S, Günthner R, Wagner M, Weidenbusch M, Lungu A, Alhaddad B, Renders L, Strom TM, Heemann U, Meitinger T, Schmaderer C, Hoefele J. Identification of disease-causing variants by comprehensive genetic testing with exome sequencing in adults with suspicion of hereditary FSGS. *Eur J Hum Genet.* 2021 Feb;29(2):262-270. doi: 10.1038/s41431-020-00719-3. Epub 2020 Sep 4. PMID: 32887937; PMCID: PMC7868362. Impact-Faktor 5,2.

20. Zhang R, Gehlen J, Kawalia A, Melissari MT, Dakal TC, Menon AM, Höfele J, **Riedhammer K**, Waffenschmidt L, Fabian J, Breuer K, Kalanithy J, Hilger AC, Sharma A, Hölscher A, Boemers TM, Pauly M, Leutner A, Fuchs J, Seitz G, Ludwikowski BM, Gomez B, Hubertus J, Heydweiller A, Kurz R, Leonhardt J, Kosch F, Holland-Cunz S, Münsterer O, Ure B, Schmiedeke E, Neser J, Degenhardt P, Märzheuser S, Kleine K, Schäfer M, Spychalski N, Deffaa OJ, Gosemann JH, Lacher M, Heilmann-Heimbach S, Zwink N, Jenetzky E, Ludwig M, Grote P, Schumacher J, Thiele H, Reutter H. Human exome and mouse embryonic expression data implicate *ZFHX3*, *TRPS1*, and *CHD7* in human esophageal atresia. *PLoS One.* 2020 Jun 5;15(6):e0234246. doi: 10.1371/journal.pone.0234246. PMID: 32502225; PMCID: PMC7274392. Impact-Faktor 3,7.

21. Kummeling J, Stremmelaar DE, Raun N, Reijnders MRF, Willemsen MH, Ruiterkamp-Versteeg M, Schepens M, Man CCO, Gilissen C, Cho MT, McWalter K, Sinnema M, Wheless JW, Simon MEH, Genetti CA, Casey AM, Terhal PA, van der Smagt JJ, van Gassen KLI, Joset P, Bahr A, Steindl K, Rauch A, Keller E, Raas- Rothschild A, Koolen DA, Agrawal PB, Hoffman TL, Powell-Hamilton NN, Thiffault I, Engleman K, Zhou D, Bodamer O, Hoefele J, **Riedhammer KM**, Schwaibold EMC, Tasic V, Schubert D, Top D, Pfundt R, Higgs MR, Kramer JM, Kleefstra T. Characterization of *SETD1A* haploinsufficiency in humans and Drosophila defines a novel neurodevelopmental syndrome. *Mol Psychiatry.* 2021 Jun;26(6):2013-2024. doi: 10.1038/s41380-020-0725-5. Epub 2020 Apr 28. PMID: 32346159. Impact-Faktor 11,0.

22. Lorenz G, Schul L, Schraml F, **Riedhammer KM**, Einwächter H, Verbeek M, Slotta-Huspenina J, Schmaderer C, Küchle C, Heemann U, Moog P. Adult macrophage activation syndrome-haemophagocytic lymphohistiocytosis: 'of plasma exchange and immunosuppressive escalation strategies' - a single centre reflection. *Lupus.* 2020 Mar;29(3):324-333. doi: 10.1177/0961203320901594. Epub 2020 Feb 3. PMID: 32013725. Impact-Faktor 2,6.

23. Hughes JJ, Alkhunaizi E, Kruszka P, Pyle LC, Grange DK, Berger SI, Payne KK, Masser-Frye D, Hu T, Christie MR, Clegg NJ, Everson JL, Martinez AF, Walsh LE, Bedoukian E, Jones MC, Harris CJ, **Riedhammer KM**, Choukair D, Fechner PY, Rutter MM, Hufnagel SB, Roifman M, Kletter GB, Delot E, Vilain E, Lipinski RJ, Vezina CM, Muenke M, Chitayat D. Loss-of-Function Variants in *PPP1R12A*: From Isolated Sex Reversal to Holoprosencephaly Spectrum and Urogenital Malformations. *Am J Hum Genet.* 2020 Jan 2;106(1):121-128. doi: 10.1016/j.ajhg.2019.12.004. Epub 2019 Dec 26. PMID: 31883643; PMCID: PMC7042489. Impact-Faktor 9,8.

24. Staufner C, Peters B, Wagner M, Alameer S, Barić I, Broué P, Bulut D, Church JA, Crushell E, Dalgıç B, Das AM, Dick A, Dikow N, Dionisi-Vici C, Distelmaier F, Bozbulut NE, Feillet F, Gonzales E, Hadzic N, Hauck F, Hegarty R, Hempel M, Herget T, Klein C, Konstantopoulou V, Kopajtich R, Kuster A, Laass MW, Lainka E, Larson-Nath C, Leibner A, Lurz E, Mayr JA, McKiernan P, Mention K, Moog U, Mungan NO, **Riedhammer KM**, Santer R, Palafoll IV, Vockley J, Westphal DS, Wiedemann A, Wortmann SB, Diwan GD, Russell RB, Prokisch H, Garbade SF, Kölker S, Hoffmann GF, Lenz D. Defining clinical subgroups and genotype-phenotype correlations in NBAS-associated disease across 110 patients. *Genet Med.* 2020 Mar;22(3):610-621. doi: 10.1038/s41436-019-0698-4. Epub 2019 Nov 25. PMID: 31761904. Impact-Faktor 8,8.

74

25. Zweier M, Begemann A, McWalter K, Cho MT, Abela L, Banka S, Behring B, Berger A, Brown CW, Carneiro M, Chen J, Cooper GM; Deciphering Developmental Disorders (DDD) Study; Finnila CR, Guillen Sacoto MJ, Henderson A, Hüffmeier U, Joset P, Kerr B, Lesca G, Leszinski GS, McDermott JH, Meltzer MR, Monaghan KG, Mostafavi R, Õunap K, Plecko B, Powis Z, Purcarin G, Reimand T, **Riedhammer KM**, Schreiber JM, Sirsi D, Wierenga KJ, Wojcik MH, Papuc SM, Steindl K, Sticht H, Rauch A. Spatially clustering *de novo* variants in *CYFIP2*, encoding the cytoplasmic FMRP interacting protein 2, cause intellectual disability and seizures. *Eur J Hum Genet*. 2019 May;27(5):747-759. doi: 10.1038/s41431-018-0331-z. Epub 2019 Jan 21. PMID: 30664714; PMCID: PMC6461771. Impact-Faktor 5,2.

26. Braunisch MC, Büttner-Herold M, Günthner R, Satanovskij R, **Riedhammer KM**, Herr PM, Klein HG, Wahl D, Küchle C, Renders L, Heemann U, Schmaderer C, Hoefele J. Heterozygous *COL4A3* Variants in Histologically Diagnosed Focal Segmental Glomerulosclerosis. *Front Pediatr*. 2018 Jun 12;6:171. doi: 10.3389/fped.2018.00171. PMID: 29946535; PMCID: PMC6007128. Impact-Faktor 2,6.

Sonstige Publikationen (Case Reports, Reviews)

1. Al Ojaimi M, Banimortada BJ, Othman A, **Riedhammer KM**, Almannai M, El-Hattab AW. Disorders of histone methylation: Molecular basis and clinical syndromes. *Clin Genet.* 2022 Sep;102(3):169-181. doi: 10.1111/cge.14181. Epub 2022 Jul 6. PMID: 35713103. Impact-Faktor 3,5.

2. Krenn M, Kepa S, Kasprian G, **Riedhammer KM**, Wagner M, Goedl-Fleischhacker U, Milenkovic I. A *de novo* truncating variant in *CSDE1* in an adult-onset neuropsychiatric phenotype without intellectual disability. *Eur J Med Genet.* 2022 Mar;65(3):104423. doi: 10.1016/j.ejmg.2022.104423. Epub 2022 Jan 11. PMID: 35026469. Impact-Faktor 1,9.

3. Hüllen A, Falkenstein K, Weigel C, Huidekoper H, Naumann-Bartsch N, Spenger J, Feichtinger RG, Schaefers J, Frenz S, Kotlarz D, Momen T, Khoshnevisan R, **Riedhammer KM**, Santer R, Herget T, Rennings A, Lefeber DJ, Mayr JA, Thiel C, Wortmann SB. Congenital disorders of glycosylation with defective fucosylation. *J Inherit Metab Dis.* 2021 Nov;44(6):1441-1452. doi: 10.1002/jimd.12426. Epub 2021 Sep 15. PMID: 34389986. Impact-Faktor 4,2.

4. Radelfahr F, **Riedhammer KM**, Keidel LF, Gramer G, Meitinger T, Klopstock T, Wagner M. Biotinidase deficiency: A treatable cause of hereditary spastic paraparesis. *Neurol Genet.* 2020 Oct 13;6(6):e525. doi: 10.1212/NXG.0000000000000525. PMID: 33134520; PMCID: PMC7577526. Impact-Faktor 3,1.

5. Finsterer J, Stöllberger C, Hasun M, **Riedhammer K**, Wagner M. Multisystem Myotilinopathy, including Myopathy and Left Ventricular Noncompaction, due to the *MYOT* Variant c.179C>T. *Case Rep Cardiol.* 2020 May 13;2020:5128069. doi: 10.1155/2020/5128069. PMID: 32509353; PMCID: PMC7244945. Kein Impact-Faktor.

76

6. Klinner J, Krüger M, Brunet T, Makowski C, **Riedhammer KM**, Mollweide A, Wagner M, Hoefele J. Congenital lymphedema as a rare and first symptom of tuberous sclerosis complex. *Gene*. 2020 Aug 30;753:144815. doi: 10.1016/j.gene.2020.144815. Epub 2020 May 29. PMID: 32479982. Impact-Faktor 3,5.

7. Macheroux EP, Braunisch MC, Pucci Pegler S, Satanovskij R, **Riedhammer KM**, Günthner R, Gross O, Nagel M, Renders L, Hoefele J. The Hypomorphic Variant p.(Gly624Asp) in *COL4A5* as a Possible Cause for an Unexpected Severe Phenotype in a Family With X-Linked Alport Syndrome. *Front Pediatr*. 2019 Nov 26;7:485. doi: 10.3389/fped.2019.00485. PMID: 31850286; PMCID: PMC6887795. Impact-Faktor 2,6.

8. **Riedhammer KM**, Leszinski GS, Andres S, Strobl-Wildemann G, Wagner M. First replication that biallelic variants in *FITM2* cause a complex deafness-dystonia syndrome. *Mov Disord*. 2018 Oct;33(10):1665-1666. doi: 10.1002/mds.27481. Epub 2018 Oct 4. PMID: 30288795. Impact-Faktor 8,6.

9. Westphal DS, **Riedhammer KM**, Kovacs-Nagy R, Meitinger T, Hoefele J, Wagner M. A *De Novo* Missense Variant in *POU3F2* Identified in a Child with Global Developmental Delay. *Neuropediatrics*. 2018 Dec;49(6):401-404. doi: 10.1055/s-0038-1669926. Epub 2018 Sep 10. PMID: 30199896. Impact-Faktor 1,4.

10. Thiel C, Wortmann S, **Riedhammer K**, Alhaddad B, Mayatepek E, Prokisch H, Distelmaier F. Severe ichthyosis in MPDU1-CDG. *J Inherit Metab Dis*. 2018 Nov;41(6):1293-1294. doi: 10.1007/s10545-018-0189-9. Epub 2018 May 2. PMID: 29721919. Impact-Faktor 4,2.

11. **Riedhammer KM**, Siegel C, Alhaddad B, Montoya C, Kovacs-Nagy R, Wagner M, Meitinger T, Hoefele J. Identification of a Novel Heterozygous *De Novo* 7-bp Frameshift Deletion in *PBX1* by Whole-Exome Sequencing Causing a Multi-Organ Syndrome Including Bilateral Dysplastic Kidneys and Hypoplastic Clavicles. *Front Pediatr*. 2017 Nov 24;5:251. doi: 10.3389/fped.2017.00251. PMID: 29226118; PMCID: PMC5705563. Impact-Faktor 2,6.

Lebenslauf

Danksagung

Ich danke den Mitgliedern meines Fachmentorats, Herrn Prof. Dr. Uwe Heemann, Frau Prof. Dr. Julia Höfele und Herrn Prof. Dr. Michael Fischereder, für die Unterstützung meines Habilitationsverfahrens.

Frau Prof. Julia Höfele danke ich insbesondere für ihre exzellente wissenschaftliche und klinische Betreuung, auch im Rahmen meiner Facharztausbildung am Institut für Humangenetik. Ohne Frau Prof. Höfele wäre meine Habilitation nicht möglich gewesen.

Ein weiterer besonderer Dank geht an Herrn Prof. Uwe Heemann, Leiter der Abteilung für Nephrologie am Klinikum rechts der Isar der Technischen Universität München, der mich in meiner gesamten bisherigen klinisch-wissenschaftlichen Weiterbildung in der Nephrologie intensiv betreut und gefördert hat und auf die grandiose Idee kam, einen Nephrologen in die Humangenetik zu schicken.

Auch möchte ich Herrn Prof. Fischereder, Leiter der Nephrologie an der Ludwig-Maximilians-Universität München, danken, dass er sich so selbstverständlich an einem Fachmentorat für einen Kollegen *rechts* der Isar beteiligt hat.

Außerdem möchte ich noch Herrn Prof. em. Dr. Thomas Meitinger, ehemaliger Direktor des Instituts für Humangenetik am Klinikum rechts der Isar der Technischen Universität München, ausdrücklich meinen Dank aussprechen, der mir mit seinem unvergleichlichen Führungsstil und seiner Persönlichkeit das gesamte Feld der Genetik eröffnet und auch das kritische wissenschaftliche Denken gelehrt hat.

Ich danke zudem allen Kolleginnen und Kollegen der Abteilung für Nephrologie sowie am Institut für Humangenetik des Klinikums rechts der Isar für die andauernde kollegiale Zusammenarbeit. In diesem Zusammenhang sind auch alle Mitglieder der Arbeitsgruppe „NephroGen" und internationalen Kooperationspartner für ihre Unterstützung dankend hervorzuheben.

Abschließend geht mein größter Dank an meine Ehefrau Johanna, meinen Sohn Julian und an meine gesamte liebevolle Familie, die mich immer in meinem Lebensweg unterstützt haben und ohne die ich die vorliegende Arbeit nicht hätte fertigstellen können.

Boston, MA, USA, 25.04.2024.

Anhang - Originalarbeiten

In der Zusammenstellung beschriebene Originalarbeiten in chronologischer Reihenfolge nach Publikationszeitpunkt

Exome Sequencing and Identification of Phenocopies in Patients With Clinically Presumed Hereditary Nephropathies

Korbinian M. Riedhammer, Matthias C. Braunisch, Roman Günthner, Matias Wagner, Clara Hemmer, Tim M. Strom, Christoph Schmaderer, Lutz Renders, Velibor Tasic, Zoran Gucev, Valbona Nushi-Stavileci, Jovana Putnik, Nataša Stajic, Marc Weidenbusch, Barbara Uetz, Carmen Montoya, Peter Strotmann, Sabine Ponsel, Baerbel Lange-Sperandio, and Julia Hoefele

Rationale & Objective: Hereditary nephropathies are clinically and genetically heterogeneous disorders. For some patients, the clinical phenotype corresponds to a specific hereditary disease but genetic testing reveals that the expected genotype is not present (phenocopy). The aim of this study was to evaluate the spectrum and frequency of phenocopies identified by using exome sequencing in a cohort of patients who were clinically suspected to have hereditary kidney disorders.

Study Design: Cross-sectional cohort study.

Setting & Participants: 174 unrelated patients were recruited for exome sequencing and categorized into 7 disease groups according to their clinical presentation. They included autosomal dominant tubulointerstitial kidney disease, Alport syndrome, congenital anomalies of the kidney and urinary tract, ciliopathy, focal segmental glomerulosclerosis/steroid-resistant nephrotic syndrome, VACTERL association, and "other."

Results: A genetic diagnosis (either likely pathogenic or pathogenic variant according to the guidelines of the American College of Medical Genetics) was established using exome sequencing in 52 of 174 (30%) cases. A phenocopy was identified for 10 of the 52 exome sequencing–solved cases (19%), representing 6% of the total cohort. The most frequent phenocopies (n = 5) were associated with genetic Alport syndrome presenting clinically as focal segmental glomerulosclerosis/steroid-resistant nephrotic syndrome. Strictly targeted gene panels (<25 kilobases) did not identify any of the phenocopy cases.

Limitations: The spectrum of described phenocopies is small. Selection bias may have altered the diagnostic yield within disease groups in our study population. The study cohort was predominantly of non-Finnish European descent, limiting generalizability. Certain hereditary kidney diseases cannot be diagnosed by using exome sequencing (eg, *MUC1*-autosomal dominant tubulointerstitial kidney disease).

Conclusions: Phenocopies led to the recategorization of disease and altered clinical management. This study highlights that exome sequencing can detect otherwise occult genetic heterogeneity of kidney diseases.

The clinical and genetic heterogeneity of hereditary nephropathies is a challenging task.[1] Knowing the exact genetic cause of a disease is more and more important with regard to therapy, management, and prognosis. For example, Alport syndrome (AS) can be

Editorial, p. 451

treated by using angiotensin-converting enzyme (ACE) inhibition to reduce proteinuria and delay the decline in kidney function. In a hereditary podocytopathy causing proteinuria, in turn, rapid kidney transplantation is advised because ACE inhibition and immunosuppression have little prospect of lowering proteinuria.[2,3]

The general definition of a "phenocopy" is a phenotype that cannot be explained by the established genotype but can be explained by a different genetic variant or by environmental factors.[4] The term comes from linkage studies, in which a phenocopy refers to an individual who, phenotypically, has a disease segregating in a family but does not have the same established genetic cause (ie, genotype) as

the other affected family members.[5] In a broader sense, the term has been used in a variety of medical specialties to describe the situation in which a patient has a phenotype that corresponds to a specific hereditary disease (eg, Huntington disease) without detection of the expected genotype but with detection of a different genotype (eg, a hexanucleotide repeat expansion in *C9ORF72* instead of a CAG repeat expansion in *HTT*).[6-12] For this study, this broader definition of phenocopy is used.

As for nephrology, phenocopies have already been identified in patients with select hereditary kidney diseases analyzed by using targeted next-generation sequencing (NGS) panels or exome sequencing: 10% of a cohort of 70 families with the clinical diagnosis of focal segmental glomerulosclerosis (FSGS) were found to have segregating pathogenic variants in the classic AS genes *COL4A3* and *COL4A4* and not, as expected, in hereditary FSGS genes.[13] In a large cohort of 300 families encompassing 335 individuals with a clinical diagnosis of steroid-resistant nephrotic syndrome (SRNS), phenocopies were identified in almost 4% of the families. Phenocopies were detected in

AS genes *COL4A5* and *COL4A3* but also in *GLA*, the gene associated with Fabry disease, which is amenable to treatment by enzyme replacement therapy.[14,15] Moreover, in 22% of patients with the clinical diagnosis of autosomal recessive polycystic kidney disease (ARPKD), pathogenic variants could be found in genes other than the established ARPKD gene *PKHD1*.[16] Furthermore, pathogenic variants in nephronophthisis genes (eg, *NPHP1*, *NPHP4*, and *TMEM213*) can appear clinically like congenital anomalies of the kidney and urinary tract (CAKUT), when small cystic kidneys are mistaken for renal hypoplasia/dysplasia.[17]

Exome sequencing, that is, the analysis of the protein-coding regions of the genome by using NGS, has successfully been used in various heterogeneous hereditary kidney diseases such as SRNS, CAKUT, and hereditary nephrolithiasis.[14,17,18] Recently, its utility has also been shown in an unselected cohort of more than 3,000 adult patients with chronic kidney disease (CKD), identifying a monogenic cause in nearly 10% of cases.[19]

In this study, we present the spectrum and frequency of phenocopies identified by using exome sequencing in a cohort of 174 unrelated index cases who were clinically suspected to have a hereditary kidney disease.

Methods

Patient Cohort and Phenotype Characterization

Between 2015 and 2018, a total of 174 index cases of unrelated families was recruited for this study. All 174 index cases carried a tentative clinical diagnosis of a hereditary kidney disease or had renal involvement without overlap with a specific monogenic kidney disease, but met at least 1 of the following additional criteria: young age at first manifestation (aged < 18 years), syndromic disease, familial occurrence, and/or consanguinity. None had a definitive genetic diagnosis and therefore all 174 index cases were considered to be genetically unsolved. If prior genetic analyses were performed, this was done at the discretion of the referring clinician. Patients were seen by adult or pediatric nephrologists or human geneticists and referred to the institute of human genetics at a tertiary care center. Phenotypes were acquired by using a standardized questionnaire and review of medical reports. Assignment to disease groups was based on the tentative clinical diagnosis (or "other" category if the case did not fit any of the prespecified hereditary kidney disease groups). Blood samples were collected after written informed consent from the patients or their legal guardians. To identify genetic diagnoses for the 174 unsolved index cases, we examined all of them by exome sequencing. *MUC1* testing (to detect a cytosine insertion in the variable number tandem repeats region of *MUC1*) was done additionally in all 3 unsolved autosomal dominant tubulointerstitial kidney disease (ADTKD) cases.

The study was approved by the local Ethics Committee of the Technical University of Munich and performed according to the standard of the Helsinki Declaration of 2013. Written informed consent was obtained from all participants or their legal guardians.

Exome Sequencing

DNA was extracted from peripheral blood using the Gentra Puregene Blood Kit (Qiagen) according to the manufacturer's instructions. Exome sequencing was performed using a Sure Select Human All Exon 60 Mb V6 Kit (Agilent) and a HiSeq4000 (Illumina) or Sure Select Human All Exon 50 Mb V5 Kit (Agilent) and a HiSeq2500 (Illumina), as previously described.[20] Mitchondrial DNA (mtDNA) was derived from off-target exome reads as previously described.[21] Reads were aligned to the human reference genome (UCSC Genome Browser build hg19) using Burrows-Wheeler Aligner (version 0.7.5a). Detection of single-nucleotide variants and small insertions and deletions (indels) was performed with SAMtools (version 0.1.19). ExomeDepth was used for the detection of copy number variations (CNVs). A noise threshold of 2.5 was accepted for diagnostic analysis.[22] Called CNVs were visualized by using the Integrative Genomics Viewer (IGV)[23] to check for sufficient coverage of the inspected region and plausibility of the CNV. CNVs were compared with publicly available control databases such as the Genome Aggregation Database (gnomAD),[24] the Database of Genomic Variants (DGV),[25] and databases for pathogenic CNVs such as DECIPHER[26] and ClinVar.[27] Rating was done according to American College of Medical Genetics (ACMG) guidelines.[28] For the analysis of *de novo*, autosomal dominant, and mitochondrial variants, only variants with a minor allele frequency (MAF) < 0.1% in the in-house database of the Helmholtz Center Munich containing more than 16,000 exomes were considered. For the analysis of autosomal recessive and X-linked variants (homozygous, hemizygous, or putative compound heterozygous) variants with an MAF < 1.0% were considered. Because there are pathogenic alleles in hereditary nephropathies with an MAF > 1.0%, such as the *NPHS2* p.Arg229Gln allele (also known as p.R229Q), in unsolved cases, an additional search for recessive and X-linked variants with an MAF up to 3% was used. The p.Arg229Gln allele is known to cause SRNS when in trans with specific 3' *NPHS2* variants.[29,30] Identified variants were compared with publicly available databases for pathogenic variants such ClinVar, the Human Gene Mutation Database (HGMD),[31] and the Leiden Open Variation Database (LOVD).[32] Only variants rated as "likely pathogenic" or "pathogenic" according to the classification of the ACMG and with a genotype in agreement with the mode of inheritance led to the designation "solved case."[28,33] Patients with no pathogenic variant, a nonexplanatory genotype, or with variants classified as benign, likely benign, or of unknown significance according to ACMG were subsequently denoted as "unsolved cases." Exome sequencing results were communicated to the patients either by the referring clinician or as part of genetic counseling.

Sanger Sequencing and Single-Nucleotide Polymorphism Array

Segregation analysis of identified variants was performed by Sanger sequencing or single-nucleotide polymorphism array, as appropriate. Oligonucleotide primer sequences are available on request. For single-nucleotide polymorphism array, a CytoScanTM 750 K Array (Affymetrix Inc) with an average space between 2 oligonucleotides of 4 kilobases (kb) was used. Scanning was performed by using the Affymetrix GeneChip Scanner 3000 7G (resolution, 0.51-2.5 μm). The data analysis was conducted using the Affymetrix Chromosome Analysis Suite Software (ChAS), version 3.0, hg19.

Targeted mtDNA NGS

For analysis of heteroplasmy levels of the mtDNA variant in different tissues of the mother of index case HN-F542-II-1, NGS of the mtDNA was performed (see Item S1). The entire mtDNA was amplified as a single amplicon using long-range polymerase chain reaction as previously published.[34] Libraries were prepared using the Nextera XT DNA Library Preparation Kit (Illumina) and sequenced using the MiSeq sequencing platform (Illumina) as paired-ends of 2×150 base pairs. Reads were aligned to the revised Cambridge Reference Sequence (rCRS accession number NC_012920.1). Variant calling was performed with the Genome Analysis Toolkit (GATK 3.8).[35]

Comparison of Diagnostic Yield of Exome Sequencing Versus Targeted Gene Panel in Phenocopy Cases

To compare the diagnostic yields of exome sequencing versus targeted gene panels in phenocopy cases, we retrospectively chose a commercial panel of a size < 25 kb (billable panel size in the German statutory health insurance system) covering the genes associated with the tentative clinical diagnosis (between 6 and 10 genes) and 1 comprehensive hereditary kidney disease panel (272 genes). See Table S3 for genes included in the different panels and the provider of the panels.

Statistical Analysis and Graphical Visualization

Descriptive statistics are displayed as median and interquartile range. Statistical analyses were performed using IBM SPSS Statistics 23 and R, version 3.5.2, software (R Foundation for Statistical Computing). Plots were generated with R version 3.5.2 software.

Results

Identification of a Monogenic Cause

The study cohort consisted of 174 index cases (53% male and 47% female) of unrelated families who carried tentative clinical diagnoses of a specific hereditary nephropathy or criteria pointing toward a hereditary nephropathy (see Methods), including FSGS/SRNS (28% of cases), AS (20%), CAKUT (17%), ciliopathies (11%), and ADTKD (3%). Five percent of cases were diagnosed with VACTERL association (V, vertebral anomalies; A, anorectal malformations; C, cardiovascular anomalies; T, tracheoesophageal fistula; E, esophageal atresia; R, renal and/or radial anomalies; L, limb defects). Disorders not fitting in the mentioned disease groups were assigned to the group "other" (eg, tubulopathies, atypical hemolytic uremic syndrome, childhood-/adolescence-onset glomerulonephritis, complex syndromes involving the kidney; 16% of cases; Fig 1). Of the 174 index cases, 133 (76%) were of non-Finnish European descent and 69 (40%) had a positive family history.

Exome sequencing established a genetic diagnosis in 52 of 174 individuals, making its diagnostic yield 30% in the overall cohort, with some variability across groups defined by tentative clinical diagnoses (50% in ADTKD [n = 6], 47% in AS [n = 34] and ciliopathy group [n = 19], 27% in CAKUT [n = 30], 16% in FSGS/SRNS [n = 49], and 30% in the other group [n = 27]). None of the 9 VACTERL cases could be solved by exome sequencing (Fig 2). See Table 1 for an overview of the cohort.

Detection of Phenocopies

In the overall cohort, 10 of 174 (6%) cases could be identified as phenocopies, which corresponds to 1 phenocopy per every fifth exome sequencing–solved case (19%; 10/52). Three phenocopies were genetically proven FSGS/SRNS that clinically presented as AS. Two phenocopies were genetically proven AS that presented clinically as FSGS/SRNS. One phenocopy was genetically proven AS displaying clinical features of immunoglobulin A (IgA) nephropathy. In another phenocopy, kidney biopsy alluded to a presumed clinical diagnosis of collagen type IV disease, which turned out to be Dent disease on genetic testing. One patient was clinically categorized to have ciliopathy, but genetic testing revealed chromosome 17q12 deletion syndrome involving the CAKUT gene *HNF1B*. The remaining 2 phenocopies presented clinically as tubulopathies; however, the genetic diagnoses were disparate from the typical genetic causes of tubulopathies. One was determined to be a mitochondriopathy (homoplasmic variant m.616T>C in *MT-TF*) and the other, a prohormone processing defect with compound heterozygous missense variants in the gene *PCSK1*. See Table 2 for a complete account of phenocopies and Item S1 of phenocopies.

Examination of Targeted NGS Panels for Identifying Phenocopies

Strictly targeted NGS panels (<25 kb; Table S3) could not have identified any of the phenocopy cases that had a tentative clinical diagnosis of a monogenic disease. In contrast, a comprehensive hereditary kidney disease panel (272 genes; Table S3) could have identified 8 of 10 (80%) phenocopies, but it would have missed cases HN-F46-II-1 (*PCSK1*) and HN-F542-II-1 (*MT-TF*) and the second monogenic disease (*ADA2*) in HN-F56-II-1.

Figure 1. Overview of clinical disease groups of the study cohort with presumed hereditary kidney diseases (n = 174 unrelated index cases). Abbreviations: ADTKD, autosomal dominant tubulointerstitial kidney disease; AS, Alport syndrome; CAKUT, congenital anomalies of the kidney and urinary tract; FSGS, focal segmental glomerulosclerosis; SRNS, steroid-resistant nephrotic syndrome; VACTERL association: V, vertebral anomalies; A, anorectal malformations; C, cardiovascular anomalies; T, tracheoesophageal fistula; E, esophageal atresia; R, renal (kidney) and/or radial anomalies; L, limb defects. See Tables 2, S1, and S2 for a list of all cases.
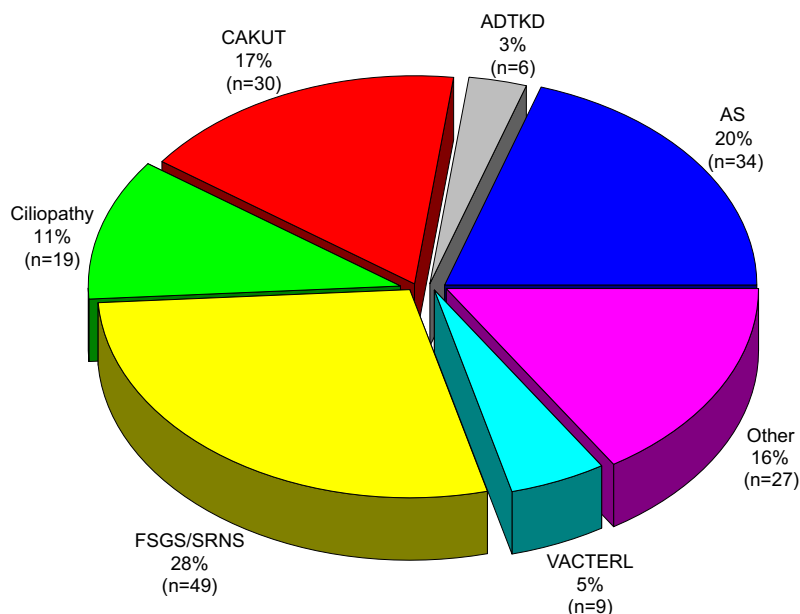
Discussion

This study illustrates the spectrum of phenocopies in a cohort of 174 index patients with a clinically presumed hereditary nephropathy. A monogenic disease could be diagnosed in 30% of cases, with every fifth case (19%) being a phenocopy. Previous reports on phenocopies come from cohorts or families with select disease groups such as AS, CAKUT, or ciliopathies.[13,14,16,37-39] A recent study of 114 families with 138 adults (median age, 48 years) with CKD analyzed by using exome sequencing showed that in 21% of exome sequencing–solved cases, genetic analysis could "correct" the clinical diagnosis. Furthermore, in another study of 92 adults (all >18 years) with CKD, exome sequencing could "reclassify" the clinical diagnosis in 27% of cases.[40,41] In contrast to the mentioned studies, the present study is not restricted to adult patients (median age, 19 years; interquartile range, 7.0-35.0) and it does not focus on a single disease group. It illustrates the spectrum of phenocopies in major hereditary kidney disorders such as AS, FSGS/SRNS, CAKUT, ciliopathies, and tubulopathies.[42] Additionally, the present study is strictly centered on phenocopies, that is, tentative clinical diagnosis of a specific disease turning out not to be caused by the expected genotype. In the study by Connaughton et al,[41] in some cases unspecific clinical diagnoses such as chronic glomerulonephritis led to the designation "corrected clinical diagnosis" if exome sequencing established a causative genotype.

As expected, "typical" phenocopies could be detected in this cohort. FSGS is an unspecific histologic phenotype shared by many kidney diseases, including hereditary nephropathies.[39,43] Therefore, it is not surprising that a genetically confirmed diagnosis of AS can present clinically as FSGS, especially if kidney biopsy is done late in the course of the disease (cases ATS-F9-II-1 and ATS-F261-II-1: kidney biopsy at ages 29 and 32 years, respectively). However, case ATS-F29-III-1 highlights that AS may only produce the histologic phenotype of minimal change disease, which in conjunction with the clinical phenotype of proteinuria may lead to the suspicion of hereditary FSGS. An unusual feature of this case is that the AS genes COL4A3, COL4A4, and COL4A5 had been tested in the patient at 12 years of age by Sanger sequencing with a false-negative result. Further demonstrating the clinical variability of AS, case ATS-F486-II-1 presented clinically as IgA nephropathy at a very early age. For this case, the patient was only 3 years of age at initial presentation and therefore kidney biopsy was not done. The expected outcome of exome sequencing was that no causative genotype could be established because IgA nephropathy is not a monogenic disease. Nevertheless, exome sequencing identified a hemizygous frameshift variant in COL4A5. The deleterious nature of the frameshift variant could explain the clinical course in this patient with intermittent macroscopic hematuria because loss-of-function variants are known to cause a more severe phenotype than missense variants.[44]

In HN-F56-II-1, the histologic findings were misleading, pointing toward a collagen type IV disease. Exome sequencing revealed a hemizygous nonsense variant in CLCN5, the gene associated with Dent disease, which is a tubulopathy. No clinically relevant variants could be detected in the AS genes COL4A3, COL4A4, or COL4A5. Judging from the clinical presentation (microscopic hematuria, proteinuria, hypercalciuria, and nephrocalcinosis), which is typical for Dent disease, the result of the kidney biopsy probably shifted the focus of the clinician. Of note, in this case another monogenic disease could be identified by exome sequencing: a hereditary
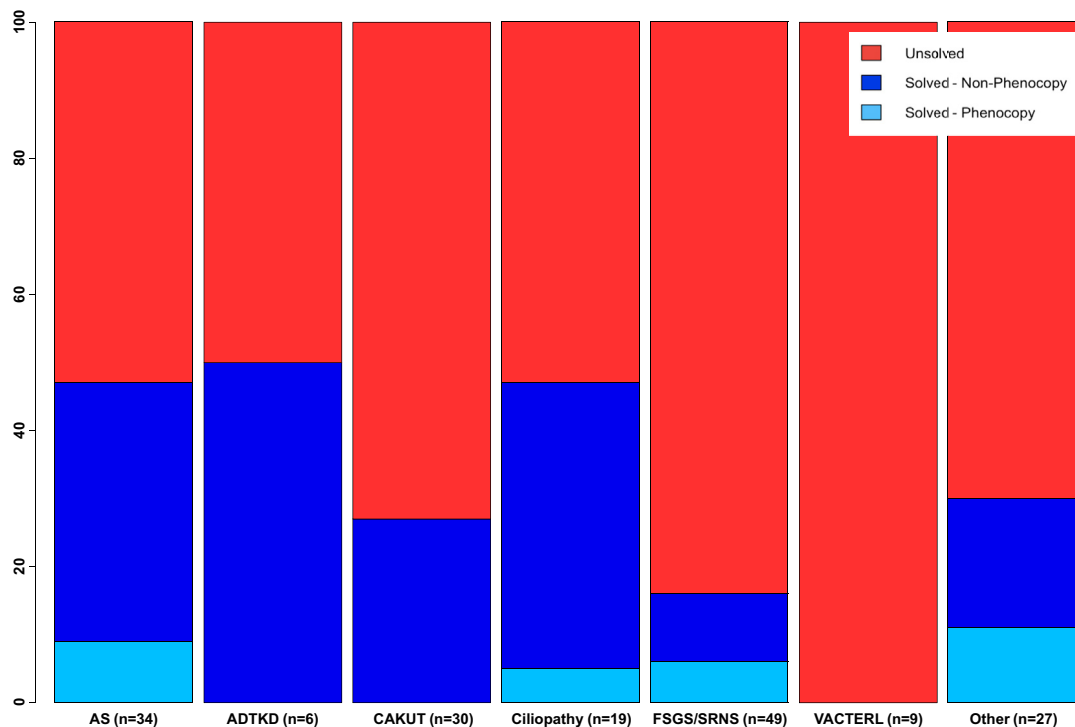
Figure 2. Diagnostic yield of respective disease groups. Abbreviations: ADTKD, autosomal dominant tubulointerstitial kidney disease; AS, Alport syndrome; CAKUT, congenital anomalies of the kidney and urinary tract; FSGS, focal segmental glomerulosclerosis; SRNS, steroid-resistant nephrotic syndrome; VACTERL association: V, vertebral anomalies; A, anorectal malformations; C, cardiovascular anomalies; T, tracheoesophageal fistula; E, esophageal atresia; R, renal (kidney) and/or radial anomalies; L, limb defects. Solved cases are cases for which exome sequencing identified a genetic diagnosis. Phenocopies are cases for which exome sequencing–derived genetic diagnosis differs from the presumed clinical diagnosis. Solved cases are divided into "Solved–Non-Phenocopy" (dark blue) and "Solved–Phenocopy" (light blue). Fractions are given in percent. The diagnostic yield of exome sequencing in the total cohort (n = 174 index cases) was 30%.

form of childhood-onset polyarteritis nodosa, called ADA2 deficiency (compound heterozygous missense variants in *ADA2*).[36]

As mentioned, AS phenocopying FSGS has been frequently described in the literature.[13] This study shows the reverse case (HN-F203-II-2) of a family clinically diagnosed with AS with no disease-causing variant identified in *COL4A3-5* and *MYH9* (Sanger sequencing performed in the index at the age of 21 years) in which exome sequencing could detect a likely pathogenic homozygous missense variant in *MYO1E* segregating in all 3 affected siblings. The index was diagnosed in 1986 with AS by kidney biopsy at 3 years of age. *MYO1E* was first published in 2011 as a monogenic FSGS gene and genetic diagnosis was made in 2017 in the index case at the age of 34 years.[45] This case shows that repeat genetic testing is warranted in families with high probability of a genetic disorder because knowledge on disease-causing genes is ever evolving.

A further previously reported phenocopy in the field of hereditary nephropathies is CAKUT mimicking ciliopathies.[46] In this cohort, there was 1 case (HN-F13-II-1) with hyperechogenic kidneys on prenatal ultrasound suggesting a clinical diagnosis of ARPKD but the genetic diagnosis was chromosome 17q12 deletion syndrome comprising the CAKUT gene *HNF1B*. Because this child was analyzed using exome sequencing in the first months of life, other potential extrarenal features of 17q12 deletion syndrome (developmental delay and maturity-onset diabetes of the young) were not recognizable yet.[47]

Case HN-F46-II-1 initially had a tubulopathy phenotype manifesting after birth, pointing toward a clinical diagnosis of distal renal tubular acidosis. Exome sequencing could identify compound heterozygous likely pathogenic missense variants in *PCSK1*, a gene associated with the monogenic disease "obesity with impaired prohormone processing" [MIM 600955]. An elevated proinsulin to insulin ratio supported the pathogenicity of the variants. Furthermore, the patient developed diabetes insipidus and hyperphagia, which is also part of the phenotypic spectrum of *PCSK1*-associated disease.[48] This underpins that constant phenotyping can help overcome the problem of phenocopies in hereditary nephropathies if comprehensive genetic analyses such as exome sequencing are not available to the clinician.

Finally, case HN-F542-II-1 sheds light on the huge phenotypic variability of mitochondriopathies. Renal phenotypes have been associated with both nuclear and

Table 1. Overview of the Study Cohort

	AS	ADTKD	CAKUT	Ciliopathy	FSGS/SRNS	VACTERL	Other	Total
No. of index cases	34/174 (20%)	6/174 (3%)	30/174 (17%)	19/174 (11%)	49/174 (28%)	9/174 (5%)	27/174 (16%)	174
Male sex	20/34 (59%)	3/6 (50%)	19/30 (63%)	7/19 (37%)	25/49 (51%)	5/9 (56%)	14/27 (52%)	93/174 (53%)
Positive family history	18/34 (53%)	5/6 (83%)	9/30 (30%)	8/19 (42%)	19/49 (39%)	0/9 (0%)	10/27 (37%)	69/174 (40%)
Reported consanguinity	0/34 (0%)	0/6 (0%)	2/30 (7%)	2/19 (11%)	5/49 (10%)	0/9 (0%)	1/27 (4%)	10/174 (6%)[a]
Age at genetic testing, y	15 [8.0-26.0]	53 [47.0-65.0]	6 [0.1-25.0]	9 [0.8-19.0]	31 [19.0-42.0]	10 [1.0-12.5]	24 [7.0-37.0]	19 [7.0-35.0]
Diagnostic yield	16/34 (47%)	3/6 (50%)	8/30 (27%)	9/19 (47%)	8/49 (16%)	0/9 (0%)	8/27 (30%)	52/174 (30%)
No. of phenocopies	3/34 (9%)	0/6 (0%)	0/30 (0%)	1/19 (5%)	3/49 (6%)	0/9 (0%)	3/27 (11%)	10/174 (6%)

Note: Solved cases (the diagnostic yield) are cases for which exome sequencing identified a genetic diagnosis. Phenocopies are cases for which exome sequencing–derived genetic diagnosis differs from the presumed clinical diagnosis. Prenatal manifestations and diagnoses were set to age "0." Age at exome sequencing was used as timepoint for age at genetic testing (equal to age at genetic diagnosis in solved cases). See Tables 2, S1, and S2 for a list of all cases. Unless otherwise indicated, values given as n/N (percentage) or median [interquartile range].

Abbreviations: ADTKD, autosomal dominant tubulointerstitial kidney disease; AS, Alport syndrome; CAKUT, congenital anomalies of the kidney and urinary tract; FSGS, focal segmental glomerulosclerosis; SRNS, steroid-resistant nephrotic syndrome; VACTERL association: V, vertebral anomalies; A, anorectal malformations; C, cardiovascular anomalies; T, tracheoesophageal fistula; E, esophageal atresia; R, renal (kidney) and/or radial anomalies; L, limb defects.

[a]All 10 index patients from consanguineous families also had other affected relatives.

mtDNA-encoded genes, among them FSGS in MELAS (mitochondrial encephalomyopathy, lactic acidosis, stroke-like episodes) syndrome and primary coenzyme Q10 deficiency (genes COQ2, COQ6, and COQ8B).[49–52] Moreover, tubular defects can be observed frequently in mitochondriopathies.[53] Case HN-F542-II-1 initially presented with renal salt wasting and seizures progressing to epileptic encephalopathy and CKD. Exome sequencing (mtDNA included) could identify the homoplasmic MT-TF variant m.616T>C (which affects the transfer RNA specific for phenylalanine), which was previously reported in families with epilepsy and kidney failure.[21,54]

Of course, when discussing phenocopies, one must acknowledge that clinical tentative diagnoses are made at a certain point in time and may change as disease and diagnostic capabilities develop (as reflected by cases HN-F13-II-1 and HN-F46-II-1 and discussed in the preceding).

The recategorization of disease due to phenocopies has several clinical implications. First, there may be different clinical management, for example, in AS (ACE inhibition to reduce proteinuria) versus FSGS/SRNS (rapid transplantation if nephrotic syndrome develops) or the focus on hormone supplementation in PCSK1-associated disease.[2,3,48] Second, reproductive choices may be altered if, at 34 years of age, an autosomal recessive instead of a potentially X-linked disease is genetically diagnosed (MYO1E-associated FSGS vs X-linked AS). Third, different genetic counseling may be warranted, for example in a tubulopathy due to an mtDNA-encoded variant versus an autosomal variant. Fourth, the recategorization may imply a different clinical course (chromosome 17q12 deletion syndrome vs ARPKD).[46,47]

Another important finding of this study is that strictly targeted gene panels (<25 kb) would not have been able to identify any of the phenocopies. This underlines the

importance of comprehensive testing in genetically heterogeneous disorders, at least if narrow panel diagnostics do not yield a positive result.

Albeit the intention of this study was to highlight the spectrum of phenocopies in hereditary nephropathies, the small number of only 10 phenocopies and the heterogeneity of disease groups covered poses a limitation as to the generalization of the findings. Additionally, the cohort is predominantly of non-Finnish European descent (76%), which also reduces the transferability of results for other ethnicities.[55] Moreover, the diagnostic yield of the different disease groups in this study differs in part from published data. NGS panels in patients with AS report diagnostic yields > 80%, whereas the yield in this study is only 47%.[56] This may be due to the many "milder" clinical phenotypes of isolated microscopic hematuria and thin basement membrane nephropathy in the unsolved cases (13/18; 72%). Selection bias can also be assumed in CAKUT cases in which the present yield (27%) is about twice as high as previously reported.[17] The median age at genetic testing of 31 years in the FSGS/SRNS group explains the diagnostic yield of 16%, which is in line with lower yields in adult patients with FSGS in 1 study (22%) compared with pediatric/adolescent patients with SRNS in another study (29.5%).[14,37,57] However, this highlights the presence of hereditary FSGS cases in adult patients and warrants further research. Concerning the 47% diagnostic yield in the ciliopathy group, this is a lower yield than reported in an exome sequencing study on nephronophthisis-related ciliopathies in 79 families (63%). However, in 76% of these families, parents were consanguineous, explaining the high yield of autosomal-recessive nephronophthisis in that cohort.[58] In our cohort, only 10% (Table 1) of index cases derive from consanguineous families. Furthermore, our ciliopathy cohort features 5 clinically suspected

Table 2. Summary of Identified Phenocopies

Index Case (Sex)	Disease Group[a]	Age at First Manifestation; Phenotype; Clinical Dx[b]	Previous Genetic Tests[c]	Genetic Diagnosis[d]	Variant[e]	MAF[f]	ClinVar Rating[g]	ACMG Rating[h]	Zygosity/ Heteroplasmy	Inheritance
ATS-F9-II-1 (M)	FSGS/SRNS (FSGS)	26 y; nephrotic proteinuria; Dx by kidney Bx at 29 y	—	AS, autosomal recessive (203780) at 32 y	COL4A3 (NM_000091.4): • c.2126-1G>C p.(?) • c.4421T>C p.(Leu1474Pro)	• —[i] • 0.003	• —[i] • 1× pathogenic, 4× VUS	• PVS1/PM2/PP3 • PS4[j] (in trans with pathogenic variants)/PM1/PM3/PP3	Compound het	Mother & father
ATS-F29-III-1 (F)	FSGS/SRNS (MCD)	3 y; proteinuria, hematuria; Dx by kidney Bx at 12 y	COL4A3, COL4A4, COL4A5	AS, autosomal recessive (203780) at 21 y	COL4A3 (NM_000091.4): • c.1831G>A p.(Gly611Arg) • c.4421T>C p.(Leu1474Pro)	• —[i] • 0.003	• —[i] • 1× pathogenic, 4× VUS	• PS4[j]/PM1/PM2 • PS4[j] (in trans with pathogenic variants)/PM1/PM3/PP3	Compound het	Mother & father
ATS-F261-II-1 (F)	FSGS/SRNS (FSGS)	5 y; hematuria & proteinuria; Dx by kidney Bx at 32 y	—	AS, X-linked (301050) at 42 y	COL4A5 (NM_000495.4): c.645+1G>T (p.(?))	—[i]	—[i]	PVS1/PM2	Het	UD
HN-F13-II-1 (F)	Ciliopathy (ARPKD)	Prenatal; hyperechogenic kidneys on US, Dx at same time	—	17q12 deletion syndrome (614527) at 4 mo	1.2 Mb deletion Chr17q12 (comprising HNF1B)[k]	—	Overlapping & similarly sized CNVs rated as pathogenic	Pathogenic	Het	Mother
HN-F20-II-1 (M)	AS (AS & sensorimotor neuropathy)	4 & 15 y; neuropathy & proteinuria/ sensorineural deafness, respectively; Dx at first respective manifestation	PMP22, MPZ, COL4A3, COL4A4, COL4A5, WT1, NPHS2	FSGS, 5 (613237); CMT disease, dominant intermediate E (614455) at 26 y	INF2 (NM_022489.3): c.224_256del p.(Asp75_Ser85del)	—[i]	—[e]	PM1/PM2/PM4	Het	UD
HN-F56-II-1 (M)	AS (collagen type IV disease)	4 y; microscopic hematuria, proteinuria, hypercalciuria, nephrocalcinosis; Dx by kidney Bx at 4 y	—	Dent disease[l] (300009) at 5 y	CLCN5 (NM_000084.4): c.292C>T p.(Arg28*)	—[i]	Pathogenic	PVS1/PM2/PP3	Hemi	Mother
HN-F203-II-2 (F)	AS	2 y; microscopic hematuria; Dx by kidney Bx at 3 y	COL4A3, COL4A4, COL4A5, MYH9	FSGS, 6 (614131) at 34 y	MYO1E (NM_004998.3): c.2060T>C p.(Leu687Ser)	—[i]	—[i]	PM1/PM2/PP1/PP3	Homo	Mother & father

(Continued)

Table 2 (Cont'd). Summary of Identified Phenocopies

Index Case (Sex)	Disease Group[a]	Age at First Manifestation; Phenotype; Clinical Dx[b]	Previous Genetic Tests[c]	Genetic Diagnosis[d]	Variant[e]	MAF[f]	ClinVar Rating[g]	ACMG Rating[h]	Zygosity/ Heteroplasmy	Inheritance
HN-F46-II-1 (F)	Other (dRTA)	3 wk; hyperchloremic acidosis, hypercalciuria, nephrocalcinosis; Dx at same time	*ATP5V0A4, ATP6V1B1, CA2, SLC4A1, SLC4A4, VIPAS39, VPS33B, OCRL*	Obesity w/ impaired prohormone processing (600955) at 2 y	*PCSK1* (NM_000439.4): • c.1346T>C p.(Leu449Pro) • c.1688C>G p.(Pro563Arg)	• —[i] • —[i]	• —[i] • —[i]	• PM1[m]/PM2/ PP3/PP4[n] • PM1[m]/PM2/ PP3/PP4[n]	Compound het	Mother & father
ATS-F486-II-1 (M)	Other (IgAN)	3 y; microscopic hematuria w/ intermittent infection-associated macroscopic hematuria; Dx at same time	—	AS, X-linked (301050) at 9 y	*COL4A5* (NM_000495.4): c.225delA p.(Gly76Leufs*79)	—[i]	—[i]	PVS1/PM2	Hemi	Mother
HN-F542-II-1 (F)	Other (Rasmussen encephalopathy w/ tubulopathy & CKD)	3 y; seizure & renal salt wasting; Dx at same time	Mitochondriopathy panel	Maternally inherited epilepsy w/ tubulointerstitial kidney disease (-) at 4 y	*MT-TF* (NC_012920.1): m.616T>C	—	Pathogenic[o]	—	Homoplasmic in blood & urine	Mother

Note: Solved cases are those for which exome sequencing identified a genetic diagnosis. Phenocopies are cases for which exome sequencing–derived genetic diagnosis differs from the presumed clinical diagnosis. See Item S1 for further clinical details.

Abbreviations: AS, Alport syndrome; ARPKD, autosomal recessive polycystic kidney disease; Bx, biopsy; CAKUT, congenital anomalies of the kidney and urinary tract; CKD, chronic kidney disease; CMT, Charcot-Marie-Tooth; CNV, copy number variant; dRTA, distal renal tubular acidosis; Dx, diagnosis; F, female; FSGS, focal segmental glomerulosclerosis; hemi, hemizygous; het, heterozygous; homo, homozygous; IgAN, immunoglobulin A nephropathy; M, male; MAF, minimal allele frequency; MCD, minimal change disease; MIM, Mendelian Inheritance in Man; SRNS, steroid-resistant nephrotic syndrome; UD, undetermined; US, ultrasound; VUS, variant of unknown significance.

[a]Based on clinical (tentative) diagnosis.
[b]Includes first manifestation (with age) and core phenotype, with age at clinical diagnosis.
[c]In all cases, genetic test results were inconspicuous.
[d]MIM (https://www.omim.org/) phenotype number provided in parentheses.
[e]Genbank accession number for reference sequence of transcript provided in parentheses after gene name.
[f]Based on Genome aggregation database (https://gnomad.broadinstitute.org/).
[g]Based on https://www.ncbi.nlm.nih.gov/clinvar/.
[h]See Richards et al[33] and Kearney et al.[28] In general PVS1 indicates a very strong level of pathogenicity, PS designations indicate strong evidence of pathogenicity, PM designations indicate a moderate level of pathogenicity, and PP designations indicate supporting evidence of pathogenicity.
[i]Not listed.
[j]Moderate.
[k]Corresponding to g.34842543-36104875 of chromosome 17 in the reference sequence hg19.
[l]A second monogenic disease was diagnosed in the patient: compound heterozygous missense variants in *ADA2*: NM_017424.2:c.140G>C (p.(G47A)) and c.752C>T (p.(P251L)), which corresponds to a genetic diagnosis of "Polyarteritis nodosa, childhood-onset" (MIM number 615688). We previously published this case.[36]
[m]Supporting.
[n]Strong (rated as strong because of highly specific phenotype consisting of hyperphagia, diabetes insipidus and elevated proinsulin/insulin ratio in blood).
[o]Also rated pathogenic on MITOMAP (https://mitomap.org//cgi-bin/search_allele?starting=616).

AJKD

autosomal-dominant polycystic kidney disease cases. Detection of pathogenic variants in the major autosomal-dominant polycystic kidney disease gene *PKD1* is limited in exome sequencing.[59] This study also features 9 VACTERL cases. There is a known association of CAKUT with VACTERL(-like) phenotypes and numerous monogenic syndromes can clinically present as VACTERL (eg, Townes-Brocks syndrome or Baller Gerold syndrome).[60] VACTERL is a term describing the nonrandom co-occurrence of several congenital anomalies and involves heterogeneous causes that can be both multifactorial and monogenic. Therefore, diagnostic yield from cohorts with phenotypes including VACTERL characteristics is low (14% in one publication).[61,62] In this cohort of only 9 patients with VACTERL, none could be genetically solved. With regard to ADTKD, exome sequencing cannot determine the complete diagnostic yield because one major cause for ADTKD, *MUC1*-related ADTKD, cannot be diagnosed using NGS.[63] All 3 solved cases were *UMOD*-related ADTKD and *MUC1*-related ADTKD was tested for before exome sequencing was done in all unsolved cases.

In this cohort of patients with clinically presumed hereditary kidney diseases, 19% of solved cases were initially clinically misdiagnosed because of phenocopies. Despite the small number of 10 identified phenocopies, it is noteworthy that exome sequencing can help unravel the broad genetic heterogeneity of hereditary nephropathies. A correct genetic diagnosis has implications on clinical management, genetic counseling, and prognosis.

Supplementary Material

Supplementary File 1 (PDF)

Item S1: Supplementary case reports of phenocopy cases.

Supplementary File 2 (XLSX)

Table S1: List of solved nonphenocopy cases.

Table S2: List of unsolved cases.

Table S3: Selected gene panels for comparison of diagnostic yields between exome sequencing and targeted NGS.

Article Information

Authors' Full Names and Academic Degrees: Korbinian M. Riedhammer, MD, Matthias C. Braunisch, MD, Roman Günthner, MD, Matias Wagner, MD, Clara Hemmer, Tim M. Strom, MD, Christoph Schmaderer, MD, Lutz Renders, MD, Velibor Tasic, MD, Zoran Gucev, MD, Valbona Nushi-Stavileci, MD, Jovana Putnik, MD, Nataša Stajic, MD, Marc Weidenbusch, MD, Barbara Uetz, MD, Carmen Montoya, MD, Peter Strotmann, MD, Sabine Ponsel, MD, Baerbel Lange-Sperandio, MD, and Julia Hoefele, MD.

Authors' Affiliations: Institute of Human Genetics (KMR, MCB, RG, MWagner, CH, JH) and Department of Nephrology (KMR, MCB, RG, CS, LR), Klinikum rechts der Isar, School of Medicine, Technical University of Munich, Munich; Institute of Neurogenomics (MWagner) and Institute of Human Genetics (MWagner, TMS), Helmholtz Zentrum München, Neuherberg, Germany; University Children's Hospital, Medical Faculty of Skopje, Macedonia (VT, ZG); Pediatric Clinic, University Clinical Center of Kosovo, Prishtina, Kosovo (VN-S); Institute for Mother and Child Health Care of Serbia "Dr Vukan Cupic," Department of Nephrology, University of Belgrade, Faculty of Medicine, Belgrade, Serbia (JP, NS); Nephrologisches Zentrum, Medizinische Klinik und Poliklinik IV, Klinikum der Universität München, Ludwig-Maximilians University (MWeidenbusch); München-Klinik Schwabing, Klinikum rechts der Isar, Technical University of Munich, Children's Hospital, Pediatric Nephrology (BU, PS); KfH-Kindernierenzentrum (BU, CM); and Division of Pediatric Nephrology, Dr. v. Hauner Children's Hospital, Ludwig-Maximilians University, Munich, Germany (SP, BL-S).

Address for Correspondence: Julia Hoefele, MD, Institute of Human Genetics, Klinikum rechts der Isar, School of Medicine, Technical University of Munich, Trogerstr. 32, 81675 Munich, Germany. E-mail: julia.hoefele@tum.de

References

1. Groopman EE, Rasouly HM, Gharavi AG. Genomic medicine for kidney disease. *Nat Rev Nephrol*. 2018;14(2):83-104.
2. Trautmann A, Schnaidt S, Lipska-Zietkiewicz BS, et al. Long-term outcome of steroid-resistant nephrotic syndrome in children. *J Am Soc Nephrol*. 2017;28(10):3055-3065.
3. Gross O, Licht C, Anders HJ, et al. Early angiotensin-converting enzyme inhibition in Alport syndrome delays renal failure and improves life expectancy. *Kidney Int*. 2012;81(5):494-501.
4. Strachan T, Read A. *Human Molecular Genetics*. 5th ed. Boca Raton, FL, USA: Taylor & Francis Inc; 2018.
5. Lescai F, Franceschi C. The impact of phenocopy on the genetic analysis of complex traits. *PLoS One*. 2010;5(7):e11876.
6. Turner JJ, Christie PT, Pearce SH, Turnpenny PD, Thakker RV. Diagnostic challenges due to phenocopies: lessons from multiple endocrine neoplasia type1 (MEN1). *Hum Mutat*. 2010;31(1):E1089-E1101.
7. Hensman Moss DJ, Poulter M, Beck J, et al. C9orf72 expansions are the most common genetic cause of Huntington disease phenocopies. *Neurology*. 2014;82(4):292-299.

8. Koutsis G, Karadima G, Kartanou C, Kladi A, Panas M. C9ORF72 hexanucleotide repeat expansions are a frequent cause of Huntington disease phenocopies in the Greek population. *Neurobiol Aging*. 2015;36(1). 547 e513-e546.

9. Mariani LL, Tesson C, Charles P, et al. Expanding the spectrum of genes involved in Huntington disease using a combined clinical and genetic approach. *JAMA Neurol*. 2016;73(9):1105-1114.

10. Neuhaus C, Eisenberger T, Decker C, et al. Next-generation sequencing reveals the mutational landscape of clinically diagnosed Usher syndrome: copy number variations, phenocopies, a predominant target for translational read-through, and PEX26 mutated in Heimler syndrome. *Mol Genet Genomic Med*. 2017;5(5):531-552.

11. Biancalana V, Romero NB, Thuestad IJ, et al. Some DNM2 mutations cause extremely severe congenital myopathy and phenocopy myotubular myopathy. *Acta Neuropathol Commun*. 2018;6(1):93.

12. Ulirsch JC, Verboon JM, Kazerounian S, et al. The genetic landscape of diamond-blackfan anemia. *Am J Hum Genet*. 2018;103(6):930-947.

13. Malone AF, Phelan PJ, Hall G, et al. Rare hereditary COL4A3/COL4A4 variants may be mistaken for familial focal segmental glomerulosclerosis. *Kidney Int*. 2014;86(6):1253-1259.

14. Warejko JK, Tan W, Daga A, et al. Whole exome sequencing of patients with steroid-resistant nephrotic syndrome. *Clin J Am Soc Nephrol*. 2018;13(1):53-62.

15. Schiffmann R, Hughes DA, Linthorst GE, et al. Screening, diagnosis, and management of patients with Fabry disease: conclusions from a "Kidney Disease: Improving Global Outcomes" (KDIGO) Controversies Conference. *Kidney Int*. 2017;91(2):284-293.

16. Szabo T, Orosz P, Balogh E, et al. Comprehensive genetic testing in children with a clinical diagnosis of ARPKD identifies phenocopies. *Pediatr Nephrol*. 2018;33(10):1713-1721.

17. van der Ven AT, Connaughton DM, Ityel H, et al. Whole-exome sequencing identifies causative mutations in families with congenital anomalies of the kidney and urinary tract. *J Am Soc Nephrol*. 2018;29(9):2348-2361.

18. Daga A, Majmundar AJ, Braun DA, et al. Whole exome sequencing frequently detects a monogenic cause in early onset nephrolithiasis and nephrocalcinosis. *Kidney Int*. 2018;93(1):204-213.

19. Groopman EE, Marasa M, Cameron-Christie S, et al. Diagnostic utility of exome sequencing for kidney disease. *N Engl J Med*. 2019;380(2):142-151.

20. Kremer LS, Bader DM, Mertes C, et al. Genetic diagnosis of Mendelian disorders via RNA sequencing. *Nat Commun*. 2017;8:15824.

21. Griffin HR, Pyle A, Blakely EL, et al. Accurate mitochondrial DNA sequencing using off-target reads provides a single test to identify pathogenic point mutations. *Genet Med*. 2014;16(12):962-971.

22. Plagnol V, Curtis J, Epstein M, et al. A robust model for read count data in exome sequencing experiments and implications for copy number variant calling. *Bioinformatics*. 2012;28(21):2747-2754.

23. Robinson JT, Thorvaldsdóttir H, Winckler W, et al. Integrative genomics viewer. *Nat Biotechnol*. 2011;29(1):24-26.

24. About gnomAD. https://gnomad.broadinstitute.org/about. Accessed December 15, 2019.

25. MacDonald JR, Ziman R, Yuen RK, Feuk L, Scherer SW. The database of genomic variants: a curated collection of structural variation in the human genome. *Nucleic Acids Res*. 2014;42(Database issue):D986-D992.

26. Firth HV, Richards SM, Bevan AP, et al. DECIPHER: Database of Chromosomal Imbalance and Phenotype in Humans using Ensembl Resources. *Am J Hum Genet*. 2009;84(4):524-533.

27. Landrum MJ, Lee JM, Benson M, et al. ClinVar: improving access to variant interpretations and supporting evidence. *Nucleic Acids Res*. 2018;46(D1):D1062-D1067.

28. Kearney HM, Thorland EC, Brown KK, Quintero-Rivera F, South ST. Working Group of the American College of Medical Genetics Laboratory Quality Assurance Committee. American College of Medical Genetics standards and guidelines for interpretation and reporting of postnatal constitutional copy number variants. *Genet Med*. 2011;13(7):680-685.

29. Tory K, Menyhard DK, Woerner S, et al. Mutation-dependent recessive inheritance of NPHS2-associated steroid-resistant nephrotic syndrome. *Nat Genet*. 2014;46(3):299-304.

30. Miko A, Menyhárd DK, Kaposi A, Antignac C, Tory K. The mutation-dependent pathogenicity of NPHS2 p.R229Q: a guide for clinical assessment. *Hum Mutat*. 2018;39(12):1854-1860.

31. Stenson PD, Mort M, Ball EV, et al. The Human Gene Mutation Database: towards a comprehensive repository of inherited mutation data for medical research, genetic diagnosis and next-generation sequencing studies. *Hum Genet*. 2017;136(6):665-677.

32. Fokkema IF, Taschner PE, Schaafsma GC, Celli J, Laros JF, den Dunnen JT. LOVD v.2.0: the next generation in gene variant databases. *Hum Mutat*. 2011;32(5):557-563.

33. Richards S, Aziz N, Bale S, et al. Standards and guidelines for the interpretation of sequence variants: a joint consensus recommendation of the American College of Medical Genetics and Genomics and the Association for Molecular Pathology. *Genet Med*. 2015;17(5):405-424.

34. Zhang W, Cui H, Wong LJ. Comprehensive one-step molecular analyses of mitochondrial genome by massively parallel sequencing. *Clin Chem*. 2012;58(9):1322-1331.

35. McKenna A, Hanna M, Banks E, et al. The Genome Analysis Toolkit: a MapReduce framework for analyzing next-generation DNA sequencing data. *Genome Res*. 2010;20(9):1297-1303.

36. Gunthner R, Wagner M, Thurm T, Ponsel S, Hofele J, Lange-Sperandio B. Identification of co-occurrence in a patient with Dent's disease and ADA2-deficiency by exome sequencing. *Gene*. 2018;649:23-26.

37. Sadowski CE, Lovric S, Ashraf S, et al. A single-gene cause in 29.5% of cases of steroid-resistant nephrotic syndrome. *J Am Soc Nephrol*. 2015;26(6):1279-1289.

38. Deltas C, Savva I, Voskarides K, Papazachariou L, Pierides A. Carriers of autosomal recessive Alport syndrome with thin basement membrane nephropathy presenting as focal segmental glomerulosclerosis in later life. *Nephron*. 2015;130(4):271-280.

39. Braunisch MC, Buttner-Herold M, Gunthner R, et al. Heterozygous COL4A3 variants in histologically diagnosed focal segmental glomerulosclerosis. *Front Pediatr*. 2018;6:171.

40. Lata S, Marasa M, Li Y, et al. Whole-exome sequencing in adults with chronic kidney disease: a pilot study. *Ann Intern Med*. 2018;168(2):100-109.

41. Connaughton DM, Kennedy C, Shril S, et al. Monogenic causes of chronic kidney disease in adults. *Kidney Int*. 2019;95(4):914-928.

42. Devuyst O, Knoers NV, Remuzzi G, et al. Rare inherited kidney diseases: challenges, opportunities, and perspectives. *Lancet*. 2014;383(9931):1844-1859.

43. Rosenberg AZ, Kopp JB. Focal segmental glomerulosclerosis. *Clin J Am Soc Nephrol*. 2017;12(3):502-517.

44. Bekheirnia MR, Reed B, Gregory MC, et al. Genotype-phenotype correlation in X-linked Alport syndrome. *J Am Soc Nephrol*. 2010;21(5):876-883.

45. Mele C, Iatropoulos P, Donadelli R, et al. MYO1E mutations and childhood familial focal segmental glomerulosclerosis. *N Engl J Med*. 2011;365(4):295-306.

46. Bergmann C. Early and severe polycystic kidney disease and related ciliopathies: an emerging field of interest. *Nephron*. 2019;141(1):50-60.

47. Bockenhauer D, Jaureguiberry G. HNF1B-associated clinical phenotypes: the kidney and beyond. *Pediatr Nephrol*. 2016;31(5):707-714.

48. Stijnen P, Ramos-Molina B, O'Rahilly S, Creemers JW. PCSK1 mutations and human endocrinopathies: from obesity to gastrointestinal disorders. *Endocr Rev*. 2016;37(4):347-371.

49. Seidowsky A, Hoffmann M, Glowacki F, et al. Renal involvement in MELAS syndrome - a series of 5 cases and review of the literature. *Clin Nephrol*. 2013;80(6):456-463.

50. Diomedi-Camassei F, Di Giandomenico S, Santorelli FM, et al. COQ2 nephropathy: a newly described inherited mitochondriopathy with primary renal involvement. *J Am Soc Nephrol*. 2007;18(10):2773-2780.

51. Park E, Ahn YH, Kang HG, et al. COQ6 mutations in children with steroid-resistant focal segmental glomerulosclerosis and sensorineural hearing loss. *Am J Kidney Dis*. 2017;70(1):139-144.

52. Korkmaz E, Lipska-Zietkiewicz BS, Boyer O, et al. ADCK4-associated glomerulopathy causes adolescence-onset FSGS. *J Am Soc Nephrol*. 2016;27(1):63-68.

53. Emma F, Bertini E, Salviati L, Montini G. Renal involvement in mitochondrial cytopathies. *Pediatr Nephrol*. 2012;27(4):539-550.

54. Zsurka G, Hampel KG, Nelson I, et al. Severe epilepsy as the major symptom of new mutations in the mitochondrial tRNA(Phe) gene. *Neurology*. 2010;74(6):507-512.

55. Petrovski S, Goldstein DB. Unequal representation of genetic variation across ancestry groups creates healthcare inequality in the application of precision medicine. *Genome Biol*. 2016;17(1):157.

56. Mallett AJ, McCarthy HJ, Ho G, et al. Massively parallel sequencing and targeted exomes in familial kidney disease can diagnose underlying genetic disorders. *Kidney Int*. 2017;92(6):1493-1506.

57. Yao T, Udwan K, John R, et al. Integration of genetic testing and pathology for the diagnosis of adults with FSGS. *Clin J Am Soc Nephrol*. 2019;14(2):213-223.

58. Braun DA, Schueler M, Halbritter J, et al. Whole exome sequencing identifies causative mutations in the majority of consanguineous or familial cases with childhood-onset increased renal echogenicity. *Kidney Int*. 2016;89(2):468-475.

59. Ali H, Al-Mulla F, Hussain N, et al. PKD1 duplicated regions limit clinical utility of whole exome sequencing for genetic diagnosis of autosomal dominant polycystic kidney disease. *Sci Rep*. 2019;9(1):4141.

60. Reutter H, Hilger AC, Hildebrandt F, Ludwig M. Underlying genetic factors of the VATER/VACTERL association with special emphasis on the "Renal" phenotype. *Pediatr Nephrol*. 2016;31(11):2025-2033.

61. Solomon BD. The etiology of VACTERL association: current knowledge and hypotheses. *Am J Med Genet C Semin Med Genet*. 2018;178(4):440-446.

62. Retterer K, Juusola J, Cho MT, et al. Clinical application of whole-exome sequencing across clinical indications. *Genet Med*. 2016;18(7):696-704.

63. Kirby A, Gnirke A, Jaffe DB, et al. Mutations causing medullary cystic kidney disease type 1 lie in a large VNTR in MUC1 missed by massively parallel sequencing. *Nat Genet*. 2013;45(3):299-303.

OXFORD

Suleiman-El-Hattab syndrome: a histone modification disorder caused by TASP1 deficiency

Korbinian M. Riedhammer [1,2], Anna L. Burgemeister[3], Vincent Cantagrel [4], Jeanne Amiel[5], Karine Siquier-Pernet[4],
Nathalie Boddaert[6], Jozef Hertecant[7], Patricia L. Kannouche [8], Caroline Pouvelle[8], Stephanie Htun[9], Anne M. Slavotinek [9],
Christian Beetz[10], Dan Diego-Alvarez[10], Kapil Kampe[10], Nicole Fleischer[11], Zain Awamleh[12], Rosanna Weksberg [12,13,14],
Robert Kopajtich [1,15], Thomas Meitinger[1], Jehan Suleiman [16,17] and Ayman W. El-Hattab [18,19,20,*]

[1]Institute of Human Genetics, Klinikum rechts der Isar, School of Medicine, Technical University of Munich, 81675 Munich, Germany
[2]Department of Nephrology, Klinikum rechts der Isar, School of Medicine, Technical University of Munich, 81675 Munich, Germany
[3]Genetikum, Genetic Counseling and Diagnostics, 70173 Stuttgart, Germany
[4]Developmental Brain Disorders Laboratory, Université Paris Cité, Imagine Institute, INSERM UMR, 75015 Paris, France
[5]Department of Genetics, AP-HP, Necker Enfants Malades Hospital, Université Paris Cité, Imagine Institute, 75015 Paris, France
[6]Département de radiologie pédiatrique, INSERM UMR 1163 and INSERM U1000, AP-HP, Necker Enfants Malades Hospital, 75015 Paris, France
[7]Division of Genetics and Metabolics, Department of Pediatrics, Tawam Hospital, Al Ain, United Arab Emirates
[8]CNRS UMR 9019, Université Paris-Saclay, Equipe labellisée Ligue contre le Cancer, Gustave Roussy, 94805 Villejuif, France
[9]Department of Pediatrics, Division of Genetics, University of California, San Francisco, San Francisco, CA 94143, USA
[10]Centogene GmbH, 18055 Rostock, Germany
[11]FDNA Inc., Boston, MA 02111, USA
[12]Genetics and Genome Biology, Research Institute, The Hospital for Sick Children, Toronto, Ontario M5G 0A4, Canada
[13]Division of Clinical and Metabolic Genetics, The Hospital for Sick Children, Toronto, Ontario M5G 1X8, Canada
[14]Department of Molecular Genetics, Institute of Medical Sciences, University of Toronto, Toronto, Ontario M5S 1A1, Canada
[15]Institute of Neurogenomics, Helmholtz Zentrum München, 85764 Neuherberg, Germany
[16]Division of Neurology, Department of Pediatrics, Tawam Hospital, Al Ain, United Arab Emirates
[17]Department of Pediatrics, College of Medicine and Health Sciences, United Arab Emirates University, Al Ain, United Arab Emirates
[18]Department of Clinical Sciences, College of Medicine, University of Sharjah, Sharjah, United Arab Emirates
[19]Pediatrics Department, University Hospital Sharjah, Sharjah, United Arab Emirates
[20]Genetics and Metabolic Department, KidsHeart Medical Center, Abu Dhabi, United Arab Emirates
*To whom correspondence should be addressed at: College of Medicine, University of Sharjah, P.O. Box 27272, Sharjah, United Arab Emirates. Tel: +971 508875123;
Fax: +97137131044; Email: elhattabaw@yahoo.com

Abstract

Background: TASP1 encodes an endopeptidase activating histone methyltransferases of the KMT2 family. Homozygous loss-of-function variants in *TASP1* have recently been associated with Suleiman-El-Hattab syndrome. We report six individuals with Suleiman-El-Hattab syndrome and provide functional characterization of this novel histone modification disorder in a multi-omics approach. *Methods:* Chromosomal microarray/exome sequencing in all individuals. Western blotting from fibroblasts in two individuals. RNA sequencing and proteomics from fibroblasts in one individual. Methylome analysis from blood in two individuals. Knock-out of *tasp1* orthologue in zebrafish and phenotyping. *Results:* All individuals had biallelic *TASP1* loss-of-function variants and a phenotype including developmental delay, multiple congenital anomalies (including cardiovascular and posterior fossa malformations), a distinct facial appearance and happy demeanor. Western blot revealed absence of TASP1. RNA sequencing/proteomics showed *HOX* gene downregulation (*HOXA4, HOXA7, HOXA1* and *HOXB2*) and dysregulation of transcription factor TFIIA. A distinct methylation profile intermediate between control and Kabuki syndrome (*KMT2D*) profiles could be produced. Zebrafish *tasp1* knock-out revealed smaller head size and abnormal cranial cartilage formation in *tasp1* crispants. *Conclusion:* This work further delineates Suleiman-El-Hattab syndrome, a recognizable neurodevelopmental syndrome. Possible downstream mechanisms of TASP1 deficiency include perturbed *HOX* gene expression and dysregulated TFIIA complex. Methylation pattern suggests that Suleiman-El-Hattab syndrome can be categorized into the group of histone modification disorders including Wiedemann–Steiner and Kabuki syndrome.

Introduction

Homozygous loss-of-function variants in *TASP1* (MIM *608270) have recently been associated with an autosomal recessive syndrome featuring developmental delay, happy demeanor, distinctive facial features and congenital anomalies (1). It has been termed 'Suleiman-El-Hattab syndrome' (MIM #618950).

TASP1 encodes taspase 1 (threonine aspartase 1, TASP1). This enzyme functions as a heterodimeric endopeptidase activating various nuclear factors, including histone methyltransferases of the evolutionarily conserved KMT2 family of proteins like KMT2A and KMT2B, which are part of the epigenetic machinery (2). Epigenetic marks are modifications of DNA (e.g.

methylation of cytosine nucleotides) or histone tails influencing transcriptional activity of genes without altering the DNA sequence itself (3). Because of this central role in regulation of transcriptional activity, it is not surprising that variation in genes of the epigenetic machinery can result in Mendelian disorders. Haploinsufficiency of *KMT2A* has been associated with Wiedemann–Steiner syndrome [MIM #605130; (4)]. Haploinsufficiency of *KMT2B* has been associated with complex childhood-onset dystonia [MIM #617284; (5)]. Another member of the evolutionary conserved KMT2 family of histone methyltransferases is KMT2D. Haploinsufficiency of *KMT2D* has been associated with Kabuki syndrome 1 [MIM #147920; (6)].

To date, Suleiman-El-Hattab syndrome has been described in four individuals. We present here six individuals with Suleiman-El-Hattab syndrome including three unreported individuals and three previously reported individuals with updated phenotypic information. We further delineate the phenotypic and genotypic spectrum of this recently described syndrome, and additionally present both *in vitro* and *in vivo* functional work showing the consequences of biallelic *TASP1* loss-of-function variants.

Results

Phenotypic characteristics

We present six individuals from five unrelated families with Suleiman-El-Hattab syndrome with biallelic putative loss-of-function variants in *TASP1*.

The six individuals were between 9 months and 10 years old. All had a neurodevelopmental phenotype featuring developmental delay with severe speech delay (older individuals remained non-verbal or only said few words) and motor delay (walking between ages two and four), hypotonia and microcephaly. Feeding difficulties were observed in all and most had failure to thrive. Happy demeanor was a common finding.

In terms of facial appearance, typical facial dysmorphies included thick and arched eyebrows, thick eyelids, periorbital fullness, synophrys, epicanthus, a broad nasal bridge, a wide mouth with a long smooth philtrum and a thin upper and thick lower lip, low-set and dysplastic ears and a preauricular skin tag (Fig. 1A, B, E, G, and I).

Congenital anomalies were common including brain malformations (especially posterior fossa malformations; Fig. 2), cardiovascular malformations (ventricular and atrial septal defects and tetralogy of Fallot), limb and skeletal deformities and cryptorchidism in males. Hirsutism and recurrent respiratory infections were also commonly observed.

Table 1 summarizes the phenotypic characteristics of the cohort and detailed clinical descriptions can be found in the Supplementary case reports.

The DeepGestalt algorithm could establish a distinct facial gestalt for Suleiman-El-Hattab syndrome [Fig. 1K; (7)]. The descriptor of photos of individuals genetically diagnosed with Suleiman-El-Hattab syndrome is distinct from all other descriptors of syndromes in the dataset (300+) achieving an area under the curve of 0.975 (95% confidence interval 88–93%).

Genotypic characteristics

Chromosomal microarray (CMA) in individual 1 revealed a homozygous deletion at 20p12.1 with a minimum deletion boundary of chr20:g.13 463 860–13 532 560 (hg19). This deletion encompasses part of *TASP1*. Breakpoint mapping revealed that this deletion is 149.4 kb in size spanning chr20:g.13 448 380–13 597 783 and includes exons 5–11 of *TASP1* [NM_017714.3; (1)]. CMA in individual 2, brother of individual 1, revealed the same deletion in a homozygous state. CMA in individual 3 revealed a homozygous deletion at 20p21.2 with a minimum deletion boundary of ch20:g.13 447 411–13 606 048. Breakpoint mapping revealed the same boundaries as in individual 1 (chr20:g.13 448 380–13 597 783), including exons 5–11 of *TASP1*. CMA in individual 4 identified a homozygous deletion with a minimum deletion boundary of chr20:g.13 466 774–13 593 390. Breakpoint mapping revealed the same boundaries as in individual 1 (chr20:g.13 448 380–13 597 783), including exons 5–11 of *TASP1* (1). For these individuals, parents were found to be heterozygous for the deletion, and none of the healthy siblings were found to have a homozygous deletion in this region (Fig. 1C, D and F). This intragenic deletion disrupts the active site of the enzyme (at amino acid position 234; NP_060184.2; see https://www.uniprot.org/uniprot/Q9H6P5/protvista) and is predicted to lead to a frameshift supporting the loss-of-function nature of this variant (1,8). It has previously been shown that individuals 1 and 4 share the same haplotype surrounding the deletion and that it is a founder deletion in the Arabian Peninsula (1).

Exome sequencing in individual 5 revealed a homozygous nonsense variant in *TASP1* c.199C > T, p.(Arg67*) (chr20:g.13 605 846G > A). The variant p.(Arg67*) was reported once in a heterozygous state in the Genome Aggregation Database (gnomAD v.2.1.1, https://gnomad.broadinstitute.org/; allele frequency of 4×10^{-6}) indicating that it is an extremely rare variant. This variant is predicted to either lead to nonsense-mediated decay or a truncated protein leading to a complete loss of function. Both parents are confirmed to be heterozygous carriers for this variant (Fig. 1H). Trio exome sequencing in individual 6 revealed compound-heterozygous frameshift variants c.81del, p.(Glu29Serfs*79) (chr20:g.13 610 645del) and c.598_599del, p.(Lys200Glufs*24) (chr20:g.13 539 731_13 539 732del). The father is heterozygous carrier of the p.(Glu29Serfs*79) variant and the mother is heterozygous carrier of the p.(Lys200Glufs*24) variant (Fig. 1J). Both variants have not been listed in over 140 000 individuals in gnomAD. Both variants are predicted to either lead to nonsense-mediated decay or a truncated protein. Figure 1L summarizes the localization of the different *TASP1* pathogenic variants within the gene and protein.

Table 1. Genotypic and phenotypic characteristics of individuals with Suleiman-El-Hattab syndrome

Individual	1	2	3	4	5	6	Case 3[a]	
Gender	Male	Male	Female	Female	Male	Female	Male	
Ethnicity	Arabian Peninsula	Arabian Peninsula	Arabian Peninsula	Arabian Peninsula	Turkish	North Africa	Arabian Peninsula	
Age	7 years	9 months	19 months	3 years	6 years	10 years	3 years	
TASP1 allele 1	Exon 5–11 deletion	Exon 5–11 deletion	Exon 5–11 deletion	Exon 5–11 deletion	c.199C > T p.(Arg67*)	c.81del p.(Glu29Serfs*79)	c.701C > T p.(Thr234Met)	
TASP1 allele 2	Exon 5–11 deletion	Exon 5–11 deletion	Exon 5–11 deletion	Exon 5–11 deletion	c.199C > T p.(Arg67*)	c.(598_599del) p.(Lys200Glufs*24)	c.701C > T p.(Thr234Met)	
Neurodevelopment								
Developmental delay	+	+	+	+	+	+	+	7/7
Hypotonia	+	+	+	+	+	–	+	6/7
Microcephaly	+	–	+	+	+	+	+	6/7
Seizures	–	–	–	–	+	–	+	2/7
Posterior fossa malformation	–	+	+	–	+	+	–	4/7
Dilated ventricles	–	+	–	–	+	+	+	4/7
Feeding and growth								
Feeding difficulties	+	+	+	+	+	+	+	7/7
Salivary drooling	+	–	+	+	–	–	+	4/7
Failure to thrive	+	+	+	+	–	–	+	5/7
Happy demeanor	+	NA (too young)	+	+	+	–	+	5/6
CVS malformation	ASD/VSD	TOF	PFO/VSD	PFO/VSD	VSD	VSD	–	6/7
Cryptorchidism	+	–	NA	NA	+	NA	+	3/4
Hirsutism	+	–	+	+	–	–	–	4/7
Recurrent respiratory infections	+	–	+	+	+	–	–	4/7
Preauricular skin tag	–	+	+	+	+	–	–	4/7
Single palmar crease	+	–	–	+	+	–	–	3/7
Facial features								
Prominent glabella	+	+	+	–	+	–	+	4/7
Excess forehead hair	+	–	+	+	–	–	–	4/7
Thick eyebrows	+	+	+	+	+	+	+	7/7
Arched eyebrows	+	+	+	+	+	+	+	7/7
Synophrys	+	+	+	+	+	+	+	7/7
Epicanthus	+	+	+	+	+	+	+	7/7
Hypertelorism	+	+	+	+	+	+	+	7/7
Downslanted eyes	–	–	+	+	–	–	–	2/7
Thick eyelids	+	+	+	+	+	+	+	7/7
Periorbital fullness	+	+	+	+	+	+	+	7/7
Broad nasal bridge	+	+	+	+	+	+	+	7/7
Long smooth philtrum	+	+	+	+	–	+	+	6/7
Wide mouth	+	+	+	+	–	+	+	6/7
Thin upper lip	+	+	+	+	+	+	+	7/7
Thick lower lip	+	+	+	+	+	+	+	7/7
Microretrognathia	–	+	+	–	+	–	–	3/7
High arched palate	–	–	+	–	+	–	–	2/7
Low-set ears	+	+	+	+	+	+	+	7/7
Dysplastic ears	+	+	+	+	+	+	+	7/7
Webbed neck	+	–	+	+	–	–	–	3/7
Ophthalmologic anomalies	–	–	–	Hyperopia	Strabismus, amblyopia, pale optic disc	Hyperopia	–	
Limb deformities	Brachydactyly, clinodactyly	Overlapping toes	–	Polydactyly	–	Short extremities, brachydactyly, broad thumb and first toe	–	
Skeletal deformities	–	–	–	–	–	Scoliosis, genu recurvatum	Short stature	
Skin	–	Lumbar skin dimple	Sacral hair tuft,	Congenital dermal melanocytosis	–	–	–	
Others	Hearing impairment	–	Umbilical hernia	Left hydronephrosis	Inguinal hernia	Choanal stenosis, anteriorly placed anus, spasticity of the lower limbs	–	

ASD, atrial septal defect; CNS, central nervous system; CVS, cardiovascular; NA, not applicable; PFO, patent foramen ovale; TOF, tetralogy of Fallot; VSD, ventricular septal defect. *TASP1* transcript NM_017714.3, TASP1 protein NP_060184.2. [a]Described in (1), no new phenotypic or functional data. Featured in the table and the discussion to present all reported individuals with Suleiman-El-Hattab syndrome.

Western blot

Western blot from primary fibroblasts from individuals 5 and 6 confirmed that TASP1 protein (alpha-subunit p28) is not observed in these cells compared with primary fibroblasts from a healthy donor (Fig. 1M). The specificity of the TASP1 antibody was verified by downregulating *TASP1* gene expression using specific siRNAs. A clear reduction of TASP1 protein levels with
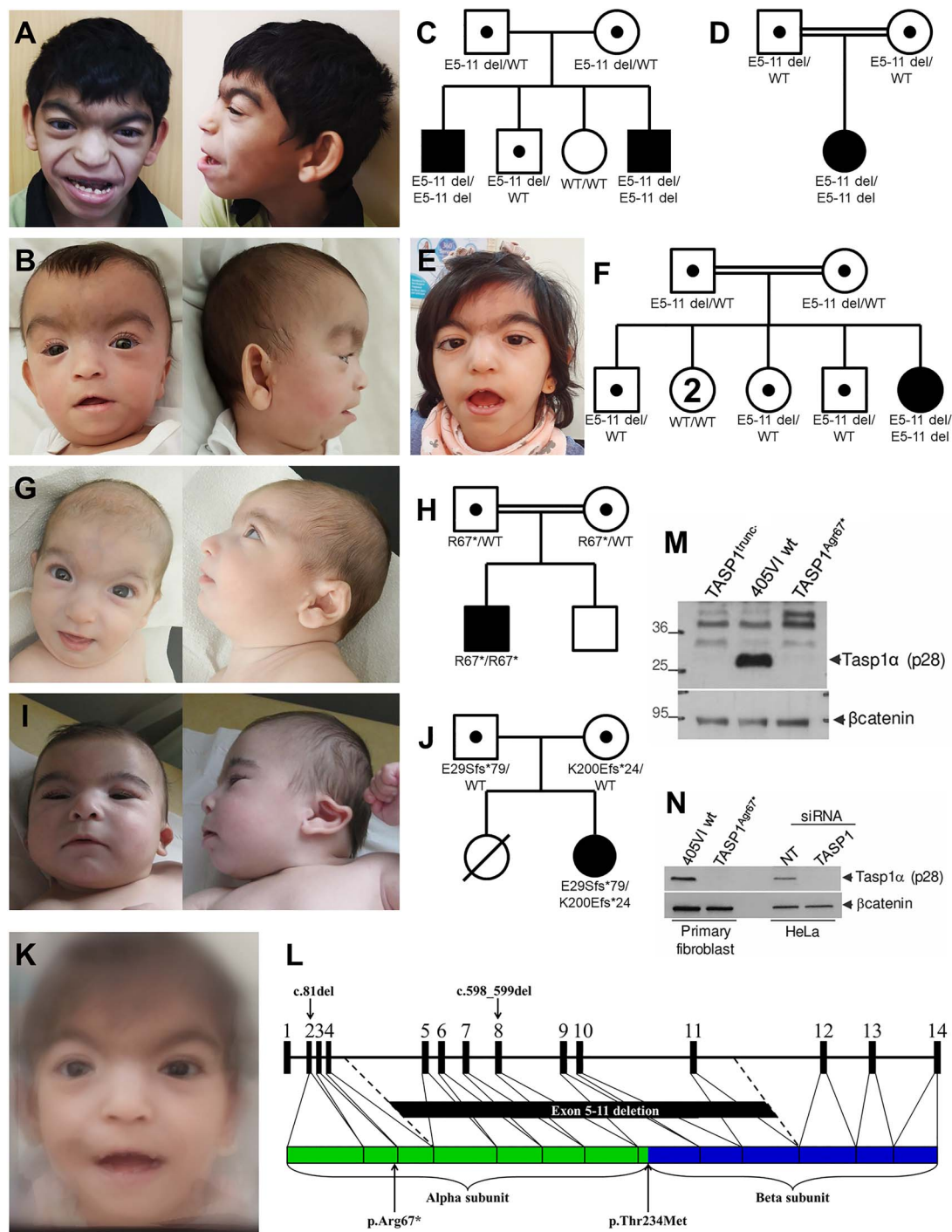
Figure 1. Pedigrees and photographs of affected individuals, DeepGestalt composite image, western blot results, and schematic image of *TASP1* gene and corresponding protein. Circles, female individual; crossed circle, deceased female individual; dot within circles/squares, heterozygous carrier of the respective *TASP1* variant and double horizontal line, consanguineous couple; squares, male individual. (**A**) Individual 1 at 7 years of age showing prominent glabella, excessive forehead hair, thick and arched eyebrows with synophrys, epicanthus, hypertelorism, periorbital fullness with thick eyelids, broad nasal bridge, long and smooth philtrum, wide mouth, thin upper lip, thick lower lip, low-set dysplastic ears and webbed neck. (**B**) Individual 2 at 6 months of age showing prominent glabella, thick and arched eyebrows with synophrys, epicanthus, hypertelorism, periorbital fullness with thick eyelids, broad and flat nasal bridge, long and smooth philtrum, wide mouth, thin upper lip, thick lower lip, microretrognathia, low-set dysplastic ears and preauricular skin tag. (**C**) Pedigree of individuals 1 and 2. (**D**) Pedigree of individual 3. Parents elected not to publish the individual's photographs. Facial features include prominent glabella, excessive forehead hair, arched and thick eyebrows with synophrys, epicanthus, downslanted palpebral fissures, hypertelorism, periorbital fullness with thick eyelids, broad nasal bridge, long and smooth philtrum, wide mouth, thin upper lip, thick lower lip, high arched palate and low-set dysplastic ears. (**E**) Individual 4 at 2 years of age showing excessive forehead hair, arched and thick eyebrows with synophrys, epicanthus, downslanted palpebral fissures, hypertelorism, periorbital fullness with thick eyelids, broad nasal bridge, long and smooth philtrum, wide mouth, thin upper lip, thick lower lip, low-set dysplastic ears and webbed neck. (**F**) Pedigree of individual 4. (**G**) Individual 5 at 4 months of age showing excessive forehead hair, thick and arched eyebrows with synophrys, epicanthus, hypertelorism, periorbital fullness with thick eyelids, broad nasal bridge, thin upper lip, thick lower lip, microretrognathia, high arched palate, low-set dysplastic ears and preauricular skin tag. (**H**) Pedigree of individual 5. (**I**) Individual 6 at 4 months of age showing thick and arched eyebrows with synophrys, epicanthus, hypertelorism, periorbital fullness with thick

siRNA transfection in HeLa cells was observed (Fig. 1N). No difference in global levels of H3K4me3 histone mark could be detected in primary fibroblasts of individual 5 compared with primary fibroblasts from a healthy donor (Supplementary Fig. S1).

RNA sequencing and proteomics

RNA sequencing from fibroblasts of individual 5 revealed 20 significant differentially expressed genes (Supplementary Table S1). Notable differentially expressed genes were: *GTF2A1* (adjusted $P = 8.15 \times 10^{-7}$), which was upregulated (log2fc = 0.55); *HOXA4* (adjusted $P = 5.02 \times 10^{-4}$; log2fc = −5.42), *HOXA7* (adjusted $P = 7.86 \times 10^{-4}$; log2fc = −5.4), *HOXB2* (adjusted $P = 9.5 \times 10^{-3}$; log2fc = −1.8) and *HOXA1* (adjusted $P = 0.0312$, log2fc = 5.15), which were all downregulated (Fig. 3A).

Quantitative proteomics from fibroblasts of individual 5 resulted in the identification of 13 significant aberrant protein levels (Supplementary Table S2). One notable significant outlier was GTF2A2 (adjusted $P = 0.001770059$; log2fc = 1.74), which was upregulated (Fig. 3B). TASP1 protein was not detected in the corresponding TMT-batch, hence proteomics was not able to provide any additional evidence on TASP1 protein stability.

DNA methylation pattern

Since the number of available *TASP1* samples is not sufficient to establish a robust disorder-specific signature, we clustered the DNA methylation (DNAm) profiles of two individuals carrying homozygous loss-of-function *TASP1* variants, individual 4 (deletion exons 5–11) and individual 5 (p.Arg67*), using the published Kabuki syndrome 1 signature (9). Principal component analysis (PCA) based on DNAm values at 114 Kabuki syndrome 1 signature sites clearly distinguishes the DNAm profile of healthy controls from DNAm profiles of the five individuals with Kabuki syndrome 1 on the first principal component (PC1) and the two individuals carrying *TASP1* variants on PC2 (Fig. 3C). Hierarchal clustering shows that, at Kabuki syndrome 1 signature sites, individuals carrying *TASP1* variants have distinct DNAm profiles that are intermediate when compared with the DNAm profiles of Kabuki syndrome 1 individuals and controls (Fig. 3D).

Zebrafish experiments

We were successfully able to target the single, *tasp1* gene in *Danio rerio* and generate homozygous, F2 larvae with an indel variant predicting loss of function, c.313_314delTC, p.Ser105Glyfs*2 (ENSDART00000133661.3; Fig. 4A). Sectioning and staining of larval heads at 6 days post fertilization (dpf) showed wildtype EKW had an average brain area of 15,596 μm^2 (Fig. 4B) compared with 14,747 $\mu m2$ in larvae homozygous for the *tasp1* indel variant (Fig. 4C). A comparison of the cranial cartilages stained with Alcian blue in wildtype larvae (Fig. 4D) and homozygous, *tasp1* indel larvae (Fig. 4G and J) showed that *tasp1* crispant larvae had smaller trabeculae and shorter ethmoid cartilages compared with wildtype larvae. Wildtype larvae also had longer ceratobranchial and ceratohyal cartilages (Fig. 4E) compared with homozygous, *tasp1* indel larvae (Fig. 4H and K). Wildtype larvae had longer lower jaw lengths and larger palatoquadrate and Meckel's cartilages (Fig. 4F) compared with homozygous, *tasp1* indel larvae (Fig. 4I and L).

Discussion

Here, we report phenotypic, genotypic and functional data on the largest cohort of individuals with the recently characterized Suleiman-El-Hattab syndrome caused by biallelic loss-of-function variants in *TASP1*. The cohort presented here features six individuals with Suleiman-El-Hattab syndrome. Also included in the discussion and Table 1 is a seventh individual, previously described as case 3 in Suleiman *et al.* [no updated data; (1)].

These seven individuals have an overlapping phenotype of global developmental delay (7/7) with delayed motor development and severe speech delay (4/5 individuals at ages 3–10 years were non-verbal), microcephaly (6/7) and brain malformations (4/7), hypotonia (6/7), feeding difficulties (7/7), a happy demeanor (5/6; individual 2 was too young) and cardiovascular malformations (6/7), which were mostly mild [ventricular septal defect/atrial septal defects (ASD/VSD) with spontaneous resolution]. However, individual 2 had severe cardiac malformation (TOF) and required surgery (Table 1).

Notably, concerning brain malformations, 4/7 individuals had cystic malformations of the posterior fossa, with variable degrees ranging from small cerebellopontine angle arachnoid cyst, dilated fourth ventricle with enlarged posterior fossa along with cerebellar vermian hypoplasia, to the full extent of classic Dandy–Walker malformation associated with hydrocephalus [individuals 2, 3, 5 and 6; Fig. 2; (10,11)]. This extends the neurologic phenotype of Suleiman-El-Hattab syndrome and might further help in recognition of this syndrome. In addition, this supports the notion that imaging findings

---

eyelids, broad and flat nasal bridge, long and smooth philtrum, wide mouth, thin upper lip, thick lower lip, low-set and dysplastic ears and a short neck. (**J**) Pedigree of individual 6. (**K**) DeepGestalt composite image generated from facial images of individuals with genetically proven Suleiman-El-Hattab syndrome. The facial gestalt is distinct from all other descriptors of syndromes in the Face2Gene dataset (300+ syndromes). (**L**) *TASP1* gene structure (NM_017714.3) and corresponding protein (NP_060184.2) with respective identified variants. Please note that the missense variant p.(Thr234Met) has been identified in a homozygous state in case 3 in Suleiman *et al.*, 2019 [no updated data; (1)]. (**M**) Western blot. TASP1 protein (alpha-subunit p28) is not observed in primary fibroblasts carrying biallelic loss-of-function variants (TASP1Arg67*, individual 5; TASP1trunc, individual 6) compared with primary fibroblasts from a healthy donor (405VI wt). (**N**) TASP1 antibody specificity was verified by downregulating *TASP1* gene expression using specific *TASP1*-targeting siRNAs. A clear reduction of TASP1 protein levels with siRNA transfection in HeLa cells was observed. NT, non-targeted siRNA; 405VI wt, primary fibroblasts of control and TASP1Arg67*, primary fibroblasts of individual 5.

of cerebellar hypoplasia and Dandy–Walker malformation are often associated with underlying genetic causes and should prompt further evaluation (12).

Affected individuals feature a distinctive facial pattern, as also mathematically proven by the DeepGestalt algorithm, involving thick and arched eyebrows with synophrys, epicanthus, downslanted palpebral fissures, hypertelorism, broad nasal bridge, long and smooth philtrum, wide mouth with thin upper lip and thick lower lip, microretrognathia and ear anomalies [dysplastic, low-set; (7)]. This makes the syndrome recognizable by clinical geneticists and the syndrome is now featured in the Face2Gene online tool (https://www.face2gene.com).

TASP1 encodes the proenzyme taspase 1 (threonine aspartase 1, TASP1), which is cleaved into two subunits, alpha and beta, in an autocatalytic fashion, which in turn form the active heterodimeric enzyme, an endopeptidase. The active enzyme uses the N-terminal threonine at amino acid position 234 (p.Thr234) of the mature beta subunit as the active-site nucleophile to proteolyze polypeptide substrates. This endopeptidase cleaves various nuclear factors after an aspartate, hence it is called threonine aspartase (taspase). For example, active TASP1 cleaves and hence activates histone methyltransferases of the KMT2 protein family like KMT2A and KMT2B. Cleavage of KMT2A (also known as MLL1) in turn is crucial for *HOX* and cyclin gene expression, which is important for cell cycle dynamics (2,13). In line with this, individual 5, who harbors a homozygous nonsense variant in *TASP1* and has no detectable TASP1 protein on Western blot (Fig. 1M), showed significant RNA downregulation of *HOX* genes *HOXA4, HOXA7, HOXA1* and *HOXB2* (Fig. 3A). Coordinated *HOX* expression is central for a correct segmental body plan (14). Hence, dysregulation of *HOX* genes likely plays a role in the congenital and neurodevelopmental anomalies observed in TASP1-deficient individuals. However, it has to be pointed out that we tested the global level of the histone mark catalyzed by KMT2A histone methyltransferase (i.e. H3K4m3) and did not find any different levels between wildtype and *TASP1* mutated cells (Supplementary Fig. S1) suggesting that the activity of KMT2A is not completely dependent of its TASP1-mediated proteolysis. This is consistent with the study of Zhao *et al.* (15–17), which showed that TASP1-dependent cleavage of KMT2A facilitates its degradation (and not its activity) to control the levels of KMT2A, reminiscent of that of TFIIA (see below). An alternative explanation for the unaffected levels of H3K4m3 in TASP1-mutated cell lines could be because of a compensatory phenomenon with other members of this histone methyltransferase family that do not required TASP1 cleavage. Hence, further studies need to be undertaken to unravel the intricate regulation of histone methyltransferases by TASP1.

Another substrate of TASP1 is transcription factor TFIIA$\alpha-\beta$ (*GTF2A1*), a general transcription factor with ubiquitous expression featuring an alpha and beta subunit. TFIIA$\alpha-\beta$ is bound to TFIIAγ (*GTF2A2*). When TASP1 cleaves the alpha and beta subunit of TFIIA$\alpha-\beta$, the heterotrimeric complex TFIIA$\alpha/\beta/\gamma$ (encoded by *GTF2A1* and *GTF2A2*, summarized as TFIIA) is susceptible to degradation by the proteasome impeding its transcriptional activity (2,17). Regulated turnover of TFIIA is key for correct embryonal cell proliferation and morphogenesis. Tasp1-deficient and Tfiia-noncleavable mice both show craniofacial anomalies such as jaw, eye and brain malformations (8). Intriguingly, on RNA sequencing of TASP1-deficient individual 5, *GTF2A1* (TFIIA$\alpha-\beta$) is upregulated; and on proteomics, GTF2A2 (TFIIAγ) is upregulated, probably illustrating the stable non-cleaved TFIIA complex (Fig. 3A and B). Hence, the neurodevelopmental phenotype including the central nervous system anomalies in Suleiman-El-Hattab syndrome could be because of TFIIA dysregulation including a positive feedback loop (*GTF2A1* upregulation on RNA sequencing). Of course, it is a limitation, that RNA sequencing and proteomics data are only available from one individual. The findings are still biologically convincing. Nonetheless, further studies are needed for replication.

As TASP1 cleaves and hence activates histone methyltransferases of the KMT2 protein family, it is expected that defects in *KMT2*-genes result in syndromes with overlapping features of Suleiman-El-Hattab syndrome. Haploinsufficiency of *KMT2A* causes a phenotypically similar disorder, Wiedemann–Steiner syndrome (MIM #605130), also featuring developmental delay, facial anomalies, alongside hypertrichosis cubiti, growth failure, skeletal malformations, cardiac anomalies and microcephaly (4). Also individuals with haploinsufficiency of *KMT2B* (MIM #617284) can have, additionally to childhood-onset dystonia, facial anomalies such as elongated face, a bulbous nasal tip and microcephaly (18). Haploinsufficiency of *KMT2D* causes Kabuki syndrome 1 (MIM #147920), which is characterized by developmental delay, distinctive facial features, hirsutism, skeletal anomalies, persistence of fetal fingertip pads, recurrent infections, growth failure, seizures and congenital anomalies (6).

Intriguingly, Kabuki syndrome 1, Wiedemann–Steiner syndrome and Suleiman-El-Hattab syndrome share remarkable phenotypic overlap. All three are syndromic intellectual disability/developmental delay syndromes featuring a distinct facial gestalt with thick and arched eyebrows, hirsutism, growth failure and multiple congenital anomalies. *KMT2A*, *KMT2B* and *KMT2D* are all part of the highly conserved COMPASS family of histone methyltransferases. The members of the COMPASS protein family catalyze histone H3 lysine 4 (H3K4) methylation and are crucial for regulation of gene expression (2,19). As the *KMT2*-genes encode histone methyltransferases, we sought to investigate the effect of TASP1 deficiency on DNAm. Alterations of the epigenetic machinery can result in distinctive and reproducible DNAm patterns ('episignatures'), as has recently been shown for 34 monogenic neurodevelopmental disorders,
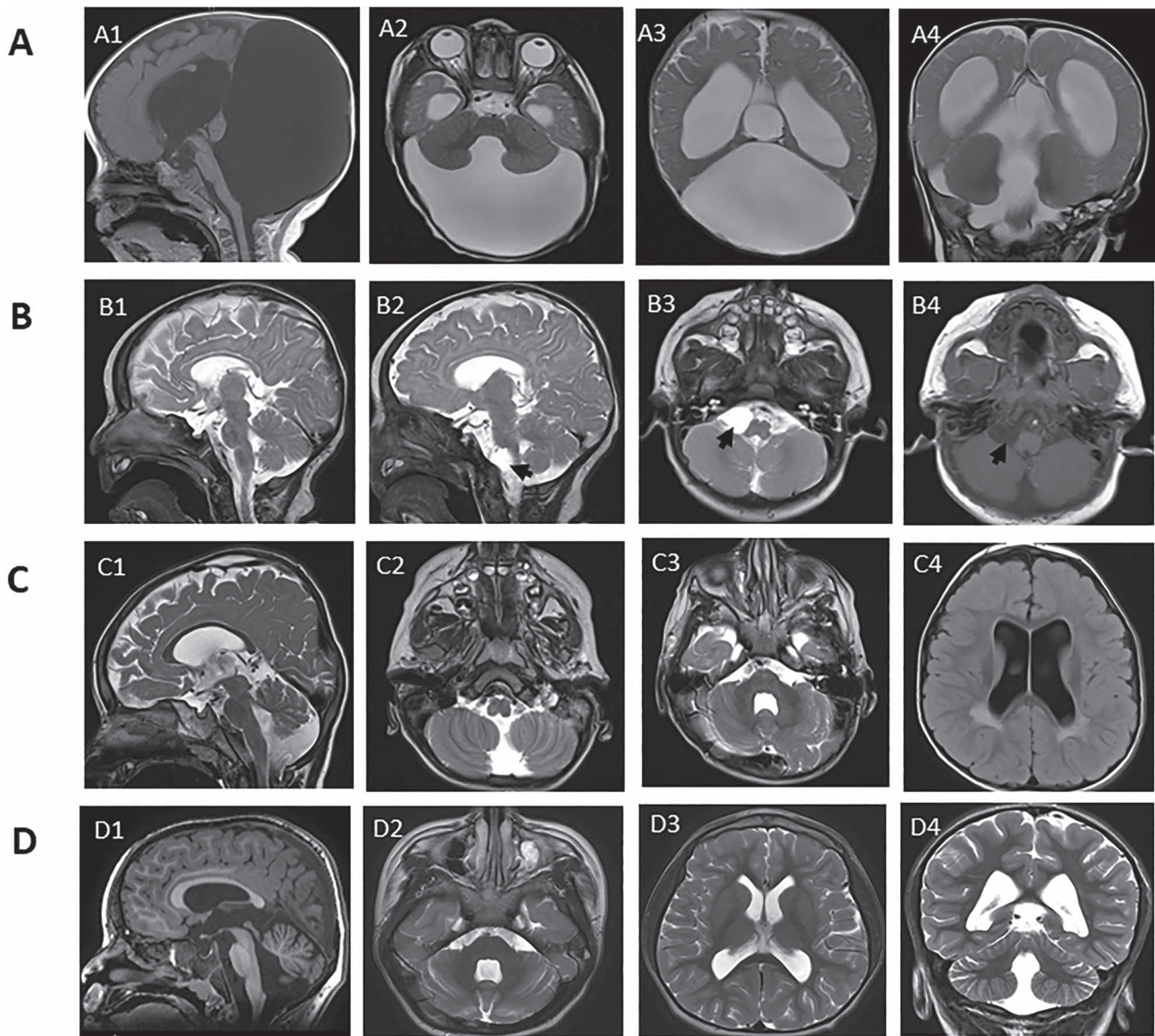
Figure 2. Cranial magnetic resonance images of four individuals with variable degrees of posterior fossa malformations. (**A**) Images of individual 2 at age 8 months; sagittal T1 (A1), axial T2 (A2 and A3) and coronal T2 (A4); showing cystic dilatation of the fourth ventricle extending posteriorly and directly communicating with a massively enlarged posterior fossa, with associated hypoplasia/dysgenesis of cerebellar vermis and small cerebellar hemispheres and cephalad rotation of the vermian remnant (Dandy–Walker malformation). In addition, significant supratentorial hydrocephalus with dilated lateral and third ventricles is seen causing stretching of the overlying corpus callosum. (**B**) Images of individual 3 at age 5 months; sagittal T2 (B1 and B2), axial T2 (B3) and axial T1 (B4); showing a well-defined right cerebellopontine angle cyst 1.2 × 1.5 × 1.5 cm (arrow in B2, 3 and 4) and hypoplasia of the splenium of the corpus callosum (best seen in B1). (**C**) Images of individual 5 at age 3 years; sagittal T2 (C1), axial T2 (C2 and C3) and axial FLAIR (C4) show dilatation of the fourth ventricle that directly communicates with a mildly enlarged posterior fossa, with associated hypoplastic inferior cerebellar vermis. In addition, dilatation of lateral and third ventricles is seen, as well as periventricular white matter hyperintensity around the posterior horn of the lateral ventricle bilaterally (seen best in C4). (**D**) Images of individual 6 at age 6 years; sagittal T1 (D1), axial T2 (D2 and D3) and coronal T2 (D4) show dilatation of the fourth ventricle that directly communicates with a retrocerebellar cyst, with associated hypoplastic inferior vermis. In addition, dilatation of lateral and third ventricles is present.

including Wiedemann–Steiner syndrome (*KMT2A*). A major advantage of this approach is that episignatures, which can be established by methylome analysis from peripheral blood, can serve as 'biomarkers' to classify variants of unknown significance in the respective genes (20). Because of the small number of investigated individuals, we could not establish a specific methylation pattern for Suleiman-El-Hattab syndrome but, interestingly, could show that the examined cases (blood DNA of individuals 4 and 5) have a distinct DNAm profile intermediate between Kabuki syndrome

1 and control profiles (Fig. 3C and D). In summary, our data suggest that Suleiman-El-Hattab syndrome can be grouped into the category of histone modification disorders.

We can also corroborate the effects of *TASP1* loss-of-function by *in vivo* data. Already in 2006, knock-out mouse experiments revealed that *Tasp1*-deficient mice were smaller in size than their wild type counterparts and cell proliferation was reduced in mutant mice (14). Indeed, also in the seven individuals with Suleiman-El-Hattab syndrome, feeding difficulties and/or failure to
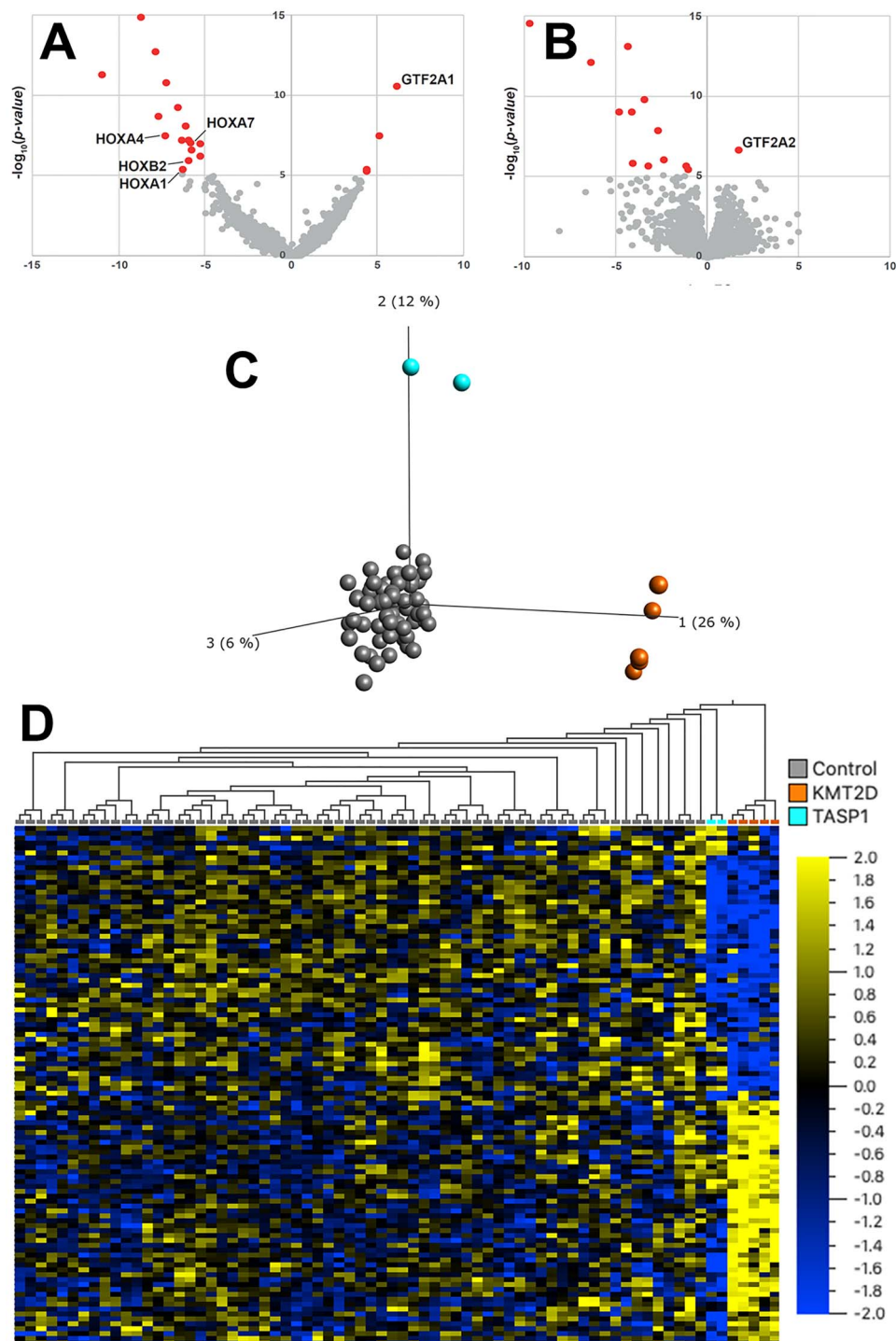
Figure 3. RNA sequencing, proteomics and DNAm (**A**) Volcano plot showing significant outliers of RNA sequencing with notable differentially expressed genes marked. (**B**) Volcano plot showing significant outliers of quantitative proteomics with notable differentially expressed protein marked. (**C**) Principal component analysis (PCA) based on DNAm values at 114 Kabuki syndrome 1 (*KMT2D*) signature sites clearly distinguishes the DNAm profile of healthy controls (*n* = 65 controls presented as grey dots), from DNAm profiles of the five individuals with Kabuki syndrome 1 (orange dots) on the first principal component (PC1) and the two individuals carrying *TASP1* variants (blue; individuals 4 and 5) on PC2 (9). (**D**) Hierarchal clustering shows that, at Kabuki syndrome 1 signature sites, individuals carrying *TASP1* variants have DNAm profiles that are intermediate when compared with the DNAm profiles of Kabuki syndrome 1 individuals and controls. Euclidean distance metric is used in the clustering dendrogram and the color gradient indicates the normalized *β* (DNAm) value ranging from −2.0 (blue) to +2.0 (yellow).

thrive was a common finding (7/7 had feeding difficulties, 5/7 failure to thrive). Microcephaly was also reported in 6/7 individuals. Reduced function for the orthologous gene, *tasp1*, in zebrafish recapitulates this difference in growth, as *tasp1* crispants have smaller head sizes in comparison with wildtype animals (Fig. 4B and C). Furthermore, *tasp1* mutants showed abnormal formation of the cranial cartilages (Fig. 4D–L). In line with this finding, individuals with Suleiman-El-Hattab syndrome feature facial anomalies, including a broad nasal bridge,

wide mouth and microretrognathia (Fig. 1K). TASP1 activates KMT2A, and it is interesting to note that zebrafish injected with antisense morpholinos targeting *kmt2a* also had significant craniofacial defects, with severe hypoplasia of the cartilaginous structures of the viscerocranium including complete loss of branchial arches 3–7, Meckel's cartilage and the ceratohyal cartilages (21). Moreover, *Tasp1* knock-out mice featured skeletal anomalies [vertebra, ribs and sternum; (14)]. In our cohort, major skeletal anomalies or dysplasia were not reported but, interestingly, there were three individuals with digital deformities (individuals 1, 4 and 6), and individual 6 also had shortened extremities. Altogether, our *in vivo* data complements and extends the *in vivo* data in the literature.

In conclusion, we further delineate the phenotypic and genotypic basis of Suleiman-El-Hattab syndrome by presenting the largest cohort of affected individuals of this recognizable syndrome. We provide functional insight in the pathophysiology of Suleiman-El-Hattab syndrome by suggesting perturbation of *HOX* gene expression and TFIIA complex dysregulation as possible downstream mechanisms of TASP1 deficiency. Furthermore, by methylation pattern analysis, we can show that Suleiman-El-Hattab syndrome can be categorized into the group of histone modification disorders including Wiedemann–Steiner and Kabuki syndrome.

Materials and methods
Recruitment of individuals
Individuals were seen in pediatric neurology and/or genetics departments of the respective institutions. Some of the individuals have been connected via GeneMatcher (22).

Molecular genetic testing
CMA for individual 1 was performed at Baylor Genetics Laboratory, Houston, TX, USA, as previously described (23). CMA for individual 2 was performed at Tawam Hospital Genetics Laboratory, Al Ain, United Arab Emirates, using CytoScan™ HD Array (Thermo Fisher Scientific, USA) as per the manufacturer's instructions. CMA for individual 3 was performed at Centogene GmbH, Rostock, Germany, using CentoArrayCyto™. Breakpoint mapping in this individual was performed using gene specific primers (F: 5′ AAGGCACTCGCAAGTAACTG 3′; R: 5′ CACTGGAAAGACAGCTTGATGC 3′) to amplify the deleted allele (1). PCR product was later sequenced on a 3730xl capillary sequencer (Applied Biosystems, USA) to identify the breakpoints. CMA for individual 4 was performed at PreventionGenetics, Marshfield, Wisconsin, USA, as previously described (24). Exome sequencing for individual 5 was performed at Helmholtz Zentrum München, Neuherberg, Germany, as previously described (25,26). Sanger sequencing was used to test the individual's parents. Trio exome sequencing for

individual 6 and parents was done at Imagine Institute, Paris, France, as previously described (27).

Distinct facial gestalt
To establish a reproducible facial gestalt for Suleiman-El-Hattab syndrome, the facial recognition algorithm DeepGestalt was used [Face2Gene, FDNA Inc., USA; (7)]. The analysis of images was first pre-processed to achieve facial detection, landmark detection and alignment. After preprocessing, the input image was cropped into facial regions. Each region was fed into a Deep Convolutional Neural Network (DCNN) to obtain a softmax vector indicating its correspondence to each syndrome in the model. The analysis of visual facial data was used to form a mathematical representation of the face (facial descriptor), which can be readily compared with other such descriptors (i.e. facial gestalt of other syndromes). To enable visualization of these vectors, a composite image was produced.

Western blot
Primary fibroblasts 405VI wt (wildtype) from a healthy donor, primary fibroblasts TASP1Arg67* (individual 5), primary fibroblasts TASP1trunc (individual 6) and tumor cells HeLa (ATCC CCL-2) were cultivated in DMEM containing 100 U/ml penicillin, 100 μg/ml streptomycin and 10% fetal calf serum (FCS). All cell lines were incubated at 37°C in an atmosphere containing 5% CO_2 and were regularly tested for mycoplasma. siRNAs were purchased from Horizon Discovery, UK: *hTASP1* (L-004745-00-0005) and non-targeting siRNA (NT, D-001810-01-05) were used as control. Cells were transfected with 30 nM of siRNAs using Interferin (Polyplus, France) according to the manufacturer's instructions and were processed 72 h later. Protein extracts were prepared and processed for SDS-PAGE as previously described (28). Membranes were then blotted with indicated antibodies: rabbit polyclonal Tasp1α (Proteintech, UK, 16739–1-AP, 1:500), mouse IgG1 β-catenin (BD Biosciences, USA, clone 14, 1:2000), rabbit polyclonal anti-Histone H3K4me3 (Abcam, UK, ab8580, 1:2000) and rabbit polyclonal anti-histone H4 (Active Motif, USA, 39 269, 1:2000).

RNA sequencing and proteomics
RNA sequencing of individual 5 was performed as strand-specific mRNA according to the TruSeq Stranded mRNA Sample Prep Guide on a NovaSeq 6000 platform (Illumina, USA) at Helmholtz Zentrum München, Neuherberg, Germany, as previously described (26). In order to detect differentially expressed genes, RNA sequencing data was analyzed using the method OUTRIDER in a cohort of 269 control samples (29).

Quantitative tandem mass tag (TMT) proteomics was performed at the BayBioMS core facility at the Technical University of Munich, Freising, Germany, and is described in detail on medRxiv (https://www.medrxiv.org/content/10.1101/2021.03.09.21253187v2.full, *in revision*).
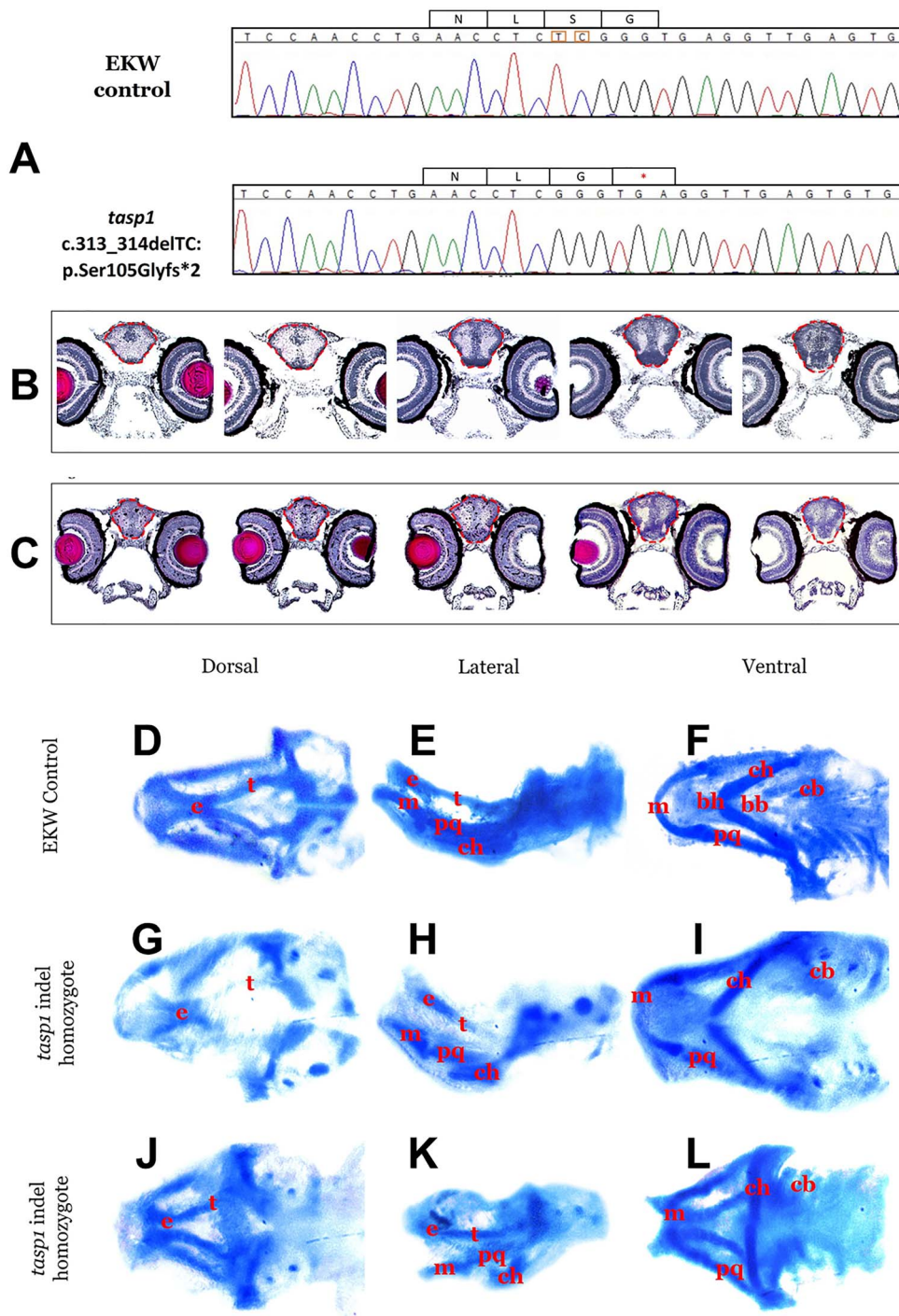
Figure 4. (**A**) Sequence of EKW control larva and a homozygous, *tasp1* larva with c.313_314delTC, predicting p.Ser105Glyfs*2 (ENSDART00000133661.3). (**B**) and (**C**) Measurement of brain area in homozygous, *tasp1* indel larvae shows a smaller size compared with wildtype control larvae. (B) Measurement of brain area from control larvae at 6 dpf. Larval brain area was measured from an average of five consecutive sections of brain containing diencephalon (red dotted line). (C) Measurement of brain area from homozygous, *tasp1* indel larvae at 6 dpf. Larval brain area was measured from an average of five consecutive sections of brain containing diencephalon (red dotted line). This difference was not statistically significant. (**D**)–(**L**) Homozygous, *tasp1* indel larvae show abnormal development and hypoplasia of the cranial cartilages at 6 dpf compared with wildtype controls. bb, basibranchial; bh, basihyal; cb, ceratobranchial; ch, ceratohyal; e, ethmoid plate; m, Meckel's cartilage; pq, palatoquadrate and t, trabeculae cranii. (D) Dorsal view of cranial cartilages in 6 dpf EKW control larvae. (E) Lateral view of cranial cartilages in 6 dpf control larvae. (F) Ventral view of cranial cartilages in 6 dpf control larvae. (G) Dorsal view of 6 dpf *tasp1* homozygous larvae with mild abnormality in cranial cartilages, showing ethmoid plate length is slighter shorter compared with EKW control. (H) Lateral view of 6 dpf *tasp1* homozygous larvae with mild abnormality in cranial cartilages, showing shorter cartilage lengths compared with EKW control. (I) Ventral view of 6 dpf *tasp1* homozygous larvae with mild abnormality in cranial cartilages, showing wider angle between ceratohyal cartilages compared with EKW control. (J) Dorsal view of 6 dpf *tasp1* homozygous larvae with more severe abnormality in cranial cartilages, showing ethmoid plate is severely shorter and trabeculae cranii are abnormally positioned by growing further toward lateral compared with EKW control. (K) Lateral view of 6 dpf *tasp1* homozygous larvae with severe abnormality in cranial cartilages, showing that trabeculae and other cartilages are abnormally positioned and appear to be more ventrally located and the ceratohyal cartilage appears to be shorter compared with EKW control. (L) Ventral view of 6 dpf *tasp1* homozygous larvae with severe abnormality in cranial cartilages, showing shorter ceratobranchial and ceratohyal cartilages and atypical basibranchial and basihyal cartilages. Palatoquadrate and Meckel's cartilage appear shorter in *tasp1* homozygous larvae and thus the lower jaw length appears shorter than the upper jaw.

DNAm pattern

Genomic DNA extracted from blood was treated with sodium bisulfite using the EpiTect PLUS Bisulfite Kit (Qiagen, Germany) and hybridized to the Illumina Infinium Human Methylation EPIC BeadChip (Illumina, USA) to interrogate more than 850 000 CpG sites at The Center for Applied Genomics (TCAG), Hospital for Sick Children Research Institute, Toronto, Ontario, Canada. The *TASP1* samples with age-and sex-matched typically developing controls were run in two batches. The minfi Bioconductor package was used to preprocess data including quality control, Illumina normalization and background subtraction and extraction of β values. Probes with detection flaws, probes near single-nucleotide polymorphisms (SNPs) with minor allele frequencies above 1%, cross-reactive probes, probes with raw beta of 0 or 1 in >0.25% of samples, non-CpG probes and sex chromosome probes were removed according to the published pipeline (30). A total of $n = 774\,558$ probes remained for interrogating DNAm levels. *TASP1* samples (blood DNA of individuals 4 and 5) were compared with DNAm data from typically developing controls ($n = 65$) and individuals diagnosed with Kabuki syndrome 1 with a pathogenic *KMT2D* variant [$n = 5$; (9)].

Zebrafish

A Clustered Regularly Interspaced Short Palindromic Repeats (CRISPR) single guide (sg)RNA targeting exon 5 of *tasp1* (ENSDART00000133661.3) was designed. sgRNA and Cas9 protein were co-injected into wildtype EKW zebrafish eggs and F0 founders with mosaicism for small indels in *tasp1* at the target site were selected. Adult F1 heterozygotes with germline *tasp1* indel variants were crossed to obtain F2, homozygous larvae. Larvae were cryosectioned and hematoxylin and eosin staining was performed. For measurements of brain size, 12-μm sections through the optic nerve of both eyes from wildtype and *tasp1* indel homozygous larvae were selected and an average of five consecutive sections containing the diencephalon were measured using Image J software (https://imagej.nih.gov/ij/); measurements were averaged for 3 larvae from each group. Alcian blue staining was performed according to prior methods (31).

Supplementary Material

Supplementary Material is available at *HMG* online.

Ethics approval, consent to participate and consent for publication

The study has been approved by the ethical committee of the Technical University of Munich (5369/12 S) and the further respective institutions and written informed consent under an IRB-approved protocol for sequencing and publication in a scientific journal (including photographs) was obtained by the legal guardians of each subject according to the Declaration of Helsinki. All animal experiments were performed under a protocol approved by the Institute for Animal Care and Use Committee at University of California, San Francisco (UCSF).

Availability of data and materials

Data and materials are available from the corresponding author upon reasonable request.

Authors' contributions

KMR and AWEH performed data analysis, designed the study and wrote the manuscript. ALB, VC, JA, KSP, JH and JS provided phenotypic and genotypic data. NB, PLK, CP, SH, AMS, DDA, CB, KK, NF, ZA, RW, RK and TM did functional and data analyses. All authors critically reviewed and revised the manuscript.

References

1. Suleiman, J., Riedhammer, K.M., Jicinsky, T., Mundt, M., Werner, L., Gusic, M., Burgemeister, A.L., Alsaif, H.S., Abdulrahim, M., Moghrabi, N.N. *et al.* (2019) Homozygous loss-of-function variants of TASP1, a gene encoding an activator of the histone methyltransferases KMT2A and KMT2D, cause a syndrome of developmental delay, happy demeanor, distinctive facial features, and congenital anomalies. *Hum. Mutat.*, **40**, 1985–1992.
2. Niizuma, H., Cheng, E.H. and Hsieh, J.J. (2015) Taspase 1: a protease with many biological surprises. *Mol. Cell. Oncol.*, **2**, e999513.
3. Bjornsson, H.T. (2015) The Mendelian disorders of the epigenetic machinery. *Genome Res.*, **25**, 1473–1481.
4. Jones, W.D., Dafou, D., McEntagart, M., Woollard, W.J., Elmslie, F.V., Holder-Espinasse, M., Irving, M., Saggar, A.K., Smithson, S., Trembath, R.C. *et al.* (2012) De novo mutations in MLL cause Wiedemann-Steiner syndrome. *Am. J. Hum. Genet.*, **91**, 358–364.
5. Zech, M., Boesch, S., Maier, E.M., Borggraefe, I., Vill, K., Laccone, F., Pilshofer, V., Ceballos-Baumann, A., Alhaddad, B., Berutti, R. *et al.* (2016) Haploinsufficiency of KMT2B, encoding the lysine-specific histone methyltransferase 2B, results in early-onset generalized dystonia. *Am. J. Hum. Genet.*, **99**, 1377–1387.
6. Ng, S.B., Bigham, A.W., Buckingham, K.J., Hannibal, M.C., McMillin, M.J., Gildersleeve, H.I., Beck, A.E., Tabor, H.K., Cooper, G.M., Mefford, H.C. *et al.* (2010) Exome sequencing identifies MLL2 mutations as a cause of Kabuki syndrome. *Nat. Genet.*, **42**, 790–793.

7. Gurovich, Y., Hanani, Y., Bar, O., Nadav, G., Fleischer, N., Gelbman, D., Basel-Salmon, L., Krawitz, P.M., Kamphausen, S.B., Zenker, M. *et al.* (2019) Identifying facial phenotypes of genetic disorders using deep learning. *Nat. Med.*, **25**, 60–64.

8. Takeda, S., Sasasgawa, S., Oyama, T., Searleman, A.C., Westergard, T.D., Cheng, E.H. and Hsieh, J.J. (2015) Taspase1-dependent TFIIA cleavage coordinates head morphogenesis by limiting Cdkn2a locus transcription. *J. Clin. Invest.*, **125**, 1203–1214.

9. Butcher, D.T., Cytrynbaum, C., Turinsky, A.L., Siu, M.T., Inbar-Feigenberg, M., Mendoza-Londono, R., Chitayat, D., Walker, S., Machado, J., Caluseriu, O. *et al.* (2017) CHARGE and Kabuki syndromes: gene-specific DNA methylation signatures identify epigenetic mechanisms linking these clinically overlapping conditions. *Am. J. Hum. Genet.*, **100**, 773–788.

10. Kollias, S.S., Ball, W.S., Jr. and Prenger, E.C. (1993) Cystic malformations of the posterior fossa: differential diagnosis clarified through embryologic analysis. *Radiographics*, **13**, 1211–1231.

11. Barkovich, A.J., Kjos, B.O., Norman, D. and Edwards, M.S. (1989) Revised classification of posterior fossa cysts and cystlike malformations based on the results of multiplanar MR imaging. *AJR Am. J. Roentgenol.*, **153**, 1289–1300.

12. Aldinger, K.A., Timms, A.E., Thomson, Z., Mirzaa, G.M., Bennett, J.T., Rosenberg, A.B., Roco, C.M., Hirano, M., Abidi, F., Haldipur, P. *et al.* (2019) Redefining the etiologic landscape of cerebellar malformations. *Am. J. Hum. Genet.*, **105**, 606–615.

13. Hsieh, J.J., Cheng, E.H. and Korsmeyer, S.J. (2003) Taspase1: a threonine aspartase required for cleavage of MLL and proper HOX gene expression. *Cell*, **115**, 293–303.

14. Takeda, S., Chen, D.Y., Westergard, T.D., Fisher, J.K., Rubens, J.A., Sasagawa, S., Kan, J.T., Korsmeyer, S.J., Cheng, E.H. and Hsieh, J.J. (2006) Proteolysis of MLL family proteins is essential for taspase1-orchestrated cell cycle progression. *Genes Dev.*, **20**, 2397–2409.

15. Zhao, Z., Wang, L., Volk, A.G., Birch, N.W., Stoltz, K.L., Bartom, E.T., Marshall, S.A., Rendleman, E.J., Nestler, C.M., Shilati, J. *et al.* (2019) Regulation of MLL/COMPASS stability through its proteolytic cleavage by taspase1 as a possible approach for clinical therapy of leukemia. *Genes Dev.*, **33**, 61–74.

16. Hoiby, T., Mitsiou, D.J., Zhou, H., Erjument-Bromage, H., Tempst, P. and Stunnenberg, H.G. (2004) Cleavage and proteasome-mediated degradation of the basal transcription factor TFIIA. *EMBO J.*, **23**, 3083–3091.

17. Zhou, H., Spicuglia, S., Hsieh, J.J., Mitsiou, D.J., Hoiby, T., Veenstra, G.J., Korsmeyer, S.J. and Stunnenberg, H.G. (2006) Uncleaved TFIIA is a substrate for taspase 1 and active in transcription. *Mol. Cell. Biol.*, **26**, 2728–2735.

18. Meyer, E., Carss, K.J., Rankin, J., Nichols, J.M., Grozeva, D., Joseph, A.P., Mencacci, N.E., Papandreou, A., Ng, J., Barral, S. *et al.* (2017) Mutations in the histone methyltransferase gene KMT2B cause complex early-onset dystonia. *Nat. Genet.*, **49**, 223–237.

19. Shilatifard, A. (2012) The COMPASS family of histone H3K4 methylases: mechanisms of regulation in development and disease pathogenesis. *Annu. Rev. Biochem.*, **81**, 65–95.

20. Aref-Eshghi, E., Kerkhof, J., Pedro, V.P., Groupe, D.I.F., Barat-Houari, M., Ruiz-Pallares, N., Andrau, J.C., Lacombe, D., Van-Gils, J., Fergelot, P. *et al.* (2020) Evaluation of DNA methylation episignatures for diagnosis and phenotype correlations in 42 Mendelian neurodevelopmental disorders. *Am. J. Hum. Genet.*, **106**, 356–370.

21. Van Laarhoven, P.M., Neitzel, L.R., Quintana, A.M., Geiger, E.A., Zackai, E.H., Clouthier, D.E., Artinger, K.B., Ming, J.E. and Shaikh, T.H. (2015) Kabuki syndrome genes KMT2D and KDM6A: functional analyses demonstrate critical roles in craniofacial, heart and brain development. *Hum. Mol. Genet.*, **24**, 4443–4453.

22. Sobreira, N., Schiettecatte, F., Valle, D. and Hamosh, A. (2015) GeneMatcher: a matching tool for connecting investigators with an interest in the same gene. *Hum. Mutat.*, **36**, 928–930.

23. Gambin, T., Yuan, B., Bi, W., Liu, P., Rosenfeld, J.A., Coban-Akdemir, Z., Pursley, A.N., Nagamani, S.C.S., Marom, R., Golla, S. *et al.* (2017) Identification of novel candidate disease genes from de novo exonic copy number variants. *Genome. Med.*, **9**, 83.

24. Alabdullatif, M.A., Al Dhaibani, M.A., Khassawneh, M.Y. and El-Hattab, A.W. (2017) Chromosomal microarray in a highly consanguineous population: diagnostic yield, utility of regions of homozygosity, and novel mutations. *Clin. Genet.*, **91**, 616–622.

25. Kremer, L.S., Bader, D.M., Mertes, C., Kopajtich, R., Pichler, G., Iuso, A., Haack, T.B., Graf, E., Schwarzmayr, T., Terrile, C. *et al.* (2017) Genetic diagnosis of Mendelian disorders via RNA sequencing. *Nat. Commun.*, **8**, 15824.

26. Riedhammer, K.M., Stockler, S., Ploski, R., Wenzel, M., Adis-Dutschmann, B., Ahting, U., Alhaddad, B., Blaschek, A., Haack, T.B., Kopajtich, R. *et al.* (2021) De novo stop-loss variants in CLDN11 cause hypomyelinating leukodystrophy. *Brain*, **144**, 411–419.

27. Ucuncu, E., Rajamani, K., Wilson, M.S.C., Medina-Cano, D., Altin, N., David, P., Barcia, G., Lefort, N., Banal, C., Vasilache-Dangles, M.T. *et al.* (2020) MINPP1 prevents intracellular accumulation of the chelator inositol hexakisphosphate and is mutated in Pontocerebellar Hypoplasia. *Nat. Commun.*, **11**, 6087.

28. Despras, E., Sittewelle, M., Pouvelle, C., Delrieu, N., Cordonnier, A.M. and Kannouche, P.L. (2016) Rad18-dependent SUMOylation of human specialized DNA polymerase eta is required to prevent under-replicated DNA. *Nat. Commun.*, **7**, 13326.

29. Brechtmann, F., Mertes, C., Matuseviciute, A., Yepez, V.A., Avsec, Z., Herzog, M., Bader, D.M., Prokisch, H. and Gagneur, J. (2018) OUTRIDER: a statistical method for detecting aberrantly expressed genes in RNA sequencing data. *Am. J. Hum. Genet.*, **103**, 907–917.

30. Choufani, S., Cytrynbaum, C., Chung, B.H., Turinsky, A.L., Grafodatskaya, D., Chen, Y.A., Cohen, A.S., Dupuis, L., Butcher, D.T., Siu, M.T. *et al.* (2015) NSD1 mutations generate a genome-wide DNA methylation signature. *Nat. Commun.*, **6**, 10207.

31. Wu, D., Mandal, S., Choi, A., Anderson, A., Prochazkova, M., Perry, H., Gil-Da-Silva-Lopes, V.L., Lao, R., Wan, E., Tang, P.L. *et al.* (2015) DLX4 is associated with orofacial clefting and abnormal jaw development. *Hum. Mol. Genet.*, **24**, 4340–4352.

ARTICLE OPEN

Check for updates

Exome sequencing in individuals with congenital anomalies of the kidney and urinary tract (CAKUT): a single-center experience

Korbinian M. Riedhammer [1,2], Jasmina Ćomić[1,2], Velibor Tasic [3], Jovana Putnik [4], Nora Abazi-Emini[3], Aleksandra Paripovic[4], Natasa Stajic[4], Thomas Meitinger[1], Valbona Nushi-Stavileci[5], Riccardo Berutti [1], Matthias C. Braunisch[2] and Julia Hoefele [1 ✉]

Individuals with congenital anomalies of the kidney and urinary tract (CAKUT) show a broad spectrum of malformations. CAKUT can occur in an isolated fashion or as part of a syndromic disorder and can lead to end-stage kidney failure. A monogenic cause can be identified in ~12% of affected individuals. This study investigated a single-center CAKUT cohort analyzed by exome sequencing (ES). Emphasis was placed on the question whether diagnostic yield differs between certain CAKUT phenotypes (e.g., bilateral kidney affection, unilateral kidney affection or only urinary tract affection). 86 unrelated individuals with CAKUT were categorized according to their phenotype and analyzed by ES to identify a monogenic cause. Prioritized variants were rated according to the recommendations of the American College of Medical Genetics and Genomics and the Association for Clinical Genomic Science. Diagnostic yields of different phenotypic categories were compared. Clinical data were collected using a standardized questionnaire. In the study cohort, 7/86 individuals had a (likely) pathogenic variant in the genes *PAX2*, *PBX1*, *EYA1*, or *SALL1*. Additionally, in one individual, a 17q12 deletion syndrome (including *HNF1B*) was detected. 64 individuals had a kidney affection, which was bilateral in 36. All solved cases (8/86, 9%) had bilateral kidney affection (diagnostic yield in subcohort: 8/36, 22%). Although the diagnostic yield in CAKUT cohorts is low, our single-center experience argues, that, in individuals with bilateral kidney affection, monogenic burden is higher than in those with unilateral kidney or only urinary tract affection.

INTRODUCTION

Congenital anomalies of the kidney and urinary tract (CAKUT) is a collective term for a group of diverse structural malformations ranging from relatively mild phenotypes like vesicoureteral reflux (VUR) to severe manifestations like bilateral renal agenesis. CAKUT can be present in isolated form (limited to the kidney and the urinary tract) or can be part of syndromic disorders [1]. It results from disturbances in embryonic development of the kidney and/or the urinary tract and is the leading cause for end-stage kidney failure in the pediatric population. CAKUT accounts for 23% of all birth defects and has a prevalence of about 3–6 per 1000 newborns [2–6].

Perturbation of renal and ureteral morphogenesis in CAKUT can be due to environmental, epigenetic, genetic factors, and the interplay of these [2]. Although alterations in renal development can be multifactorial, there are also hereditary forms of CAKUT resulting from single-gene defects ("monogenic CAKUT"). This is underscored by familial clustering of CAKUT, knockout mouse models recapitulating CAKUT phenotypes, and complex heritable syndromes involving CAKUT [1, 7]. Hence, it is not surprising that disease-causing variants in more than 50 different genes and with different modes of inheritance (e.g., autosomal dominant,

autosomal recessive, X-linked) have been described in the literature [8]. Additionally, numerical chromosomal alterations, deletions or duplications are known to cause CAKUT [9, 10].

However, in only about 16% of individuals affected by CAKUT, a monogenic cause can be identified, with diagnostic yields varying between 6% and 33% depending on study population. It has been shown that the diagnostic yield is higher if there is familial or syndromic occurrence of CAKUT [11]. Furthermore, there is some evidence that individuals with a severe CAKUT phenotype, such as renal agenesis or renal dysplasia, have a higher diagnostic yield (17% in one publication) but more detailed data on the relationship between phenotypic variation (e.g., bilateral vs. unilateral vs. only urinary tract affection) and the respective diagnostic yield in CAKUT is lacking [6, 12].

Molecular genetic techniques like next-generation sequencing including exome sequencing (ES), linkage analyses, homozygosity mapping combined with ES for recessive diseases, and array analysis are the current approaches to identify disease-causing variants in known disease-associated CAKUT genes, but also to discover new candidate genes [2, 8, 13–15]. This study investigated a tertiary care center CAKUT cohort analyzed by ES. Focus

[1]Institute of Human Genetics, Klinikum rechts der Isar, Technical University of Munich, School of Medicine, Munich, Germany. [2]Department of Nephrology, Klinikum rechts der Isar, Technical University of Munich, School of Medicine, Munich, Germany. [3]University Children's Hospital, Medical Faculty of Skopje, Skopje, North Macedonia. [4]Institute for Mother and Child Health Care of Serbia "Dr Vukan Čupić", Department of Nephrology, University of Belgrade, Faculty of Medicine, Belgrade, Serbia. [5]Pediatric Clinic, University Clinical Center of Kosovo, Prishtina, Kosovo. ✉email: julia.hoefele@tum.de

was specifically laid on whether diagnostic yield is different in certain CAKUT phenotypes (e.g., bilateral kidney affection, unilateral kidney affection or only urinary tract affection).

MATERIAL AND METHODS
Study population
A cohort of 86 unrelated index cases with a CAKUT phenotype was collected at our institute between October 2015 and February 2019 after referral by their clinician (Fig. 1). This study was performed according to the standards of the Declaration of Helsinki 2013 and approved by the local Ethics Committee of the Technical University of Munich (approval number 521/16S). Written informed consent was obtained from all individuals or their legal guardians. Clinical and phenotypic data were obtained from clinical reports and medical history. A standardized questionnaire was used to assess the clinical information.

Each individual was assigned to one group each in a two-step process:
First, all individuals were categorized into one of the following groups based on their renal/urinary tract phenotype (according to ref. [16]). These groups are as follows: group I: duplication of the ureter, pelvis and kidney; group II: ectopic kidney and/or horseshoe kidney; group III: other kidney anomaly; group IV: obstructive uropathy; group V: VUR; group VI: posterior ureteral valves; and group VII: other lower urinary tract malformations.

Secondly, the individuals were divided into the following three groups encompassing a broader phenotypic spectrum; group I: "bilateral kidney affection", in which cases with any bilateral renal affection were included; group II: "unilateral kidney affection", in which unilateral kidney affection and cases with unilateral ectopic kidney and/or a horseshoe kidney were included; group III: "isolated urine transport affection" (i.e., without known parenchymal kidney affection), in which cases with duplication of the ureter, pelvis and kidney, obstructive uropathy, posterior ureteral valves, VUR and other lower urinary tract malformations phenotypes were included.

Genetic testing
Peripheral blood was used for DNA isolation using the automated nucleic acid purification instrument Chemagic™ 360 (PerkinElmer, Waltham, MA, USA) according to the manufacturer's protocol.

Exome sequencing
ES was performed with Sure Select Human All Exon V5 (50 Mb) Kit (Agilent Technologies, Inc., Santa Clara, CA, United States of America) and a HiSeq2500 (Illumina, Inc., San Diego, CA, United States of America) or with Sure Select Human All Exon V6 (60 Mb) Kit (Agilent Technologies, Inc., Santa Clara, CA, United States of America) and a HiSeq4000 (Illumina, Inc., San Diego, CA, United States of America) [17]. Mitochondrial DNA was derived from off-target exome reads as previously described [18]. Reads were aligned to the Genome Reference Consortium Human Build 37 (UCSC Genome Browser build hg19) using Burrows-Wheeler Aligner (v.0.7.5a). SAMtools (version 0.1.19) was employed for detection of single-nucleotide variants (SNVs) and small insertions and deletions (indels). ExomeDepth was used to detect copy number variations (CNVs). A noise threshold of 2.5 was accepted for diagnostic analysis [19]. The retrieved CNVs were visualized using Integrative Genomics Viewer (IGV, https://software.broadinstitute.org/software/igv/) to verify that the regions examined were adequately covered and that the CNVs were plausible. CNVs were then compared with publicly available control databases like the Genome Aggregation Database (gnomAD, https://gnomad.broadinstitute.org/about), the Database of Genomic Variants (DGV, http://dgv.tcag.ca/dgv/app/home), and databases for disease-causing CNVs like DECIPHER (https://decipher.sanger.ac.uk/) and ClinVar (https://www.ncbi.nlm.nih.gov/clinvar/).

Sanger sequencing
Segregation analysis of a variant previously identified with ES was performed by Sanger sequencing in the parents to determine inheritance or to confirm a de novo status (if parents had not been exome sequenced in the first place). The oligonucleotide primer sequences are available upon request.

Variant interpretation
For the analysis of de novo, autosomal dominant and mitochondrial variants, only variants with a minor allele frequency (MAF) of less than 0.1% in the in-house database of the Helmholtz Zentrum Munich containing more than 20,000 exomes were considered. For the analysis of autosomal recessive and X-linked variants (homozygous, hemizygous or [putative] compound heterozygous), variants with a MAF of less than 1.0% and a SNV quality of 30 were considered [20, 21]. Variants were checked in publicly available databases for (likely) pathogenic variants. These databases were ClinVar (https://www.ncbi.nlm.nih.gov/clinvar/), the Human Gene Mutation Database (HGMD® Professional, http://www.hgmd.cf.ac.uk), and the Leiden Open Variation Database (LOVD, https://www.lovd.nl). The variants were rated in accordance with the guidelines of the American College of Medical Genetics (ACMG) and current amendments [22–25]. Individuals with a (likely) pathogenic variant and a fitting genotype were classified as "solved cases" or, if no disease-causing (i.e., likely pathogenic or pathogenic) variant could be identified, we designated them as "unsolved cases".
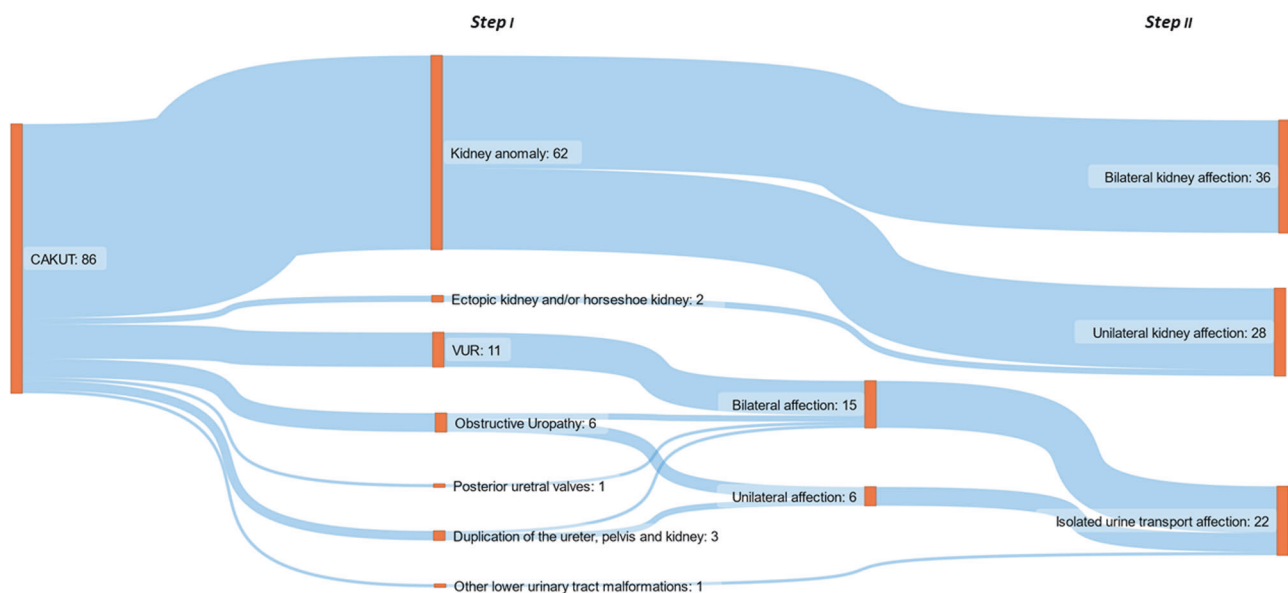

Fig. 1 Cohort overview according to renal and urinary tract phenotype (two-step process, see Methods section). This figure was created with the free web-based tool SankeyMATIC (http://sankeymatic.com/build/). CAKUT congenital anomalies of the kidney and urinary tract, VUR vesicoureteral reflux.

RESULTS

Study population
The total study cohort consisted of 86 index cases, 29/86 (34%) were female and 57/86 (66%) were male (Table 1). ES was performed in all index cases, 51 individuals were analyzed by proband-only ES, one by duo ES (index case and mother) and 34 by trio ES (index case and parents). Most of these cases were of non-Finnish origin (74/86; 86%; Germany, Serbia, and North Macedonia). 15/86 (17%) cases had a positive family history for CAKUT. Among those with reported parental consanguinity (7/86; 8%), family history was positive in 2/7 (29%) cases, and among those with no parental consanguinity (79/86; 92%), family history was positive in 13/79 (16%) cases. The median age at ES was 9 years (range 0 to 61 years). Extrarenal manifestations (syndromic CAKUT) were present in 33/86 (38%) cases and complex CAKUT (i.e., several CAKUT manifestations in an individual) in 24/86 (28%) cases (Table 1).

All individuals were classified using a two-step process
Step I: Detailed renal and urinary tract phenotype. All 86 individuals were categorized into groups based on their renal and urinary tract phenotype (as per [16]; Fig. 1): group I: duplication of the ureter, pelvis and kidney: 3/86 (4%) cases; group II: ectopic kidney and/or horseshoe kidney: 2/86 (2%) cases; group III: other kidney anomaly: 62/86 (72%) cases; group IV: obstructive uropathy: 6/86 (7%) cases; group V: VUR: 11/86 (13%) cases: 11/86 (13%) cases; group VI: posterior ureteral valves: 1/86 (1%) cases; group VII: other lower urinary tract malformations: 1/86 (1%) cases.

Step II: Broader phenotype - bilateral or unilateral kidney affection or isolated urine transport affection. Grouping the individuals according to extent of affection, the following distribution was seen: group I: "bilateral kidney affection": 36/86 (42%) cases; group II: "unilateral kidney affection": 28/86 (32%) cases; group III: "isolated urine transport affection": 22/86 (26%) cases (Fig. 1, Table 1).

Diagnostic yield. Monogenic causes of CAKUT could be identified in 8/86 (9%) cases (Table 2 and Supplementary Table 1). All solved cases were in the "bilateral kidney affection" group (8/36; 22%; Fig. 2). 6/8 (75%) solved cases additionally had extrarenal manifestations (i.e., syndromic CAKUT).

Of the 22 complex CAKUT cases, only one (5%) case was solved. This case (HN-F541-II-2) presented with bilateral kidney hypoplasia, urogenital malformations, dysplastic ears, and bilateral hexadactyly (Tables 1, 2). 3/8 (38%) solved cases had a positive family history (HN-F262-II-1, HN-F502-II-1 and HN-F316-I-1). In all solved cases, there was no parental consanguinity (Table 2).

Of the 8 solved cases (Table 2), heterozygous disease-causing variants in *PBX1* were identified in 2/8 (25%) cases compatible with the genetic diagnosis of CAKUTHED (MIM #617641). In 2/8 (25%) cases, Townes-Brocks syndrome 1 (MIM #107480) was diagnosed, with one pathogenic and one likely pathogenic variant in *SALL1*. In 2/8 (25%) cases, Branchiootorenal syndrome 1 (MIM # 113650) was diagnosed, with a likely pathogenic and a pathogenic variant in *EYA1*. 1/8 (13%) cases had a papillorenal syndrome (MIM #120330) caused by a likely pathogenic variant in *PAX2*. Additionally, in 1/8 (13%) cases, a chromosome 17q12 deletion syndrome [MIM #614527] was detected which included *HNF1B*. 5/8 (63%) disease-causing variants have not been described in the literature so far. Of note, 6/8 (75%) of solved cases also had syndromic features (Table 2).

Supplementary Table 2 lists homozygous stretches in exome sequencing data and homozygous rare variants (only variants in OMIM-listed [https://www.omim.org/] disease-associated genes; MAF < 1.0%) within these stretches in consanguineous cases (all unsolved). Supplementary Table 3 lists rare de novo variants (MAF < 0.1%; CADD [https://cadd.gs.washington.edu/] >15) and rare homozygous/compound heterozygous/hemizygous variants (MAF < 1.0%) in unsolved trio ES cases (also only variants in OMIM-listed disease-associated genes).

Diagnostic yields in different CAKUT groups
All solved cases had a bilateral kidney affection. No disease-causing variant could be found in individuals with a unilateral renal or an isolated urinary tract phenotype.

DISCUSSION
Diagnostic yield
In this single-center cohort comprising 86 unrelated individuals, comprehensive genetic testing with ES resulted in a diagnostic yield of monogenic CAKUT of 9%. This is comparable with the reported diagnostics yields of unselected CAKUT cohorts in the literature. For example, in the study by van der Ven et al. 2018, in 29/232 (13%) families, disease-causing variants in genes associated with monogenic CAKUT were identified [6]. All eight solved cases of our cohort had bilateral kidney affection (8/36 individuals, diagnostic yield of 22% in this subcohort). Interestingly, in the above-mentioned study by van der Ven et al., cases with kidney involvement (renal agenesis or renal dysplasia; defined as "severe"

Table 1. Clinical characteristics of the 86 index cases.

Clinical characteristics	Total cohort (*n* = 86 index cases)
Sex	
Female	29 (34%)
Male	57 (66%)
Non-Finnish European descent	
Yes	74 (86%)
No	12 (14%)
Reported family history regarding CAKUT	Familial CAKUT
Yes	15 (17%)
No	71 (83%)
Reported parental consanguinity	
Yes	7 (8%)
No	79 (92%)
Syndromic CAKUT	
Yes	33 (38%)
No	53 (62%)
Syndromic features	
Skeletal malformations	9 (27%)
Eye anomalies	3 (9%)
Hearing impairment	3 (9%)
Intellectual disability	6 (18%)
Heart defect	6 (18%)
Complex CAKUT	
Yes	24 (30%)
No	62 (72%)
CAKUT phenotype	
Bilateral kidney affection	36 (42%)
Unilateral kidney affection	28 (33%)
Isolated urine transport affection	22 (25%)
Solved cases*	
Yes	8 (9%)
No	78 (91%)

CAKUT congenital anomalies of the kidney and urinary tract; *Solved cases are those in which a genetic diagnosis could be made by exome sequencing.

Table 2. Phenotypic and genotypic details on genetically solved index cases in the cohort.

ID	Sex	Phenotype	Gene (transcript)	Chromosomal position (hg19)	Nucleotide and amino acid change	gnomAD v2.1.1 MAF[†]	Zygosity	Inheritance	Genetic diagnosis (MIM phenotype number)[**]	Classification according to applied ACMG criteria/CNV score[***]	Accession number in ClinVar[****]	Individual ID in LOVD[#]	Syndromic disease (0 = no; 1 = yes)
HN-F262-II-1	f	Bilateral renal hypoplasia	PAX2 (NM_000278.3)	chr10:g.102509535dup	c.76dup p.(Val26Glyfs*28)	0.00002834	Heterozygous	Father	Papillorenal syndrome (#120330)	Likely pathogenic (PVS1 PS4_moderate)	SCV001149865.1	-	0
HN-F75-II-1	m	Bilateral renal dysplasia, developmental delay, growth retardation, skeletal anomalies	PBX1 (NM_002585.3)	chr1:g.164761878_164761884del	c.413_419del p.(Gly138Valfs*40)	Not listed	Heterozygous	de novo	CAKUTHED (#617641)	Pathogenic (PVS1 PS2 PM2)	SCV000680322.1	-	1
HN-F317-II-3	f	Bilateral renal agenesis, skeletal anomalies	EYA1 (NM_000503.4)	chr8:g.72211430G>T	c.678C>A p.(Tyr226*)	Not listed	Heterozygous	de novo	Branchiootorenal syndrome 1, with or without cataracts (#113650)	Pathogenic (PVS1 PS2 PM2)	SCV001149770.1	-	1
HN-F541-II-2	f	Bilateral renal hypoplasia (cysts in right kidney), urogenital malformations, dysplastic ears, bilateral hexadactyly	SALL1 (NM_002968.2)	chr16:g.51175307G>A	c.826C>T p.(Arg276*)	Not listed	Heterozygous	de novo	Townes-Brocks syndrome 1 (#107480)	Pathogenic (PVS1 PS2 PS4_moderate PM2)	SCV001430043.1	-	1
HN-F197-II-1	f	Bilateral renal cystic dysplasia	chr17q12 (-)	Approx.chr17:g.34842543-36104875	1.2 Mb deletion (including HNF1B)	0.0001393	Heterozygous	de novo	Chromosome 17q12 deletion syndrome (#614527)	Pathogenic (1,00)	-	00404564	0
HN-F305-II-1	m	Right renal agenesis, left renal hypoplasia, short stature, facial dysmorphies, choanal atresia	PBX1 (NM_002585.3)	chr1:g.164769086G>T	c.661G>T p.(Glu221*)	Not listed	Heterozygous	de novo	CAKUTHED (#617641)	Pathogenic (PVS1 PS2 PM2)	SCV001149866.1	-	1
HN-F502-II-1	m	Bilateral renal hypoplasia, imperforate anus, dysplastic ears, right triphalangeal thumb	SALL1 (NM_002968.2)	chr16:g.51173444_51173447dup	c.2686_2689dup p.(Val897Glyfs*6)	Not listed	Heterozygous	Undetermined	Townes-Brocks syndrome 1(#107480)	Likely pathogenic (PVS1 PM2)	SCV001149911.1	-	1
HN-F316-I-1	m	Branchiootorenal syndrome, congenital hypertrophic cardiomyopathy	EYA1 (NM_000503.4)	chr8:g.72127964C>T	c.1361-1G>A p.(?)	Not listed	Heterozygous	Undetermined	Branchiootorenal syndrome 1, with or without cataracts (#113650)	Likely pathogenic (PVS1 PM2)	SCV001149769.1	-	1

CAKUT congenital anomalies of the kidney and urinary tract; *f* female; *m* male; *https://gnomad.broadinstitute.org/; **https://www.omim.org/; ***variant is classified as likely pathogenic/pathogenic as per ACMG and amendments [24, 25]; ****https://www.ncbi.nlm.nih.gov/clinvar/; #https://www.lovd.nl.
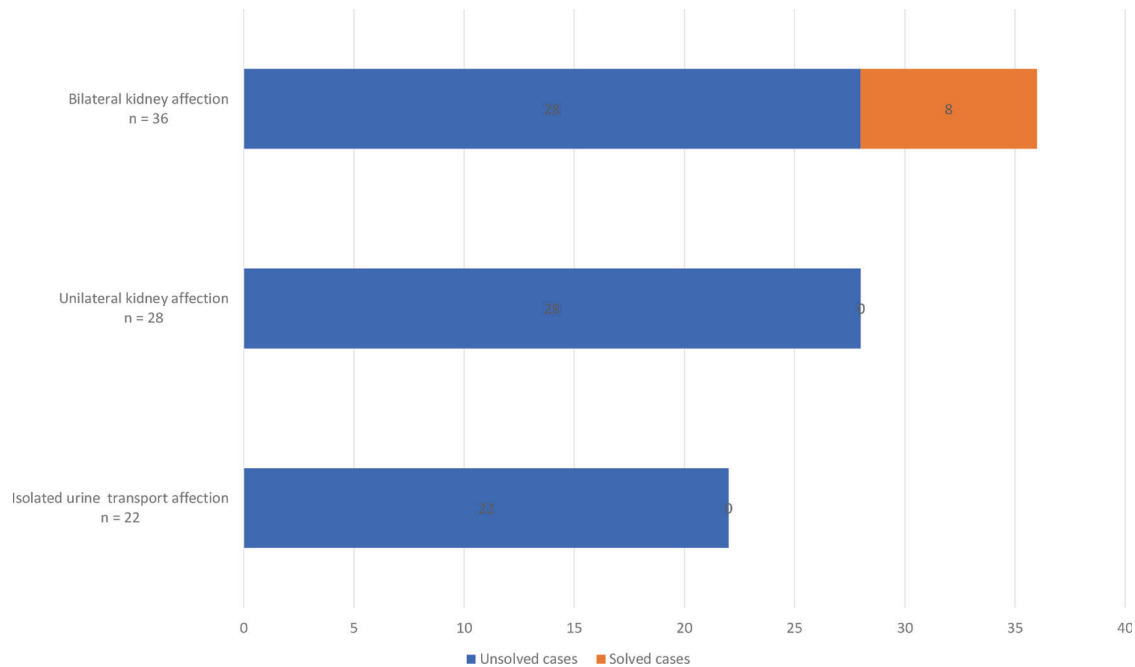
Fig. 2 Distribution of solved cases in the CAKUT cohort consisting of 86 index cases grouped according to broader phenotype categories. Solved cases are those in which a genetic diagnosis could be made by exome sequencing.

CAKUT) also had a higher diagnostic yield of 17%. Discrepancies could be explainable by different compositions of the study cohorts, e.g., based on different inclusion criteria and the variability of the clinical phenotypes of the affected individuals. Of note, a precise differentiation between the diagnostic yields of unilateral and bilateral affections was not made in the study by van der Ven et al. Bekheirnia et al. 2017 identified pathogenic SNVs in 5% of the examined 62 families [26]. Precise information on individuals with unilateral or bilateral affection was not given in this study, therefore, a comparison to the present study is only possible to a limited extent. Furthermore, it has to be pointed out that 6/8 (75%) solved cases had syndromic features additionally to bilateral kidney involvement and the diagnostic yield in syndromic cases was 18% (6/33). Also in the study by van der Ven et al., syndromic cases had a higher diagnostic yield than the total cohort (29% vs. 13%) [6]. Hence, our study, of course with limited sample size, encourages that syndromic features should actively be investigated in CAKUT cases with bilateral kidney involvement.

In this study, diagnostic yields were calculated on CAKUT phenotypic subgroups and individuals with bilateral kidney affection were grouped separately from individuals with unilateral kidney affection. This showed that all solved cases presented with bilateral kidney affection implying that, in individuals with bilateral kidney affection, comprehensive genetic testing should be considered, even in non-syndromic cases (2/8 of solved cases had bilateral kidney affection without reported extrarenal manifestations).

Genetic diagnoses

All eight genetic diagnoses featured autosomal dominant syndromic monogenic CAKUT disorders (Table 2). However, only 6/8 (75%) solved cases had syndromic phenotypes as per medical records/ referring clinicians. Reverse phenotyping of the two individuals without syndromic features after the molecular genetic result confirmed the isolated renal phenotype. And exactly these cases not featuring a syndromic phenotype carried a heterozygous disease-causing variant in *PAX2* (papillorenal syndrome, MIM #120330) and a heterozygous 1.2 Mb deletion on Chr17q12 encompassing *HNF1B* as the only disease-associated gene (17q12 deletion syndrome, MIM #614527). *PAX2* and *HNF1B* are the genes most frequently associated

with autosomal dominant syndromic CAKUT accounting for 5–15% of cases in some studies [27]. An explanation for this observation could be that extrarenal manifestations can be subtle and missed by clinicians and that expressivity of CAKUT is highly variable and age-dependent (e.g., maturity-onset diabetes of the young and neuropsychiatric disorders in 17q12 deletion syndrome; the individual with 17q12 deletion syndrome was two years old at genetic testing and [reverse] phenotyping) [27]. Nonetheless, as mentioned above, our study makes the case that common syndromic monogenic CAKUT disorders could be present in bilateral kidney affection cases without apparent extrarenal manifestation, as phenotypes can be subtle and evolve over time.

Interestingly, in 2/8 solved cases, heterozygous disease-causing variants in *PBX1* could be identified, a fairly novel disease-associated gene at the time of ES [28]. This could illustrate an underestimated burden of *PBX1*-associated disease (CAKUTHED, MIM #617641) in monogenic CAKUT.

Two cases each carried disease-causing variants in *SALL1* and *EYA1*, both well-known autosomal dominant syndromic monogenic CAKUT genes (Townes-Brocks syndrome 1, MIM #107480; and branchiootorenal syndrome 1, MIM #113650) [27].

Limitations

Although these are interesting observations, it has to be pointed out that this study has a small sample size. Therefore, and to confirm the findings, future larger studies should focus on diagnostic yields in phenotypic subgroups of CAKUT. This might allow the development of a clinical score for genetic testing in CAKUT in order to optimize clinical management.

A further limitation is the uneven distribution between our cases with unilateral/bilateral kidney affection (64/86; 74%) and isolated urine transport affection (22/86; 26%). The observed discrepancy between these two groups can probably be explained by the small study size and could change in a larger cohort.

For CAKUT cohorts, consanguinity of the parents is known to result in a higher diagnostic yield [13]. In our CAKUT cohort, however, this association was not present. This could refer to the overall limited number of cases with reported parental consanguinity (7/86, 8%) within this study.

CONCLUSION

In this study, all solved cases had bilateral kidney involvement and 75% had syndromic disease showing this phenotypic presentation is a strong sign for an underlying hereditary cause in individuals with CAKUT. In future studies, a larger cohort of individuals with CAKUT is needed to develop a clinical score in order to increase the diagnostic yield in individuals with a CAKUT phenotype as molecular genetic diagnosis with ES can help to improve clinical management of individuals with CAKUT.

DATA AVAILABILITY

The data that support the findings of this study are available on request from the corresponding author.

REFERENCES

1. Vivante A, Kohl S, Hwang DY, Dworschak GC, Hildebrandt F. Single-gene causes of congenital anomalies of the kidney and urinary tract (CAKUT) in humans. Pediatr Nephrol. 2014;29:695–704.
2. Nicolaou N, Renkema KY, Bongers EM, Giles RH, Knoers NV. Genetic, environmental, and epigenetic factors involved in CAKUT. Nat Rev Nephrol. 2015;11:720–31.
3. Saisawat P, Tasic V, Vega-Warner V, Kehinde EO, Gunther B, Airik R, et al. Identification of two novel CAKUT-causing genes by massively parallel exon resequencing of candidate genes in patients with unilateral renal agenesis. Kidney Int. 2012;81:196–200.
4. Soliman NA, Ali RI, Ghobrial E, Habib EI, Ziada AM. Pattern of clinical presentation of congenital anomalies of the kidney and urinary tract among infants and children. Nephrology. 2015;20:13–18.
5. Song R, Yosypiv IV. Genetics of congenital anomalies of the kidney and urinary tract. Pediatr Nephrol. 2011;26:353–64.
6. van der Ven AT, Connaughton DM, Ityel H, Mann N, Nakayama M, Chen J, et al. Whole-exome sequencing identifies causative mutations in families with congenital anomalies of the kidney and urinary tract. J Am Soc Nephrol. 2018;29:2348–61.
7. Bulum B, Ozcakar ZB, Ustuner E, Dusunceli E, Kavaz A, Duman D, et al. High frequency of kidney and urinary tract anomalies in asymptomatic first-degree relatives of patients with CAKUT. Pediatr Nephrol. 2013;28:2143–7.
8. van der Ven AT, Vivante A, Hildebrandt F. Novel insights into the pathogenesis of monogenic congenital anomalies of the kidney and urinary tract. J Am Soc Nephrol. 2018;29:36–50.
9. Sanna-Cherchi S, Westland R, Ghiggeri GM, Gharavi AG. Genetic basis of human congenital anomalies of the kidney and urinary tract. J Clin Investig. 2018;128:4–15.
10. Weber S, Landwehr C, Renkert M, Hoischen A, Wuhl E, Denecke J, et al. Mapping candidate regions and genes for congenital anomalies of the kidneys and urinary tract (CAKUT) by array-based comparative genomic hybridization. Nephrol Dial Transpl. 2011;26:136–43.
11. Kagan M, Pleniceanu O, Vivante A. The genetic basis of congenital anomalies of the kidney and urinary tract. Pediatr Nephrol. 2022;37:2231–43.
12. Rasmussen M, Sunde L, Nielsen ML, Ramsing M, Petersen A, Hjortshoj TD, et al. Targeted gene sequencing and whole-exome sequencing in autopsied fetuses with prenatally diagnosed kidney anomalies. Clin Genet. 2018;93:860–9.
13. Vivante A, Hwang DY, Kohl S, Chen J, Shril S, Schulz J, et al. Exome sequencing discerns syndromes in patients from consanguineous families with congenital anomalies of the kidneys and urinary tract. J Am Soc Nephrol. 2017;28:69–75.
14. Hildebrandt F, Heeringa SF, Ruschendorf F, Attanasio M, Nurnberg G, Becker C, et al. A systematic approach to mapping recessive disease genes in individuals from outbred populations. PLoS Genet. 2009;5:e1000353.
15. Gee HY, Otto EA, Hurd TW, Ashraf S, Chaki M, Cluckey A, et al. Whole-exome resequencing distinguishes cystic kidney diseases from phenocopies in renal ciliopathies. Kidney Int. 2014;85:880–7.
16. Verbitsky M, Westland R, Perez A, Kiryluk K, Liu Q, Krithivasan P, et al. The copy number variation landscape of congenital anomalies of the kidney and urinary tract. Nat Genet. 2019;51:117–27.
17. Kremer LS, Bader DM, Mertes C, Kopajtich R, Pichler G, Iuso A, et al. Genetic diagnosis of Mendelian disorders via RNA sequencing. Nat Commun. 2017;8:15824.
18. Griffin HR, Pyle A, Blakely EL, Alston CL, Duff J, Hudson G, et al. Accurate mitochondrial DNA sequencing using off-target reads provides a single test to identify pathogenic point mutations. Genet Med. 2014;16:962–71.
19. Plagnol V, Curtis J, Epstein M, Mok KY, Stebbings E, Grigoriadou S, et al. A robust model for read count data in exome sequencing experiments and implications for copy number variant calling. Bioinformatics. 2012;28:2747–54.
20. Tory K, Menyhard DK, Woerner S, Nevo F, Gribouval O, Kerti A, et al. Mutation-dependent recessive inheritance of NPHS2-associated steroid-resistant nephrotic syndrome. Nat Genet. 2014;46:299–304.
21. Miko A, Dóra KM, Kaposi A, Antignac C, Tory K. The mutation-dependent pathogenicity of NPHS2 p.R229Q: A guide for clinical assessment. Hum Mutat. 2018;39:1854–60.
22. Abou Tayoun AN, Pesaran T, DiStefano MT, Oza A, Rehm HL, Biesecker LG, et al. Recommendations for interpreting the loss of function PVS1 ACMG/AMP variant criterion. Hum Mutat. 2018;39:1517–24.
23. Kearney HM, Thorland EC, Brown KK, Quintero-Rivera F, South ST, Working Group of the American College of Medical Genetics Laboratory Quality Assurance C. American College of Medical Genetics standards and guidelines for interpretation and reporting of postnatal constitutional copy number variants. Genet Med. 2011;13:680–5.
24. Richards S, Aziz N, Bale S, Bick D, Das S, Gastier-Foster J, et al. Standards and guidelines for the interpretation of sequence variants: a joint consensus recommendation of the American College of Medical Genetics and Genomics and the Association for Molecular Pathology. Genet Med. 2015;17:405–24.
25. Ellard S, Baple EL, Berry I, Forrester N, Turnbull C, Owens M, et al. ACGS best practice guidelines for variant classification 2019. https://www.acgsukcom/media/11631/uk-practice-guidelines-for-variant-classification-v4-01-2020.pdf.
26. Bekheirnia MR, Bekheirnia N, Bainbridge MN, Gu S, Coban Akdemir ZH, Gambin T, et al. Whole-exome sequencing in the molecular diagnosis of individuals with congenital anomalies of the kidney and urinary tract and identification of a new causative gene. Genet Med. 2017;19:412–20.
27. Murugapoopathy V, Gupta IR. A primer on congenital anomalies of the kidneys and urinary tracts (CAKUT). Clin J Am Soc Nephrol. 2020;15:723–31.
28. Heidet L, Moriniere V, Henry C, De Tomasi L, Reilly ML, Humbert C, et al. Targeted exome sequencing identifies PBX1 as involved in monogenic congenital anomalies of the kidney and urinary tract. J Am Soc Nephrol. 2017;28:2901–14.

AUTHOR CONTRIBUTIONS

Research and study design: KMR, JH; data analysis/interpretation: JC, KMR, TM, JH; statistical analysis: JC; proband acquisition: VT, JP, NAE, VNS, AP, NT, VNS, MCB, JH; drafting and revising the article: JC, KMR, JH; supervision or mentorship: JH; revising and final approval of the submitted manuscript: KMR, MCB, JH. Each author contributed important intellectual content during manuscript drafting or revision and agrees to be personally accountable for the individual's own contributions and to ensure that questions pertaining to the accuracy or integrity of any portion of the work, even one in which the author was not directly involved, are appropriately investigated and resolved, including with documentation in the literature if appropriate.

COMPETING INTERESTS

The authors declare no competing interests.

ETHICAL APPROVAL

This study was performed according to the standards of the Declaration of Helsinki 2013 and approved by the local Ethics Committee of the Technical University of Munich (approval number 521/16S).

ADDITIONAL INFORMATION

Supplementary information The online version contains supplementary material available at https://doi.org/10.1038/s41431-023-01331-x.

Correspondence and requests for materials should be addressed to Julia Hoefele.

Reprints and permission information is available at http://www.nature.com/reprints

Implication of transcription factor FOXD2 dysfunction in syndromic congenital anomalies of the kidney and urinary tract (CAKUT)

Check for updates

OPEN

Korbinian M. Riedhammer[1,2,37], Thanh-Minh T. Nguyen[3,37], Can Koşukcu[4,37], Julia Calzada-Wack[5], Yong Li[6], Nurit Assia Batzir[7], Seha Saygılı[8], Vera Wimmers[9,10], Gwang-Jin Kim[9], Marialena Chrysanthou[3], Zeineb Bakey[3,10], Efrat Sofrin-Drucker[7], Markus Kraiger[5], Adrián Sanz-Moreno[5], Oana V. Amarie[5], Birgit Rathkolb[5,11,12], Tanja Klein-Rodewald[5], Lillian Garrett[5,13], Sabine M. Hölter[5,13,14], Claudia Seisenberger[5], Stefan Haug[6], Pascal Schlosser[6,15], Susan Marschall[5], Wolfgang Wurst[13,14,16,17], Helmut Fuchs[5], Valerie Gailus-Durner[5], Matthias Wuttke[6], Martin Hrabe de Angelis[5,12,18], Jasmina Ćomić[1,2], Özlem Akgün Doğan[19], Yasemin Özlük[20], Mehmet Taşdemir[21], Ayşe Ağbaş[8], Nur Canpolat[8], Naama Orenstein[7,22], Salim Çalışkan[8], Ruthild G. Weber[23], Carsten Bergmann[24,25], Cecile Jeanpierre[26], Sophie Saunier[26], Tze Y. Lim[27], Friedhelm Hildebrandt[28], Bader Alhaddad[1], Lina Basel-Salmon[22,29,30], Yael Borovitz[22,31], Kaman Wu[3], Dinu Antony[3,10], Julia Matschkal[2], Christian W. Schaaf[1,2], Lutz Renders[2], Christoph Schmaderer[2], Manuel Rogg[32], Christoph Schell[32], Thomas Meitinger[1], Uwe Heemann[2], Anna Köttgen[6,33], Sebastian J. Arnold[9,33], Fatih Ozaltin[4,34,35,36], Miriam Schmidts[3,10,33,38] and Julia Hoefele[1,38]

[1]Institute of Human Genetics, Klinikum rechts der Isar, Technical University of Munich, TUM School of Medicine and Health, Munich, Germany; [2]Department of Nephrology, Klinikum rechts der Isar, Technical University of Munich, TUM School of Medicine and Health, Munich, Germany; [3]Department of Human Genetics, Radboud Institute for Molecular Life Sciences, Radboud University Medical Center, Nijmegen, The Netherlands; [4]Department of Bioinformatics, Hacettepe University Institute of Health Sciences, Ankara, Türkiye; [5]Institute of Experimental Genetics, German Mouse Clinic, Helmholtz Zentrum München, German Research Center for Environmental Health, Neuherberg, Germany; [6]Institute of Genetic Epidemiology, Medical Center – University of Freiburg, Faculty of Medicine, University of Freiburg, Germany; [7]Pediatric Genetics Unit, Schneider Children's Medical Center of Israel, Petah Tikva, Israel; [8]Department of Pediatric Nephrology, Istanbul University-Cerrahpasa, Cerrahpasa Faculty of Medicine, Istanbul, Türkiye; [9]Institute of Experimental and Clinical Pharmacology and Toxicology, Faculty of Medicine, University of Freiburg, Germany; [10]Center for Pediatrics and Adolescent Medicine, Medical Center – University of Freiburg, Faculty of Medicine, University of Freiburg, Germany; [11]Institute of Molecular Animal Breeding and Biotechnology, Gene Center, Ludwig-Maximilians-University Munich, Munich, Germany; [12]German Center for Diabetes Research (DZD), Neuherberg, Germany; [13]Institute of Developmental Genetics, Helmholtz Zentrum München, German Research Center for Environmental Health, Neuherberg, Germany; [14]Chair of Developmental Genetics, TUM School of Life Sciences (SoLS), Technical University of Munich, Freising, Germany; [15]Department of Epidemiology, Johns Hopkins University Bloomberg School of Public Health, Baltimore, Maryland, USA; [16]Deutsches Institut für Neurodegenerative Erkrankungen (DZNE) Site Munich, Munich, Germany; [17]Munich Cluster for Systems Neurology (SyNergy), Adolf-Butenandt-Institut, Ludwig-Maximilians-University Munich, Munich, Germany; [18]Chair of Experimental Genetics, TUM School of Life Sciences (SoLS), Technical University of Munich, Freising, Germany; [19]Department of Pediatrics, Division of Pediatric Genetics, Acibadem Mehmet Ali Aydinlar University, School of Medicine, Istanbul, Türkiye; [20]Department of Pathology, Istanbul University, Istanbul Faculty of Medicine, Istanbul, Türkiye; [21]Department of Pediatric Nephrology, Istinye University Faculty of Medicine, Istanbul, Türkiye; [22]Faculty of Medicine, Tel Aviv University, Tel Aviv, Israel; [23]Department of Human Genetics, Hannover Medical School, Hannover, Germany; [24]Medizinische Genetik Mainz, Limbach Genetics, Mainz, Germany; [25]Department of Medicine IV, Medical Center – University of Freiburg, Faculty of Medicine, University of Freiburg, Germany; [26]Laboratoire des Maladies Rénales Héréditaires, Institut Imagine, Université Paris Cité, INSERM UMR 1163, Paris, France; [27]Department of Medicine, Division of Nephrology, Columbia University, New York, New York, USA; [28]Division of Nephrology, Boston Children's Hospital, Harvard Medical School, Boston, Massachusetts, USA; [29]Raphael Recanati Genetics Institute, Rabin Medical Center, Petah Tikva, Israel; [30]Felsenstein Medical Research Center, Petah Tikva, Israel; [31]Institute of Nephrology, Schneider Children's Medical Center of Israel, Petah Tikva, Israel; [32]Institute of Surgical Pathology, Medical Center – University of Freiburg, Faculty of Medicine, University of Freiburg, Germany; [33]CIBSS – Center for Integrative Biological Signaling Studies, University of Freiburg, Freiburg, Germany; [34]Department of Pediatric Nephrology, Hacettepe University Faculty of Medicine, Sihhiye, Ankara, Türkiye; [35]Nephrogenetics Laboratory, Hacettepe University Faculty of Medicine, Sihhiye, Ankara, Türkiye; and [36]Center for Genomics and Rare Diseases, Hacettepe University, Sihhiye, Ankara, Türkiye

Correspondence: Julia Hoefele, Institute of Human Genetics, Klinikum rechts der Isar, Technical University of Munich, TUM School of Medicine and Health, Trogerstr. 32, 81675 Munich, Germany. E-mail: julia.hoefele@tum.de; or Miriam Schmidts, Center for Pediatrics and Adolescent Medicine, Medical Center – University of Freiburg, Faculty of Medicine, University of Freiburg, Mathildenstr. 1, 79106 Freiburg, Germany. E-mail: miriam.schmidts@uniklinik-freiburg.de; or Fatih Ozaltin, Department of Pediatric Nephrology,

Hacettepe University Faculty of Medicine, 06100, Sihiye, Ankara, Türkiye. E-mail: fozaltin@hacettepe.edu.tr

[37]These first authors contributed equally to the work.

[38]These senior authors contributed equally to the work.

Congenital anomalies of the kidney and urinary tract (CAKUT) are the predominant cause for chronic kidney disease below age 30 years. Many monogenic forms have been discovered due to comprehensive genetic testing like exome sequencing. However, disease-causing variants in known disease-associated genes only explain a proportion of cases. Here, we aim to unravel underlying molecular mechanisms of syndromic CAKUT in three unrelated multiplex families with presumed autosomal recessive inheritance. Exome sequencing in the index individuals revealed three different rare homozygous variants in *FOXD2*, encoding a transcription factor not previously implicated in CAKUT in humans: a frameshift in the Arabic and a missense variant each in the Turkish and the Israeli family with segregation patterns consistent with autosomal recessive inheritance. CRISPR/Cas9-derived *Foxd2* knockout mice presented with a bilateral dilated kidney pelvis accompanied by atrophy of the kidney papilla and mandibular, ophthalmologic, and behavioral anomalies, recapitulating the human phenotype. In a complementary approach to study pathomechanisms of FOXD2-dysfunction–mediated developmental kidney defects, we generated CRISPR/Cas9-mediated knockout of *Foxd2* in ureteric bud–induced mouse metanephric mesenchyme cells. Transcriptomic analyses revealed enrichment of numerous differentially expressed genes important for kidney/urogenital development, including *Pax2* and *Wnt4* as well as gene expression changes indicating a shift toward a stromal cell identity. Histology of *Foxd2* knockout mouse kidneys confirmed increased fibrosis. Further, genome-wide association studies suggest that *FOXD2* could play a role for maintenance of podocyte integrity during adulthood. Thus, our studies help in genetic diagnostics of monogenic CAKUT and in understanding of monogenic and multifactorial kidney diseases.

Lay Summary

Congenital anomalies of the kidney and urinary tract are the predominant cause of impaired kidney function in infants, children, and adolescents. The symptoms are diverse, ranging from relatively mild manifestations such as vesicoureteral reflux (backward flow of urine to the kidneys) to severe forms such as renal agenesis (absent kidneys). So far, in only ∼10% of the affected individuals, disease-causing variants in known disease-associated genes can be identified. Within this study, in 3 families with children affected by congenital anomalies of the kidney and urinary tract, rare variants in the gene *FOXD2* (forkhead box D2) could be identified. Further analyses, for example, of mice and renal cells, suggested that *FOXD2* could play a role in the renal and urogenital development and seems to be important for maintenance of the filtering function of the kidneys. The focus of this study was therefore on the characterization of *FOXD2* as a gene associated with the development of congenital anomalies of the kidney and urinary tract and its underlying pathomechanisms.

C ongenital anomalies of the kidney and urinary tract (CAKUT) are the most important cause of renal replacement therapy in children aged 0 to 14 years in Europe (41.3%) and the most frequent cause of chronic kidney disease (CKD) up to the age of 30 years.[1,2] CAKUT comprises a broad spectrum of malformations of the kidney and urinary tract, ranging from vesicoureteral reflux to renal agenesis leading to kidney failure requiring dialysis and kidney transplantation.[3] CAKUT can occur in either isolated or syndromic forms.[4,5]

Much progress has been made over the last years concerning disease-associated gene identification by using next-generation sequencing approaches. Several monogenic forms of CAKUT have been identified, mostly inherited in an autosomal dominant, but also autosomal recessive, fashion. More than 45 genes associated with isolated monogenic CAKUT and >135 genes associated with syndromic CAKUT are known.[6,7] Furthermore, copy number variants play an important role in CAKUT.[4] Nevertheless, only ∼10% of CAKUT cases can be genetically solved, and incomplete penetrance and variable expressivity are often observed. Monogenic CAKUT is more frequent if severe kidney affection occurs (renal agenesis/dysplasia) in syndromic/familial cases and if there is parental consanguinity.[3,8] Judging from familial clustering of CAKUT and a large number of CAKUT manifestations in monogenic mouse models, there is evidence for not yet described monogenic causes of CAKUT in humans.[3,9]

Among the genes implicated in CAKUT by mouse models are 2 encoding transcription factors of the forkhead box (*FOX*) gene family: *Foxd1* and *Foxd2*. Both genes are highly similar in structure and sequence and likely have partially redundant functions.[10] No human individuals with CAKUT resulting from *FOXD1* or *FOXD2* disease-causing variants have been described to date. Here, we report the identification of a homozygous frameshift variant and 2 homozygous missense variants in *FOXD2* in 3 unrelated families implicated in autosomal recessive syndromic CAKUT with renal hypoplasia, facial dysmorphies, and proteinuria. Systematic phenotyping of *Foxd2* knockout (KO) mice did not only confirm the renal anomalies previously reported in the literature but also recapitulated extrarenal features observed in affected individuals.[10] Transcriptome analyses in a *Foxd2* mutant mouse metanephric mesenchyme cell line suggests
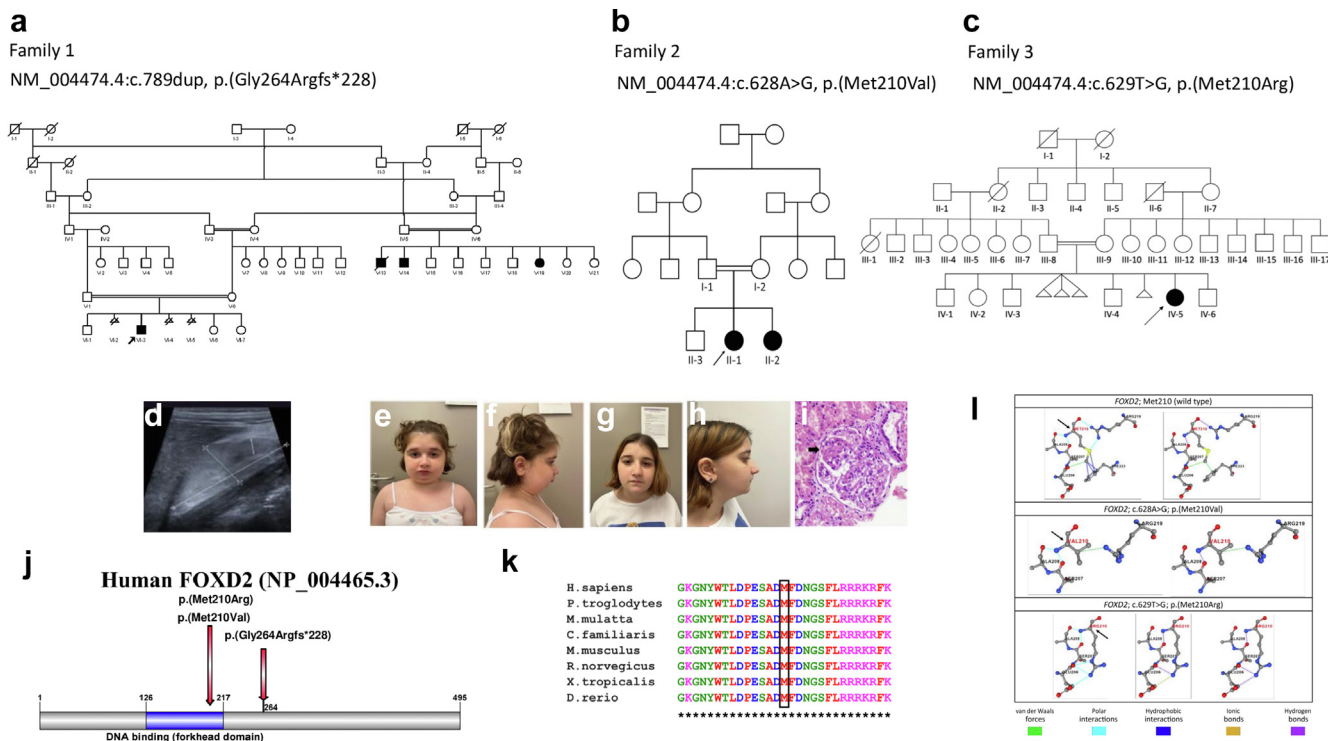
Figure 1 | Pedigree of (a) the Arabic family, (b) the Turkish family, and (c) the Israeli family. The solid symbols indicate affected individuals; circles, females; squares, males; arrows, index and also affected cousin. The double horizontal bars indicate consanguinity. **(d)** Renal ultrasound of the Arabic index individual (right kidney). **(e–h)** Facial photographs of the siblings of the Turkish family (downslanting palpebral fissures, deeply set eyes, laterally extended eyebrows, micro-retrognathia, and mild ptosis on the left eye). **(i)** Renal biopsy of individual II-2 of the Turkish family. Note glomerular hypertrophy, mesangial increase, and segmental sclerosis (arrow; hematoxylin and eosin stain). **(j)** Illustration of the FOXD2 (forkhead box D2) protein showing location of the variants. **(k)** Multiple alignment analysis using Clustal X software (http://www.clustal.org/clustal2) demonstrating that methionine (M) in position 210 of *FOXD2* is evolutionary conserved. **(l)** Three-dimensional structural analyses showing the noncovalent interactions between the mutated site and its surrounding residues for the p.(Met210Val) and p.(Met210Arg) variants in *FOXD2*. (i) Wild-type structure of residue MET210 having 4 polar interactions (sky blue), 2 van der Waals interactions (green), 4 hydrophobic interactions (blue), and 2 hydrogen bonds (purple). (ii) Mutant-type residue 210VAL (family 2) having 2 polar interactions (sky), 1 van der Waals interaction (green), and 1 hydrogen bond (purple). (iii) Mutant-type residue 210ARG (family 3) having 5 polar interactions (sky blue), 3 hydrogen bonds (purple), and 1 ionic bond (gold). Duplicate/triplicate structures are illustrated to make overlapping interactions or bonds visible. To optimize viewing of this image, please see the online version of this article at www.kidney-international.org.

Pax2 and *Wnt4* as *Foxd2* downstream targets, providing a putative pathomechanism potentially involving diversion of the lineage identity toward renal stroma cells.

METHODS
Detailed methods can be found in the Supplementary Methods.

Human genetics
In case of family 1 (Figure 1a), the study was approved by the local ethics committee of the Technical University of Munich (521/16 S) and performed according to the standard of the Helsinki Declaration of 2013. Written informed consent was obtained from all participants or their legal guardians. The family described in this study is part of a larger hereditary kidney disease cohort ("NephroGen"; >1000 families), including 313 CAKUT families, located at the Institute of Human Genetics, Technical University of Munich, Munich, Germany.

A DNA sample of the index case (VI-3) was analyzed by exome sequencing (ES) using the SureSelect Human All Exon 60 Mb V6 kit (Agilent) and the HiSeq 4000 (Illumina) sequencer as previously described.[11] Other family members were analyzed by targeted Sanger

sequencing using the ABI capillary sequencer 3730 (Applied Biosystems). To identify additional individuals affected by CAKUT and carrying biallelic damaging *FOXD2* variants, a number of collaborating laboratories (total of 5000 cases analyzed) were contacted and a *GeneMatcher* search was conducted.[12]

Family 2 (Figure 1b) was identified through *GeneMatcher*,[12] and all individuals participating in this study were enrolled after obtaining signed informed consent in accordance with human subject research protocols approved by the Ethics Committee of Istanbul University – Cerrahpasa, Cerrahpasa Medical Faculty (No.: 139896, Date: October 22, 2020).

Microarray studies were performed in affected individuals (II-1 and II-2) using the Illumina Infinium HumanCytoSNP-12 v2.1 (300K) microarray chip and Illumina BlueFuse Multi v4.5 Software. ES was performed in the 2 affected girls, 1 unaffected boy, and their parents (i.e., II-1, II-2, II-3, I-1, and I-2; Figure 1b) using the Human Core Exome Panel v3.0 (Twist Bioscience) and the MGI-T7 (MGI Tech) sequencer. Homozygosity mapping was performed using ES data via HomSI software (a homozygous stretch identifier from next-generation sequencing data), which was developed by the Advanced Genomics and Bioinformatics Research Center in the Scientific and Technological Research Council of Türkiye.[13] Sanger sequencing was

performed in all individuals of the family to validate the sequence variation prioritized by ES using the ABI 3130 genetic analyzer.

In case of family 3 (Figure 1c), the study was approved by the Rabin Medical Center Institutional Review Board (6826). Signed informed consent for participation in the study was received from the family. Chromosomal microarray analysis was performed using the CytoScan 750K Array (Applied Biosystems). The index case underwent commercial multigene panel testing (Blueprint Genetics). Subsequently, duo ES for the proband (Figure 1c, IV-5) and her mother (Figure 1c, III-9) was performed at the Genetics Institute in the Tel Aviv Sourasky Medical Center. Targeted capture of protein-coding regions was performed using xGen Exome Hyb Panel v2 (Integrated DNA Technologies). Paired-end libraries were sequenced on the NovaSeq 6000 system (Illumina). At least 97% of target bases were covered at $\geq 20\times$ (95% at $>100\times$). Data analysis was performed at the Raphael Recanati Genetics Institute, Petah Tikva, Israel, using the Emedgene platform (Emedgene Technologies) and the Franklin genetic analysis and variant classification platform (Franklin by genoox; https://franklin.genoox.com). Because no disease-causing variant was identified, data were subsequently reanalyzed for suspicious, rare homozygous variants, and a variant in FOXD2 was prioritized. While this manuscript was in preparation, a preprint version describing the findings in families 1 and 2 was published in medRxiv.[14] Upon reanalysis, the striking clinical and molecular similarities between the affected individuals in these families and the index case in family 3 were noted.

The GeneBank (National Center for Biotechnology Information) sequence FOXD2 NM_004474.4 (corresponding to the canonical Ensembl transcript ENST00000334793.6) was used as reference. NP_004465.3 protein sequence was also selected for further bioinformatic analyses.

In silico *prediction and multiple sequence alignment for missense variants, and protein modeling for* FOXD2 p.(Met210Val) *and* p.(Met210Arg) *missense variants (families 2 and 3).* In silico predictions were performed using Sorting Intolerant From Tolerant (SIFT; https://sift.bii.a-star.edu.sg/), Protein Variation Effect Analyzer (PROVEAN; http://provean.jcvi.org/index.php/), Polymorphism Phenotyping v2 (PolyPhen-2; http://genetics.bwh.harvard.edu/pph2/), Mutation Taster (https://www.mutationtaster.org/), Combined Annotation Dependent Depletion (CADD; https://cadd.gs.washington.edu/), Rare Exome Variant Ensemble Learner (REVEL; https://sites.google.com/site/revelgenomics/?pli=1),[15] ClinPred (https://sites.google.com/site/clinpred/),[16] and MutPred2 (http://mutpred.mutdb.org/).[17]

Multiple sequence protein alignment was performed using Clustal Omega version 1.2.2 (https://www.ebi.ac.uk/Tools/msa/clustalo/).

FOXD2 protein structure and Protein Data Bank (PDB) files were absent in the RCSB Protein Data Bank (https://www.rcsb.org/). Therefore, the preexisting model based in the AlphaFold database (https://alphafold.ebi.ac.uk/entry/O60548) was used. Gibbs free energy minimization of the wild-type (wt) protein structure was performed with the RepairPDB command of FoldX software[18] with the following syntax:

foldx –command=RepairPDB –pdb= AF-O60548-F1-model_v2.pdb –water=CRYSTAL.

Four in silico tools, which estimate the impact of missense variants on protein stability and calculate the changes in unfolding Gibbs free energy, $\Delta\Delta G$, were used. Protein stability predictions were calculated with DynaMut2,[19] INPS-3D,[20] FoldX,[18] and PremPS[21] using the AlphaFold structure of FOXD2 as an input PDB file.

The $\Delta\Delta G$ values between the wt protein and results of altered amino acid substitution were calculated for the p.Met210Val and p.Met210Arg variants in FOXD2. Finally, 3-dimensional (3D) structures of the wt and altered FOXD2 protein structures were generated with DynaMut2. The $\Delta\Delta G$ values (in kilocalorie per mole) for both variants were interpreted as follows: Predicted $\Delta\Delta G < 0$ is destabilizing in the case of DynaMut2 and INPS-3D. Predicted $\Delta\Delta G > 0$ is destabilizing in the case of FoldX 5.0 and PremPS.

Clustered regularly interspaced short palindromic repeats (CRISPR)/Cas9 gene editing in mice and mouse phenotyping

Mice were maintained in individually ventilated cages with water and standard mouse chow according to the Directive 2010/63/EU, German laws, and German Mouse Clinic (GMC) housing conditions. All tests were approved by the responsible authority of the district government of Upper Bavaria, Germany.

The Foxd2 KO mouse model was derived using CRISPR/Cas9 technology using the web-based CRISPOR design tool[22] and systematically characterized in the GMC phenotyping screen as previously described.[23,24] Homozygous Foxd2 KO mice (10 males, 7 females), heterozygous Foxd2 KO mice (8 males, 10 females), and wt controls (33 males, 36 females) were analyzed by the GMC at Helmholtz Zentrum München, Neuherberg, Germany (http://www.mouseclinic.de).[23–25] The phenotypic tests were part of the GMC screen and performed according to standardized protocols as previously described.[26–29] More details and the description of the immunohistochemistry and image analysis can be found in the Supplementary Methods.

Cell culture, *Foxd2*-deficient metanephric mesenchyme cell model generation using CRSPR/Cas9 technology, and transcriptome analyses

CRISPR/Cas9 gene targeting on mk4 metanephric mouse cells was performed as previously described.[30,31] Bioinformatics analysis was performed using the Galaxy platform (https://usegalaxy.org/) as previously described.[32] Quantitative polymerase chain reaction (qPCR) in different mk4 clones carrying different homozygous frameshift alleles to exclude clonal effects was performed using the GoTaq qPCR Master Mix (Promega; catalog number A6001). Immunofluorescence analyses were performed as previously described (anti-Pax2 antibody: ab79389 [Abcam], 1:200).[33] Gel electrophoresis and Western blotting were likewise performed as previously described (anti-Pax2 antibody: ab150391, EPR8586 [Abcam]).[34]

3D cell culture

CMUB-1 and mK cells were cultured in Dulbecco's modified Eagle's medium with GlutaMax medium with addition of 10% fetal bovine serum, 1% penicillin/streptomycin, and 1% sodium pyruvate at 37 °C under 5% CO_2. To obtain the mK3 cell supernatant, mK3 cells were cultured 48 hours in serum-free medium before medium collection. Thirty milliliters of medium were then filtered using a 0.2 μm filter and added to a centrifugation concentration filter system with cutoff pore sizes of 3 kDa and centrifugation performed at $4000g$ for 30 minutes, resulting in an ∼50-times concentration. For CMUB-1 3D Matrigel cell cultures, Lab-Tek II Chamber Slides (Thermo Fisher) were coated with a Matrigel–cell suspension and 150 μl of medium was added after solidification.

FOXD2 genome-wide association study locus fine mapping

A previous genome-wide association study (GWAS) meta-analysis of the urinary albumin-to-creatinine ratio (UACR) has identified the *FOXD2* locus.[35] We therefore attempted to identify the responsible variants underlying the association signal by using the statistical fine-mapping method SuSiE.[36] SuSiE selects single nucleotide polymorphisms (SNPs) with a high probability to causally affect a given trait—here the UACR—even if a genetic locus contains many highly correlated genetic variants and/or multiple SNPs with a causal effect. We used the R package susieR (version 0.12.27) to fine-map the 1 MB genomic region centered at the SNP showing the strongest statistical association with UACR, rs1337526. For linkage disequilibrium matrix calculation, we used a genotype set of 15,000 randomly selected participants of European ancestry from the UK Biobank as in Teumer et al.[35] To match the linkage disequilibrium reference as closely as possible, GWAS summary statistics of UACR based on data from 436,392 participants of the UK Biobank (application number 20272) were used as input. We used the default parameters in susieR functions, except for setting var_y to 1 and max_iter to 100000. The identified credible set SNPs were screened for their association with the UACR in up to 127,862 independent participants of the CKDGen Consortium.[35] For visualization, credible set SNPs were positioned in the IGV browser of the human kidney snATAC-seq open chromatin peaks (http://www.susztaklab.com/human_kidney/igv/) from Sheng et al.[37] to examine their position with respect to cell type–specific open chromatin peaks. The regional association plot was created by LocusZoom version 1.4.[38] The podocyte cis-coaccessibility network was kindly provided by Muto et al.[39] Only connections with a coaccessibility score of >0.25 targeting the *FOXD2* promoter were displayed.

We performed phenome-wide association studies of the 2 most likely causal fine-mapped variants using GWAS summary statistics of human traits and diseases from the UK Biobank[40] (TOPMed-imputed PheWeb at https://pheweb.org/UKB-TOPMed/) and Finn-Gen[41] (release DF9 data at https://r9.finngen.fi/). Phenome-wide association study queries were based on the rs identifier of the variants.

Kidney gene expression profiles

To determine the localization of *FOXD2* gene expression within the adult human kidney, we leveraged publicly available single-cell RNA sequencing data from 47 samples from the Kidney Precision Medicine Project (accessible through https://atlas.kpmp.org/). Lake et al. provided a detailed description of the experimental setup and cell type identification processes.[42]

Code availability

Codes for transcriptome analysis and plotting are available under https://github.com/gwangjinkim/foxd2_analysis.

Ethics approval and consent to participate

This project has received approval from the local ethics committee of the Technical University of Munich (521/16 S), from the Ethics Committee of Istanbul University – Cerrahpasa, Cerrahpasa Medical Faculty (No: 139896, Date: October 10, 2020), as well as from the Rabin Medical Center Institutional Review Board in Petah Tikva (6826). Human samples collected as part of the Kidney Precision Medicine Project (KPMP) consortium (https://KPMP.org) were obtained with informed consent and approved under a protocol by the KPMP single institutional review board of the University of Washington Institutional Review Board (IRB 20190213). All participants provided informed consent, and the research conformed to the principles of the Helsinki Declaration.

RESULTS

Clinical case

Family 1 (Arabian Peninsula). In this consanguineous family, the index individual (VI-3) had facial dysmorphism (low-set ears, hypertelorism, downslanting palpebral fissures, and retrognathia), developmental delay, and congenital bilateral hypoplastic kidneys (Figure 1d) and underwent allogenic kidney transplantation at 11 years of age. At 7 years of age, he had CKD G4 (estimated glomerular filtration rate 26 ml/min per 1.73 m^2 [modified Schwartz formula][43]) and proteinuria of 2.7 g/24 h. His parents are first-degree cousins. Three first cousins once removed—individuals V-13, V-14, and V-19 (see Figure 1a for a detailed pedigree of the family)—were similarly affected. V-19 had bilateral hypoplastic kidneys, developmental delay, and retrognathia. At 6 years of age, she had CKD G3 (estimated glomerular filtration rate 11 ml/min per 1.73 m^2) and proteinuria of 5.0 g/24 h. Allogenic kidney transplantation was done at 7 years of age. Relatives V-13 and V-14, brothers of V-19, were also affected by a similar phenotype (Table 1; Supplementary Case Report).

Family 2 (Türkiye). In this consanguineous family, the female index individual (II-1) was diagnosed with kidney failure at the age of 6 years. Initial ultrasonography showed bilateral hypoplastic kidneys with increased echogenicity. She received a preemptive kidney transplant from her father at the age of 6 years. In addition to kidney failure, the individual had dysmorphic findings including downslanting palpebral fissures, deeply set eyes, laterally extended eyebrows, micro-retrognathia, and mild ptosis on the left eye (Figure 1e and f and Table 1), as well as high palate, dental crowding, fusiform fingers, sandal gap in both sides, and central obesity noted on physical examination. Eye examination performed at the age of 6 years showed left esotropia and bilateral posterior subcapsular cataract as well as grade I hypertensive retinopathy.

The sister of the index individual (II-2) was referred to the pediatric nephrology department because of persistent proteinuria at the age of 7 years. Her height was 117 $\pm$ −2.61 cm, and she also had dysmorphic findings (Figure 1g and h and Table 1). Serum creatinine level was normal for the age (i.e., 0.35 mg/dl, corresponding to an estimated glomerular filtration rate of 138 ml/min per 1.73 m^2; creatinine-based "bedside Schwartz" equation [2009]).[43] Renal ultrasound showed bilateral increased renal parenchymal echogenicity and left kidney hypoplasia. Kidney biopsy was compatible with focal segmental glomerulosclerosis (FSGS; Figure 1i). Dysmorphic features included downslanting palpebral fissures, laterally extended eyebrows, micro-retrognathia, left deviation of nasal axis, tapering of distal phalanges of fingers, sandal gap in both sides, short toes, and central obesity. A full ophthalmological examination was found to be normal. At 17 years of age, laboratory findings were compatible with CKD G3

Table 1 | Overview of the clinical phenotype of the affected individuals of the Arabic, the Turkish, and the Israeli family

	Family 1: Arabic family				Family 2: Turkish family		Family 3: Israeli family
	VI-3	V-13	V-14	V-19	II-1	II-2	
Genetic and proband data							
FOXD2 variant, chromosomal position (hg19)	chr1:g.47904596dup	n.t.	n.t.	chr1:g.47904596dup	chr1:g.47904435A>G	chr1:g.47904435A>G	chr1:g.47904436T>G
FOXD2 variant, cDNA position and protein position (NM_004474.4, NP_004465.3)	c.789dup, p.(Gly264Argfs*228)	n.t.	n.t.	c.789dup, p.(Gly264Argfs*228)	c.628A>G, p.(Met210Val)	c.628A>G, p.(Met210Val)	c.629T>G, p.(Met210Arg)
gnomAD MAF	0	0	0	0	0	0	0
Zygosity	Homozygous	—	—	Homozygous	Homozygous	Homozygous	Homozygous
Inheritance	From parents	—	—	Only mother tested (heterozygous carrier)	From parents	From parents	Only mother tested (heterozygous carrier)
Consanguinity	+	+	+	+	+	+	+
Sex	Male	Male	Male	Female	Female	female	Female
Age at the last examination, yr	8	Deceased at age 6 yr	n.d.	n.d.	12.7	16.9	7
Kidney							
Congenital anomalies of the kidney and urinary tract	+ (Bilateral kidney hypoplasia)	+ (Hypospadias)	+ (Horseshoe kidney, hypospadias)	+ (Bilateral kidney hypoplasia)	+ (Bilateral kidney hypoplasia)	+ (Kidney hypoplasia on the left side)	+ (Bilateral kidney hypoplasia)
KF	+ (10 yr)	n.d.	+	+ (6 yr)	+ (6 yr)	-	+ (5 yr)
Kidney transplantation	+ (11 yr; allogenic)	—	+ (6 yr, 25 yr; allogenic)	+ (7 yr; allogenic)	+ (6 yr)	-	+ (7 yr; allogenic)
Neurodevelopment							
Developmental delay	+	+	+	+	+	+	+
Dysmorphic features							
Facial dysmorphies	+ (Mandibular retrognathia, micrognathia, severe dental abnormalities, high-arched palate, hypertelorism, downslanting palpebral fissures, exophthalmos, flat nasal bridge, low-set dysplastic ears)	+ (Micrognathia)	+ (Micrognathia, crowded teeth)	+ (Micrognathia, discrete retrognathia)	+ (Downslanting palpebral fissures, deeply set eyes, laterally extended eyebrows, micro-retrognathia, mild ptosis on the left eye, high palate, dental crowding)	+ (Downslanting palpebral fissures, laterally extended eyebrows, micro-retrognathia, left deviation of the nasal axis)	+ (Downslanting palpebral fissures, ptosis, mild retrognathia)

Table 1 | (Continued) Overview of the clinical phenotype of the affected individuals of the Arabic, the Turkish, and the Israeli family

	Family 1: Arabic family				Family 2: Turkish family		Family 3: Israeli family
	VI-3	V-13	V-14	V-19	II-1	II-2	
Other				■ Imperforate anus (surgically treated as a neonate) ■ Corneal abrasions	■ Fusiform fingers ■ Sandal gap in both sides ■ Central obesity ■ Left esotropia and bilateral posterior subcapsular cataract	■ Tapering of distal phalanges of fingers ■ Sandal gap in both sides ■ Short toes ■ Central obesity	■ Trivial pulmonic stenosis ■ Esotropia, hypermetropia ■ Preauricular pit (also in mother and healthy brother)

FOXD2, forkhead box 2; gnomAD, Genome Aggregation Database (v.2.1.1, https://gnomad.broadinstitute.org); KF, kidney failure; MAF, minor allele frequency; n.d., no data; n.t., not tested.

with an estimated glomerular filtration rate of 38 ml/min per 1.73 m² (modified Schwartz formula).[43]

Family 3 (Israel). The proband was born to parents of Bedouin descent who are first cousins. During pregnancy, at 35 weeks of gestation, small kidneys were noted. On the third day of life, she had an elevated creatinine level of 1.7 mg/dl, which gradually decreased. Around age 2 years, she first presented with nephrotic syndrome, which did not respond to steroid treatment. Renal ultrasound showed bilateral dysplastic kidneys, and the left kidney was noted to be in the left central abdomen with small hypoechogenic findings suspicious for cysts and possibly dilated renal pelvis. Kidney biopsy was planned but not done owing to difficult access to the kidneys. She was treated with angiotensin-converting enzyme inhibitors and angiotensin receptor blockers with fluctuations in the degree of proteinuria, but levels always remained within the nephrotic range. Treatment with tacrolimus was also attempted but discontinued because of a rapid increase in the individual's creatinine levels and hyperkalemia. Her renal functions worsened over time, and, at the age of 5 years and a half, she was started on peritoneal dialysis. At the age of 7 years, she underwent allogenic kidney transplantation. Medical history is also significant for mild developmental delay, which resolved, esotropia, and hypermetropia. She follows up with cardiology for left ventricular dysfunction attributed to hypertension, which improved with treatment. She also had short stature below the third percentile in the growth chart since age 3 years, likely because of chronic kidney failure.

On the last examination, she had microcephaly (2.8 SDs below the mean), downslanting palpebral fissures, ptosis, mild retrognathia, and a small, prominent chin. She had a unilateral preauricular pit also seen in her mother and an unaffected brother.

Genetic results

Family 1 (Arabian Peninsula). ES of individual VI-3 (index) led to the prioritization of a homozygous frameshift variant in *FOXD2* NM_004474.4:c.789dup, p.(Gly264Argfs*228). The variant is not listed in gnomAD (Genome Aggregation Database, v.2.1.1, http://gnomad.broadinstitute.org/) and predicted to result in a protein of nearly the same length as wt FOXD2 but with a changed amino acid composition within the C-terminal half of the protein, leaving the DNA-binding domain intact (Figure 1j). As *FOXD2* is a single-exon gene (NM_004474.4), nonsense-mediated decay due to the frameshift variant cannot be expected (see Supplementary Methods for details on the filtering process of ES and Supplementary Table S1 for a list of homozygous variants below minor allele frequency 1.0% detected with ES in the index individual of family 1). Supporting the hypothesis that *FOXD2* represents an essential gene during mammalian development, no *FOXD2* homozygous loss-of-function variants are reported in gnomAD v.2.1.1.

Subsequent Sanger sequencing confirmed the segregation of the variant: parents of VI-3 are heterozygous carriers of the

variant. The clinically similarly affected maternal first cousin once removed (V-19) was found to be a homozygous carrier, while the maternal great-aunt (IV-6) and mother of V-19 are heterozygous carriers of this variant (Supplementary Figure S1). Further segregation of the variant could not be performed because of limited accessibility/missing consent of relatives.

Family 2 (Türkiye). Homozygosity mapping revealed runs of homozygosity located in chromosome 1, ~11.6 Mb long (chr1:g.47,607,000-59,155,000, hg19). The identified homozygous stretch showed that both affected siblings were sharing the runs of homozygosity; however, parents and the unaffected sibling were heterozygous for the region of interest (Supplementary Figure S2A). ES was then performed for the index case (II-1), affected and unaffected siblings (II-2 and II-3), as well as healthy consanguineous parents (I-1 and I-2). ES analyses resulted in the prioritization of a homozygous missense variant NM_004474.4:c.628A>G, p.(Met210Val) in *FOXD2* (predicted as deleterious with CADD, REVEL, ClinPred, and MutPred2), which is located within the disease-segregating homozygous region and is not listed in gnomAD (see Supplementary Table S2 for a list of filtered candidate variants detected with ES in the Turkish index individual).

Sanger sequencing results confirmed that the p.Met210Val variant in *FOXD2* is segregating with the disease in the family (Supplementary Figure S2B). The homozygous missense variant is located at the methionine residue at amino acid position 210 within the DNA-binding domain of FOXD2 (NP_004465.3), which is completely conserved among different species until the level of *Danio rerio* (Figure 1j and k).

Family 3 (Israel). A chromosomal microarray analysis (Raphael Recanati Genetics Institute) was inconspicuous, but showed regions of homozygosity ≥3 Mb in 6.4% of all autosomal regions tested. A renal malformation panel and nephrotic syndrome panel (Blueprint Genetics) followed by ES for the index individual and her mother were negative for disease-causing variants that fully explained the index individual's phenotype. Variants of uncertain significance in *FN1* and *TBC1D8B* and a single variant in *PKHD1* were detected, all of which were inherited from the unaffected mother (see Supplementary Table S3).

Because of parental consanguinity, revision of the exome data focusing on rare homozygous variants was performed, which identified a homozygous missense variant NM_004474.4:c.629T>G, p.(Met210Arg) in *FOXD2*. This variant is absent from the gnomAD database. It affects the same conserved amino acid as seen in family 2. The CADD PHRED score for this variant is 28.6.

Gibbs free energy calculation and the change in 3D protein structure in FOXD2 missense variants c.628A>G, p.(Met210Val) and c.629T>G, p.(Met210Arg) (families 2 and 3)

The starting free energy ΔG for the FOXD2 protein model was 817.623 kcal/mol, and it was lowered to 719.079 kcal/mol to a more stable state after the RepairPDB command of FoldX was applied. 3D protein models for wt FOXD2 and the potential changes in noncovalent bonds caused by the p.(Met210Val) and p.(Met210Arg) variants are displayed in Figure 1l. The p.(Met210Val) variant decreased protein stability and was predicted as "destabilizing" with all 4, and the p.(Met210Arg) variant decreased protein stability and was predicted as "destabilizing" with 3 of 4 different protein stability prediction tools upon point mutations. The $\Delta\Delta G$ scores calculated for both variants are displayed in Supplementary Table S4.

Fine mapping of the FOXD2 UACR GWAS locus prioritizes 2 underlying variants. The *FOXD2* locus (1p33) has been previously associated with UACR in large GWAS meta-analyses of adult study participants.[35] In agreement, the affected individuals carrying rare biallelic *FOXD2* variants show significant proteinuria, with one of them even showing the histological finding of FSGS on kidney biopsy. We now performed fine mapping of UACR-associated genetic variants in the *FOXD2* locus in 436,392 participants of the UK Biobank to prioritize the variants most likely to cause the association signal (Figure 2; see Methods). Fine mapping yielded 2 independent sets of UACR-associated variants that contained 8 and 21 variants, all of which were also associated with UACR in a direction-consistent manner in an independent sample of up to 127,862 participants of the CKDGen Consortium (Supplementary Table S5).[35] The variants with the highest posterior probability to cause the association signal with UACR in each set were both common SNPs upstream of *FOXD2*, rs17453832 and rs1337526 (Figure 2b). Interestingly, using publicly available scATAC-seq data from the human kidney,[37] rs17453832 overlaps accessible chromatin regions exclusively in podocytes, the relevant cell type for albuminuria of glomerular origin, as observed in FSGS (Figure 2c). Moreover, a cis-coaccessibility network derived from podocytes in an independent scATAC-seq data set[39] revealed a putative connection between rs17453832 and the *FOXD2* promoter/exon (Figure 2d; see Methods), further supporting rs17453832 as a regulatory variant of *FOXD2* in podocytes that leads to an association with UACR. Additional investigation of *FOXD2* in single-cell RNA-sequencing expression data (see Methods) showed >2.69-fold enriched expression in podocytes compared to all other cell types ($P = 5.9 \times 10^{-120}$). Fine-mapped variants in the *FOXD2* locus were not associated with other diseases in the UK Biobank or the FinnGen data sets after correction for multiple testing (see Methods); the association with the lowest P value was with "gestational edema and proteinuria without hypertension" ($P = 3 \times 10^{-5}$; FinnGen).

Foxd2 deficiency in mice leads to multidevelopmental phenotypes. To investigate the consequences of Foxd2 dysfunction in mice, *Foxd2* KO mice were generated using CRISPR/Cas9 technology and comprehensively phenotyped. Reverse transcription polymerase chain reaction and cDNA analysis confirmed the absence of *Foxd2* transcript in homozygous mutant animals (Supplementary Figure S3A). Homozygous *Foxd2* KO mice were viable and were born
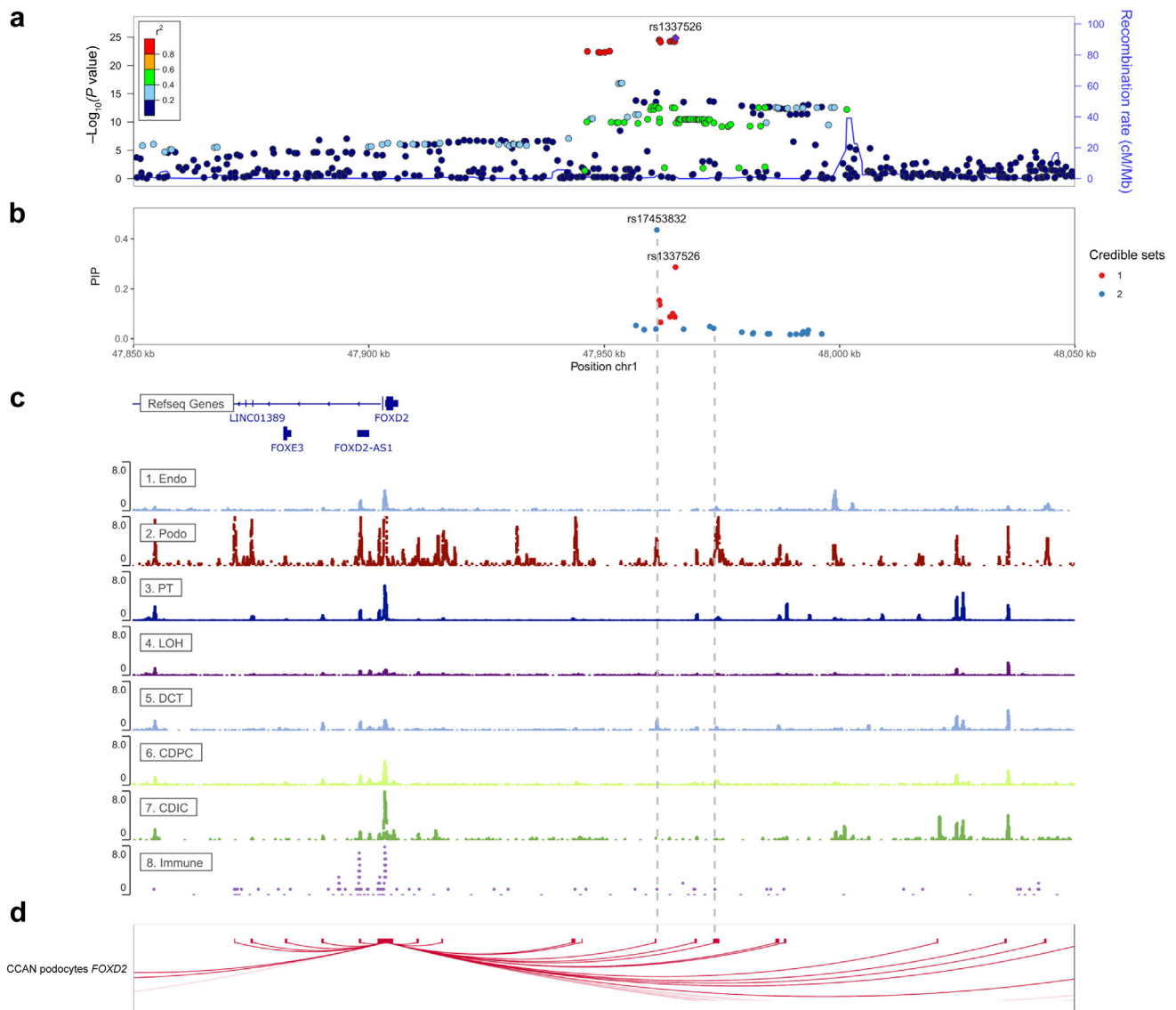
Figure 2 | From top to bottom: (a) regional association plot, (b) posterior inclusion probability (PIP) plot, (c) RefSeq gene track and 8 snATAC-seq peak tracks, and (d) podocyte cis-coaccessibility network (CCAN) at the *FOXD2* (forkhead box D2) locus. In the regional association plot, the association *P* values from a genome-wide association study of the urine albumin-to-creatinine ratio (UACR) from the UK Biobank were plotted on the $-\log_{10}$ scale. The correlation (r^2) of genetic variants in the region with the lead single nucleotide polymorphism (SNP) rs1337526 is indicated as color gradients. The r^2 was based on 1000 Genomes EUR genotype data phase 3, November 2014 release. In the PIP plot, only SNPs in 95% credible sets (i.e., the set of SNPs that contains a variant with effect on UACR with probability $\geq$ 95%) are shown. The color indicates the credible set membership. The vertical axis indicates the PIP value of the SNPs. The 8 ATAC-seq open chromatin tracks were retrieved from http://www.susztaklab.com/human_kidney/igv/. Two gray vertical dashed lines were placed at positions where credible set SNPs overlap with open chromatin peaks in a podocyte, a relevant cell type for albuminuria. The CCAN plot shows all connections with a coaccessibility score of >0.25 targeting the *FOXD2* promoter as red curved lines. CDIC, collecting duct intercalated cell; CDPC, collecting duct principal cell; chr1, chromosome 1; DCT, distal convoluted tubule; Endo, endothelial cell; Immune, immune cell; LOH, loop of Henle; Podo, podocyte; PT, proximal tubule.

approximately according to Mendelian distribution. Compared with wt and heterozygous littermates, more homozygous newborns died shortly after birth (Supplementary Figure S3B).

At 16 weeks, micro–computed tomography analyses revealed a changed mandible morphology in homozygous *Foxd2* KO mice (Figure 3a–d; $n = 4$ wt and $n = 2$ homozygous females and $n = 4$ wt and $n = 4$ homozygous males; using landmarks that have already been described in

rodents[44]), including an abnormally shortened condylar process and a flattened tip of the coronoid process in male homozygous *Foxd2* KO mice (Figure 3b–d). Importantly, homozygous *Foxd2* KO mice display smaller mandibles (micrognathia or mandibular hypoplasia), as measured with distance 3–5 (Figure 3d).

Ophthalmic evaluation identified changes in the appearance of the optic disc, imaged using the *en face* optical
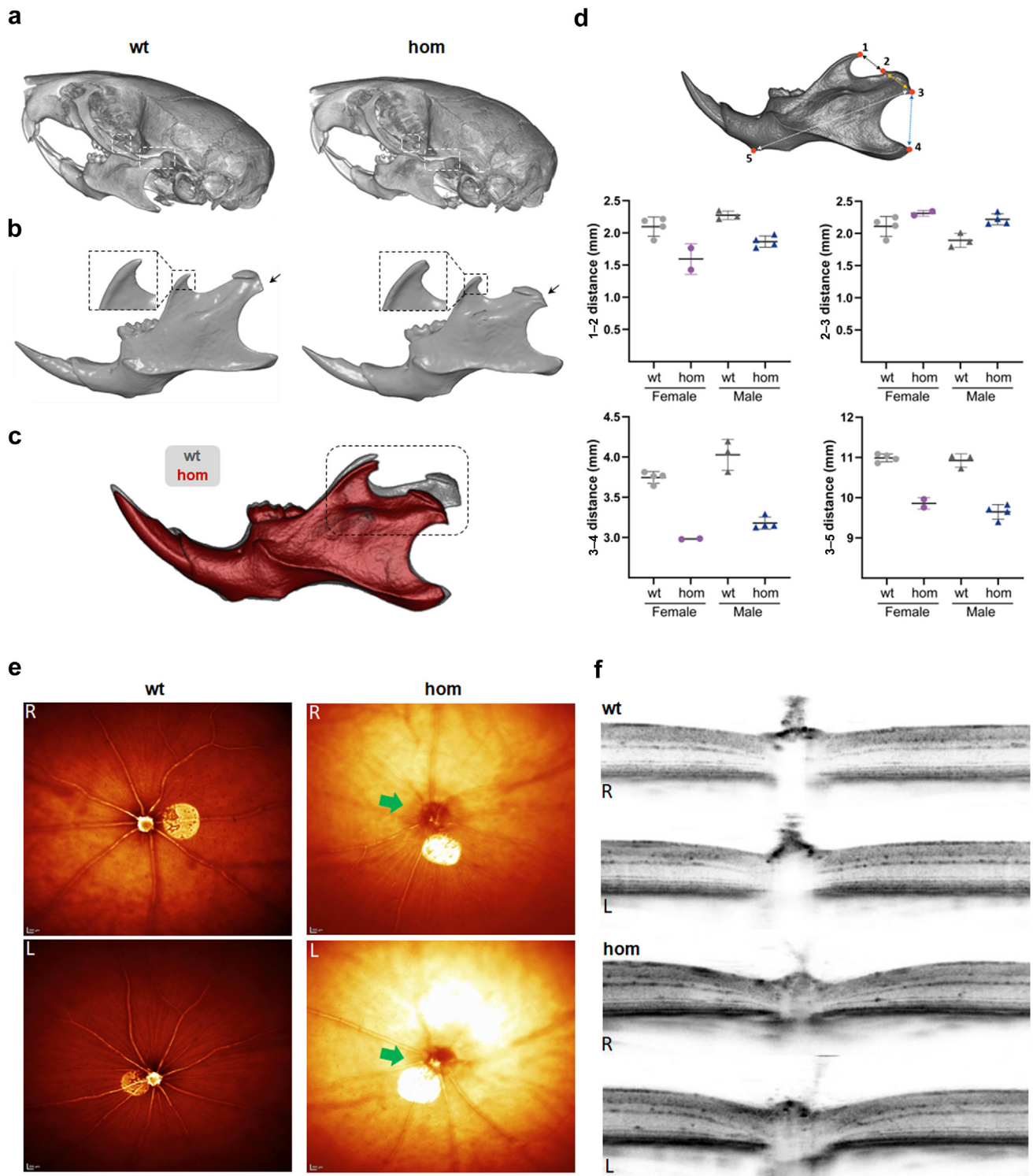
Figure 3 | Mandibular alterations and defective optic disc in homozygous (hom) *Foxd2* **(forkhead box D2) knockout (KO) mice.** Micro–computed tomography representative images of the (**a**) skull and (**b**) mandible from control (wild-type [wt]) and hom *Foxd2* KO male mice. In (**a**), the coronoid (left side) and condylar (right side) processes are highlighted by dash line rectangles; and in (**b**), by a magnified inset and arrows, respectively. (**c**) Volume matching of male control (gray) and mutant (red) mandibles at an identical scale, allowing easy qualitative comparison of the described morphological changes. (**d**) Mandibular morphometric analysis comparing distance measurements between several anatomical landmarks: (1) dorsal-most point of the coronoid process; (2) anterodorsal side of the condylar process; (3) ventral-most point of the condylar process; (4) posterior-most point of the angular process; and (5) ventral-most point of the front lower part of the mandible. The condylar process is shorter (distances 1–2 and 3–4) and slightly wider (distance 2–3) in mutants than in control animals. These landmarks have already been described in rodents.[44] $n = 4$ wt and $n = 2$ homozygous females and $n = 4$ wt and $n = 4$ homozygous males. Single values and mean ± SD values are shown. Test for statistical significance was not performed because of the low animal (continued)

coherence tomography modality as a darker ring around the optic nerve head (Figure 3e). Spectral-domain optical coherence tomography images revealed that homozygous *Foxd2* KO mice have posterior deformation of the optic nerve head surface (Figure 3f). We noted different severity in the alterations of the optic nerve in these mice. The total retinal thickness was not significantly altered; only for severely affected eyes, a much thinner total retinal thickness was measured (data not shown).

Although macroscopy did not reveal malformations of the urinary system, microscopic analysis by standard hematoxylin and eosin staining detected bilateral dilation of the renal pelvis. Among 6 homozygous *Foxd2* KO mice examined (4 males, 2 females), bilateral dilation of the renal pelvis was present in 2 homozygous males (33% penetrance; Figure 4a). A clearly narrowed cortex and a decreased size of the renal papilla (Figure 4a and b) accompanied the dilation. For better visualization of the papilla, we used immunohistochemical staining with aquaporin-2 as a marker for the collecting tubules and detected a reduction in the diameter of the ducts (Figure 4c). To rule out that the bilateral dilation of the renal pelvis observed in homozygous mutants represented a background lesion, we performed hematoxylin and eosin staining of kidneys from 126 wt animals randomized by age and background strain. We detected bilateral renal pelvis dilation in only 4 of 126 wt animals (Fisher exact test, $P = 0.0239$). Taken together, our results support the diagnosis of a renal pelvis dilation in homozygous mutant mice with a penetrance of 33%. The bilateral dilation of the renal pelvis was apparently not secondary to an obstructive lower urinary tract lesion. Additional histological parameters of the kidneys are described in Supplementary Table S6A and B and Supplementary Figure S4.

Further, we found a significantly increased (on average doubled) cytokeratin 8 expression level in the renal cortex of homozygous *Foxd2* KO mice compared with wt controls, determined by algorithm-based cell counting (2-sample *t* test, $P < 0.001$; Figure 5; Supplementary Figure S5), indicating tubular epithelial injury.

Plasma clinical chemistry parameters affected by renal dysfunction showed mild to moderate deviations in homozygous *Foxd2* KO mice compared with wt controls analyzed in parallel. Although sodium levels, and in trend also chloride levels, were slightly decreased predominantly in female homozygous *Foxd2* KO mice, maybe as a sign of volume overload due to reduced urine output, a significant increase in plasma potassium and urea levels in male homozygous *Foxd2* KO mice was observed (Figure 4d–f and h). The index

individual of family 1 also had increased plasma potassium and urea levels owing to reduced kidney function, but plasma sodium levels were normal. Interestingly, although in general no increase in plasma creatinine concentrations in homozygous *Foxd2* KO mice was observed, 2 homozygous *Foxd2* KO animals showed high values compared with controls (Figure 4g). One of them was studied by histological analyses, and the high creatinine and elevated urea levels were in line with the already described histopathological alterations in the kidneys, including increased cytokeratin 8 expression compatible with increased fibrosis (Figure 5; Supplementary Figure S5).

Behavioral alterations consequent to Foxd2 loss were also observed. In the open field test of spontaneous reactions to a novel environment, 8-week-old homozygous *Foxd2* KO mice were clearly hypoactive and hypoexploratory (Supplementary Figure S6). This was indexed by decreased total distance traveled (2-way analysis of variance genotype effect: $F_{1,81} = 19.93$; $P < 0.0001$) and total rearing activity (2-way analysis of variance genotype effect: $F_{1,81} = 59.36$; $P < 0.0001$) compared to wt controls. Heterozygous *Foxd2* KO mice were also hypoactive and hypoexploratory compared with wt mice, albeit with less severity than homozygous KO mice (Supplementary Table S7).

Generation of Foxd2-deficient metanephric mesenchyme cell models. To further investigate FOXD2 function for proper renal development and to understand how biallelic FOXD2 dysfunction may cause bilateral renal hypodysplasia/CAKUT in humans and mice, *Foxd2*-deficient immortalized mouse metanephric cell models (mk4 cells) were generated using CRISPR/Cas9 technology. mk4 cells represent ureteric bud–induced metanephric mesenchyme cells undergoing epithelial conversion.

The targeted *FOXD2* region was chosen to closely replicate the homozygous frameshift variant identified in family 1. Four suitable mk4 clones carrying different homozygous *Foxd2* variants resulting in a change in the reading frame were chosen (Table 2; Supplementary Figure S7 [only clone F7 shown]). Foxd2 is a transcription factor previously implicated in renal development in mice[10]; however, at the time of *Foxd2* KO mouse analysis, RNA sequencing analysis was unavailable and the precise role of mammalian renal development has remained elusive. Therefore, transcriptome analysis comparing the homozygous mutant mk4 with control mk4 cells transfected with nontargeting single guide RNA (sgRNA) was performed. Clone F7 carrying the frameshift variant NM_00859.3:c.801insT (p.Tyr268Leufs*109) was chosen as the frameshift that most closely resembles the one predicted

---

Figure 3 | (continued) number. (**e**) Representative images of eyes of 16-week-old hom *Foxd2* KO mice and age-matched wt littermates using the *en face* optical coherence tomography modality. *Foxd2*$^{-/-}$ fundus appearance around the optic nerve displays a darker signal, indicating alterations of the optic disc (green arrow). (**f**) Spectral-domain optical coherence tomography images through the optic nerve showed altered optic nerve morphology. Eleven of 17 hom *Foxd2* KO mice showed clear optic disc alterations. To optimize viewing of this image, please see the online version of this article at www.kidney-international.org.
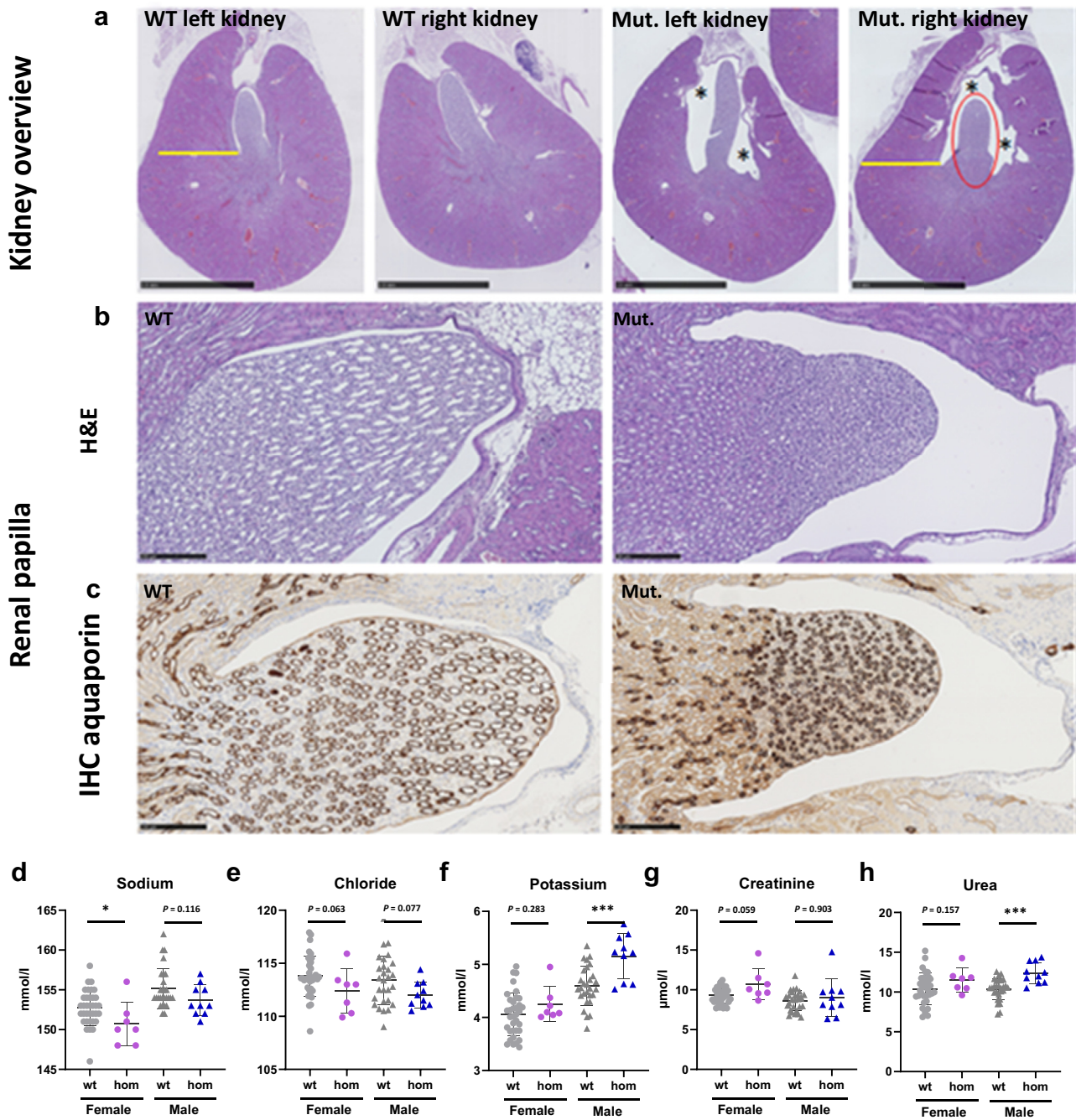
Figure 4 | Histopathological renal alterations in 16-week-old mice. (a) Representative overview pictures of hematoxylin and eosin (H&E) staining from the left and right kidneys of wild-type (wt) and homozygous (hom) *Foxd2* (forkhead box D2) knockout (KO) mice. Note the normal kidney morphology observed in the wt animal compared with bilateral mild renal pelvis dilation (marked with an asterisk) in the hom KO mouse. Note the reduced size of the renal papilla (marked in red) and the cortex, which is clearly narrowed (yellow). (b) H&E stains show a higher magnification of the renal papilla. (c) Immunohistochemistry (IHC) aquaporin-2 clearly shows a reduction in diameter of the collecting ducts in the mutant mouse. (d–h) Plasma clinical chemistry analyses of parameters frequently altered in the case of renal dysfunction, including plasma levels of (d–f) electrolytes, (g) creatinine, (h) and urea. Significance according to the Mann-Whitney test: $*P < 0.05$, $***P < 0.001$. Mut., mutant; NS, not significant. To optimize viewing of this image, please see the online version of this article at www.kidney-international.org.

for the allele of the index individual. Five biological replicates per condition were used for transcriptome analysis.

RNA sequencing results. Transcriptomics analyses revealed a number of differentially regulated genes (Figure 6a). Gene

Ontology (GO) term analysis of differentially expressed genes comparing clone F7 with a control clone revealed extracellular matrix organization (GO:0043062, $P = 3.46 \times 10^{-8}$)/extracellular matrix (GO:0030198, $P = 3.378 \times 10^{-7}$) as top hits
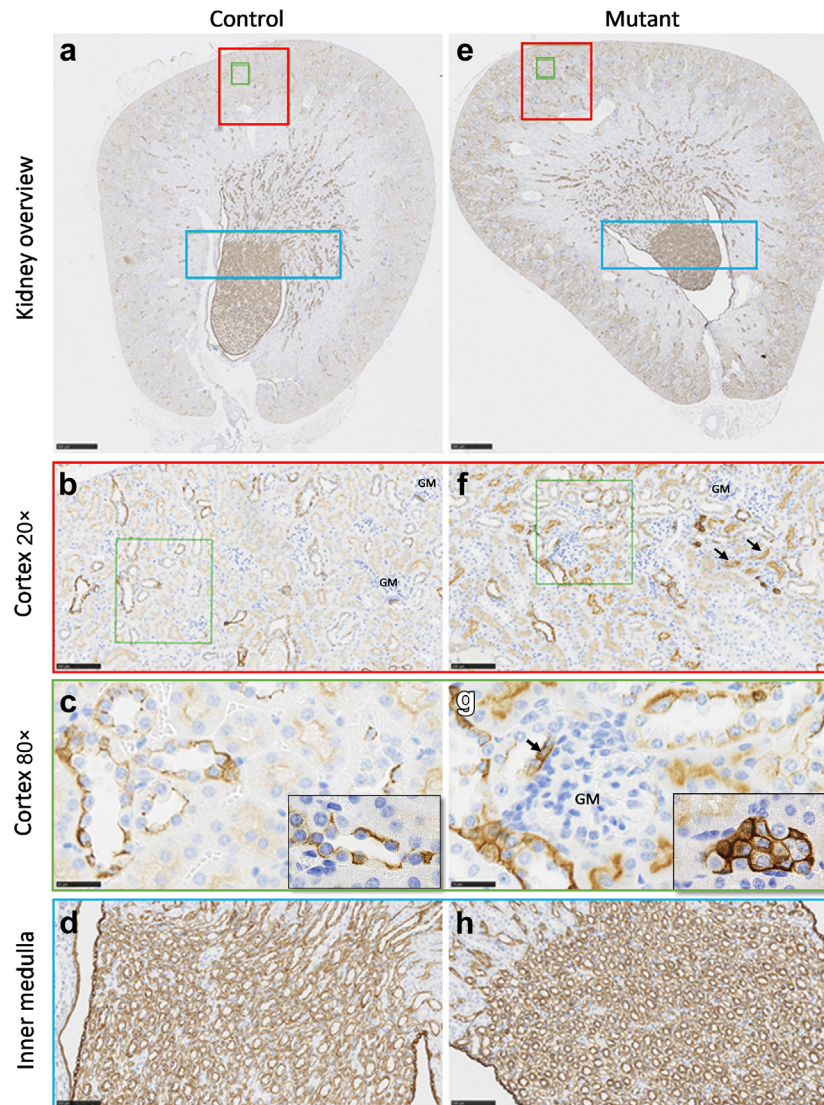
Figure 5 | Homozygous *Foxd2* (forkhead box D2) knockout (KO) increases cortical cytokeratin 8 (CK8) expression. Representative examples of CK8 staining tissue image analysis of the renal cortex. Kidney overview with the marked cortex and inner medulla of (**a**) a control (wild type) and (**e**) a mutant (homozygous KO) animal. The magnified renal cortex of (**b,c**) a control and (**f,g**) a mutant kidney. The magnified inner medulla of (**d**) a control and (**h**) a mutant kidney. Brown indicates CK8 H-DAB (hematoxylin and 3,3'-diaminobenzidine) immunohistochemistry (see also Supplementary Figure S5). GM, glomerulus. To optimize viewing of this image, please see the online version of this article at www.kidney-international.org.

followed by several terms related to renal/urogenital development as top hits among genes downregulated in the mutant clone: kidney development (GO:0001822, $P = 5.73 \times 10^{-7}$), renal system development (GO:0072001, $P = 6.57 \times 10^{-7}$), and urogenital development (GO:0001655, $P = 7.45 \times 10^{-7}$) with 24 to 27 of 6331 genes (adjusted $P = 0.000655$ for all 3 terms). Genes comprised were *Mmp17, Smad9, Fgf1, Emx2, Col4a4, Tfap2a, Sim1, Wnt2b, Adamts1, Tgfb2, Aqp1, Cys1, Pax2, Npnt, Egr1, Agt, Lrp4, Prlr, Col4a3, Igf1, Wnt4, Fgfr2, Id3, Fras1, Gli2, Pygo1,* and *Enpep* (Supplementary Figure S8A and B). Interestingly, among upregulated genes in *Foxd2* mutant versus control cells, top Gene Ontology term hits were related to leukocyte migration, antigen presentation, and chemotaxis followed by regulation of mitogen-activated protein kinase

activity (GO:0043405, $P = 2.96 \times 10^{-10}$; Table 3; Supplementary Figure S8A and B). Transcriptome analysis of *Foxd2* mutant clone F7 compared with unedited control cells further suggested a significant upregulation of *Nfia* ($\log_2$ fold change $= 7.27$; adjusted $P = 3.358 \times 10^{-7}$; Figure 6a; Supplementary Figure S9A).

qPCR validation of a set of selected targets showed a highly significant correlation with the relative expression levels determined by RNA sequencing (Pearson $R = 0.8955$; $P < 0.0001$; Supplementary Figure S9A). To exclude clone-specific effects, top gene hits from the Gene Ontology analysis with potential influence on renal development were confirmed by qPCR, comparing control cells with different *Foxd2* mutant mk4 clones (E4, F6, F7, and H9). These

Table 2 | *Foxd2* variants created for *in vitro* experiments using CRISPR/Cas9 technology

Clone	cDNA NM_00859.3
mk4 clone E4	c.794insA
	p.(Tyr265fs*)
mk4 clone F6	c.794A>G,792-793delTAinsGGG
	p.(Tyr265Trypfs*88)
mk4 clone F7	c.801insT
	p.(Tyr268Leufs*109)
mk4 clone H9	c.800-803delCTTA
	p.(Tyr268Alafs*83)

CRISPR, clustered regularly interspaced short palindromic repeats; *Foxd2*, forkhead box D2.

included single gene hits related to early kidney development and/or known to cause renal hypoplasia, such as *Pax2*, *Wnt4*, and *Fgfr2*. In addition, *Emx2* was found to be downregulated in *Foxd2* mutant mk4 cells compared with control cells. Although qPCR confirmed downregulation in all clones compared with control cells, the log 2 relative expression value for *Emx2* was <1, suggesting a rather minor effect (data not shown). In addition, higher gene expression of *Fat4* in mutant clones was confirmed compared with wt cells. qPCR also confirmed the strong downregulation of *Fat2* in all mutant clones compared with control cells (see Supplementary Figures S8C and S9B for a full set of qPCR-validated genes).

To investigate *Foxd2* KO on protein level, Western blotting was performed to confirm *Pax2* downregulation. This revealed markedly reduced Pax2 protein levels in *Foxd2*-deficient cells (3 independent experiments with 3 replicates each per condition; Figure 6b and c).

3D tubuloid models. The human probands we identified presented with renal hypoplasia, which could be a result of impaired renal tubule development/branching morphogenesis defect during renal development to which reduced *Pax2* expression could contribute. Given the low penetrance of the CAKUT phenotype in *Foxd2* mutant mice also previously observed by Hogan and coworkers,[10] in line with the "3R" principles for animal procedures, we decided to validate the effects of FOXD2 dysfunction on renal tubule formation using 3D tubuloid models to reduce the number of animals killed. To study the effect of Foxd2 dysfunction in metanephric mesenchyme cells on ureteric bud–derived tubule formation, we used so-called conditioned medium from wt and *Foxd2* mutant metanephric mesenchyme cells. This revealed significantly lower rates of tubule formation when conditioned medium from mutant cells was applied compared with conditioned medium derived from wt cells or medium treated with glial cell line–derived neurotrophic factor (GDNF) and fibroblast growth factor (FGF) additions (Supplementary Figure S10).

DISCUSSION

FOXD2 encodes a transcription factor of the large, evolutionarily conserved, forkhead box gene family important for various processes in humans, such as organogenesis or metabolism.[45] FOX genes share a "winged helix" DNA-binding domain consisting of 3 N-terminal a-helices, 3 b-strands, and 2 loops toward the C-terminal region. Different FOX genes have been associated with inherited human diseases and carcinogenesis.[46] Notably, *FOXC1*, a gene associated with syndromic ophthalmological disease (Axenfeld-Rieger
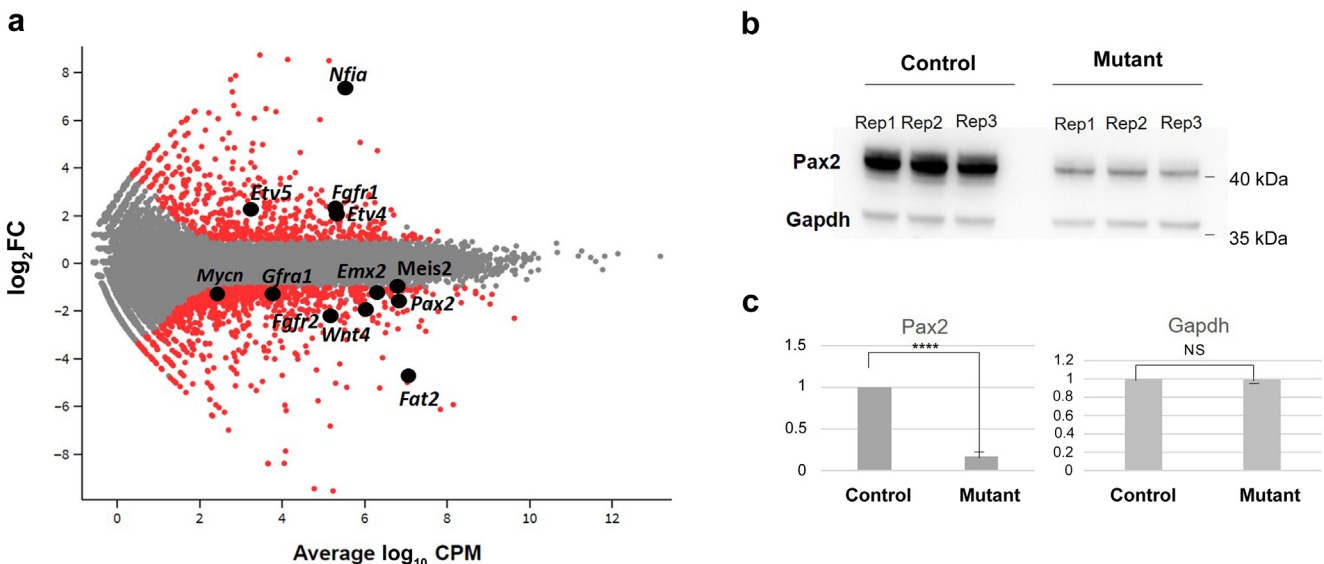
Figure 6 | Differential gene expression in *Foxd2* (forkhead box D2) mutant cells. (**a**) Glimma plot visualizing hits of interest. (**b**) Western blot analysis showing a strong reduction of Pax2 protein in mutant (clone E4) versus control cells using glyceraldehyde-3-phosphate dehydrogenase (Gapdh) as a loading control. *n* = 3 biological replicates per condition. (**c**) Quantitative analysis of Pax2 levels combining the 3 biological replicates per condition and Gapdh as a control protein, confirming a lower Pax2 protein amount in mutant cells than in controls. Student *t* test, ****P < 0.0001. CPM, counts per million; FC, fold change; NS, not significant; Rep, replicate. To optimize viewing of this image, please see the online version of this article at www.kidney-international.org.

Table 3 | Gene Ontology term analysis comparing mk4 clone F7 with wild type

	P	Adjusted P
Down		
Extracellular matrix organization	3.456442E−8	0.000152
Renal system development	6.571659E−7	0.000655
Urogenital system development	7.447146E−7	0.000655
Positive regulation of the steroid metabolic process	3.479562E−6	0.002186
Inner ear development	3.807702E−6	0.002186
Up		
Cell chemotaxis	6.340431E−11	4.250202E−8
Positive regulation of vasculature development	1.506551E−10	7.765204E−8
Antigen processing and presentation of endogenous antigen	1.544546E−10	7.765204E−8
Regulation of MAP kinase activity	2.957847E−10	1.321828E−7
Regulation of protein serine/threonine kinase activity	1.459391E−9	3.668544E−7

MAP, mitogen-activated protein.

syndrome, type 3; Mendelian Inheritance in Men, MIM #602482), has recently been linked to autosomal dominant CAKUT.[47]

In addition, several other *FOX* genes (*FOXL2*, *FOXA2*, and *FOXA3*) have been proposed as candidate genes for monogenic CAKUT in a recent ES study.[48]

However, no representative of the "D" subfamily has been linked to a monogenic disease in humans thus far. *FOXD2* (*FREAC-9* and *MF-2*) is well expressed in the renal cortex.[49] Of note, the *FOXD2* locus (1p33) has recently been associated with urinary albumin levels in genome-wide meta-analyses[35] and *Foxd2* RNA is highly enriched in podocytes and was implicated in maintenance of podocyte integrity.[50] Proteinuria up to the nephrotic range was reported in the index individual of family 1 and his female first cousin once removed, albuminuria with FSGS on kidney biopsy was present in individual II-2 of family 2, and nephrotic syndrome was reported in the affected individual of family 3 (see clinical cases in the Results section and Supplementary Case Report). In line with this, fine mapping of the *FOXD2* UACR GWAS locus revealed a likely podocyte-specific regulatory SNP (Figure 2). Together, this could support a role of *FOXD2* in podocyte maintenance and hence in proteinuric kidney disease in general.

Our study suggests that the abrogation of FOXD2 function can result in CAKUT. *Foxd2* KO mice have previously been reported to show renal hypoplasia and hydroureters, however, at a reduced penetrance of 40%.[10] Also, in KO mice generated for this study, renal anomalies could only be identified at a reduced penetrance of 33% and were rather subtle (Figure 4a–c), underlining the variable expressivity of CAKUT. *Foxd2* shares close sequence homology with *Foxd1*
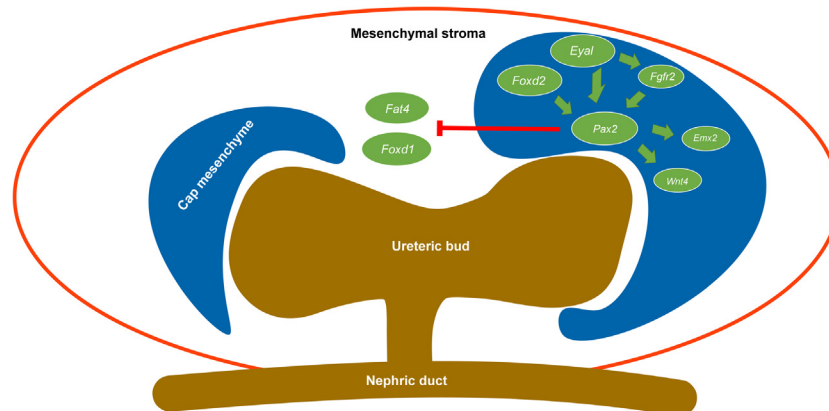

Figure 7 | Key players in the network of assumed Foxd2 (forkhead box D2) function. Although *Foxd1* expression in the developing mouse kidney is largely restricted to the mesenchymal stroma, *Foxd2* is found in the cap mesenchyme where it plays a role in *Pax2* expression.[10,74] Foxd2 dysfunction leads to reduced PAX2 protein levels (see the Results section and Figure 6b and c). *Eya1* is important for *Pax2* expression in the ureteric bud–induced metanephric mesenchyme (embryonic day 11.5 in the mouse), and *Eya1* upregulation in *Foxd2* mutant cells may indicate a compensatory mechanism for reduced *Pax2* expression via a feedback loop.[76] *Pax2* activates *Wnt4* expression in the metanephric mesenchyme during mammalian kidney development, and *Wnt4* expression is downregulated in *Foxd2* mutant cells.[70] *Pax2* enhances *Emx2* gene expression, and *Emx2* expression is downregulated in *Foxd2* mutant cells.[61] Nephron progenitor cells lacking Pax2 can change into Foxd1-positive renal interstitium–like cell types, suggesting that Pax2 represses a renal interstitial cell program.[62] This is supported by the upregulation of *Fat4* in *Foxd2* mutant cells as *Fat4* encodes an atypical cadherin expressed by stromal cells inhibiting nephron progenitor renewal.[64] *Fgfr2* (and *Fgfr1*) is believed to act downstream of *Eya1* and upstream of *Pax2* in the metanephric mesenchyme.[77] Conditional knockout of *Fgfr2* in metanephric mesenchyme cells leads to congenital anomalies of the kidney and urinary tract in mice and deficiency of Fgfr2 in stromal cells[69] (see Discussion for further details). Adapted from McMahon AP. Development of the mammalian kidney. *Curr Top Dev Biol.* 2016;117:31–64[74] and Walker KA, Sims-Lucas S, Bates CM. Fibroblast growth factor receptor signaling in kidney and lower urinary tract development. *Pediatr Nephrol.* 2016;31:885–895.[75]

(*Bf2*). A (partial) redundancy of the 2 could explain the reduced penetrance of CAKUT in *Foxd2* KO mice.[10,51] Of note, in contrast to *Foxd2* mutant mice, homozygous *Foxd1* KO mice die shortly after birth of kidney failure due to hypoplastic kidneys.[52] Furthermore, despite their phylogenetic relation and genomic homology, humans and mice are known to not respond completely alike to interventions/gene KO. This could also explain the differences in expressivity between the renal mouse and human phenotypes in this study (milder in mice than in affected individuals).[53]

In Northern blot experiments, mRNA transcripts of *Foxd2* were detected in the kidney, facial regions (tongue, nose, and maxilla), and brain.[51] Developmental delay presenting as delayed motor milestone achievement and delayed speech development was noted in the affected individuals of families 1 and 2 (see clinical case in the Results section and Supplementary Case Report). Unfortunately, no cranial magnetic resonance imaging data were available except for individual II-1 of family 2, in whom enlarged ventricles and an enlarged subarachnoid space were noted at the age of 13 years (see Supplementary Case Report). Furthermore, facial anomalies in affected individuals were compatible with the previously detected expression patterns. A neurological phenotype was not reported in *Foxd2* KO mice in the literature. However, *Foxd1* KO mice present with small cerebral hemispheres with reduced development of the ventral telencephalon.[10,54,55] Facial alterations, in turn, were not reported in *Foxd2* mice in the literature, but could be detected in the meticulously phenotyped *Foxd2* KO mice of this study (Figure 3a–d), in line with the facial dysmorphies of the affected individuals of families 1 to 3 (Figure 1e–h and Table 1).[10,51,56,57] Furthermore, behavioral changes were identified in *Foxd2* KO mice of this study (hypoactivity in the open field test; Supplementary Figure S6). This can be indicative of neurodevelopmental alterations in *Foxd2* KO mice. Taken together, it can be assumed that *FOXD2* plays an important role in neuronal, branchial arch, and facial development.

Transcriptome analysis of mk4 CRISPR/Cas9-mediated homozygous *Foxd2* frameshift mutants gave a valuable insight into the possible mechanisms of CAKUT in the described families. Pathway analysis showed significant enrichment of differentially expressed genes important for the development of the renal/urogenital system (Table 3). *Pax2* was downregulated in all mk4 clones (Figure 6a; Supplementary Figure S8C) as were Pax2 protein levels on the Western blot (Figure 6b and c). *PAX2* haploinsufficiency is known to be associated with papillorenal syndrome in humans (MIM #120330), which comprises a CAKUT phenotype with eye anomalies.[58] Of note, no overt eye anomalies were reported in the affected individuals described in this study. However, there is *Foxd2* RNA expression around the eye vesicle in mice during embryonic development.[59] In line with this, the generated *Foxd2* KO mice showed alterations of the optic disc and nerve (Figure 3e and f), which might have been missed on routine ophthalmological examination of the affected individuals. Interestingly, there were alterations on eye examination of

individual II-1 of family 2 and in the index individual of family 3. However, these did not involve the optic nerve and disc (see clinical case in the Results section).

Foxd2 is strongly expressed in renal condensed mesenchyme at embryonic day 11.5, similarly to *Pax2*.[10] *Pax2* is activated in the mesenchyme in response to induction by the ureteric bud and is subsequently downregulated in more differentiated cells derived from the mesenchyme. With reduced Pax2 protein levels, kidney mesenchyme cells fail to aggregate and do not undergo the sequential morphological changes characteristic of epithelial cell formation, demonstrating an essential role for Pax2 function for early mesenchymal-epithelial transition.[60] Interestingly, we also detected a downregulation of *Emx2* in *Foxd2* mutant versus control cells by transcriptomics. *Pax2* enhances *Emx2* gene expression, and digenic loss of function of *Pax2* and *Emx2* is known to result in CAKUT similar to what is found in *Foxd2* KO mice and to the phenotype observed in the affected individuals of this study.[10,61]

Intriguingly, *Pax2* is also implicated in establishing the nephron-interstitium boundary during kidney development: nephron progenitor cells lacking Pax2 fail to differentiate into nephron cells, but can switch fates into Foxd1-positive renal interstitium–like cell types, suggesting that Pax2 function maintains nephron progenitor cells by repressing a renal interstitial cell program.[62] Our findings suggest that the lack of Foxd2 results in reduced Pax2 levels. Therefore, it seems possible that Foxd2 dysfunction will divert lineage identity toward renal stroma cells. In line with this hypothesis, we could detect significantly increased cytokeratin 8 expression in the renal cortex of homozygous *Foxd2* KO mice compared with wt controls (Figure 5; Supplementary Figure S5). Keratins such as cytokeratin 8 are markers of tubular epithelial injury preceding renal fibrotic changes.[63] Fittingly, individual II-2 of family 2 featured fibrotic changes on kidney biopsy in terms of FSGS (Figure 1i).

This hypothesis is further supported by the upregulation of *Fat4* in *Foxd2* mutants (Supplementary Figure S8C). *Fat4* encodes an atypical cadherin expressed by stromal cells inhibiting nephron progenitor renewal.[64] In contrast, there was a marked downregulation of *Fat2* in *Foxd2* mutant cells (Figure 6a; Supplementary Figure S8C). Although *Fat4* has been shown to play a role in kidney tubule elongation and planar cell polarity in renal cells, the role of *Fat2* in renal development and homeostasis is unclear.[65] The *Drosophila* orthologue *fat* has been implicated in cell proliferation and morphogenesis in a contact-dependent manner.[66] We also observed a strong upregulation of *Nfia* in *Foxd2* mutant cells (Figure 6a). Haploinsufficiency of *NFIA* has been associated with brain malformations and CAKUT, and upregulation could be a compensatory mechanism in *Foxd2* KO cells.[67,68]

In contrast, *Fgfr2* was downregulated in mutant *Foxd2* cells versus controls (Figure 6a). Conditional KO of *Fgfr2* in metanephric mesenchyme cells leads to CAKUT in mice including hypo-/dysplastic kidneys and hydroureters.

Interestingly, in these mice devoid of mesenchymal *Fgfr2* expression, there is no Fgfr2 in stromal cells either, also indicating a disturbance in stromal cells in *Fgfr2* KO mice.[69]

Further, *Pax2* activates *Wnt4* expression in the metanephric mesenchyme during mammalian kidney development,[70] potentially explaining reduced *Wnt4* gene expression in *Foxd2* mutant cells (Figure 6a; Supplementary Figure S8C). Wnt4 protein plays a role in mesenchymal-epithelial transition and is essential for tubulogenesis in the developing kidney through a noncanonical Wnt-signaling pathway.[71,72] Of note, Wnt4 signaling can be substituted by other Wnt proteins such as Wnt7b,[73] which was also downregulated in *Foxd2* mutant mk4 cells (Supplementary Figure S9B). Figure 7[10,61,62,64,69,70,74–77] summarizes the network of assumed Foxd2 function (adapted from McMahon[74] and Walker *et al.*[75]; with the presumed feedback loop[76]).

In line with the hypothesis of an impaired Pax2-Wnt4 axis due to Foxd2 dysfunction abrogating proper mesenchymal-epithelial transition and tubulogenesis, we could indeed show significantly lower rates of tubule formation when conditioned medium from *Foxd2* mutant cells was applied compared with conditioned medium derived from wt cells in 3D tubuloid models (Supplementary Figure S10).

In addition, we observed higher *Eya1* expression in *Foxd2* mutant cells compared with control cells (Supplementary Figure S8C). *Eya1* is important for *Pax2* expression in the ureteric bud–induced metanephric mesenchyme, and *Eya1* upregulation in *Foxd2* mutant cells may indicate a compensatory mechanism for reduced *Pax2* expression via a feedback loop.[76] *Gdnf* expression, which is vital for ureteric bud induction, was unchanged in *Foxd2* mutants (Supplementary Figure S9B). This is in line with *Eya1* upregulation in the context of reduced Pax2 levels, as both genes regulate *Gdnf* expression.[76,78] Hence, it does not seem likely that the renal hypoplasia phenotype observed in the index individuals of the presented families is a result of impaired *Gdnf* expression.

This study has several limitations. The affected individuals of families 1 to 3 do not share the same type of variant. Family 1 segregates a homozygous frameshift variant in *FOXD2*, families 2 and 3 feature a homozygous missense variant affecting the same codon. However, as *FOXD2* is a single-exon gene (NM_004474.4), nonsense-mediated decay cannot be assumed, and this makes the frameshift variant not a clear-cut loss-of-function variant but probably leads to an altered protein. Interestingly, no homozygous truncating variants are listed in gnomAD, illustrating that there is constraint for this type of variant in *FOXD2*. This supports a causative role of the frameshift variant. Unfortunately, no patient-derived cells could be obtained in affected individuals of family 1 to clarify *FOXD2* expression. This limits the transferability of the KO experiments in this study. In contrast, it cannot be denied that *Foxd2* KO recapitulates the phenotype of the affected individuals of this study (all families 1–3). Furthermore, family 2 segregates a protein-altering variant—identified by a stringent filtering process—and features striking phenotypic overlap in affected

individuals in comparison to family 1. In families 2 and 3, it could be shown by *in silico* analysis that the missense variant, located in the DNA-binding domain, destabilizes the mature protein. Hence, we believe that both missense variants abrogate proper FOXD2 function, which can be related to by KO experiments. Of course, further studies are needed to experimentally clarify causality of the described variants in *FOXD2* (according to MacArthur *et al.*[79]). Finally, a limitation of our cell culture model is that we investigated similar but not identical *FOXD2* variants *in vitro* compared with the variants we identified in human individuals with CAKUT.

In conclusion, our findings indicate that the syndromic CAKUT phenotype in the presented families is caused by FOXD2 dysfunction, putatively causing a shift of nephron progenitor cells undergoing mesenchymal-epithelial transition toward a stromal cell identity, resulting in fibrotic changes in the kidney. The observed human and *Foxd2* KO mouse phenotypes highlight an important role of *Foxd2* in kidney and craniofacial development. The observed kidney alterations are in line with the enrichment of differentially expressed genes important in extracellular matrix organization and renal/urogenital development in *Foxd2* mutant metanephric mesenchyme cells.

It is intriguing that FOXD2 dysfunction could result in a phenotype of both renal malformation and podocyte damage. As the *FOXD2* locus was also previously associated with urinary albumin in genome-wide meta-analyses[35] and we have now identified a likely podocyte-specific regulatory SNP within this locus, FOXD2 could represent an interesting target in common kidney diseases in terms of tackling proteinuria and renal fibrosis. Consequently, our findings are building bridges between rare monogenic and common complex kidney disease.

APPENDIX
Web resources

1000 Genomes Project human polymorphism database, http://www.1000genomes.org/
AlphaFold database, https://alphafold.ebi.ac.uk/entry/O60548
ANNOVAR, https://annovar.openbioinformatics.org/en/latest/
Burrows-Wheeler aligner, https://bio-bwa.sourceforge.net/
Combined Annotation Dependent Depletion (CADD) https://cadd.gs.washington.edu/
ClinPred, https://sites.google.com/site/clinpred/
ClinVar, https://www.ncbi.nlm.nih.gov/clinvar/
Clustal Omega, https://www.ebi.ac.uk/Tools/msa/clustalo/
Database of Genomic Variants (DGV) http://dgv.tcag.ca/dgv/app/home
dbSNP, http://www.ncbi.nlm.nih.gov/SNP/
DECIPHER, https://decipher.sanger.ac.uk/
DynaMut2, https://bio.tools/dynamut
Expression atlas, https://www.ebi.ac.uk/gxa/home
FinnGen release DF9, https://r9.finngen.fi/
FoldX, https://foldxsuite.crg.eu/
Galaxy platform12, https://usegalaxy.org/
Genome Analysis Tool Kit, https://gatk.broadinstitute.org/hc/en-us
Genome Aggregation Database (gnomAD v.2.1.1), http://gnomad.broadinstitute.org/
Homozygous Stretch Identifier (HomSI), https://bio.tools/homsi
Human Gene Mutation Database (HGMD®), http://www.hgmd.cf.ac.uk
Human Kidney snATAC-seq Peaks, http://www.susztaklab.com/human_kidney/igv/
Leiden Open Variation Database (LOVD), https://www.lovd.nl

INPS-3D, https://inpsmd.biocomp.unibo.it/inpsSuite/default/index3D
Mutation Taster, https://www.mutationtaster.org
MutPred2, http://mutpred.mutdb.org/
National Heart, Lung, and Blood Institute Exome Sequencing Project, http://evs.gs.washington.edu/EVS/
Online Mendelian Inheritance in Man®, http://www.omim.org/
Picard tool, https://broadinstitute.github.io/picard
Polymorphism Phenotyping v2 (PolyPhen-2), http://genetics.bwh.harvard.edu/pph2/
PremPS, https://bio.tools/premps
Protein Variation Effect Analyzer (PROVEAN), http://provean.jcvi.org/index.php/
Primer3, http://frodo.wi.mit.edu/primer3/input.htm
QuPath, https://QuPath.github.io/
Rare Exome Variant Ensemble Learner (REVEL), https://sites.google.com/site/revelgenomics/?pli=1
RCSB Protein Data Bank, https://www.rcsb.org/
Sorting Intolerant From Tolerant (SIFT), https://sift.bii.a-star.edu.sg
susieR, https://stephenslab.github.io/susieR/
The Human Protein Atlas, https://www.proteinatlas.org/
UK Biobank TOPMed-imputed PheWeb, https://pheweb.org/UKB-TOPMed/
UniProt, https://www.uniprot.org/

DISCLOSURE

All the authors declared no competing interests.

DATA STATEMENT

Exome data

Human next-generation sequencing data sets for families 1 to 3 are not openly available, as the private nature of disease-causing *FOXD2* (forkhead box D2) variants in these data sets would make individuals identifiable. Data can be made available on personal request. Monogenic *FOXD2* disease alleles in families 1 to 3 and corresponding phenotypes have been submitted to ClinVar.

Genome-wide association study analyses

The data supporting the findings of this study are described in Teumer *et al.*[35] Genome-wide summary statistics from the publication are publicly available in repository https://ckdgen.imbi.uni-freiburg.de/. The data from the UK Biobank used in fine-mapping analyses were obtained and analyzed under application number 20272. All other analyses used publicly available data sets as described in the Methods section.

Transcriptomics analyses in renal cells

The RNA sequencing data supporting the findings of this study are openly available in Gene Expression Omnibus (GEO; https://www.ncbi.nlm.nih.gov/geo/query/acc.cgi?acc=GSE168582). Codes for analyses and plotting are available under https://github.com/gwangjinkim/foxd2_analysis.

CONSENT FOR PUBLICATION

Participants whose pedigree data are presented in this manuscript gave consent to publish the family history in pedigree or summarized format.

SUPPLEMENTARY MATERIAL

Supplementary File (Word)
Supplementary Methods.
Supplementary Results. Supplementary Case Report Families 1, 2, and 3.
Supplementary Figure S1. Chromatograms of the homozygous frameshift variant NM_004474.4:c.789dup, p.(Gly264Argfs*228) in *FOXD2* (forkhead box D2) of family 1. The wild-type reading frame in the chromatogram is CTACGGCG. Affected individuals carried the variant homozygously (VI-3 and V-19), whereas the healthy parents/relatives were heterozygous for the variant (V-6, V-1, IV-6, IV-4).
Supplementary Figure S2. (**A**) Homozygosity mapping of family 2. The overlapping homozygous stretches shared in 2 affected individuals (II-1 and II-2) are ∼11.6 Mb in size between genomic

positions of 47,600,000 and 59,200,000 on chromosome 1 (box). *FOXD2* (forkhead box D2) resides here. (**B**) Chromatograms of the missense variant NM_004474.4:c.628 A>G), p.(Met210Val) observed in *FOXD2*. Affected individuals carried the variant homozygously, whereas the healthy parents were heterozygous for the variant. The unaffected sibling had a wild-type sequence.

Supplementary Figure S3. (**A**) Reverse transcription polymerase chain reaction and cDNA synthesis confirm the absence of *Foxd2* (forkhead box D2) transcript in homozygous (hom) knockout (KO) animals. (**B**) Decreased viability in hom *Foxd2* KO newborns. Pie charts representing different genotype proportions. The "expected" genotype percentages are those anticipated according to Mendelian distribution after double heterozygous (het) mating. The "born offspring" genotype proportions show the genotype proportions determined in pups born from such mating, and the "viable offspring" show the genotype percentages in offspring that survived weaning. Percentages were calculated by dividing the observed number of pups with the respective genotype by the total number of offspring ($n = 143$ born; $n = 116$ weaned) that was genotyped multiplied by 100. wt, wild type.

Supplementary Figure S4. Other histopathological renal alterations in 16-week-old mice. (**A**) Representative images of periodic acid–Schiff (PAS) staining of a wild-type (wt) mouse and a *Foxd2* (forkhead box D2) homozygous knockout (KO) mouse. No alterations such as thickening of the glomerular and tubular basement membrane or increased proliferation of mesangial cells or Bowman's capsule are observed. (**B**) Hematoxylin and eosin (H&E) staining shows mild and focal alterations found only in homozygous KO mice. From left to right: examples of tubular basophilia, hyaline intratubular cast, and presence of clear vacuoles (arrows) in the renal tubular epithelium.

Supplementary Figure S5. (**A**) *Foxd2* (forkhead box D2) homozygous knockout (KO) increases cortical cytokeratin 8 (CK8) expression. *Foxd2* homozygous KO mice show highly increased CK8 expression. Data are expressed as mean $\pm$ SD. Two-sample *t* test, ***$P < 0.001$. Representative examples of tissue image analysis CK8 staining of the renal cortex. Overview of (**B**) kidney with the marked cortex, section wild-type (**C**) preanalysis and (**D**) postanalysis, and homozygous KO mice (**E**) preanalysis and (**F**) postanalysis. Yellow indicates marked region; red, positive cells; blue, negative cells; and brown, CK8 H-DAB immunohistochemistry.

Supplementary Figure S6. *Foxd2* (forkhead box D2) homozygous (hom) knockout (KO) causes hypoactivity and hypoexploration in a novel mildly stressful environment. *Foxd2* hom KO mice show clear (**A**) hypoactivity (decreased distance traveled) and (**B**) hypoexploration (decreased rearing) during the 20-minute open field test compared with wild-type (wt) controls at 8 weeks. Data are expressed as mean $\pm$ SD. ***$P < 0.001$, genotype effect in 2-way analysis of variance.

Supplementary Figure S7. (**A**) Illustration of Foxd2 (forkhead box D2) protein showing *Foxd2* mutant clone F7. (**B**) Amino acid sequence of human wild-type (WT) *FOXD2* (NP_004465.3), human mutant *FOXD2* p.(Gly264Argfs*228), mouse WT *Foxd2* (NP_032619.1), and mouse *Foxd2* clone F7.

Supplementary Figure S8. Transcriptome analysis results of *Foxd2* (forkhead box D2) mutant cells versus controls. (**A**) Heatmap Gene Ontology term kidney morphogenesis. (**B**) Heatmap Gene Ontology term mitogen-activated protein kinase (MAPK) signaling. (**C**) Quantitative polymerase chain reaction (PCR). Confirmation of the selected genes of interest from transcriptomics in all 4 different clones versus control cells using real-time PCR analysis (*y* axis: log 2 relative expression values [Log$_2$RQ]). In agreement with RNA sequencing results, we could not detect differences in *Foxd1* gene expression; however, they confirmed downregulation of *Fgfr2*, *Wnt4*, *Fat2*, and

Pax2 and upregulation of *Eya1* and *Fat4* in *Foxd2* mutant versus control cells. Data shown for $n = 1$ biological experiment. Error bars indicate the SD of technical duplicates.

Supplementary Figure S9. (**A**) Pearson correlation of quantitative polymerase chain reaction (qPCR) validated genes showing a highly significant correlation with the relative expression levels determined by RNA sequencing (Pearson $R = 0.8955$; $P < 0.0001$). (**B**) qPCR validation of the selected genes of interest found to be differentially regulated by transcriptomics (*y* axis: log 2 relative expression values [Log$_2$RQ]; see also Figure 6 in the main text).

Supplementary Figure S10. (**A**) Schematic overview of the CMUB-1 Matrigel culture. Cell culture medium from mk3 *Foxd2* (forkhead box D2) mutant or wild-type cells was concentrated by centrifugation and added to wild-type CMUB-1 cells in Matrigel on day 0 ("conditioned medium"). Normal (nonconditioned) medium containing additional GDNF and FGF1 served as a positive control. Differentiation of CMUB-1 cells into 3-dimensional (3D) tubuloids was visualized by fluorescence microscopy. Graphics created with BioRender.com. (**B–E**) Confocal images of 3D CMUB-1 cell culture shows formation of different types of 3D structures after 7 days of differentiation. A graphical abstract of structure types is presented in (**G**). Immunofluorescence was performed using the cell surface marker Na/K adenosine triphosphatase (Na/K-ATPase) or β-catenin (both in green), cytoskeleton marker F-actin (red), and nucleus marker 4',6-diamidino-2-phenylindole (DAPI; blue). Bar = 30 μm. (**B**) CMUB-1 cells under addition of GDNF/FGF1 (positive control). (i) Confocal overview image displaying different ureteric bud tubuloid types. The arrow indicates outgrowing tubule. The cross indicates lumen. (ii) Tubule with lumen (cross). (iii) The arrows mark round cyst with budding (top) and elongation (right). (**C**) Negative control, CMUB-1 cells plus normal culture medium barely showed tubule formation. (i) Overview image. (ii) Round cyst with lumen (cross). (**D**) Addition of wild-type conditioned medium resulted in tubule formation similar to what we observed upon addition of GDNF- and FGF-treated medium. (i) Overview image showing a tubule with elongation (arrow). (ii) Tubule with continuous lumen (cross) developed. (iii) Structures with several elongations (arrow) was observed. (**E**) Conditioned medium from *Foxd2* mutant cells resulted in reduced tubulogenesis and budding/elongation as compared with wild-type conditioned medium. (i) Overview image. (ii) Close-up of a cyst with lumen (cross) typically seen in ureteric bud culture plus mutant conditioned medium. (**F**) Statistical analysis of structure types observed. The positive control GDNF/FGF1 showed significantly increased tubule formation as well as elongations/buddings and protuberances compared with negative control and both mutant conditioned media. Negative control (normal medium) as well as both mutant conditioned media resulted in the formation of cysts/spheroids without signs of budding or elongation, while wild-type conditioned medium showed a significant increase in tubulogenesis, elongations/buddings, and protuberance formations compared with both mutant conditioned media and negative control. $n = 3$ independent experiments. Per experiment, 94 to 102 structures were counted. For *P*-value calculation, an unpaired Student *t* test was conducted. *$P < 0.05$. (**G**) Graphical description and definition of structures seen in ureteric bud 3D culture. (**H**) Diameter of structures of each condition was analyzed. GDNF/FGF1 treatment resulted in diameters of ~50 μm, reflecting a collecting tubule diameter. Nonconditioned and mutant conditioned media resulted in diameters of ~25 μm, while wild-type conditioned medium resulted in diameters of ~35 μm. $n = 2$ independent experiments. Per experiment, 94 to 101 structures were counted. An unpaired Student *t* test was performed to analyze *P* value. *$P < 0.05$, ***$P < 0.001$, ****$P < 0.0001$. ns, not significant.

Supplementary References.

Supplementary Table S2. List of filtered candidate variants detected with exome sequencing in the index individual (II-1) of family 2.

Supplementary Table S3. Additional variants reported on next-generation sequencing in the index case of family 3.

Supplementary Table S4. Online *in silico* analysis tools used for evaluating protein stability changes on the p.(Met210Val) and p.(Met210Arg) missense variants in *FOXD2* (forkhead box D2), and Gibbs free energy calculation results. INPS-3D and DynaMut2: $\Delta\Delta G < 0$ is destabilizing; $\Delta\Delta G > 0$ is stabilizing PremPS and FoldX: $\Delta\Delta G > 0$ is destabilizing; $\Delta\Delta G < 0$ is stabilizing.

Supplementary Table S6. (**A,B**) Histological parameters of the examined kidneys. GM, glomeruli; H&E, hematoxylin and eosin; hom, homozygous knockout; NAD, no alteration determined; wt, wild type.

Supplementary Table S7. Total distance traveled and total rearing activity of wild-type (wt) control mice and heterozygous (het) and homozygous (hom) *Foxd2* (forkhead box D2) knockout mice.

Supplementary File (Excel)

Supplementary Table S1, Sheet 1. List of homozygous variants at minor allele frequency (MAF) 1.0% detected with exome sequencing in the index individual of family 1. Variants listed as "benign" or likely "benign" in ClinVar (https://www.ncbi.nlm.nih.gov/clinvar/) have been deleted for the sake of clarity. Only intronic variants ± 20 bp to the exon-intron boundary are shown.

Supplementary Table S1, Sheet 2. List of rare homozygous variants detected with exome sequencing in the index individual of family 3. Filters applied included homozygosity in the proband but not the mother, absence from the gnomAD database, high or moderate quality as determined by the automated pipeline, and variant type that included missense, splice, or intronic variants.

Supplementary File (Excel)

Supplementary Table S5. Summary statistics of fine-mapped urinary albumin-to-creatinine ratio (UACR)–associated variants at *FOXD2* (forkhead box D2) locus in the UK Biobank and CKDGen Consortium.

REFERENCES

1. Pohl M, Bhatnagar V, Mendoza SA, Nigam SK. Toward an etiological classification of developmental disorders of the kidney and upper urinary tract. *Kidney Int*. 2002;61:10–19.
2. Chesnaye N, Bonthuis M, Schaefer F, et al. Demographics of paediatric renal replacement therapy in Europe: a report of the ESPN/ERA-EDTA registry. *Pediatr Nephrol*. 2014;29:2403–2410.
3. van der Ven AT, Connaughton DM, Ityel H, et al. Whole-exome sequencing identifies causative mutations in families with congenital anomalies of the kidney and urinary tract. *J Am Soc Nephrol*. 2018;29: 2348–2361.
4. Verbitsky M, Westland R, Perez A, et al. The copy number variation landscape of congenital anomalies of the kidney and urinary tract. *Nat Genet*. 2019;51:117–127.
5. Vivante A, Mann N, Yonath H, et al. A dominant mutation in nuclear receptor interacting protein 1 causes urinary tract malformations via dysregulation of retinoic acid signaling. *J Am Soc Nephrol*. 2017;28:2364–2376.
6. Sanna-Cherchi S, Westland R, Ghiggeri GM, Gharavi AG. Genetic basis of human congenital anomalies of the kidney and urinary tract. *J Clin Invest*. 2018;128:4–15.
7. Connaughton DM, Hildebrandt F. Disease mechanisms of monogenic congenital anomalies of the kidney and urinary tract. *Am J Med Genet C Semin Med Genet*. 2022;190:325–343.
8. Vivante A, Hwang DY, Kohl S, et al. Exome sequencing discerns syndromes in patients from consanguineous families with congenital anomalies of the kidneys and urinary tract. *J Am Soc Nephrol*. 2017;28:69–75.
9. Vivante A, Kohl S, Hwang DY, et al. Single-gene causes of congenital anomalies of the kidney and urinary tract (CAKUT) in humans. *Pediatr Nephrol*. 2014;29:695–704.
10. Kume T, Deng K, Hogan BL. Minimal phenotype of mice homozygous for a null mutation in the forkhead/winged helix gene, Mf2. *Mol Cell Biol*. 2000;20:1419–1425.
11. Kremer LS, Bader DM, Mertes C, et al. Genetic diagnosis of Mendelian disorders via RNA sequencing. *Nat Commun*. 2017;8:15824.
12. Sobreira N, Schiettecatte F, Valle D, Hamosh A. GeneMatcher: a matching tool for connecting investigators with an interest in the same gene. *Hum Mutat*. 2015;36:928–930.
13. Gormez Z, Bakir-Gungor B, Sagiroglu MS. HomSI: a homozygous stretch identifier from next-generation sequencing data. *Bioinformatics*. 2014;30: 445–447.
14. Riedhammer KM, Nguyen TT, Kosukcu C, et al. Implication of FOXD2 dysfunction in syndromic congenital anomalies of the kidney and urinary tract (CAKUT). Preprint. *medRxiv*. 2023.03.21.23287206. Posted online March 22 2023. https://doi.org/10.1101/2023.03.21.23287206
15. Ioannidis NM, Rothstein JH, Pejaver V, et al. REVEL: an ensemble method for predicting the pathogenicity of rare missense variants. *Am J Hum Genet*. 2016;99:877–885.
16. Alirezaie N, Kernohan KD, Hartley T, et al. ClinPred: prediction tool to identify disease-relevant nonsynonymous single-nucleotide variants. *Am J Hum Genet*. 2018;103:474–483.
17. Pejaver V, Urresti J, Lugo-Martinez J, et al. Inferring the molecular and phenotypic impact of amino acid variants with MutPred2. *Nat Commun*. 2020;11:5918.
18. Schymkowitz J, Borg J, Stricher F, et al. The FoldX web server: an online force field. *Nucleic Acids Res*. 2005;33:W382–W388 (Web Server issue).
19. Rodrigues CHM, Pires DEV, Ascher DB. DynaMut2: assessing changes in stability and flexibility upon single and multiple point missense mutations. *Protein Sci*. 2021;30:60–69.
20. Savojardo C, Fariselli P, Martelli PL, Casadio R. INPS-MD: a web server to predict stability of protein variants from sequence and structure. *Bioinformatics*. 2016;32:2542–2544.
21. Chen Y, Lu H, Zhang N, et al. PremPS: predicting the impact of missense mutations on protein stability. *PLoS Comput Biol*. 2020;16:e1008543.
22. Haeussler M, Schonig K, Eckert H, et al. Evaluation of off-target and on-target scoring algorithms and integration into the guide RNA selection tool CRISPOR. *Genome Biol*. 2016;17:148.
23. Gailus-Durner V, Fuchs H, Becker L, et al. Introducing the German Mouse Clinic: open access platform for standardized phenotyping. *Nat Methods*. 2005;2:403–404.
24. Fuchs H, Aguilar-Pimentel JA, Amarie OV, et al. Understanding gene functions and disease mechanisms: phenotyping pipelines in the German Mouse Clinic. *Behav Brain Res*. 2018;352:187–196.
25. Fuchs H, Gailus-Durner V, Adler T, et al. The German Mouse Clinic: a platform for systemic phenotype analysis of mouse models. *Curr Pharm Biotechnol*. 2009;10:236–243.
26. Rathkolb B, Hans W, Prehn C, et al. Clinical chemistry and other laboratory tests on mouse plasma or serum. *Curr Protoc Mouse Biol*. 2013;3:69–100.
27. Fuchs H, Gailus-Durner V, Adler T, et al. Mouse phenotyping. *Methods*. 2011;53:120–135.
28. Puk O, de Angelis MH, Graw J. Longitudinal fundus and retinal studies with SD-OCT: a comparison of five mouse inbred strains. *Mamm Genome*. 2013;24:198–205.
29. Holter SM, Garrett L, Einicke J, et al. Assessing cognition in mice. *Curr Protoc Mouse Biol*. 2015;5:331–358.
30. Oud MM, Latour BL, Bakey Z, et al. Cellular ciliary phenotyping indicates pathogenicity of novel variants in IFT140 and confirms a Mainzer-Saldino syndrome diagnosis. *Cilia*. 2018;7:1.
31. Mohammed SG, Arjona FJ, Verschuren EHJ, et al. Primary cilia-regulated transcriptome in the renal collecting duct. *FASEB J*. 2018;32:3653–3668.
32. Tosic J, Kim GJ, Pavlovic M, et al. Eomes and Brachyury control pluripotency exit and germ-layer segregation by changing the chromatin state. *Nat Cell Biol*. 2019;21:1518–1531.
33. Rehman AU, Najafi M, Kambouris M, et al. Biallelic loss of function variants in PPP1R21 cause a neurodevelopmental syndrome with impaired endocytic function. *Hum Mutat*. 2019;40:267–280.
34. Loges NT, Antony D, Maver A, et al. Recessive DNAH9 loss-of-function mutations cause laterality defects and subtle respiratory ciliary-beating defects. *Am J Hum Genet*. 2018;103:995–1008.
35. Teumer A, Li Y, Ghasemi S, et al. Genome-wide association meta-analyses and fine-mapping elucidate pathways influencing albuminuria. *Nat Commun*. 2019;10:4130.

36. Zou Y, Carbonetto P, Wang G, Stephens M. Fine-mapping from summary data with the "Sum of Single Effects" model. *PLoS Genet*. 2022;18: e1010299.
37. Sheng X, Guan Y, Ma Z, et al. Mapping the genetic architecture of human traits to cell types in the kidney identifies mechanisms of disease and potential treatments. *Nat Genet*. 2021;53:1322–1333.
38. Pruim RJ, Welch RP, Sanna S, et al. LocusZoom: regional visualization of genome-wide association scan results. *Bioinformatics*. 2010;26:2336–2337.
39. Muto Y, Wilson PC, Ledru N, et al. Single cell transcriptional and chromatin accessibility profiling redefine cellular heterogeneity in the adult human kidney. *Nat Commun*. 2021;12:2190.
40. Bycroft C, Freeman C, Petkova D, et al. The UK Biobank resource with deep phenotyping and genomic data. *Nature*. 2018;562:203–209.
41. Kurki MI, Karjalainen J, Palta P, et al. FinnGen provides genetic insights from a well-phenotyped isolated population. *Nature*. 2023;613:508–518.
42. Lake BB, Menon R, Winfree S, et al. An atlas of healthy and injured cell states and niches in the human kidney. *Nature*. 2023;619:585–594.
43. Schwartz GJ, Munoz A, Schneider MF, et al. New equations to estimate GFR in children with CKD. *J Am Soc Nephrol*. 2009;20:629–637.
44. Fabre PH, Herrel A, Fitriana Y, et al. Masticatory muscle architecture in a water-rat from Australasia (Murinae, Hydromys) and its implication for the evolution of carnivory in rodents. *J Anat*. 2017;231:380–397.
45. Carlsson P, Mahlapuu M. Forkhead transcription factors: key players in development and metabolism. *Dev Biol*. 2002;250:1–23.
46. Benayoun BA, Caburet S, Veitia RA. Forkhead transcription factors: key players in health and disease. *Trends Genet*. 2011;27:224–232.
47. Wu CW, Mann N, Nakayama M, et al. Phenotype expansion of heterozygous FOXC1 pathogenic variants toward involvement of congenital anomalies of the kidneys and urinary tract (CAKUT). *Genet Med*. 2020;22:1673–1681.
48. Zheng B, Seltzsam S, Wang C, et al. Whole exome sequencing identifies FOXL2, FOXA2 and FOXA3 as candidate genes for monogenic congenital anomalies of the kidneys and urinary tract. *Nephrol Dial Transplant*. 2022;37:1833–1843.
49. Ernstsson S, Betz R, Lagercrantz S, et al. Cloning and characterization of freac-9 (FKHL17), a novel kidney-expressed human forkhead gene that maps to chromosome 1p32-p34. *Genomics*. 1997;46:78–85.
50. Okabe M, Motojima M, Miyazaki Y, et al. Global polysome analysis of normal and injured podocytes. *Am J Physiol Renal Physiol*. 2019;316: F241–F252.
51. Wu SC, Grindley J, Winnier GE, et al. Mouse mesenchyme forkhead 2 (Mf2): expression, DNA binding and induction by sonic hedgehog during somitogenesis. *Mech Dev*. 1998;70:3–13.
52. Hatini V, Huh SO, Herzlinger D, et al. Essential role of stromal mesenchyme in kidney morphogenesis revealed by targeted disruption of Winged Helix transcription factor BF-2. *Genes Dev*. 1996;10:1467–1478.
53. Perlman RL. Mouse models of human disease: an evolutionary perspective. *Evol Med Public Health*. 2016;2016:170–176.
54. Newman EA, Kim DW, Wan J, et al. Foxd1 is required for terminal differentiation of anterior hypothalamic neuronal subtypes. *Dev Biol*. 2018;439:102–111.
55. Xuan S, Baptista CA, Balas G, et al. Winged helix transcription factor BF-1 is essential for the development of the cerebral hemispheres. *Neuron*. 1995;14:1141–1152.
56. Millington G, Elliott KH, Chang YT, et al. Cilia-dependent GLI processing in neural crest cells is required for tongue development. *Dev Biol*. 2017;424:124–137.
57. Jeong J, Mao J, Tenzen T, et al. Hedgehog signaling in the neural crest cells regulates the patterning and growth of facial primordia. *Genes Dev*. 2004;18:937–951.
58. Sanyanusin P, Schimmenti LA, McNoe LA, et al. Mutation of the PAX2 gene in a family with optic nerve colobomas, renal anomalies and vesicoureteral reflux. *Nat Genet*. 1995;9:358–364.
59. Sasaki H, Hogan BL. Differential expression of multiple fork head related genes during gastrulation and axial pattern formation in the mouse embryo. *Development*. 1993;118:47–59.
60. Rothenpieler UW, Dressler GR. Pax-2 is required for mesenchyme-to-epithelium conversion during kidney development. *Development*. 1993;119:711–720.
61. Boualia SK, Gaitan Y, Murawski I, et al. Vesicoureteral reflux and other urinary tract malformations in mice compound heterozygous for Pax2 and Emx2. *PLoS One*. 2011;6:e21529.
62. Naiman N, Fujioka K, Fujino M, et al. Repression of interstitial identity in nephron progenitor cells by Pax2 establishes the nephron-interstitium boundary during kidney development. *Dev Cell*. 2017;41: 349–365.e363.
63. Djudjaj S, Papasotiriou M, Bulow RD, et al. Keratins are novel markers of renal epithelial cell injury. *Kidney Int*. 2016;89:792–808.
64. Das A, Tanigawa S, Karner CM, et al. Stromal-epithelial crosstalk regulates kidney progenitor cell differentiation. *Nat Cell Biol*. 2013;15: 1035–1044.
65. Saburi S, Hester I, Fischer E, et al. Loss of Fat4 disrupts PCP signaling and oriented cell division and leads to cystic kidney disease. *Nat Genet*. 2008;40:1010–1015.
66. Saburi S, Hester I, Goodrich L, McNeill H. Functional interactions between Fat family cadherins in tissue morphogenesis and planar polarity. *Development*. 2012;139:1806–1820.
67. Rao A, O'Donnell S, Bain N, et al. An intragenic deletion of the NFIA gene in a patient with a hypoplastic corpus callosum, craniofacial abnormalities and urinary tract defects. *Eur J Med Genet*. 2014;57:65–70.
68. Nyboe D, Kreiborg S, Kirchhoff M, Hove HB. Familial craniosynostosis associated with a microdeletion involving the NFIA gene. *Clin Dysmorphol*. 2015;24:109–112.
69. Hains D, Sims-Lucas S, Kish K, et al. Role of fibroblast growth factor receptor 2 in kidney mesenchyme. *Pediatr Res*. 2008;64:592–598.
70. Torban E, Dziarmaga A, Iglesias D, et al. PAX2 activates WNT4 expression during mammalian kidney development. *J Biol Chem*. 2006;281:12705–12712.
71. Tanigawa S, Wang H, Yang Y, et al. Wnt4 induces nephronic tubules in metanephric mesenchyme by a non-canonical mechanism. *Dev Biol*. 2011;352:58–69.
72. Stark K, Vainio S, Vassileva G, McMahon AP. Epithelial transformation of metanephric mesenchyme in the developing kidney regulated by Wnt-4. *Nature*. 1994;372:679–683.
73. Kispert A, Vainio S, McMahon AP. Wnt-4 is a mesenchymal signal for epithelial transformation of metanephric mesenchyme in the developing kidney. *Development*. 1998;125:4225–4234.
74. McMahon AP. Development of the mammalian kidney. *Curr Top Dev Biol*. 2016;117:31–64.
75. Walker KA, Sims-Lucas S, Bates CM. Fibroblast growth factor receptor signaling in kidney and lower urinary tract development. *Pediatr Nephrol*. 2016;31:885–895.
76. Sajithlal G, Zou D, Silvius D, Xu PX. Eya 1 acts as a critical regulator for specifying the metanephric mesenchyme. *Dev Biol*. 2005;284:323–336.
77. Poladia DP, Kish K, Kutay B, et al. Role of fibroblast growth factor receptors 1 and 2 in the metanephric mesenchyme. *Dev Biol*. 2006;291: 325–339.
78. Brophy PD, Ostrom L, Lang KM, Dressler GR. Regulation of ureteric bud outgrowth by Pax2-dependent activation of the glial derived neurotrophic factor gene. *Development*. 2001;128:4747–4756.
79. MacArthur DG, Manolio TA, Dimmock DP, et al. Guidelines for investigating causality of sequence variants in human disease. *Nature*. 2014;508:469–476.

ORIGINAL ARTICLE

CLINICAL GENETICS WILEY

Is there a dominant-negative effect in individuals with heterozygous disease-causing variants in *COL4A3/COL4A4*?

Korbinian M. Riedhammer[1,2] | Hannes Simmendinger[1] | Velibor Tasic[3] |
Jovana Putnik[4] | Nora Abazi-Emini[3] | Natasa Stajic[4] | Riccardo Berutti[1] |
Marc Weidenbusch[5] | Ludwig Patzer[6] | Adrian Lungu[7] |
Gordana Milosevski-Lomic[4] | Roman Günthner[2] | Matthias C. Braunisch[2] |
Jasmina Ćomić[1,2] | Julia Hoefele[1]

[1]Institute of Human Genetics, Klinikum rechts der Isar, Technical University of Munich, TUM School of Medicine and Health, Munich, Germany

[2]Department of Nephrology, Klinikum rechts der Isar, Technical University of Munich, TUM School of Medicine and Health, Munich, Germany

[3]Medical Faculty of Skopje, University Children's Hospital, Macedonia

[4]Institute for Mother and Child Health Care of Serbia "Dr Vukan Čupić", Department of Nephrology, University of Belgrade, Faculty of Medicine, Belgrade, Serbia

[5]Nephrologisches Zentrum, Medizinische Klinik und Poliklinik IV, Klinikum der Universität München, Ludwig-Maximilians University, Munich, Germany

[6]Department of Pediatric Nephrology, Children's Hospital St. Elisabeth and St. Barbara, Halle/Saale, Germany

[7]Pediatric Nephrology Department, Fundeni Clinical Institute, Bucharest, Romania

Correspondence
Julia Hoefele, Institute of Human Genetics, Klinikum rechts der Isar, School of Medicine, Technical University of Munich, Trogerstr. 32, 81675 Munich, Germany.
Email: julia.hoefele@tum.de

Funding information
Deutsche Forschungsgemeinschaft, Grant/Award Number: HO 2583/13-1; European Society for Paediatric Nephrology, Grant/Award Number: ESPN #2.2020

Abstract

Alport syndrome (AS) shows a broad phenotypic spectrum ranging from isolated microscopic hematuria (MH) to end-stage kidney disease (ESKD). Monoallelic disease-causing variants in *COL4A3/COL4A4* have been associated with autosomal dominant AS (ADAS) and biallelic variants with autosomal recessive AS (ARAS). The aim of this study was to analyze clinical and genetic data regarding a possible genotype–phenotype correlation in individuals with disease-causing variants in *COL4A3/COL4A4*. Eighty-nine individuals carrying at least one *COL4A3/COL4A4* variant classified as (likely) pathogenic according to the American College of Medical Genetics guidelines and current amendments were recruited. Clinical data concerning the prevalence and age of first reported manifestation of MH, proteinuria, ESKD, and extrarenal manifestations were collected. Individuals with monoallelic non-truncating variants reported a significantly higher prevalence and earlier diagnosis of MH and proteinuria than individuals with monoallelic truncating variants. Individuals with biallelic variants were more severely affected than those with monoallelic variants. Those with biallelic truncating variants were more severely affected than those with compound heterozygous non-truncating/truncating variants or individuals with biallelic non-truncating variants. In this study an association of heterozygous non-truncating *COL4A3/COL4A4* variants with a more severe phenotype in comparison to truncating variants could be shown indicating a potential dominant-negative effect as an explanation for this observation. The results for individuals with ARAS support the, still scarce, data in the literature.

KEYWORDS
Alport syndrome, *COL4A3*, *COL4A4*, dominant-negative effect, genotype–phenotype correlation

---

1 | INTRODUCTION

Type-IV-collagen-related nephropathy is an umbrella term comprising X-linked, autosomal recessive and autosomal dominant Alport syndrome (AS), the latter formerly known as thin basement membrane nephropathy (TBMN).[1–7] AS is characterized by microscopic hematuria (MH) and proteinuria leading to end-stage kidney disease (ESKD). Additionally, extrarenal manifestations like high-frequency sensorineural hearing impairment and eye abnormalities can be observed.[8] Disease-causing variants in *COL4A5*, which is located on the X chromosome (X-linked AS; XLAS; hemizygous [male] or heterozygous [female]), as well as biallelic and monoallelic disease-causing variants in *COL4A3* or *COL4A4* (autosomal recessive AS, ARAS; autosomal dominant AS, ADAS) have been described.[9] The histology-derived term TBMN has now mostly been replaced by "autosomal dominant AS" (ADAS). However, the designation ADAS is still contested.[10,11] Furlano et al. propose that individuals with a heterozygous disease-causing variant in *COL4A3* or *COL4A4* should be designated as having ADAS, whereas Savige et al. argue that AS implies a highly-penetrant phenotype of ESKD, which only occurs in a maximum of a third of ADAS cases (mostly above 50 years of age), and extrarenal manifestations, which are uncommon in ADAS.[12,13] In this manuscript, albeit its limitations, the term ADAS for individuals carrying monoallelic disease-causing variants in *COL4A3*/*COL4A4* is used for the sake of clarity.

Of note, focal segmental glomerulosclerosis (FSGS), one of the most common features seen in glomerular injury, can also be observed in kidney biopsies of individuals with disease-causing variants in *COL4A3-5*, mostly in the late course of AS.[14–16] However, it has to be pointed out that FSGS is only a descriptive pathological term and does not represent an own disease entity.[17]

Several studies on genotype–phenotype correlation in individuals with biallelic disease-causing variants in *COL4A3* or *COL4A4* implicate that the type of variant influences the phenotype.[13,18] These studies show that individuals with missense variants develop MH and proteinuria later than individuals with loss-of-function (i.e., truncating) variants. Furthermore, individuals with missense variants present extrarenal manifestations significantly less frequent compared to individuals with other types of variants. By comparison, loss-of-function variants or a combination of a loss-of-function variant and a missense variant in these individuals lead to an earlier development of ESKD than missense variants.[19–21] For individuals with monoallelic disease-causing variants, only limited data are available in the literature. Furlano et al. could recently show that individuals with a monoallelic disease-causing variant in *COL4A3* or *COL4A4* did not exhibit a clear genotype–phenotype correlation.[10]

The focus of this retrospective study was the reevaluation of the phenotype and genotype of 89 individuals with autosomal AS.

2 | METHODS

2.1 | Study population

For this study, individuals with disease-causing variants in *COL4A3* or *COL4A4* were investigated. These individuals have been recruited between October 2015 and January 2021 in a tertiary-care center (Institute of Human Genetics, Klinikum rechts der Isar, Technical University of Munich, TUM School of Medicine and Health, Munich, Germany). In all individuals, molecular genetic testing using exome sequencing (ES), next-generation sequencing (NGS)-based panel diagnostics, or Sanger sequencing had been performed and genetic data were available (see Section 3 and Supplementary Table 1). This study was carried out according to standards of the 2013 Helsinki Declaration and authorized by the local Ethics Committee of the Technical University of Munich. Informed and written consents were obtained from all individuals or their legal guardians.

2.2 | Clinical case information

Phenotypic information was first obtained from clinical reports and medical history. Additionally, a standardized questionnaire, filled out by the reffering clincian, was used to evaluate clinical information such as microscopic hematuria and proteinuria. To further corroborate the information, individuals and referring clinicians were additionally contacted by phone. All this information was collected independently of the disease-causing variant of the individuals. Assignment to the clinical disease group ARAS, ADAS or FSGS was based on the tentative clinical diagnosis of the referring clinician. The individuals were assigned to one of the following genotypic groups: (i) individuals with a monoallelic disease-causing variant in *COL4A3* or *COL4A4*; (ii) individuals with biallelic disease-causing variants in *COL4A3* or *COL4A4*. Within these two groups, five further subgroups were generated: individuals with a monoallelic non-truncating variant (missense, in-frame insertion/deletion), individuals with a monoallelic truncating variant (frameshift, nonsense, canonical splice site, and copy number variant), individuals with biallelic non-truncating variants, individuals with a non-truncating and a truncating variant (termed as non-truncating/truncating), and individuals with biallelic truncating variants. Age of onset of kidney failure in individuals was determined as the beginning of renal replacement therapy (hemodialysis or peritoneal dialysis) or pre-emptive kidney transplantation.

2.3 | Genetic analysis

Genetic testing was performed with ES, NGS-based panel diagnostics, or Sanger sequencing (see Section 3 and Supplementary Table 1).

2.4 | Exome sequencing

For extraction of DNA from peripheral blood the automated nucleic acid purification instrument Chemagic™ 360 (PerkinElmer, Waltham, MA, USA) according to the manufacturer's protocol was used. ES was performed in 22/38 (58%) index cases (see Section 3 and Supplementary Table 1) with Sure Select Human All Exon 60 Mb V6 Kit (Agilent) and a HiSeq4000 (Illumina) in the index cases.[22] Mitochondrial DNA

was derived from off-target exome reads as previously described.[23] Reads were aligned to the human reference genome (UCSC Genome Browser build hg19) using Burrows-Wheeler Aligner (v.0.7.5a). Using SAMtools (version 0.1.19), detection of single-nucleotide variants (SNVs) and small insertions and deletions (indels) was accomplished. ExomeDepth was used to investigate for copy number variants (CNVs). A noise threshold of 2.5 was accepted.[24] The Integrative Genomics Viewer (IGV, https://software.broadinstitute.org/software/igv/) was used to visualize called CNVs and to check if there was enough coverage of the examined regions as well as for plausibility of the CNVs. CNVs were then compared with publicly available control databases like the Genome Aggregation Database (gnomAD, https://gnomad.broadinstitute.org/about) and the Database of Genomic Variants (DGV, http://dgv.tcag.ca/dgv/app/home), and databases for pathogenic CNVs like DECIPHER (https://decipher.sanger.ac.uk/), and ClinVar (https://www.ncbi.nlm.nih.gov/clinvar/). For the analysis of *de novo*, autosomal dominant and mitochondrial SNVs and indels, only variants with a minor allele frequency (MAF) of less than 0.1% (Munich Exome Server with over 26 000 exomes) were considered. For the analysis of autosomal recessive and X-linked SNVs and indels (homozygous, hemizygous or [putatively] compound heterozygous), only variants with a MAF of less than 1.0% were considered. Cases, in which disease-causing variants with a genotype fitting to the phenotype were identified, were considered as genetically solved.

2.5 | Panel diagnostics

Customized NGS-based gene panels of variable size including *COL4A3-5* were performed in 11/38 (29%) index cases by an accredited external laboratory (see Section 3 and Supplementary Table 1). These panels included CNV analysis of the *COL4A3-5* genes.

2.6 | Sanger sequencing

Sequencing of *COL4A3-5* for identification of disease-causing variants (in 5/38 index cases [13%]) and segregation analysis was conducted by Sanger sequencing (see Section 3 and Supplementary Table 1). Oligonucleotide primer sequences are available upon request.

2.7 | Variant interpretation

The following publicly available databases for (likely) pathogenic variants were used for comparison of all variants found and described in this study: ClinVar, the Human Gene Mutation Database (HGMD®, http://www.hgmd.cf.ac.uk), and the Leiden Open Variation Database (LOVD, https://www.lovd.nl). The variants were rated in accordance with American College of medical Genetics and Genomics (ACMG) guidelines and current amendments.[3–6] Likely pathogenic and pathogenic variants are summarized as "disease-causing variant" in the text (at times shortened to just "variants" for better readability).

2.8 | Statistical analysis

For the comparison of categorial variables Fisher's exact test, for the comparison of quantitative variables Mann–Whitney test or Kruskal–Wallis test were used. Cumulative incidence curves for the first diagnosis of microscopic hematuria or proteinuria stratified by monoallelic truncating and non-truncating variants were calculated and compared using the logrank test. An event was retrospectively defined as the age at the first reported manifestation (i.e., first diagnosis) of MH/proteinuria. Individuals were censored if MH or proteinuria were absent at the age at the time of data collection. Statistical analysis was done with SPSS® Statistics 23 (IBM®, Ehningen, Germany) and R Version 4.2.2 (R Foundation for statistical Computing, Vienna, Austria). All tests were performed two-sided and a significance level of $p \leq 0.05$ was used for all tests.

3 | RESULTS

3.1 | Study population

The total study cohort consisted of 89 individuals out of 38 unrelated families. Complete phenotypic and genotypic data can be found in the Supplementary Table 1. 46/89 (52%) individuals were female, 43/89 (48%) male. 84/89 (94%) were of Non-Finnish European origin. 5/89 (6%) individuals were reported to be from consanguineous parents. The median age of individuals at data collection was 33 years ranging from 2 years up to 86 years of age. 29/89 (33%) individuals were <18 years of age, 60/89 (67%) individuals ≥18 years of age. 86/89 (97%) had a positive family history.

According to the tentative clinical diagnosis made by the referring clinician, the individuals were grouped as follows: 19× ARAS, 56× ADAS, and 4× FSGS. 10/89 (11%) individuals had a reported inconspicuous kidney function. These individuals were collected in the course of treatment of a clinically affected relative.

33/89 (37%) individuals were primarily examined by ES (22/38 [58%] index cases), 14/89 (16%) by NGS-based panel diagnostics (11/38 [29%] index cases), and 42/89 (47%) by Sanger sequencing of *COL4A3-5* (5/38 [13%] index cases; see Supplementary Table 1).

3.2 | Distribution of identified disease-causing variants in the study cohort

72/89 (81%) individuals carried a monoallelic disease-causing variant in *COL4A3* or *COL4A4*, whereas 17/89 (19%) had biallelic disease-causing variants in *COL4A3* or *COL4A4* (Figure 1). 24/72 (33%) individuals with a monoallelic variant carried a truncating variant, 48/72 (67%) individuals a non-truncating variant. In the 17 individuals with biallelic disease-causing variants, 5/17 (29%) had biallelic non-truncating variants, 6/17 (35%) had compound heterozygous truncating and non-truncating variants, and 6/17 (35%) had biallelic truncating variants. Due to the limited number of different variants in both genes a genotype–phenotype correlation for each variant was not performed. Detailed information on the characteristics of the identified variants can be found in Table 1.
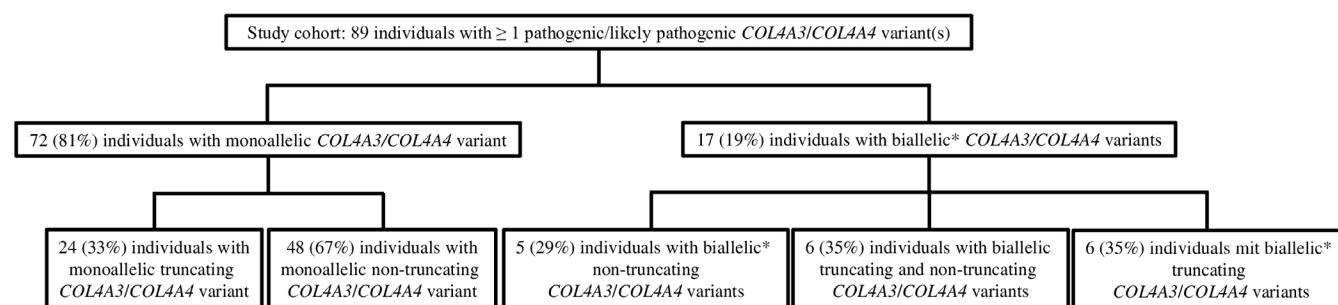
FIGURE 1 Flow chart of the study cohort. *Compound heterozygous or homozygous.

TABLE 1 Overview of the distribution of the identified variants.

Individuals/Variants	Total cohort	COL4A3	COL4A4
Individuals	89/89	61 (69%)	28 (31%)
Male	43/89	30 (70%)	13 (30%)
Female	46/89	31 (67%)	15 (33%)
Non-Finnish European origin	84/89	57 (68%)	27 (32%)
Consanguinity	5/89	4 (80%)	1 (20%)
Positive family history	86/89	60 (70%)	26 (30%)
Zygosity			
Monoallelic	72/89	47 (65%)	25 (35%)
Biallelic	17/89	14 (82%)	3 (18%)
Compound heterozygous	12/17	11 (92%)	1 (8%)
Homozygous	5/17	3 (60%)	2 (40%)
Variants			
Number of identified variants	106/106	75 (71%)	31 (29%)
Number of different variants	42/42	27 (64%)	15 (36%)
Once in cohort	9/42	6 (67%)	3 (33%)
Multiple times in cohort	33/42	21 (64%)	12 (36%)
Type of variant			
Truncating	42/106	26 (62%)	16 (38%)
Nonsense	19/42	10 (53%)	9 (47%)
Frameshift	7/42	6 (86%)	1 (14%)
Canonical splice site variant	13/42	8 (62%)	5 (38%)
CNV (multi-exon deletion)	1/42	0 (0%)	1 (100%)
Affecting start codon	2/42	2 (100%)	0 (0%)
Non-truncating	64/106	49 (77%)	15 (23%)
Missense	53/64	40 (75%)	13 (25%)
In-frame deletion	4/64	2 (50%)	2 (50%)
In-frame duplication	7/64	7 (100%)	0 (0%)

Abbreviation: CNV, copy number variant (multi-exon deletion, see Supplementary Table 1).

3.3 | Genotype–phenotype correlation of the study cohort

Because of limited or conflicting clinical data questioning the clinical tentative diagnosis submitted by the referring clinician, a genetic diagnosis was not made in 4/89 (4%) individuals (see Section 4). Therefore, only 85/89 (96%) individuals were classified as genetically solved. A detailed distribution of the clinical and genotypic status of the individuals separated in individuals with a monoallelic (72 individuals) variant and biallelic (17 individuals) variants can be found in Table 2.

3.3.1 | Microscopic hematuria

78/89 (88%) individuals had MH. The median age of first reported manifestation (i.e., age at first diagnosis) of MH was 11 years of age

TABLE 2 Overview of the distribution of phenotype and genotype.

		COL4A3/COL4A4 variants	Clinical tentative diagnosis				Cases solved	
			Reported as asymptomatic	ADAS	FSGS	ARAS/XLAS	Yes	No
Genetic diagnosis	ADAS	Monoallelic	10/72	56/72	2/72	4/72	68/72	4/72
		Monoallelic n. t.	1/48	43/48	2/48	2/48	46/48	2/48
		Monoallelic t.	9/24	13/24	0/24	2/24	22/24	2/24
	ARAS	Biallelic	0/17	0/17	2/17	15/17	17/17	0/17
		Biallelic n. t.	0/5	0/5	1/5	4/5	5/5	0/5
		Biallelic t./n. t.	0/6	0/6	1/6	5/6	6/6	0/6
		Biallelic t.	0/6	0/6	0/6	6/6	6/6	0/6

Abbreviations: ARAS, autosomal recessive Alport syndrome; ADAS, autosomal dominant Alport syndrome; FSGS, focal segmental glomerulosclerosis; n.t., non-truncating; t., truncating; X-linked Alport syndrome.

TABLE 3 Overview of the distribution of the clinical phenotypes depending on the type of variant.

COL4A3/COL4A4 variants	Microscopic hematuria yes	no	Age at first reported manifestation of microscopic hematuria median (min/max)	Proteinuria yes	no	Age at first reported manifestation of proteinuria median (min/max)	ESKD yes	no	Age at ESKD median (min/max)	Extrarenal manifestation yes	no	Age at first reported manifestation of extrarenal manifestation median (min/max)
Study cohort	78/89 (88%)	11/89 (12%)	11 (1/66)	42/89 (47%)	47/89 (53%)	11 (1/82)	8/89 (9%)	81/89 (91%)	28 (10/68)	12/89 (13%)	77/89 (87%)	12 (7/23)
monoallelic	61/72 (85%)	11/72 (15%)	20 (1/66)	25/72 (35%)	47/72 (65%)	25 (1/82)	4/72 (6%)	68/72 (94%)	37 (23/68)	2/72 (3%)	70/72 (97%)	14 (12/15)
monoallelic n.t.	46/48 (96%)	2/48 (4%)	18 (1/66)	21/48 (44%)	27/48 (56%)	25 (1/82)	3/48 (6%)	45/48 (94%)	42 (31/68)	1/48 (2%)	47/48 (98%)	12 (12/12)
monoallelic t.	15/24 (63%)	9/24 (37%)	26 (3/50)	4/24 (17%)	20/24 (83%)	17 (3/40)	1/24 (4%)	23/24 (96%)	23 (23/23)	1/24 (4%)	23/24 (96%)	15 (15/15)
biallelic	17/17 (100%)	0/17 (0%)	3 (1/18)	17/17 (100%)	0/17 (0%)	6 (1/26)	4/17 (24%)	13/17 (76%)	26 (10/29)	10/17 (59%)	7/17 (41%)	11 (7/23)
biallelic n.t.	5/5 (100%)	0/5 (0%)	6 (3/10)	5/5 (100%)	0/5 (0%)	9 (3/17)	0/5 (0%)	5/5 (100%)	-	2/5 (40%)	3/5 (60%)	17 (11/23)
biallelic n.t./t.	6/6 (100%)	0/6 (0%)	6 (1/18)	6/6 (100%)	0/6 (0%)	9 (3/26)	1/6 (17%)	5/6 (83%)	27 (27/27)	4/6 (67%)	2/6 (33%)	10 (7/19)
biallelic t.	6/6 (100%)	0/6 (0%)	3 (1/6)	6/6 (100%)	0/6 (0%)	3 (1/6)	3/6 (50%)	3/6 (50%)	24 (10/29)	4/6 (67%)	2/6 (33%)	10 (9/13)

Note: *$p \le 0.05$. Age in years.
Abbreviations: ESKD, end-stage kidney disease; n.t., non-truncating; t., truncating.

(range 1–66 years of age). 61/72 (85%) individuals with a monoallelic variant and 17/17 (100%) individuals with biallelic variants had MH (no significant difference; Table 3 and Figure 2). However, individuals with biallelic variants had a significantly earlier age of first reported manifestation of MH than individuals harboring a monoallelic variant (3 years vs. 20 years, $p < 0.001$; Table 3).

Individuals with a monoallelic non-truncating variant reported a significantly higher prevalence of MH compared to individuals with a monoallelic truncating variant (46/48 [96%] vs. 14/24 [63%], $p = 0.001$; Table 3 and Figure 2). Individuals with monoallelic non-truncating variants had a significantly earlier diagnosis of MH than individuals with monoallelic truncating variants ($p = 0.015$). At the age of 20 years, the incidence of MH was 55% and 25% in the non-truncating and truncating group, respectively. At the age of 40 years, the incidence of microscopic hematuria was 79% and 59% in the non-truncating and truncating group, whilst the corresponding incidence of MH at 60 years was 96% and 74%, respectively (Figure 3A).

Individuals with biallelic truncating variants had a significantly lower median age at first reported manifestation of MH than individuals with biallelic non-truncating variants (3 years vs. 6 years, $p = 0.030$; Table 3).

3.3.2 | Proteinuria

42/89 (47%) individuals had reported proteinuria. The median age of first reported manifestation (i.e., age at first diagnosis) of proteinuria was 11 years of age (range 1–82 years of age). 25/72 (35%) individuals with a monoallelic variant and all 17 (100%) individuals with biallelic

variants had proteinuria ($p < 0.001$; Table 3 and Figure 2). Furthermore, individuals with biallelic variants had a significantly earlier age of first reported manifestation of proteinuria than individuals harboring a monoallelic variant (6 years vs. 25 years, $p = 0.003$; Table 3).

Individuals with a monoallelic non-truncating variant had a significantly higher prevalence of proteinuria compared to individuals with a monoallelic truncating variant (21/48 [44%] vs. 4/24 [17%], $p = 0.035$; Table 3 and Figure 2). Individuals with monoallelic non-truncating variants had a significantly earlier diagnosis of proteinuria than individuals with monoallelic truncating variants ($p = 0.046$). At the age of 20 years, the incidence of proteinuria was 18% and 8% in the non-truncating and truncating group, respectively, whilst the corresponding incidence of proteinuria at 40 years was 37% and 21%, respectively (Figure 3B).

Individuals with biallelic truncating variants had a significantly lower median age at first reported manifestation of proteinuria than individuals with biallelic non-truncating variants (3 years vs. 9 years, $p = 0.017$) or individuals with compound heterozygous non-truncating/truncating variants (median 3 years vs. 9 years, $p = 0.015$; Table 3).

3.3.3 | End-stage kidney disease

8/89 (9%) individuals already had ESKD. The median age of onset was 28 years of age (range 10–68 years of age). 4/72 (6%) individuals with a monoallelic variant and 4/17 (24%) individuals with biallelic variants had ESKD. Hence, individuals with biallelic variants had ESKD significantly more often compared to individuals with a monoallelic variant ($p = 0.040$; Table 3 and Figure 2).

3.3.4 | Extrarenal manifestations

12/89 (13%) individuals had extrarenal manifestations including ocular anomalies and/or hearing impairment. The median age of reported onset was 12 years of age (range 7–23 years of age). 2/72 (3%) individuals with a monoallelic variant and 10/17 (59%) individuals with biallelic variants developed extrarenal manifestations. Therefore, individuals with biallelic variants had extrarenal manifestations significantly more often than individuals with a monoallelic variant ($p < 0.001$; Table 3 and Figure 2).

3.3.5 | RAAS blockade

28/89 (31%) individuals had a reported therapy with RAAS blockade. 13/72 (18%) individuals with a monoallelic variant and 15/17 (88%) individuals with biallelic variants had a RAAS blockade ($p < 0.001$). Individuals with monoallelic non-truncating variants had a RAAS blockade in 12/48 (25%) cases, individuals with monoallelic truncating variants in 1/24 (4%) cases ($p = 0,048$).

4 | DISCUSSION

Alport syndrome comprises various phenotypes like classic (highly-penetrant) AS (XLAS and ARAS) and ADAS (monoallelic disease-causing variant in COL4A3/COL4A4). Individuals with ADAS are known to be affected milder than individuals with classic AS.[13,14,25–30] This was also observed in the present study. Individuals with a monoallelic disease-causing variant in COL4A3/COL4A4 had a significantly lower prevalence for the development of proteinuria, ESKD, and extrarenal manifestations compared to individuals with biallelic disease-causing variants (Figure 2). Furthermore, individuals with a monoallelic disease-causing variant developed MH and proteinuria significantly later compared to individuals with biallelic disease-causing variants (Table 3). Of note, the prevalence of MH was not significantly different for monoallelic vs. biallelic variant carries. This makes the case that MH is the unifying phenotypic trait in all forms of AS.

Interestingly, individuals with a monoallelic non-truncating variant had a significantly higher prevalence of MH and proteinuria compared to individuals with a monoallelic truncating variant (Table 3 and Figure 2). Importantly, a more severe phenotype in individuals with monoallelic non-truncating variants compared to individuals with monoallelic truncating variants could be shown by a significantly younger cumulative age at the first diagnosis of microscopic hematuria and proteinuria (Figure 3). Fittingly, individuals with a monoallelic non-truncating variant had a reported therapy with RAAS blockade significantly more often than individuals with a monoallelic truncating variant. Of note, age at first diagnosis of MH and proteinuria was recorded before initiation of RAAS blockade, hence this phenotypic data is not biased by treatment.

To our knowledge, this finding of a more severe phenotype in individuals harboring heterozygous non-truncating disease-causing variants in COL4A3/COL4A4 compared to those with heterozygous truncating variants is not often described in the literature so far and is contrary to the current literature stating that truncating variants are responsible for a more severe and earlier phenotype.[13] To our knowledge, there is only the manuscript of Solanki et al. focusing on this topic.[31] Of note, 28/39 (72%; 58% of all non-truncating variants) monoallelic missense variants in COL4A3/COL4A4 changed glycine residues in the triple-helical domain of the respective proteins into highly destabilizing residues (Arg, Glu, Asp, and Val), which are known to lead to increased rates of hematuria.[18,30] This could also explain the high rate of hematuria in the non-truncating variant group. Furthermore, one meta-analysis of $n = 74$ cases with heterozygous disease-causing variants in COL4A3/COL4A4 ($n = 20$ truncating, rest being missense variants, mostly altering glycine residues), showed a significantly lower age of ESKD-onset in the truncating variant group vs. the missense variant group (47.1 vs. 55.2 years, $p = 0.03$).[29] Unfortunately, there were only four individuals with ESKD in the monoallelic variant group, hence a statistical comparison of the ESKD rate between individuals with monoallelic non-truncating ($n = 3$) versus non-truncating variants ($n = 1$) was not done. Nonetheless, our data implicates that individuals with monoallelic non-truncating variants are more severely affected than individuals with monoallelic truncating variants, which could be due to potential dominant-negative effect. This finding is well known in other autosomal dominant collagen-related diseases like osteogenesis imperfecta (OI; genes COL1A1 and COL1A2) where quantitative impacts on type 1 collagen leading to a heterozygous loss of function tend to result in a milder classic non-deforming OI phenotype compared to qualitative changes due to a dominant-negative effect (e.g., heterozygous missense variants altering glycine residues in the triple helical domain of the respective type 1 collagen) associated with the perinatally lethal form of OI.[32] However, it is important to note that this dominant-negative effect has not yet been described for diseases caused by disease-causing variant in COL4A3-5 genes, since it is currently assumed that slightly defective collagen trimers are better than nothing. Furthermore, other influencing factors like environment cannot be excluded. Nevertheless, our observations should now be further investigated in other AS cohorts with monoallelic disease-causing variants in COL4A3 and COL4A4 as well as in vitro.

Focusing on the individuals with biallelic variants in COL4A3/COL4A4, the observed prevalence and age at first reported manifestation concerning MH, proteinuria and extrarenal manifestations were comparable to the literature data.[9,19,20] The prevalence for ESKD, however, is higher in the literature compared to the present study but might be caused by the low median age of 33 years at data collection.[19,20,33]

Individuals with biallelic truncating variants are known to have a significantly higher prevalence of hearing impairment and ocular anomalies and a lower age at ESKD compared to individuals with biallelic non-truncating variants.[19–21] These data could be confirmed in the present study, although the results within this study were not significant (Table 3).

In the present study, four individuals with FSGS on kidney biopsy carried variants in COL4A3/4 resulting in the genetic diagnosis of ADAS and ARAS, respectively. The histologic lesion of
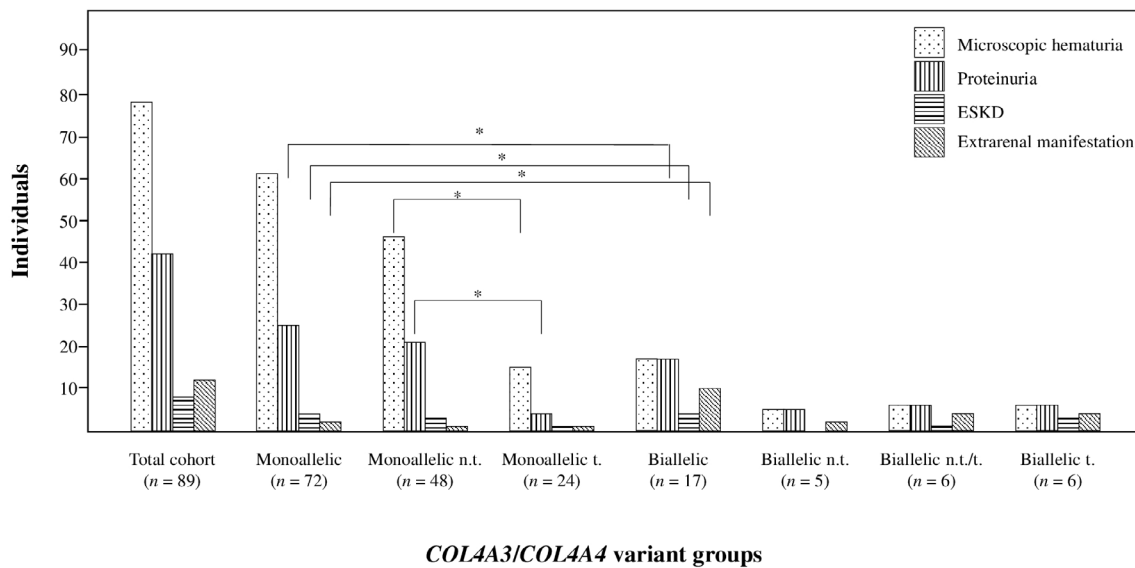
FIGURE 2 Statistical overview of the study cohort grouped according to genotype and phenotype (i.e., microscopic hematuria, proteinuria, end-stage kidney disease, and extrarenal manifestations). ESKD, end-stage kidney disease; n.t., non-truncating; t., truncating; *$p \leq 0.05$.
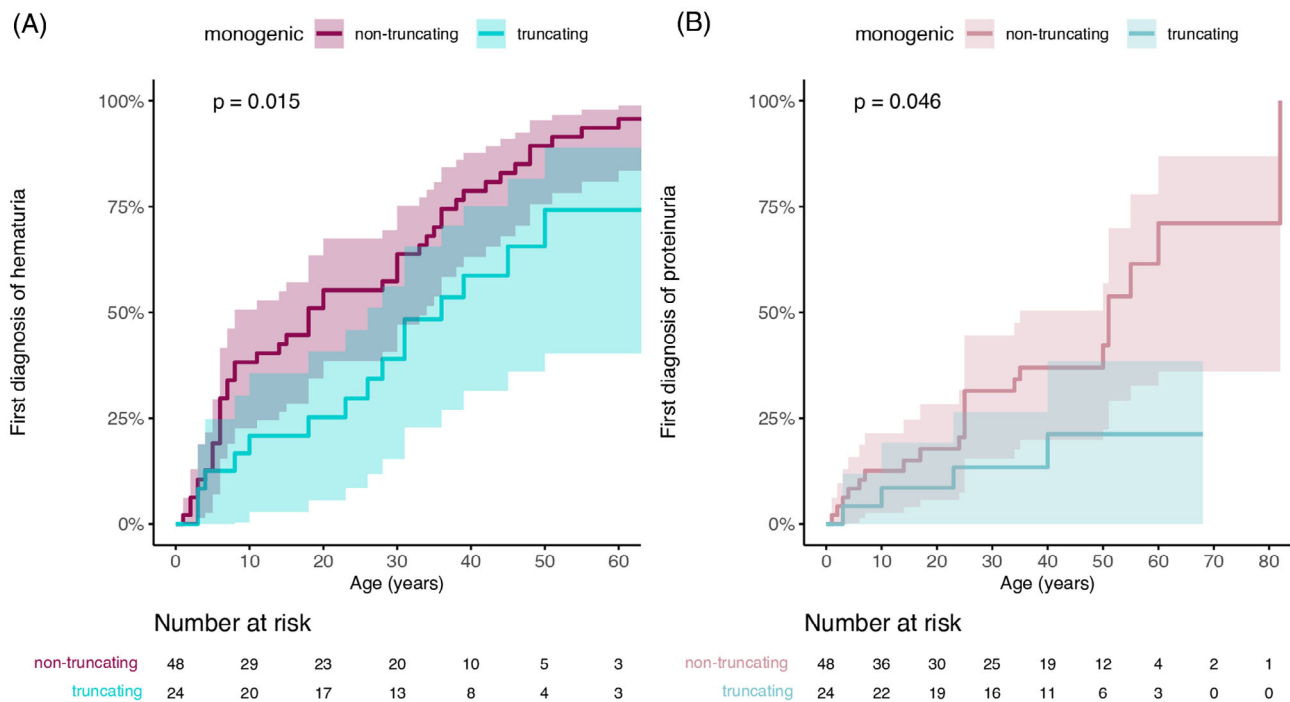

FIGURE 3 Cumulative incidence curves for the age at the first diagnosis of microscopic hematuria (A) or proteinuria (B) stratified by monoallelic non-truncating (red) and truncating (blue) variants. [Colour figure can be viewed at wileyonlinelibrary.com]

FSGS has already been described in individuals with disease-causing variants in *COL4A3*, *COL4A4*, and *COL4A5*.[9,34–36] In the study of Malone et al., 10% of individuals with monoallelic or biallelic disease-causing variants in *COL4A3/COL4A4* presented with clinical suspicion of familial FSGS.[36] As FSGS is an unspecific histologic phenotype in the process of several kidney diseases, it is not surprising to be seen in individuals with disease-causing *COL4A3/COL4A4* variants, which explains the observation of the present study.

Four individuals with ESKD or extrarenal manifestations and a monoallelic disease-causing variant had the clinical tentative diagnosis of AS. In none of these families, a further individual with an AS phenotype was observed and therefore an unequivocal genetic diagnosis of ADAS could not be made in these individuals. Apart from being *de novo* variants, this observation would be compatible with the hypothesis of Savige et al. 2018, that in individuals with the phenotype of classic AS and the finding of just a monoallelic disease-causing variant in *COL4A3* or *COL4A4*, the second disease-causing variant on the

other allele might have been missed by routine (exome-restricted) NGS-based diagnostics[11] Nonetheless, these results should be reported back to the treating physician in order to recheck the clinical diagnosis of classic Alport syndrome and to perform a re-phenotyping. If necessary, the diagnosis may subsequently change.

A limitation of this study is the small cohort size (especially the subcohort of individuals with biallelic disease-causing variants) and the fact that some individuals belong to the same family which both might have influenced the results. Additionally, although data was diligently collected for as many family members as possible, we could not collect phenotypic and genotypic information of all parents and relatives of the index cases. Therefore, there might be a selection bias which could influence the observed results. Furthermore, not all individuals of this study are index cases. Hence, oligo- or non-symptomatic relatives impact the results. This might influence at least the age of first reported manifestation of MH and proteinuria, but, importantly, this bias is irrespective of the genotype. A further limitation was the retrospective kind of this study. Individuals with a mild phenotype could often not precisely remember the exact age of onset of first identified symptoms or of performed examinations. Some of them were first detected as affected individuals after familial targeted sequencing. Therefore, in this study, the age at symptom onset is defined as "first manifestation reported" instead of "first manifestation occurred". Furthermore, this study also included children. This inclusion may have introduced a bias, as the complete phenotype may not yet have fully manifested in children. To ensure unbiased results in future studies, it is recommended to separate pediatric and adult cohorts which was not done in this study due to the small total cohort size. Finally, 5/38 (13%) index cases had only been genetically analyzed by targeted Sanger sequencing of COL4A3-5 and 11/38 (29%) only by NGS-based panel diagnostics. Hence, other genetic diagnoses could have been missed. Nonetheless, the majority of index cases (22/38 [58%]) had been analyzed by comprehensive genetic testing via ES. Lastly, it has to be mentioned that other relevant factors potentially influencing the phenotype, for example, data on blood pressure, smoking, and body mass index could not be collected for this study.

5 | CONCLUSION

This study illustrates an association of monoallelic non-truncating COL4A3/COL4A4 variants with a more severe phenotype in ADAS implicating a potential dominant-negative effect as an explanation for this observation. This hypothesis is supported by the fact that this phenomenon has already been observed in other collagenopathies.

AUTHOR CONTRIBUTIONS

Research and study design: Korbinian M. Riedhammer, Julia Hoefele. Data analysis/interpretation: Hannes Simmendinger, Jasmina Ćomić, Korbinian M. Riedhammer, Julia Hoefele. Statistical analysis: Hannes Simmendinger, Korbinian M. Riedhammer, Riccardo Berutti, Matthias C. Braunisch. Patient acquisition: Velibor Tasic, Jovana Putnik, Nora Abazi-Emini, Natasa Stajic, Marc Weidenbusch, Ludwig Patzer, Adrian Lungu, Gordana Milosevski-Lomic, Matthias C. Braunisch, Roman Günthner. Drafting and revising the article: Korbinian M. Riedhammer, Hannes Simmendinger, Julia Hoefele. Supervision or mentorship: Korbinian M. Riedhammer, Julia Hoefele. Final approval of the version to be published: Julia Hoefele. Each author contributed important intellectual content during manuscript drafting or revision and agrees to be personally accountable for the individual's own contributions and to ensure that questions pertaining to the accuracy or integrity of any portion of the work, even one in which the author was not directly involved, are appropriately investigated and resolved, including with documentation in the literature if appropriate.

CONFLICT OF INTEREST STATEMENT

The authors declare no conflicts of interest.

DATA AVAILABILITY STATEMENT

The data that support the findings of this study are available from the corresponding author upon reasonable request.

ETHICS STATEMENT

This study was approved by the local Ethics Committee of the Technical University of Munich (approval number: 521/16S).

ORCID

Korbinian M. Riedhammer https://orcid.org/0000-0002-7503-5801
Julia Hoefele https://orcid.org/0000-0002-7917-7129

REFERENCES

1. Funk SD, Lin MH, Miner JH. Alport syndrome and Pierson syndrome: diseases of the glomerular basement membrane. Matrix Biol. 2018;71-72:250-261.
2. Weber S, Strasser K, Rath S, et al. Identification of 47 novel mutations in patients with Alport syndrome and thin basement membrane nephropathy. Pediatr Nephrol. 2016;31(6):941-955.
3. Abou Tayoun AN, Pesaran T, DiStefano MT, et al. Recommendations for interpreting the loss of function PVS1 ACMG/AMP variant criterion. Hum Mutat. 2018;39(11):1517-1524.
4. Kearney HM, Thorland EC, Brown KK, Quintero-Rivera F, South ST. Working Group of the American College of Medical Genetics Laboratory Quality Assurance C. American College of Medical Genetics standards and guidelines for interpretation and reporting of postnatal constitutional copy number variants. Genet Med. 2011;13(7):680-685.
5. Richards S, Aziz N, Bale S, et al. Standards and guidelines for the interpretation of sequence variants: a joint consensus recommendation of the American College of Medical Genetics and Genomics and the Association for Molecular Pathology. Genet Med. 2015;17(5):405-424.

6. Ellard S, Baple EL, Berry I, et al. ACGS Best Practice Guidelines for Variant Classification. 2019 https://www.acgs.uk.com/media/11631/uk-practice-guidelines-for-variant-classification-v4-01-2020.pdf

7. Gibson J, Fieldhouse R, Chan MMY, et al. Prevalence estimates of predicted pathogenic COL4A3-COL4A5 variants in a population sequencing database and their implications for Alport syndrome. *J Am Soc Nephrol*. 2021;32(9):2273-2290.

8. Hudson BG, Tryggvason K, Sundaramoorthy M, Neilson EG. Alport's syndrome, Goodpasture's syndrome, and type IV collagen. *N Engl J Med*. 2003;348(25):2543-2556.

9. Kashtan CE. Alport Syndrome. In: Adam MP, Ardinger HH, Pagon RA, et al., eds. *GeneReviews* (®). University of Washington; 2019 Seattle, Copyright © 1993–2021, University of Washington, Seattle. GeneReviews is a registered trademark of the University of Washington, Seattle. All rights reserved.

10. Furlano M, Martínez V, Pybus M, et al. Clinical and genetic features of autosomal dominant Alport syndrome: a cohort study. *Am J Kidney Dis*. 2021;78(4):560-570.e561.

11. Savige J. Should we diagnose autosomal dominant Alport syndrome when there is a pathogenic heterozygous COL4A3 or COL4A4 variant? *Kidney Int Rep*. 2018;3(6):1239-1241.

12. Furlano M, Martinez V, Pybus M, et al. Clinical and genetic features of autosomal dominant Alport syndrome: a cohort study. *Am J Kidney Dis*. 2021;78:560-570.e1.

13. Savige J. Heterozygous pathogenic COL4A3 and COL4A4 variants (autosomal dominant Alport syndrome) are common, and not typically associated with end-stage kidney failure, hearing loss, or ocular abnormalities. *Kidney Int Rep*. 2022;7(9):1933-1938.

14. Deltas C, Savva I, Voskarides K, Papazachariou L, Pierides A. Carriers of autosomal recessive Alport syndrome with thin basement membrane nephropathy presenting as focal segmental glomerulosclerosis in later life. *Nephron*. 2015;130(4):271-280.

15. Braunisch MC, Buttner-Herold M, Gunthner R, et al. Heterozygous COL4A3 variants in histologically diagnosed focal segmental Glomerulosclerosis. *Front Pediatr*. 2018;6:171.

16. Frese J, Kettwig M, Zappel H, et al. Kidney injury by variants in the COL4A5 gene aggravated by polymorphisms in slit diaphragm genes causes focal segmental Glomerulosclerosis. *Int J Mol Sci*. 2019;20(3):519.

17. Miner JH. Pathology vs. molecular genetics: (re)defining the spectrum of Alport syndrome. *Kidney Int*. 2014;86(6):1081-1083.

18. Gibson JT, Huang M, Shenelli Croos Dabrera M, et al. Genotype-phenotype correlations for COL4A3-COL4A5 variants resulting in Gly substitutions in Alport syndrome. *Sci Rep*. 2022;12(1):2722.

19. Storey H, Savige J, Sivakumar V, Abbs S, Flinter FA. COL4A3/COL4A4 mutations and features in individuals with autosomal recessive Alport syndrome. *J Am Soc Nephrol*. 2013;24(12):1945-1954.

20. Lee JM, Nozu K, Choi DE, Kang HG, Ha IS, Cheong HI. Features of autosomal recessive Alport syndrome: a systematic review. *J Clin Med*. 2019;8(2):178.

21. Savige J, Storey H, Il Cheong H, et al. X-linked and autosomal recessive Alport syndrome: pathogenic variant features and further genotype-phenotype correlations. *PloS One*. 2016;11(9):e0161802.

22. Kremer LS, Bader DM, Mertes C, et al. Genetic diagnosis of Mendelian disorders via RNA sequencing. *Nat Commun*. 2017;8:15824.

23. Griffin HR, Pyle A, Blakely EL, et al. Accurate mitochondrial DNA sequencing using off-target reads provides a single test to identify pathogenic point mutations. *Genet Med*. 2014;16(12):962-971.

24. Plagnol V, Curtis J, Epstein M, et al. A robust model for read count data in exome sequencing experiments and implications for copy number variant calling. *Bioinformatics*. 2012;28(21):2747-2754.

25. Imafuku A, Nozu K, Sawa N, Nakanishi K, Ubara Y. How to resolve confusion in the clinical setting for the diagnosis of heterozygous COL4A3 or COL4A4 gene variants? Discussion and suggestions from nephrologists. *Clin Exp Nephrol*. 2020;24(8):651-656.

26. Nozu K, Nakanishi K, Abe Y, et al. A review of clinical characteristics and genetic backgrounds in Alport syndrome. *Clin Exp Nephrol*. 2019;23(2):158-168.

27. Pierides A, Voskarides K, Athanasiou Y, et al. Clinico-pathological correlations in 127 patients in 11 large pedigrees, segregating one of three heterozygous mutations in the COL4A3/ COL4A4 genes associated with familial haematuria and significant late progression to proteinuria and chronic kidney disease from focal segmental glomerulosclerosis. *Nephrol Dial Transplant*. 2009;24(9):2721-2729.

28. Voskarides K, Damianou L, Neocleous V, et al. COL4A3/COL4A4 mutations producing focal segmental glomerulosclerosis and renal failure in thin basement membrane nephropathy. *J Am Soc Nephrol*. 2007;18(11):3004-3016.

29. Matthaiou A, Poulli T, Deltas C. Prevalence of clinical, pathological and molecular features of glomerular basement membrane nephropathy caused by COL4A3 or COL4A4 mutations: a systematic review. *Clin Kidney J*. 2020;13(6):1025-1036.

30. Savige J, Huang M, Croos Dabrera MS, Shukla K, Gibson J. Genotype-phenotype correlations for pathogenic COL4A3-COL4A5 variants in X-linked, autosomal recessive, and autosomal dominant Alport syndrome. *Front Med (Lausanne)*. 2022;9:865034.

31. Solanki KV, Hu Y, Moore BS, et al. The phenotypic Spectrum of COL4A3 heterozygotes. *Kidney Int Rep*. 2023;8(10):2088-2099.

32. Steiner RD, Basel D. COL1A1/2 Osteogenesis Imperfecta. https://www.ncbi.nlm.nih.gov/books/NBK1295/

33. Jais JP, Knebelmann B, Giatras I, et al. X-linked Alport syndrome: natural history in 195 families and genotype- phenotype correlations in males. *J Am Soc Nephrol*. 2000;11(4):649-657.

34. Gast C, Pengelly RJ, Lyon M, et al. Collagen (COL4A) mutations are the most frequent mutations underlying adult focal segmental glomerulosclerosis. *Nephrol Dial Transplant*. 2016;31(6):961-970.

35. Riedhammer KM, Braunisch MC, Gunthner R, et al. Exome sequencing and identification of phenocopies in patients with clinically presumed hereditary nephropathies. *Am J Kidney Dis*. 2020;76(4):460-470.

36. Malone AF, Phelan PJ, Hall G, et al. Rare hereditary COL4A3/COL4A4 variants may be mistaken for familial focal segmental glomerulosclerosis. *Kidney Int*. 2014;86(6):1253-1259.

SUPPORTING INFORMATION

Additional supporting information can be found online in the Supporting Information section at the end of this article.